



FACULTY OF SCIENCE AND TECHNOLOGY

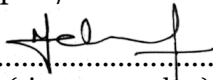
## MASTER THESIS

Study programme / specialisation:  
Computational Engineering

The spring semester, 2022

Author: Nikhil Goud Donthi

Open / ~~Confidential~~

  
.....  
(signature author)

Course coordinator: Aksel Hiorth

Supervisor(s): Ove Mikkelsen (UiS) and Jostein Lindalen (TechnipFMC)

Thesis title: Study of Stress Concentration Factors at Pipe Welds in Relation to Hydrogen Induced Stress Cracking using Finite Element Method and Response Surface Modeling

Credits (ECTS): 30

Keywords: HISC, SCF, FEM, RSM, GPR,  
Gaussian Process Regression, Pipe welds,  
Stress Concentration, Finite Element,  
Duplex Steel

Pages: 78

+ appendix: 41

Stavanger, 15.06.2022  
date/year

## Abstract

Duplex stainless steels, which are extensively used in the energy industry for subsea piping, have seen some significant failures, especially at the weld locations of cathodic protected piping components due to hydrogen induced stress cracking (HISC). This is because of the high stress concentrations at the weld hotspots. Estimating these stress concentration factors is an area of interest in the industry for studying and qualifying the welds for HISC acceptance as per the industry recommended practice, DNVGL-RP-F112.

In this thesis study, stress concentration factors at various pipe welds of different sizes and geometric parameters are estimated using the finite element method (FEM) and response surface modeling (RSM). The critical weld geometric parameters and fabrication tolerances that have a significant influence on the stress concentration are identified and studied how they affect the stress distribution in the model. The additional stress concentration induced by the secondary bending moments in the model due to centerline misalignment between the components is estimated using the 3D finite element model of the weld. The analysis models are simplified to axisymmetric models wherever possible by making reasonable approximations with the available FEM data to save computational time and expense.

The stress magnification factors estimated at some weld geometries are compared with the values calculated using the formulae from DNVGL-RP-C203, wherever applicable, and they are in line with the analytical calculations. A fillet weld between doubler plate and pipe, with high stress concentrations that couldn't meet the linear elastic assessment criteria, is checked with the actual loads from project pipe stress analysis and qualified using non-linear assessment.

Gaussian process regression modeling is used to predict the stress concentration factors at different combinations of geometric parameters based on the available FEM data and is found to be reasonably accurate when tested with random values from the estimated FEM data. It was found that the local surface penalty/ magnification factors are almost the same for different header sizes checked, provided they are of the same thickness and weld parameters. The estimated local surface penalty/ magnification factors for different combinations of wall thickness and toe fillet radius are calculated and plotted.

# Table of Contents

<b>Abstract</b> .....	ii
<b>Acknowledgements</b> .....	vi
<b>Abbreviations</b> .....	vii
<b>Symbols</b> .....	viii
<b>List of Figures</b> .....	ix
<b>List of Tables</b> .....	xi
<b>1. Introduction</b> .....	1
<b>1.1 Background</b> .....	1
<b>1.2 State of the art</b> .....	2
<b>2. Hydrogen Induced Stress Cracking in Duplex steels</b> .....	5
<b>2.1 Hydrogen formation and diffusion</b> .....	5
<b>2.2 Microstructure of the material</b> .....	6
<b>2.3 Influence of stress on HISC</b> .....	7
<b>3. HISC Assessment Criteria</b> .....	8
<b>3.1 Category 1: Semi analytical linear-elastic assessment</b> .....	8
<b>3.1.1 Smag (stress magnification factor)</b> .....	9
<b>3.1.2 LSPF<sub>cat1</sub> (Local surface penalty factor)</b> .....	9
<b>3.2 Category 2: Solid FEA based non-linear assessment</b> .....	10
<b>3.2.1 LSMF<sub>cat2</sub> (Local surface magnification factor)</b> .....	11
<b>3.3 Stress linearization</b> .....	12
<b>3.3.1 Selection of stress linearization path (or) stress classification line</b> .....	12
<b>3.3.2 Stress linearization using the stress integration method</b> .....	13
<b>3.3.3 Stress linearization example from FEA</b> .....	14
<b>4. FEA Modeling</b> .....	17
<b>4.1 Analysis models</b> .....	17
<b>4.2 Analysis loads and boundary conditions</b> .....	18
<b>4.3 Material properties</b> .....	19
<b>4.4 Meshing element types</b> .....	21
<b>4.5 Mesh convergence</b> .....	21
<b>4.5.1 Mesh convergence for linear analysis</b> .....	21
<b>5. Finite Element Analysis and Results</b> .....	26
<b>5.1 Equal weld between 6-inch pipe and winghub</b> .....	26

5.1.1 Analysis model dimensions.....	26
5.1.2 Analysis model mesh details.....	27
5.1.3 Boundary conditions.....	28
5.1.4 Analysis results.....	28
5.1.5 Analysis results with flat transition on the weld .....	30
5.1.6 Analysis Result Summary .....	32
<b>5.2 Unequal weld between 6-inch pipe and winghub.....</b>	<b>33</b>
5.2.1 Analysis model dimensions.....	33
5.2.2 Analysis model mesh details.....	34
5.2.3 Boundary conditions.....	34
5.2.4 Analysis results.....	35
5.2.5 Analysis results with flat transition on the weld .....	37
5.2.6 Analysis result summary .....	38
<b>5.3 Fillet weld between 6-inch pipe and doubler Plate .....</b>	<b>39</b>
5.3.1 Analysis model dimensions.....	39
5.3.2 Analysis model mesh details.....	39
5.3.3 Steady-state thermal analysis.....	40
5.3.4 Loads and boundary conditions.....	41
5.3.5 Non-linear analysis results .....	41
5.3.6 Calculation of LSMF using linear elastic analysis .....	42
<b>5.4 Equal welds between HIP headers and hubs.....</b>	<b>44</b>
5.4.1 Analysis model dimensions.....	44
5.4.2 Analysis model mesh details.....	44
5.4.3 Boundary conditions.....	45
5.4.4 Analysis results.....	45
<b>5.5 Unequal welds between HIP headers and hubs.....</b>	<b>48</b>
5.5.1 Analysis model dimensions.....	48
5.5.2 Analysis model mesh details.....	48
5.5.3 Boundary conditions.....	49
5.5.4 Analysis results.....	49
<b>5.6 Welds between HIP headers and valves.....</b>	<b>52</b>
5.6.1 Analysis model dimensions.....	52
5.6.2 Analysis model mesh details.....	53
5.6.3 Boundary conditions.....	53

5.6.4 Analysis results.....	54
<b>6. Response Surface Modeling and Results .....</b>	<b>57</b>
<b>6.1 RSM coupled with FEM.....</b>	<b>57</b>
<b>6.2 Gaussian process regression.....</b>	<b>58</b>
6.2.1 Theory .....	58
<b>6.3 LSPF estimation using Gaussian process regression .....</b>	<b>59</b>
6.3.1 Training the GPR model .....	59
6.3.2 Testing the GPR model.....	61
<b>6.4 Estimated LSPF values.....</b>	<b>63</b>
<b>7. Result Discussion and Conclusions.....</b>	<b>64</b>
Scope for future work.....	65
<b>References.....</b>	<b>66</b>

## **Appendices**

**Appendix – A SCF calculation at the equal weld between HIP header and hub**

**Appendix – B SCF calculation at the unequal weld between header and hub**

**Appendix – C SCF calculation at the unequal weld between header and valve**

**Appendix – D SCF calculation for valve/hub welds - headers with lower wall thickness**

**Appendix – E Input for GPRM training and estimated LSPF values**

**Appendix – F Stress linearization data and calculations**

## **Acknowledgements**

This thesis study is the final work that concludes my master's degree in Computational Engineering at the University of Stavanger. The thesis topic is proposed by TechnipFMC, Kongsberg, and the thesis work is carried out at the University of Stavanger during the period January 2022 to June 2022.

I want to express my gratitude for the guidance and support offered by the following individuals in completing my master thesis. Firstly, I would like to thank my thesis supervisors, Ove Mikkelsen (UiS) and Jostein Lindalen (TechnipFMC), for their continuous support and guidance starting from the early stages of the thesis proposal until the end of the thesis study. Next, I would like to thank Bjørn Pahlm and Dagfinn Furustad from TechnipFMC, Kongsberg, for their valuable inputs and technical guidance. I would also like to thank Manikandan Mariappan from TechnipFMC, Kongsberg, for his support in making this collaboration happen.

Stavanger, 15<sup>th</sup> June 2022

Nikhil Goud Donthi

## Abbreviations

<b>Abbreviation</b>	<b>Definition</b>
ASME	American Society of Mechanical Engineers
BPVC	Boiler and Pressure Vessel Code
Cat1	Category 1
Cat2	Category 2
CES	Computationally Expensive Simulations
DNV	Det Norske Veritas
DNVGL	Det Norske Veritas and Germanischer Lloyd
EVS	Explained Variance Score
FE	Finite Element
FEA	Finite Element Analysis
FEM	Finite Element Method
GPR	Gaussian Process Regression
GPRM	Gaussian Process Regression Model
HAZ	Heat Affected Zone
HIP	Hot Isostatic Pressing
HISC	Hydrogen Induced Stress Cracking
ID	Inner Diameter
LSMF	Local Surface Magnification Factor
LSPF	Local Surface Penalty Factor
MAE	Mean Absolute Error
OD	Outer Diameter
OMAE	Offshore Mechanics and Arctic Engineering
RP	Recommended Practice
RSM	Response Surface Model
RMSE	Root Mean Square Error
SCF	Stress Concentration Factor
SCL	Stress Classification Line
Smag	Stress Magnification Factor
SMYS	Specified Minimum Yield Strength

## Symbols

Symbol	Description
$\alpha$	Factor to determine influence of residual stresses on acceptable stress level
$\beta$	Factor to determine influence of weld transition angle on acceptable stress level
$\gamma$	Material factor reflecting influence of microstructure
$\varepsilon$	Strain
$\varepsilon_c$	Maximum allowable surface strain in category 2 assessment
$\varepsilon_{mem}$	Non-linear membrane strain
$\varepsilon_{peak}$	Peak surface strain
$K_{PT}$	Covariance function matrix for the input prediction points in GPRM
$K_{TT}$	Covariance function matrix for the input training points in GPRM
$L_{res}$	Length of zone assumed to be influenced by weld residual stresses
$\nu$	Poisson's ratio
$m$	Prediction mean in GPRM
$\sigma$	Stress
$\sigma_i$	Stress in principal direction
$\sigma_{max}$	Maximum principal surface stress
$\sigma_{mem}$	Membrane stress
$\sigma_{mem,i}$	Membrane stress in principal direction $i$
$\sigma_{bending}$	Bending stress
$\sigma_{lin}$	Linearized stress
$\sigma_{out}$	Outer fiber stress
$\sigma_{out,i}$	Outer fiber stress in the principal direction $i$
$\sigma_{therm}$	Stress due to potential thermal gradients over the wall thickness
$S_{mag}$	Stress magnification factor
$S$	Covariance matrix in GPRM
$t$	Thickness of the component
$\Theta$	Hyper parameters in GPRM



# List of Figures

**Figure 1** An overview of subsea equipment where duplex steel components are commonly used (From TechnipFMC.com, 2021)..... 1

**Figure 2** (a) A typical failure at the pipe weld due to HISC (From HAIHAO Piping, 2021) (b) Stress plot from FEM showing the weld hotspots (From Donthi and Keprate, 2021) ..... 2

**Figure 3** Factors Influencing Hydrogen Induced Stress Cracking ..... 5

**Figure 4** Hydrogen formation and diffusion mechanism (From Paul, 2022)..... 6

**Figure 5** Micrographs comparing (a) Fine grain austenite microstructure (b) coarse grain austenite microstructure (From Kjetil, 2013)..... 7

**Figure 6** Stress Classification Line Orientation and Validity Guidelines (From ASME, 2019)..... 13

**Figure 7** Principal stress direction along the stress classification line ..... 15

**Figure 8** Stress linearization example - plot from the manual calculations ..... 16

**Figure 9** Stress linearization example - plot from ANSYS ..... 16

**Figure 10** Modeling the weld centerline misalignment in 3D..... 17

**Figure 11** Example - weld cross-section details of an analysis model..... 18

**Figure 12** Example - Analysis model boundary conditions for a 2D axisymmetric model ..... 18

**Figure 13** Multilinear material isotropic hardening curves generated for 22 Cr duplex steel..... 20

**Figure 14** Multilinear material isotropic hardening curves generated for 25Cr duplex steel..... 20

**Figure 15** Linear elastic mesh convergence study- levels of mesh refinement and corresponding total maximum principal stress at the weld toe..... 22

**Figure 16** Linear elastic mesh convergence study- convergence criteria..... 23

**Figure 17** Non-linear analysis mesh convergence study- levels of mesh refinement and corresponding total maximum principal strain at the weld toe..... 24

**Figure 18** Non-linear analysis mesh convergence study- convergence criteria ..... 24

**Figure 19** Analysis model dimensions - equal weld between 6” pipe and winghub..... 26

**Figure 20** Analysis model mesh details - equal weld between 6” pipe and winghub ..... 27

**Figure 21** Analysis model boundary conditions - equal weld between 6” pipe and winghub ..... 28

**Figure 22** Maximum principal stress plot - equal weld between 6” pipe and winghub ..... 28

**Figure 23** Calculation of LSPF and  $S_{mag}$  using linearization of stress – weld root of the equal weld between 6” pipe and winghub..... 29

**Figure 24** Calculation of LSPF and  $S_{mag}$  using linearization of stress – weld toe of the equal weld between 6” pipe and winghub..... 30

**Figure 25** Analysis results comparison between 2D axisymmetric model and 3D model with centerline misalignment - weld toe of the equal weld between 6” pipe and winghub..... 31

**Figure 26** Calculation of LSPF and  $S_{mag}$  using linearization of stress – weld toe of the equal weld with the flat transition between 6” pipe and winghub..... 32

**Figure 27** Analysis model dimensions - unequal weld between 6-inch pipe and winghub ..... 33

**Figure 28** Analysis model mesh details - unequal weld between 6” pipe and winghub ..... 34

**Figure 29** Analysis model boundary conditions - unequal weld between 6” pipe and winghub ..... 35

**Figure 30** Maximum principal stress plot - unequal weld between 6” pipe and winghub ..... 35

**Figure 31** Calculation of LSPF and  $S_{mag}$  using linearization of stress – weld toe of the unequal weld between 6” pipe and winghub..... 36

**Figure 32** Calculation of LSPF and  $S_{mag}$  using linearization of stress – weld root of the equal weld between 6” pipe and winghub..... 37

<b>Figure 33</b> Calculation of LSPF and $S_{mag}$ using linearization of stress – weld toe of the unequal weld with the flat transition between 6” pipe and winghub.....	38
<b>Figure 34</b> Analysis model dimensions – fillet weld between the 6-inch pipe and doubler plate .....	39
<b>Figure 35</b> Analysis model mesh details – fillet weld between 6” pipe and doubler plate.....	40
<b>Figure 36</b> Temperature plot from the steady-state thermal analysis - 6” pipe and doubler plate.....	40
<b>Figure 37</b> Analysis boundary conditions - weld between the 6-inch pipe and doubler plate.....	41
<b>Figure 38</b> Total maximum principal strain plot - weld between the 6” pipe and doubler plate .....	41
<b>Figure 39</b> Calculation of membrane strain - weld between the 6-inch pipe and doubler plate.....	42
<b>Figure 40</b> Calculation of LSMF from linear elastic analysis - weld between the 6-inch pipe and doubler plate.....	43
<b>Figure 41</b> Analysis model dimensions – equal welds between HIP headers and hubs .....	44
<b>Figure 42</b> Analysis model mesh details – equal welds between HIP headers and hubs .....	45
<b>Figure 43</b> Analysis model boundary conditions - equal welds between HIP headers and hubs .....	45
<b>Figure 44</b> Maximum principal stress plot - equal welds between HIP headers and hubs .....	46
<b>Figure 45</b> Calculation of LSPF and $S_{mag}$ using linearization of stress – equal welds between HIP headers and hubs .....	46
<b>Figure 46</b> Analysis model dimensions – unequal welds between HIP headers and hubs .....	48
<b>Figure 47</b> Analysis model mesh details – unequal welds between HIP headers and hubs .....	49
<b>Figure 48</b> Analysis model boundary conditions - unequal welds between HIP headers and hubs .....	49
<b>Figure 49</b> Maximum principal stress plot - unequal welds between HIP headers and hubs .....	50
<b>Figure 50</b> Calculation of LSPF and $S_{mag}$ using linearization of stress – unequal welds between HIP headers and hubs .....	50
<b>Figure 51</b> Analysis model dimensions –welds between HIP headers and valves .....	52
<b>Figure 52</b> Analysis model mesh details – welds between HIP headers and valves .....	53
<b>Figure 53</b> Analysis model boundary conditions - welds between HIP headers and valves .....	54
<b>Figure 54</b> Maximum principal stress plot - welds between HIP headers and valves .....	54
<b>Figure 55</b> Calculation of LSPF and $S_{mag}$ using linearization of stress – welds between HIP headers and valves.....	55
<b>Figure 56</b> Variation of weld parameters used for GPRM training .....	60
<b>Figure 57</b> Correlation coefficients between the input and output variables.....	61
<b>Figure 58</b> Actual (FEA) vs. Predicted (GPRM) LSPF values for the weld toe (70 test points).....	62
<b>Figure 59</b> Estimated LSPF variation for welds between headers and valves.....	63

## List of Tables

<b>Table 1</b> Non-linear strain criterion .....	11
<b>Table 2</b> Linear elastic material properties .....	19
<b>Table 3</b> Thermal conductivity of materials .....	19
<b>Table 4</b> Meshing - Element type details.....	21
<b>Table 5</b> Types of welds analyzed .....	25
<b>Table 6</b> Analysis result summary - equal weld between 6” pipe and winghub.....	32
<b>Table 7</b> Analysis result summary - unequal weld between 6” pipe and winghub.....	38
<b>Table 8</b> Analysis result summary - equal welds between HIP headers and hubs.....	47
<b>Table 9</b> Analysis result summary - unequal welds between HIP headers and hubs.....	51
<b>Table 10</b> Analysis result summary - welds between HIP headers and valves.....	56
<b>Table 11</b> performance metrics for the GPR model.....	62

# 1. Introduction

## 1.1 Background

The energy industry has been extensively using 22Cr and 25Cr duplex stainless steels for subsea piping and equipment as a more robust solution in terms of design and manufacturing compared to the use of regular carbon steels (Solnørðal et al., 2009; DNVGL, 2019). These types of steels have been primarily used in subsea equipment like manifolds, Christmas trees, and jumpers as rolled or extruded pipes, small bore tubing, hubs, pipe fittings, and valve bodies manufactured by castings, forgings, or hot isostatic pressing (HIP) (DNVGL, 2019).

*Figure 1* shows some of the typical subsea equipment where duplex steel pipes and components are used.

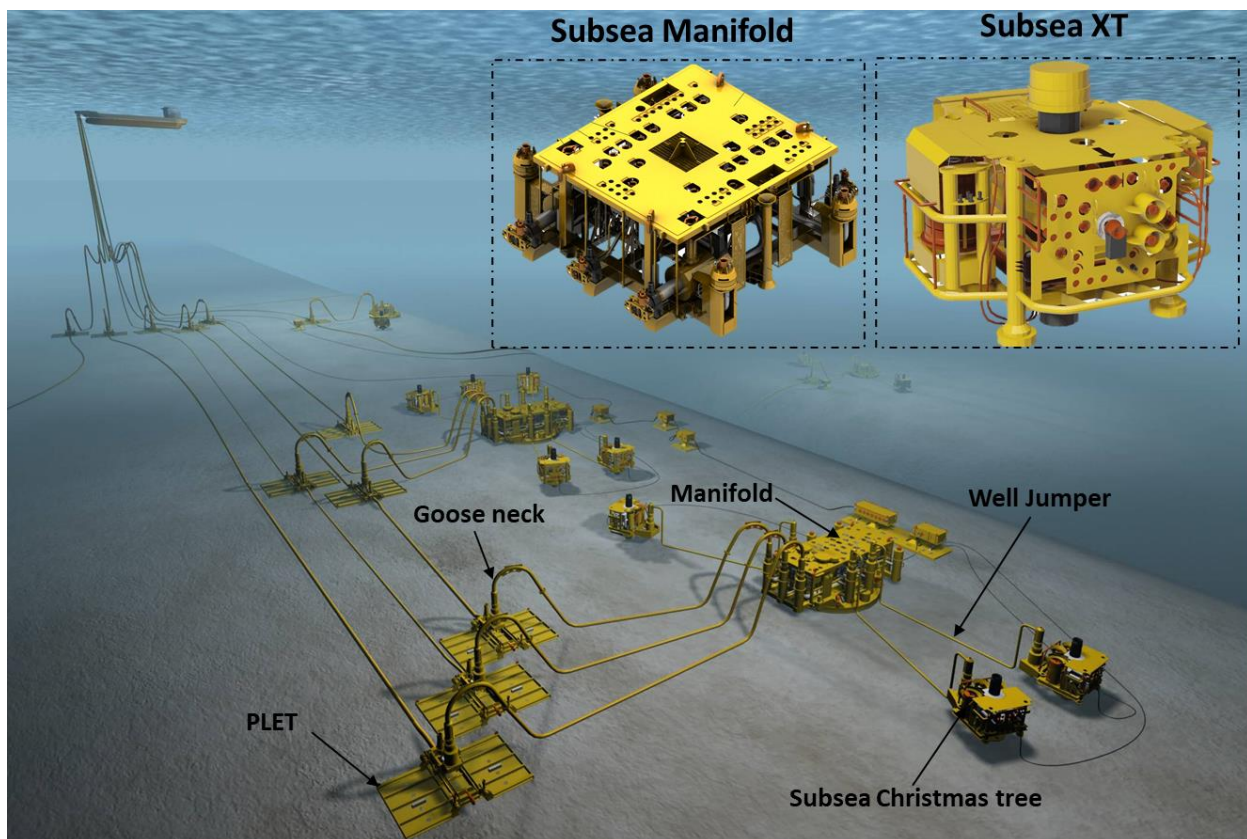


**Figure 1** An overview of subsea equipment where duplex steel components are commonly used (From TechnipFMC.com, 2021)

Though the general experience with these steels is good, some significant failures have occurred in the cathodic protected subsea components. The cause for these failures has been attributed to a combination of the tensile stress and ingress of hydrogen formed on the surface

of the steel (DNVGL, 2019). This type of failure is referred to as hydrogen induced stress cracking (HISC). HISC failures in cathodic protected duplex steel components generally occur at locations with high stress concentrations.

The most common HISC field failure locations are near the stress raisers and welds (DNVGL, 2019). This is because the critical weld features generally experience the most significant stresses and loads, needing special attention (DNVGL, 2019). Knowing the stress distribution and hotspot stresses around the weld geometry help accurately assess the HISC failures. A typical example of a weld failure due to HISC is shown in *Figure 2*.

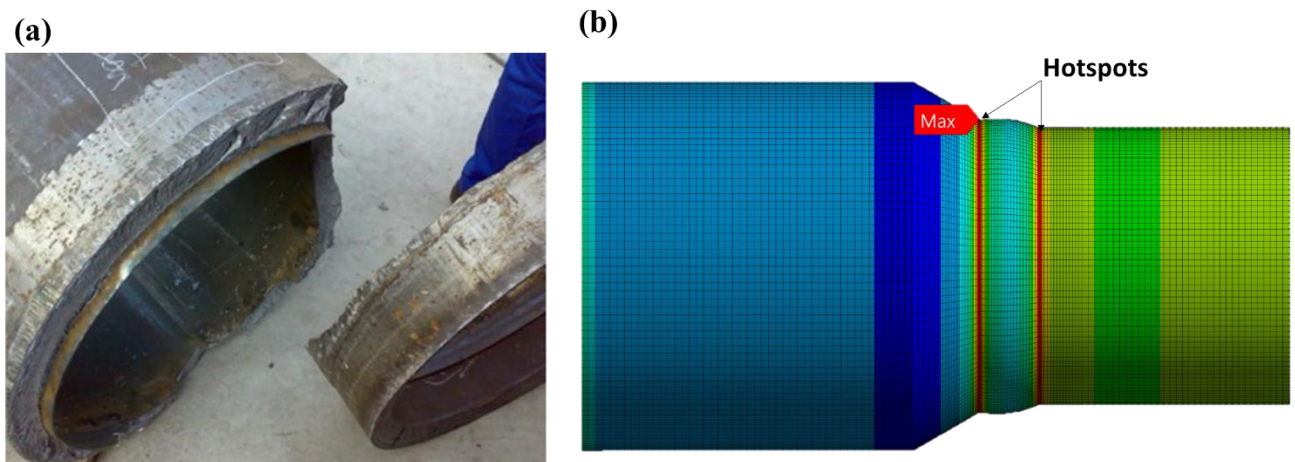


**Figure 2** (a) A typical failure at the pipe weld due to HISC (From HAIHAO Piping, 2021)  
(b) Stress plot from FEM showing the weld hotspots (From Donthi and Keprate, 2021)

## 1.2 State of the art

The current industry practice of qualifying the pipe welds against HISC is by doing either a semi-analytical assessment or a non-linear finite element analysis to calculate stresses/ strains and checking them against the acceptable limits specified in the industry recommended practice DNVGL-RP-F112. For example, Solnørdal et al. (2009) briefly present the finite element method of calculating and interpreting stresses in relation to HISC avoidance criteria defined in DNVGL (2019). The semi-analytical linear assessment requires calculating stress concentration factors, which are generally approximated using the analytical formulae from DNVGL-RP-C203 (DNVGL, 2016) or calculated using linear elastic finite element analysis depending on the complexity of the geometry.

It is helpful to calculate these stress concentration factors at the welds and study them varying the influential geometric parameters. It helps reuse these values for HISC assessment of the welds for different loads from different projects and avoids re-analysis every time. Response surface models (RSM) can be used along with the calculated values from FEA to predict the stress concentration factors for similar geometries with different dimensions. Studies have been done previously on estimating stress concentration factors using FEM and surrogate models. FEM and RSM together can be effective for predicting stress concentration factors at pipe weld transitions (Donthi and Keprate, 2021). The influence of different geometric parameters of the weld on the stress distribution and change in SCF at various hot spots were studied using response surface models (Donthi and Keprate, 2021).

### **1.3 Aim of the study**

This thesis study aims to simplify the stress analysis process of qualifying pipe welds for the HISC avoidance criteria. The agenda is to calculate the stress concentration factors at the welds using finite element analysis (FEA) and study the influence of various weld geometric parameters on the stress concentration in relation to HISC assessment. Then, estimating the SCFs for similar welds with different dimensions using response surface modeling (RSM) and the available FEA result data. This can make the qualification process both time and cost-effective compared to the individual qualification of the welds for HISC.

### **1.3 Objectives**

The major objectives thought out to achieve the aim of this thesis study are given below:

- Analyzing various welds of different sizes and geometries using the finite element method and studying the hotspot regions in the models.
- Identifying the critical geometric parameters of the weld that have a significant influence on the stress concentration and seeing how the variation of these parameters changes the stress distribution in the model.
- Studying the effect of centerline misalignment using a 3D finite element model of the weld and calculating the additional stress concentration induced by the secondary bending moments in the model.
- Studying the impact of fabrication tolerance combinations on the location of the hotspot and the value of the stress concentration.

- Simplifying the analysis models wherever possible to save computational expense by making reasonable approximations using the already available FEA data.
- Comparing the FEA evaluated SCFs with the values calculated using the relevant analytical formulae from DNVGL-RP-C203.
- Qualifying the welds by non-linear FEA using the actual loads from the global stress analysis if there are any cases where the SCFs are too high to meet the linear elastic assessment criteria for HISC avoidance.
- Identifying a suitable response surface model (RSM) and using it with FEA data to predict and plot the variation of the SCF values for similar models with different dimensions.
- Checking the accuracy and precision of the RSM in predicting SCFs for the given range of weld dimensions.

## 2. Hydrogen Induced Stress Cracking in Duplex steels

Duplex stainless steels are highly prone to HISC when exposed to cathodic protection, and it is generally caused by the influence of three major factors: tensile stress in the component, microstructure of the material, and ingress of hydrogen formed at the steel surface due to the cathodic protection. HISC failure can occur only when these three factors act together on the component. This idea is represented as a Venn diagram in *Figure 3* below.

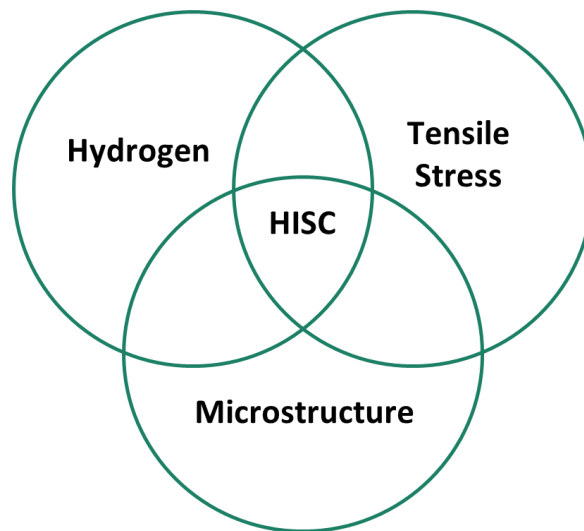


**Figure 3** Factors Influencing Hydrogen Induced Stress Cracking

### 2.1 Hydrogen formation and diffusion

The main reason for the hydrogen formation on the steel components in the subsea environment is the cathodic protection around them. Generally, duplex stainless steel pipes and components are corrosion resistant and do not require cathodic protection (Cassagne and Busschaert, 2005). However, the structure around them is usually not corrosion resistant, and it might need cathodic protection by using sacrificial anodes (Krosness, 2014). It is very difficult to isolate the piping and structure electrically, leading to cathodic protection of duplex steel components as well. Hydrogen ions formed on the cathodic protected surface slowly diffuse through the thickness and get trapped in the voids present in the material as shown in *Figure 4*.



Formation of hydrogen ions

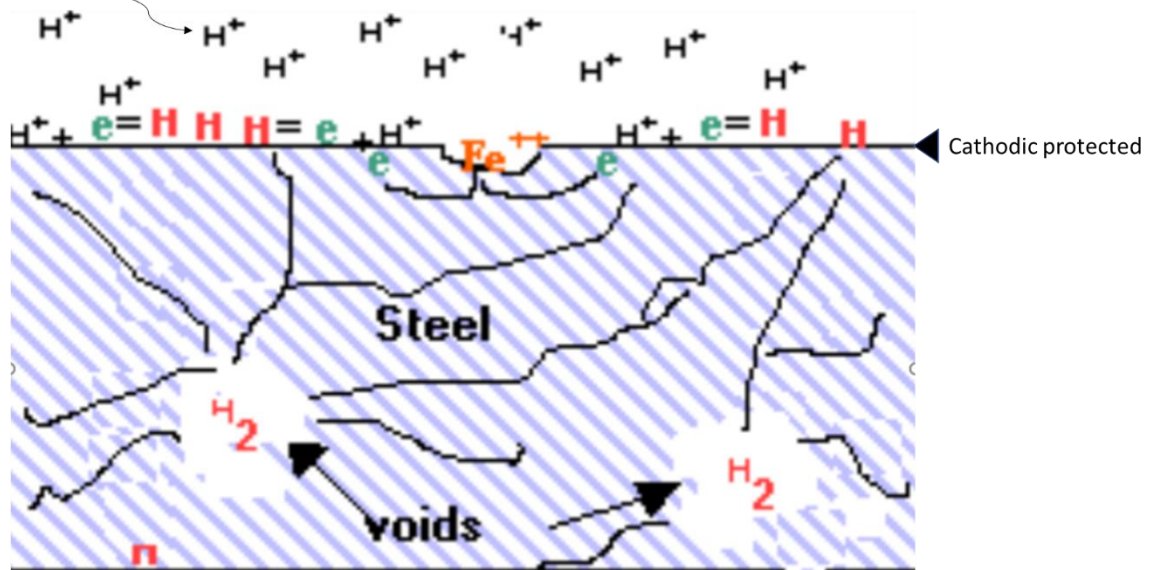


**Figure 4** Hydrogen formation and diffusion mechanism (From Paul, 2022)

These trapped hydrogen ions form hydrogen atoms releasing energy and when there is enough tensile stress present in the material, it may initiate a crack and cause HISC. However, hydrogen diffusion is a very slow process that takes place over the years. According to the diffusion depth table in DNVGL-RP-F112, it takes about 25 years for the hydrogen to diffuse through a thickness of 28 mm of the component whose surface temperature is  $121^\circ\text{C}$ . So, HISC may not be a concern at those locations in the component where sufficient hydrogen cannot diffuse through the thickness to reach them (DNVGL, 2019).

## 2.2 Microstructure of the material

Duplex and super duplex stainless steels have a two-phase microstructure comprising austenite volumes within a ferrite matrix (Solnørdal et al., 2009). The hydrogen diffusion rate is generally higher in the ferrite phase compared to that in the austenite phase, which suggests that the ferrite can quickly get saturated with hydrogen compared to austenite (Solnørdal et al., 2009). The propagation of a HISC crack is generally a straight cleavage-like fracture through the ferrite phase. Depending on the crack size, concentration of hydrogen, and tensile stress levels in the material, the crack may be arrested or propagate around or through the austenite phase (DNVGL, 2019). **Figure 5** below shows micrographs comparing fine phase spacing and coarse phase spacing.

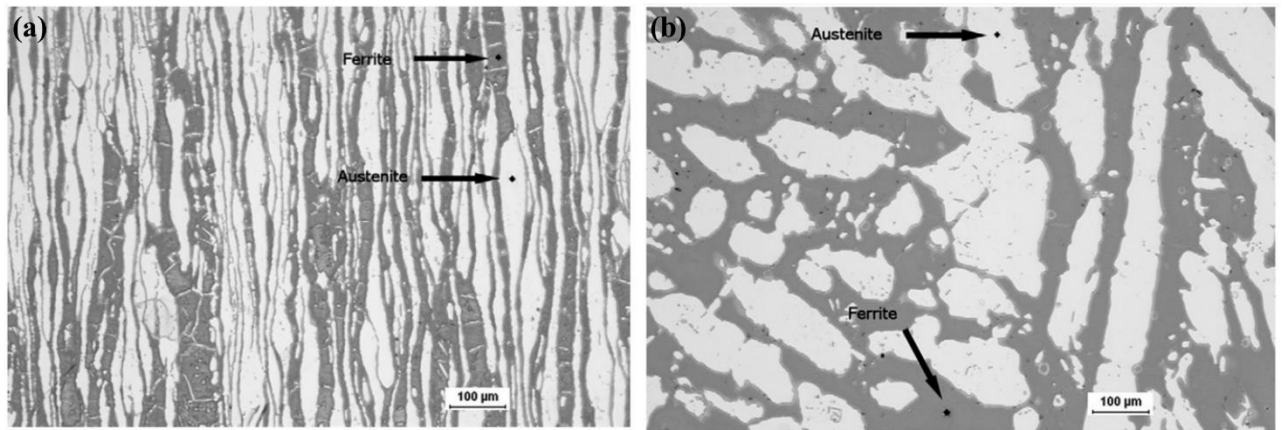


**Figure 5** Micrographs comparing (a) Fine grain austenite microstructure (b) coarse grain austenite microstructure (From Kjetil, 2013)

There is enough evidence of confirmation from testing that materials with finer austenite spacing have better resistance to HISC than the materials with coarse austenite spacing. (DNVGL, 2019). Manufacturing techniques can control this austenite spacing. The fabrication techniques that tend to decrease austenite spacing are favorable for reducing the risk of HISC. The same material can have different austenite spacing based on the fabrication method. In general, components formed by the HIP process, tubes and pipes made by extrusion, seamless rolling, or drawing have finer austenite spacing compared to the forged components (DNVGL, 2019) (Krosness, 2014). Most of the welds analyzed in this report are for the HIP header components, which have fine austenite spacing. The heat affected zone (HAZ) near the weld can be assumed to have the same austenite spacing as the base material (DNVGL, 2019).

### 2.3 Influence of stress on HISC

The most important factor influencing the occurrence of HISC in relation to this thesis study is the presence of mechanical stress in the material. Stresses can arise in a component from operational loads, accidental loads, installation loads, and misalignments. It is found from experiments and testing that it is only the tensile stress, not compressive, which is responsible for HISC (DNVGL, 2019). It is crucial to study the stress distribution in a component and identify the hotspots with high stress concentrations to understand the possible HISC failure locations in the component. The HISC assessment criteria, based on the allowable stress/strain in the material, as per the industry recommended practice DNVGL-RP-F112 are given in *Section 3* of this report.

### 3. HISC Assessment Criteria

For a long time, HISC has been an area with insufficient data to quantify failure probability as a function of parameters such as stress and strain until DNV came up with a recommended practice RP-F112 in 2008, based on the results from a joint industry project (JIP). This recommended practice provides guidance on how to avoid HISC in the design of subsea equipment made from duplex stainless steels, setting the criteria for stress and strain in the material. The values presented in the recommended practice are based on laboratory testing and reflect the material's resistance (DNVGL, 2019). DNVGL-RP-F112 provides two categories of HISC assessment for duplex stainless steels subjected to cathodic protection, namely category 1 and category 2 assessment criteria. While category 1 is a Semi analytical linear-elastic assessment, category 2 is a Nonlinear FEA-based assessment.

#### 3.1 Category 1: Semi analytical linear-elastic assessment

DNVGL-RP-F112 recommends semi-analytical analysis for components that have cross-sections with rotational symmetry and moderate transitions where global piping stress and/or analytical evaluations are applicable. These include components like global spools, elbows/bends, and transition pipes/ hubs including welds. Most of the pipe welds which are axisymmetric can be analyzed using the category 1 assessment. The components designed using the category 1 assessment shall fulfill the following design criteria (DNVGL, 2019):

$$\sigma_{mem} \leq 0.8 \cdot \gamma \cdot SMYS$$

$$(\sigma_{out.i} \cdot S_{mag.i} + \sigma_{therm}) \leq \alpha \cdot \beta \cdot \gamma \cdot (1.1 - 0.07 \cdot LSPF_{Cat1}) \cdot SMYS$$

Where,

$\alpha$ ,  $\beta$  and  $\gamma$  are the residual stress, transition angle and material factors respectively.  $\sigma_{mem}$  and  $\sigma_{out.i}$  are the membrane and outer fiber stresses in the principal direction  $i$ , respectively and  $\sigma_{therm}$  is the stress due to potential thermal gradient over the wall thickness.

$S_{mag}$  and  $LSPF_{Cat1}$  are stress magnification factor and local surface penalty factor respectively, which are defined elaborately in **section 3.1.1 and 3.1.2** respectively.

Stresses for this assessment are usually estimated from the global pipe stress analysis.  $S_{mag}$  can be calculated using analytical formulae for simple geometries and  $LSPF_{cat1}$  can be assumed as 3 conservatively. However, for a more accurate and less conservative assessment, it is required to estimate these stress concentration factors using FEA.

### 3.1.1 Smag (stress magnification factor)

The purpose of the stress magnification factor,  $S_{mag}$ , is to capture the increase in surface stress compared to the outer fiber stress,  $\sigma_{out}$ , because of the secondary bending moments created due to transitions or misalignments in the component. It should be noted that stress due to primary bending moments (actual applied bending loads) should not be confused for the additional stress due to secondary bending moments (caused by the geometry of the component). The stresses calculated using  $S_{mag}$  should not include the effect of local geometric features like notches or fillets (DNVGL, 2019).

Mathematically, it can be written as:

$$S_{mag} = \frac{\sigma_{lin}}{\sigma_{mem}}$$

Where,

$\sigma_{mem}$  = membrane stress - the average stress acting normal to the path from the outside to the inside of the component in the principal direction.

$\sigma_{lin}$  = linearized stress =  $\sigma_{mem} + \sigma_{bending}$  - the linearized stress (membrane and bending) at the hotspot across the thickness of the component in the principal direction.

### 3.1.2 LSPF<sub>cat1</sub> (Local surface penalty factor)

$LSPF_{cat1}$  (hereinafter referred to as simply “LSPF”) captures the additional stress due to local geometric features like fillets or weld toes which affect the stresses and strains locally at the hotspot region on the surface of the component. This will affect the allowable values on the stresses due to primary loads and secondary bending moments due to local geometric features like fillets, weld toes, notches, etc. (DNVGL, 2019). The idea is to calculate this factor using finite element analysis and to include the local stress level in the allowable stress criteria.

DNVGL-RP-F112 recommends that the SCF expressions found in DNVGL-RP-C203 shall not be used to estimate LSPF.

$$LSPF = \frac{\sigma_{max}}{\sigma_{lin}}$$

Where,

$\sigma_{max}$  = Total maximum principal surface stress at the hotpot caused due to local geometric features like notches and fillets.

$\sigma_{lin}$  = linearized stress =  $\sigma_{mem} + \sigma_{bending}$  - the linearized stress (membrane and bending) at the hotspot across the thickness of the component in the principal direction.

If it is not required to do FEM for low utilized components, an LSPF value of 3 can be used conservatively without further calculation for fillets with radius,  $r$ , equal to or greater than 10% of the wall thickness, for local notches in machined transitions with a radius larger than 1mm and for weld toes (DNVGL, 2019). Local features like notches that reduce the wall thickness should always be analyzed using the category 2 assessment (DNVGL, 2019).

### **3.2 Category 2: Solid FEA based non-linear assessment**

The Category 2 Non-linear assessment is recommended in DNVGL-RP-F112 for complex geometries with complex loadings, for which analytical calculations and/or global piping stress results are not applicable, or category 1 acceptance criteria are not fulfilled. These include components like connectors, valve bodies, outboard and inboard hubs, complex shaped HIP/ forged components, etc. The components designed using the category 2 assessment shall fulfill the following design criteria (DNVGL, 2019):

$$\varepsilon_{mem} \leq 0.3\%$$

$$\varepsilon_{peak} \leq \varepsilon_c$$

Where,

$\varepsilon_{mem}$  is the average strain normal to wall thickness.

$\varepsilon_{peak}$  is the maximum principal surface strain.

$\varepsilon_c$  is the maximum allowable surface strain which is determined as per **Table 1**.

**Table 1** Non-linear strain criterion

	$\epsilon_c$ (%)	
	Outside $L_{res}$ and no cold forming	Inside $L_{res}$ or cold formed material
Fine austenite spacing	$0.5 \cdot LSMF_{cat2}$	$0.45 \cdot LSMF_{cat2}$
Coarse austenite spacing	$0.35 \cdot LSMF_{cat2}$	$0.30 \cdot LSMF_{cat2}$

Here,  $L_{res}$  is the length of zone assumed to be influenced by weld residual stresses and  $LSMF_{cat2}$  is the local surface magnification factor for category 2 assessment (hereinafter referred to as simply “LSMF”), which is defined elaborately in *section 3.2.1*.

The recommended practice suggests that either a linear or non-linear FEA may be used to calculate LSMF. However, it is not appropriate to linearize stresses from an elastic-plastic analysis if yielding has occurred though it is conservative. Linear elastic analysis can be used to calculate LSMF like LSPF calculation. In fact, LSPF and LSMF are mathematically the same, except that LSPF reduces the allowable stress in category 1 assessment hence termed penalty factor and LSMF increases the allowable strain in category 2 assessment hence termed magnification factor.

### 3.2.1 $LSMF_{cat2}$ (Local surface magnification factor)

Calculation of LSMF is like LSPF except that it is used in category 2 assessment and as the name suggests, it increases (magnifies) allowable strain value for the assessment, unlike the penalty factor for category 1 assessment.

$$LSMF = \frac{\sigma_{max}}{\sigma_{lin}}$$

or can be approximated using the applicable analytical formula based on nominal stresses using the following equation:

$$LSMF = \frac{SCF_{analytical}}{2}$$

Where,  $SCF_{analytical}$  = the value of the stress concentration factor extracted from the analytical formula.

It is always acceptable to perform a category 2 assessment assuming  $LSMF_{cat2} = 1$  (DNVGL, 2019).

### 3.3 Stress linearization

In order to estimate stress magnification and the local surface factors, it is required to calculate the linearized stress through the wall thickness of the component (DNVGL, 2019). Though DNVGL-RP-F112 talks about linearized stress, the exact procedure to linearize the stress into the membrane, bending, and peak stress is not discussed in the recommended practice.

ASME Boiler & Pressure Vessel Code (BPVC) Section VIII Div. 2 gives specific guidance about the linearization of stress results for stress classification in pressure vessels. So, the guidance/ recommendations given in ANNEX 5-A of Section VIII Div. 2 about post-processing of the elastic finite element stress analysis results for stress linearization are used for this thesis study.

#### 3.3.1 Selection of stress linearization path (or) stress classification line

In order to linearize the stress, the path through the thickness of the analyzed component should be chosen carefully. The path should start at the peak/ maximum stress location in the area of interest. This typically starts at the stress raisers like weld toes, inside weld root, and end of transitions.

The orientation of the stress linearization path or stress classification line (SCL) should be normal to the direction of the maximum principal stress (DNV, 2008; ASME, 2019). In some complex geometries, this may be difficult to implement, and similar accuracy can be obtained by orienting the SCL approximately normal to the mid-surface of the cross-section of the component as shown in *Figure 6* (a) (ASME, 2019).

The distribution of hoop, meridional (longitudinal) stress components and through-thickness stress on the SCL should be monotonically increasing or decreasing, excluding the effects of stress concentrations as shown in *Figure 6* (b) (c) (ASME, 2019). The distribution of shear stress should be either parabolic as shown in *Figure 6* (d) or low relative to the hoop and longitudinal stresses (ASME, 2019).

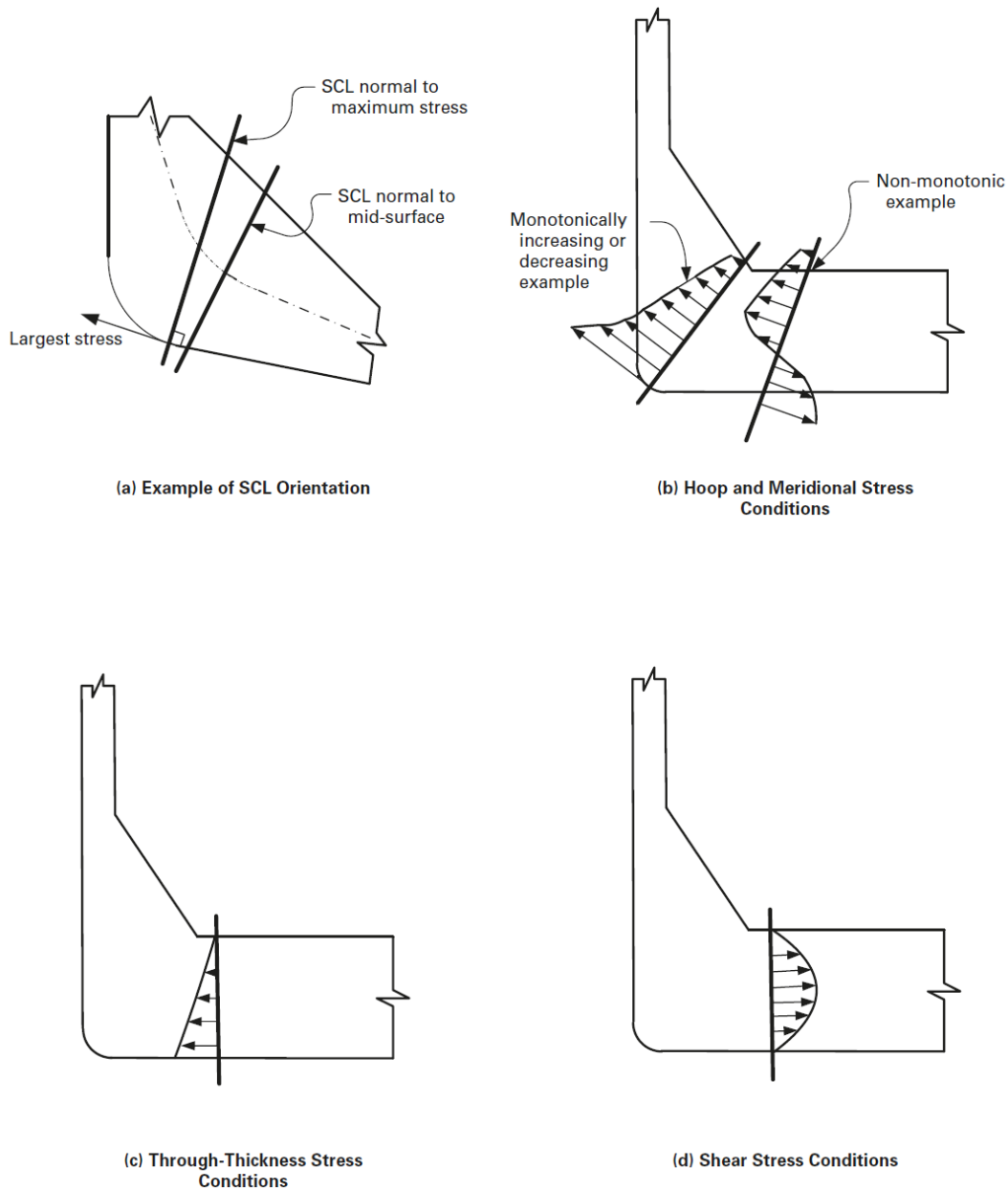


**Figure 6** Stress Classification Line Orientation and Validity Guidelines (From ASME, 2019)

### 3.3.2 Stress linearization using the stress integration method

Though ANNEX 5-A (ASME, 2019) provides three different approaches for stress linearization, the stress integration method is recommended to linearize the stress results derived from a finite element analysis utilizing two-dimensional or three-dimensional continuum elements. The components of stress can be integrated along the linearization path across the wall thickness to estimate the membrane and bending stress components. The peak stress component can be calculated by subtracting the linearized stress distribution (membrane plus bending) from the total stress distribution (ASME, 2019).



## Membrane stress

Membrane stress is the average stress acting normal to the path from the outside to the inside of the component in the principal direction. The membrane stress tensor comprised of the average of each stress component along the stress classification line is calculated as:

$$\sigma_{mem} = \frac{1}{t} \int_0^t \sigma_{ij} dx$$

Where,  $t$  is the thickness of the component along the linearization path and  $\sigma_{ij}$  is the total stress component  $i$  at point  $j$  along the path.

## Bending stress

Bending stress is the linearly varying stress across the thickness, which is the difference in stresses from inside to outside surface of the component. The bending stress tensor is comprised of the linear varying portion of each stress component along the stress classification line and is calculated as:

$$\sigma_{bending} = \frac{6}{t^2} \int_0^t \sigma_{ij} \left( \frac{t}{2} - x \right) dx$$

Here,  $t$  is the thickness of the component along the linearization path and  $\sigma_{ij}$  is the total stress component  $i$  at point  $j$  along the path.

### 3.3.3 Stress linearization example from FEA

Linearization of the stress from FEM involves the calculation of membrane and bending stresses from the total stress data available at the finite number of points along the linearization path. Note that for the HISC assessment, only maximum principal stress shall be used for linearization, not the Von Mises equivalent stress (DNVGL, 2019).

The stress linearization path shall be chosen to start from the node at the peak stress location (either external or internal surface of the model) and normal to the maximum principal direction of the peak/ maximum stress as shown in **Figure 7**, where the path is normal to the principal direction indicated by red arrows. The linearization path is also approximately normal to the mid-surface of the cross-section.

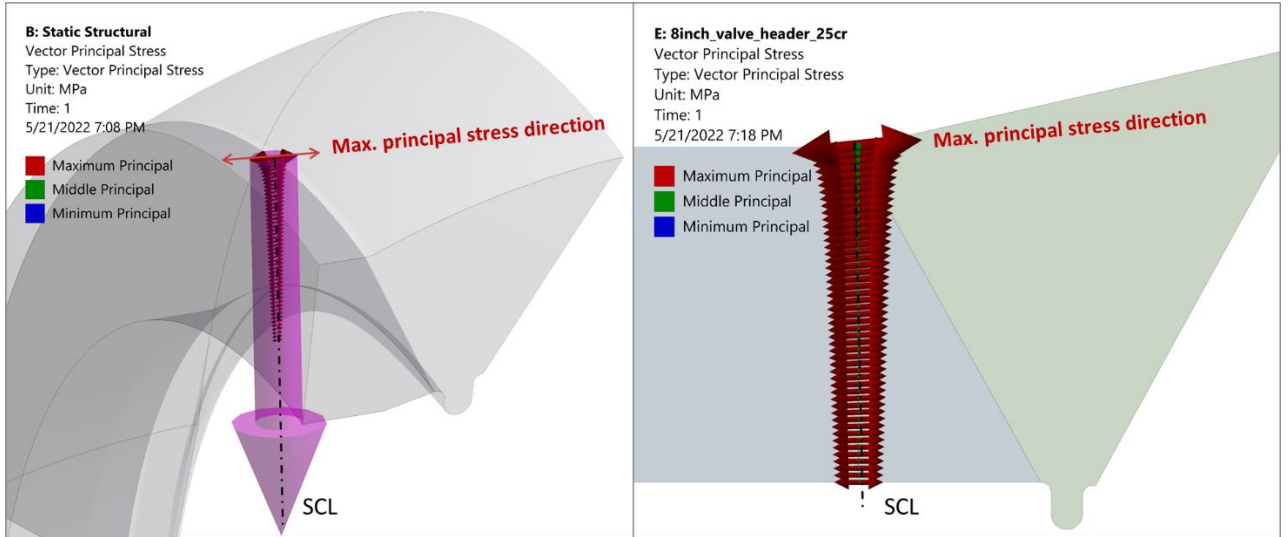


**Figure 7** Principal stress direction along the stress classification line

ANSYS (*ANSYS Mechanical, Finite Element Analysis Software for Structural Engineering*, 2021) can do stress linearization automatically without the need for manual calculations.

However, for this study manual calculation is done for an example case to make sure that the ANSYS results are in line with the guidance given in ASME BPVC Section VIII Div. 2.

By default, ANSYS generates total stress values for 49 points along the linearization path and the same are used in this calculation. The membrane stress along the path is calculated as:

$$\sigma_{memi} = \frac{1}{48} \left[ \frac{\sigma_{i1}}{2} + \frac{\sigma_{i49}}{2} + \sum_{j=2}^{48} \sigma_{ij} \right]$$

Where,  $\sigma_{ij}$  is total stress component  $i$  at point  $j$  along path.

The bending stress at the hot spot (peak stress location) is calculated as:

$$\sigma_{bending} = \frac{6}{t^2} \int_0^t \sigma_{ij} \left( \frac{t}{2} - x \right) dx$$

The integral part in the above equation for a finite number of points can be approximated using the alternative extended Simpson's rule (Press et al., 1989) which is,

$$\int_a^b f(x) dx \approx \frac{h}{48} \left[ 17f(x_0) + 59f(x_1) + 43f(x_2) + 49f(x_3) + 48 \sum_{i=4}^{n-4} f(x_i) + 49f(x_{n-3}) + 43f(x_{n-2}) + 59f(x_{n-1}) + 17f(x_n) \right]$$

The FEA data and corresponding calculations for linearization are shown in **Appendix F** of this report. The plot for calculated linearized stress for the example case is shown in **Figure 8** whose values are in-line with the ANSYS generated plot shown in **Figure 9**. From this, we can infer that ANSYS results are in line with the guidance given in ASME BPVC Section VIII Div. 2 and shall be used directly to estimate linearized stress for the weld models analyzed in this thesis study.

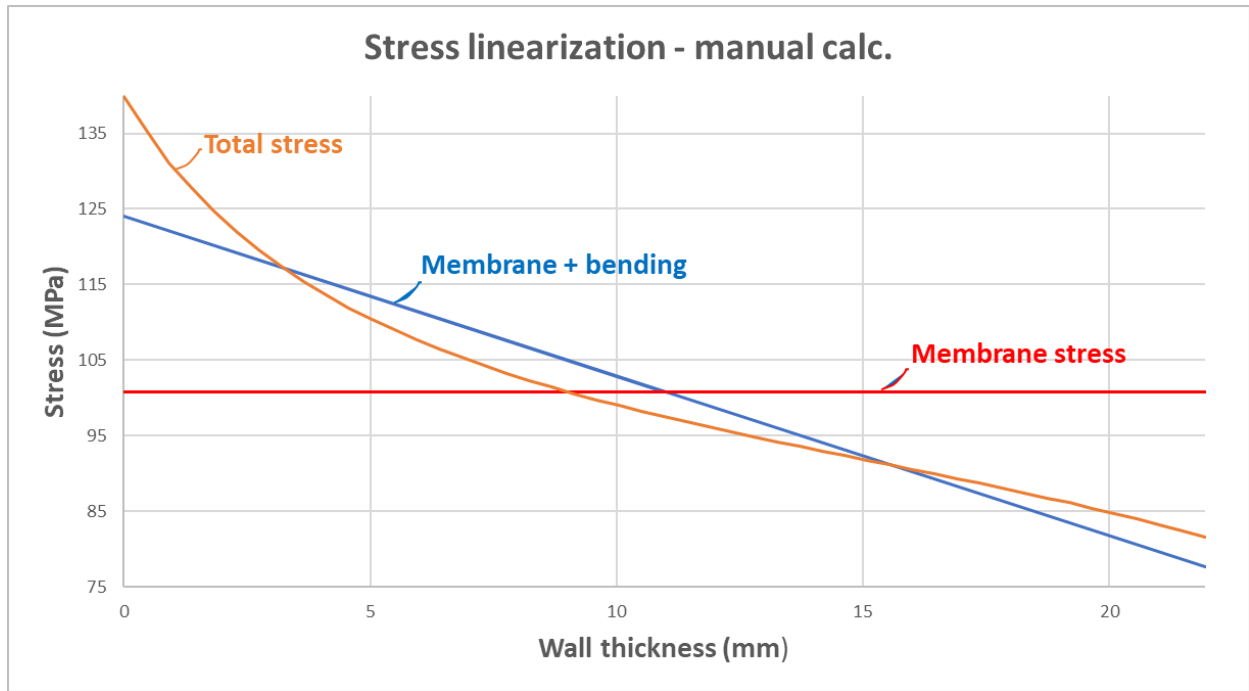


**Figure 8** Stress linearization example - plot from the manual calculations

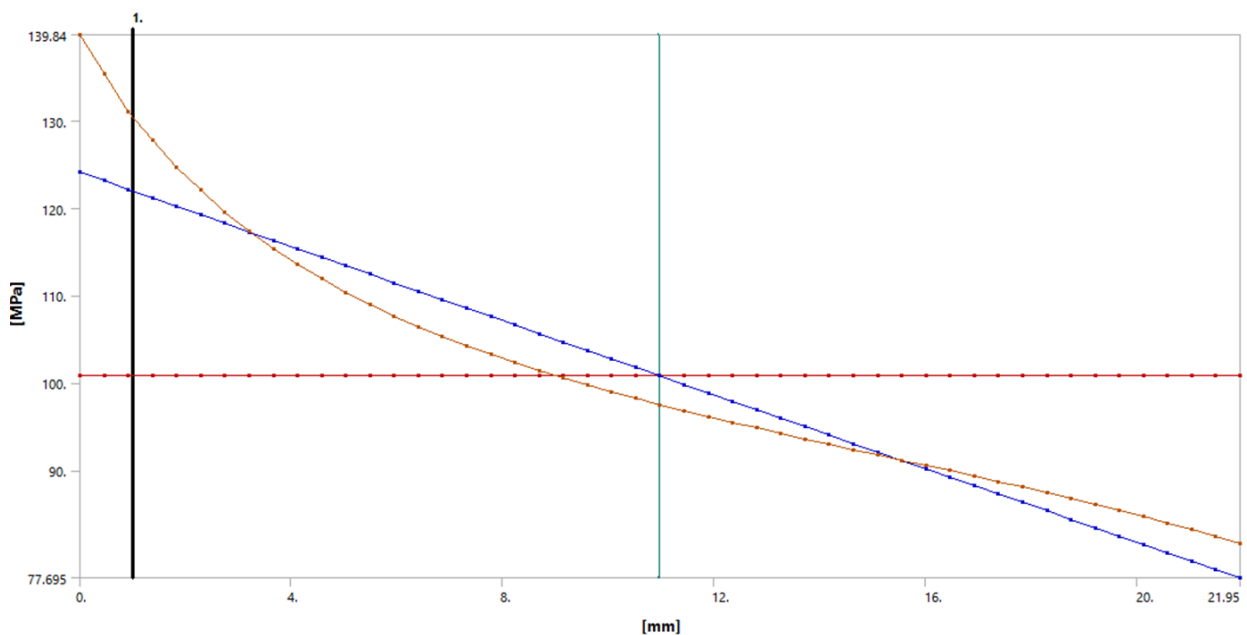


**Figure 9** Stress linearization example - plot from ANSYS

## 4. FEA Modeling

### 4.1 Analysis models

All the welds with centerline misalignment between the pipes/components are modeled in 3D as the weld geometry is not axisymmetric and changes its dimensions along the circumference. Initially, both the components with weld preparation are modeled in 3D with a misalignment between their centers. Then, multiple drafts of the weld cross-section are created along the circumference of the weld and swept through the smooth splines to create a solid that approximately represents the weld between the components having centerline misalignment. An example of such a model created in SpaceClaim (*Ansys SpaceClaim - 3D CAD Modeling Software*, 2021) is shown in **Figure 10** below.

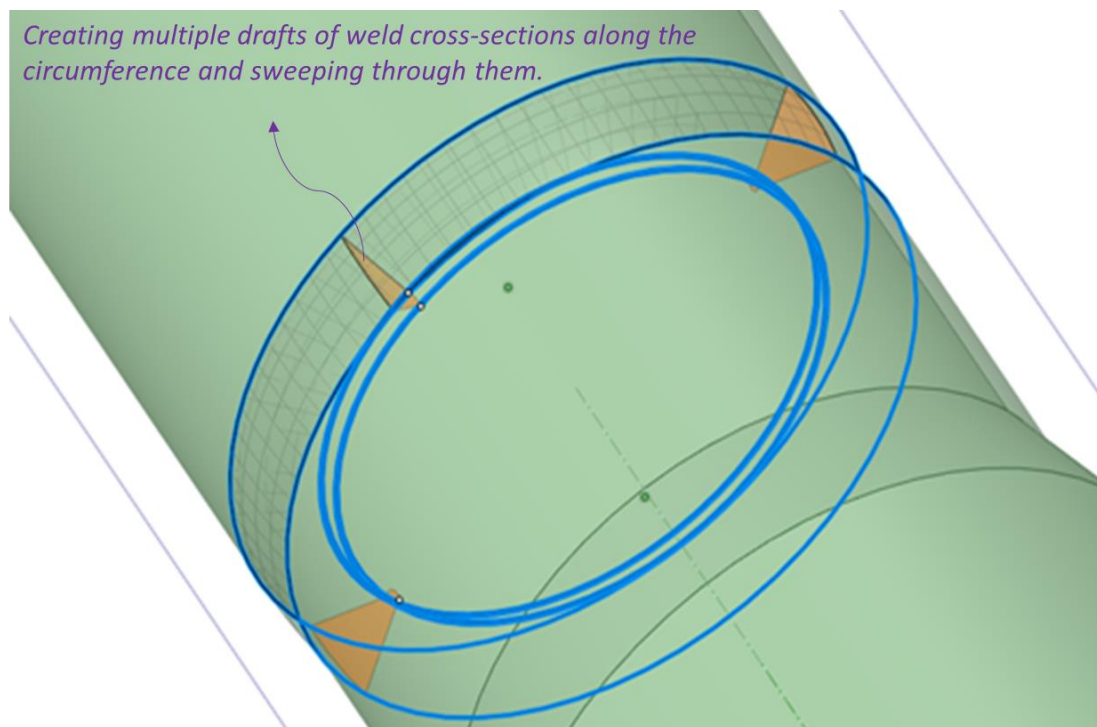


**Figure 10** Modeling the weld centerline misalignment in 3D

This centerline misalignment is considered as 1mm for the 6-inch winghub welds as a TechnipFMC design requirement for fatigue. No centerline misalignment was considered for the fillet weld between the 6-inch pipe and doubler plate. For all other welds, this misalignment is considered a maximum of 1.6 mm as a TechnipFMC requirement for fabrication. The models without centerline misalignment are modeled in 2D for an axisymmetric analysis reducing the number of elements and saving the computational time significantly.

All the weld geometries analyzed in this study are modeled including all the critical geometric details like weld preparation, flank angle, toe fillet radius, root fillet radius, transitions and component dimensions including relevant tolerance combinations. The weld cross-section details of one of the analysis models (weld between header and valve) is shown in **Figure 11** below for reference.

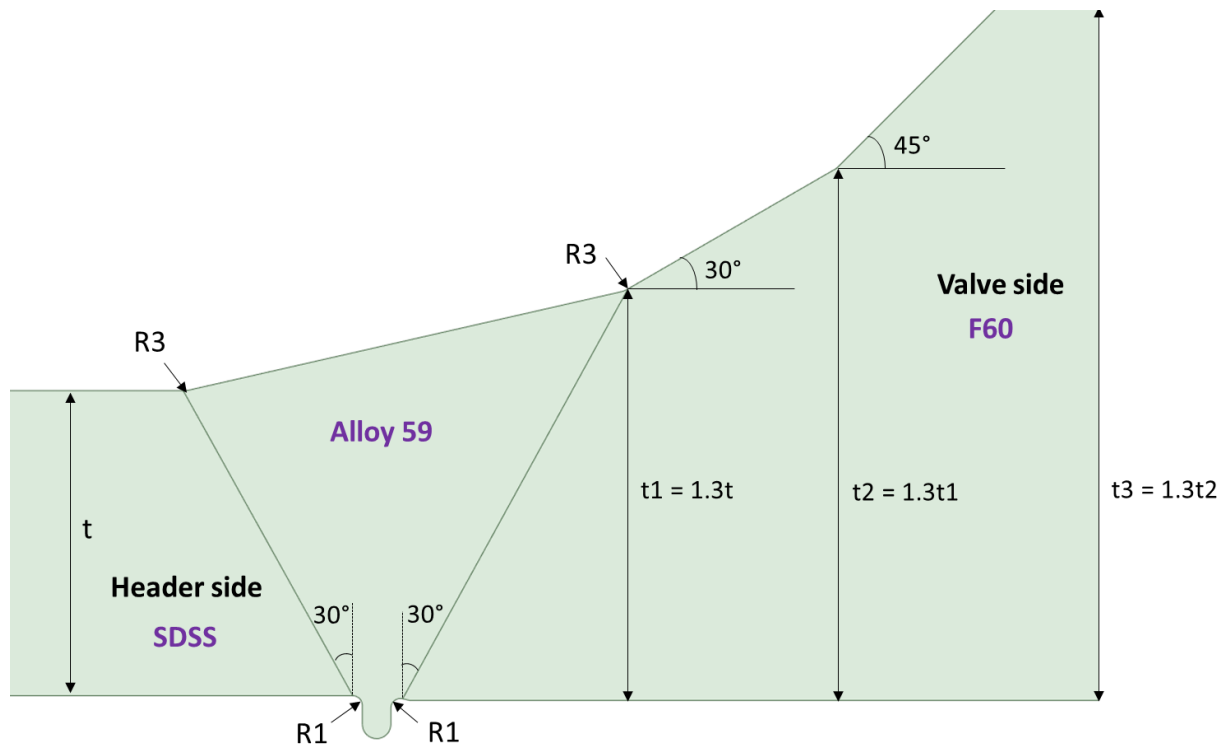


**Figure 11** Example - weld cross-section details of an analysis model

## 4.2 Analysis loads and boundary conditions

For HISC assessment, DNVGL-RP-F112 recommends using the operational and installation loads as well as the deformation loads, such as thermal and residual stresses. However, using them for this study is not required as the area of interest is only the calculation of SCF, which is load independent. For this study, all the analysis models are loaded with a simple tensile force at one end and is rigidly fixed at the other end as shown in **Figure 12** below. No other external loads (like pressure, temperature, or bending moments) are applied except for one case where the model is checked for actual loads from the project.



**Figure 12** Example - Analysis model boundary conditions for a 2D axisymmetric model

In the cases where the HISC assessment needs to be checked for the actual loads from the project, it is required to construct the model in 3D. In this thesis study, for the fillet weld between the doubler plate and the pipe, the actual loads are not axisymmetric. However, some information was available regarding the longitudinal stress (calculated as per ASME B31.8) from the pipe stress analysis. So, a 2D axisymmetric analysis is done with a simple tensile load equivalent to the longitudinal stress from the piping analysis, to calculate the corresponding peak stress/ strain.

### 4.3 Material properties

The linear elastic analysis is used for the calculation of stress concentration factors of all the models presented in this report. The material properties used for the linear FEA are given in **Table 2** below.

**Table 2** Linear elastic material properties

Material	Modulus of Elasticity (GPa)	Poisson's ratio
22 Cr Duplex	190	0.3
25 Cr Duplex	190	0.3
F60	200	0.3
F65	207	0.3
Alloy 59	205	0.3

For the steady state thermal analysis of the weld between the doubler plate and pipe presented in **Section 5.3**, the following material properties are used.

**Table 3** Thermal conductivity of materials

Thermal conductivity of Duplex steel	16 W/mK
Thermal conductivity of epoxy paint	0.35 W/mK

For the non-linear analysis of weld between doubler plate and pipe, multilinear material isotropic hardening curves are generated for 22 Cr duplex and 25 Cr duplex (UNS S32760) at various temperatures between 4°C and 85 °C according to ASME VIII (ASME, 2019) and are shown in **Figure 13** and **Figure 14** respectively.

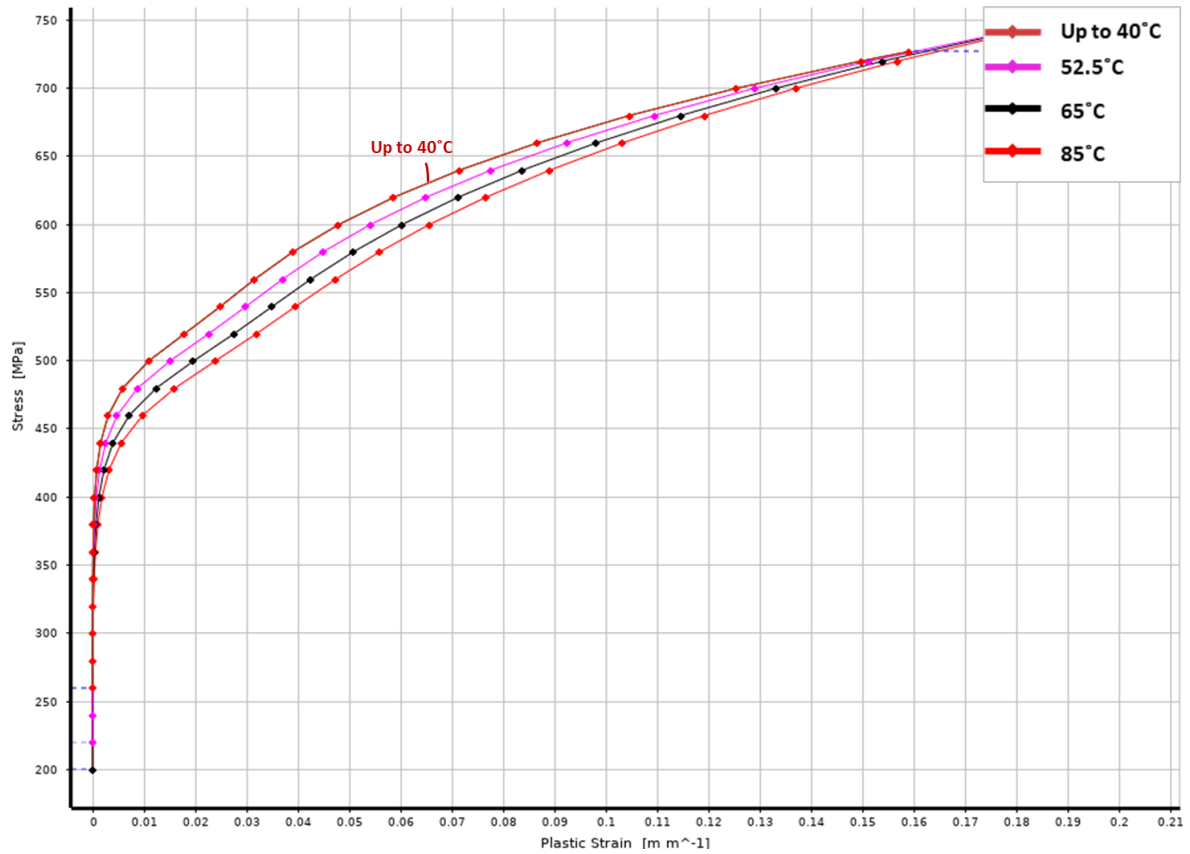


**Figure 13** Multilinear material isotropic hardening curves generated for 22 Cr duplex steel

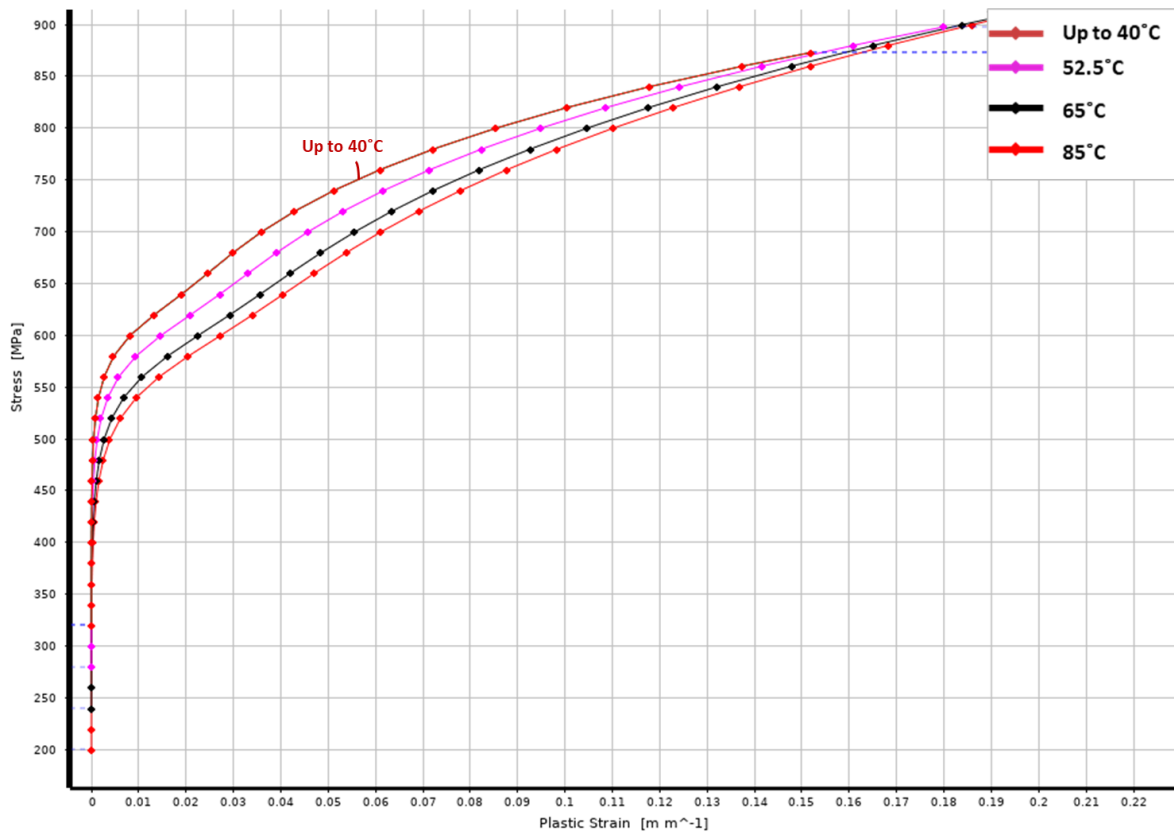


**Figure 14** Multilinear material isotropic hardening curves generated for 25Cr duplex steel

## 4.4 Meshing element types

The element types that are used for these analyses mostly are hexahedral for 3D and quadrilateral for 2D assessments. Triangular and tetrahedral elements are avoided as much as possible, especially in the critical locations of interest, because they are comparatively stiffer and don't capture bending accurately unless the mesh is very refined (Skotny, 2019). Second-order elements are used at the critical locations of the model near the weld (especially around the weld toe and weld root) to capture the accurate geometric representation and more realistic deformation.

In the areas of less interest, linear elements are used if there is a significant reduction in the total node count and analysis run time provided the mesh quality, quality, model stiffness, and accuracy in the geometric representation are taken care of. Element types used in most of the models analyzed in this study are presented in **Table 4**. Irrespective of the type of the elements, order, and size, the mesh should always be checked for convergence as per the mesh convergence criteria defined in DNVGL-RP-F112.

**Table 4** Meshing - Element type details

Model	Mesh area	Element type	ANSYS Terminology
3D	Critical areas	3D 20-node solid (Second order)	SOLID186
	Rest of the model	3D 8-node solid (First order)	SOLID185
2D	Entire model	2D 8-node plane (Second order)	PLANE 183

## 4.5 Mesh convergence

The results of a finite element analysis cannot be considered reliable if they are not checked for mesh convergence. Generally, the change in mesh size impacts the results of an FEA model and it is important to refine the mesh to the extent that any further refinement of the mesh will not significantly affect the system response and the results converge to a solution.

### 4.5.1 Mesh convergence for linear analysis

An example of a mesh convergence study for a linear analysis of a weld toe is shown in **Figure 15**. In this case, analysis is done on the weld toe of a butt weld for four different mesh sizes. Starting with a coarse mesh, halving of the local element size is applied three times until the finest mesh is reached.



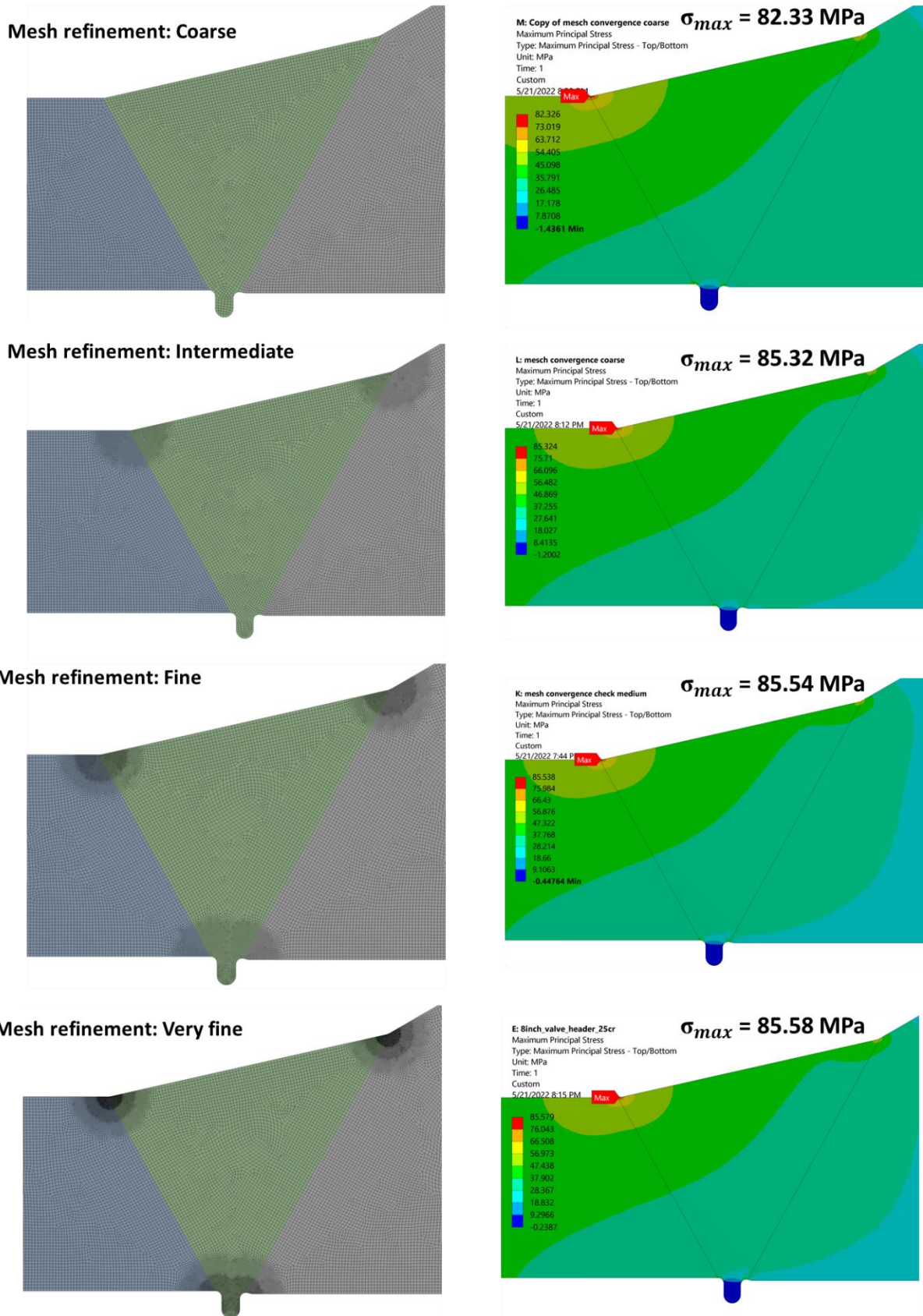


**Figure 15** Linear elastic mesh convergence study- levels of mesh refinement and corresponding total maximum principal stress at the weld toe

The maximum principal stress at the weld toe is calculated for the four mesh sizes and then a graph is plotted for the peak stress against the three mesh sizes. According to the mesh convergence criteria defined in DNVGL-RP-F112, for linear analysis, the convergence error should be less than 3%. Here, the convergence error on peak stress from coarse to intermediate mesh is 3.6 % and from intermediate to fine mesh is 0.25% as shown in the **Figure 16**. As the mesh is already converged at the fine mesh, the results from any further refinement of the mesh are valid as per the mesh convergence criteria. Similarly, convergence for membrane stress is also checked.

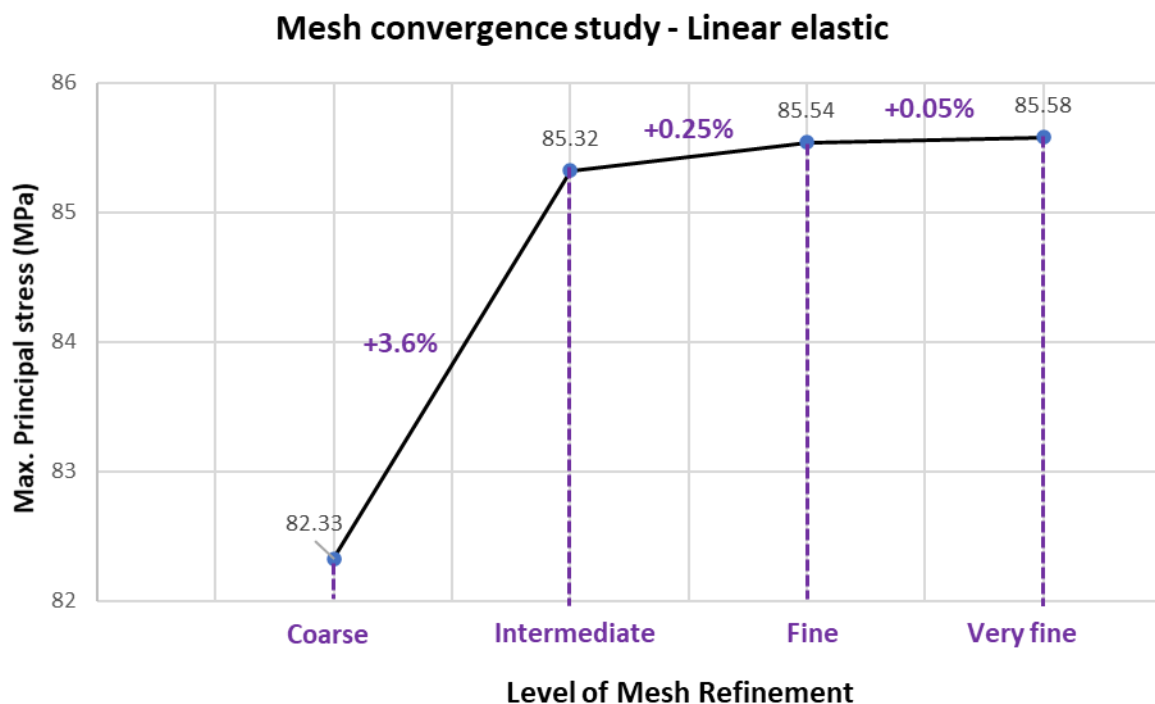


**Figure 16** Linear elastic mesh convergence study- convergence criteria

#### 4.5.2 Mesh convergence for non-linear analysis

An example of a mesh convergence study for a non-linear analysis on a weld toe is shown in **Figure 17**. In this case, analysis is done on the weld toe of a fillet weld for three different mesh sizes. Starting with a coarse mesh, halving of the local element size is applied to reach intermediate mesh refinement and then the finest mesh is reached by further halving the element size locally. The total maximum principal strain (peak strain) at the weld toe is calculated for the three mesh sizes and then a graph is plotted for the peak strain against the three mesh sizes as shown in **Figure 18**.

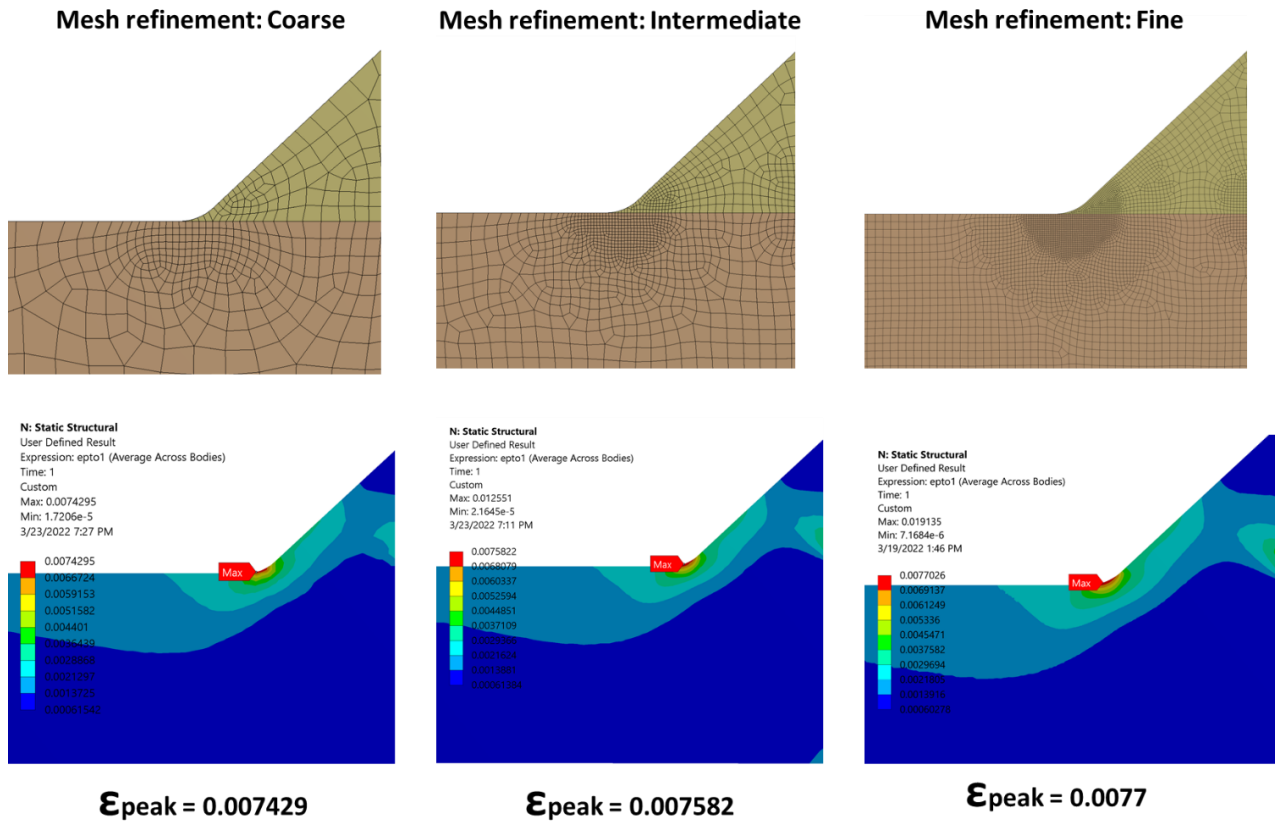


**Figure 17** Non-linear analysis mesh convergence study- levels of mesh refinement and corresponding total maximum principal strain at the weld toe

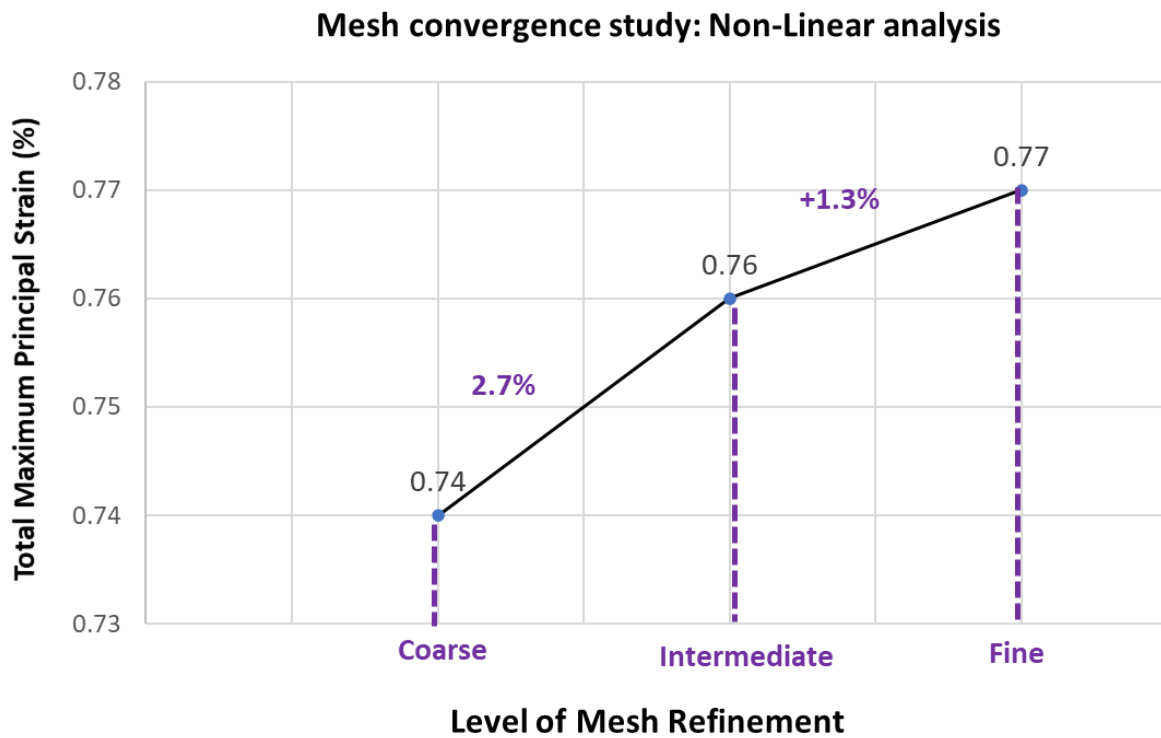


**Figure 18** Non-linear analysis mesh convergence study- convergence criteria

According to the mesh convergence criteria defined in DNVGL-RP-F112, for non-linear analysis, the convergence error should be less than 5%. Here, the convergence error on total strain from coarse to intermediate mesh is 2.1% and from intermediate to fine mesh is 1.5% as shown in **Figure 18**. As the mesh is already converged at the intermediate mesh, the results of both intermediate and fine mesh are valid as per the mesh convergence criteria. Similarly, convergence for membrane strain is also checked.

The mesh convergence check can be extended only to the same location of similar models with similar loading. While extending the mesh convergence, especially in non-linear analyses, care should be taken that the results are on the same stress/ strain gradient. If there's a significant increase in the magnitude of loading, it will increase the stress/strain gradient, resulting in less accuracy to the fixed allowable stress/strain (DNVGL, 2019).

In this thesis study, six different types of welds, as shown in **Table 5**, are analyzed using FEM. Here, the welds with the components having the same nominal thickness are termed equal welds and the ones with different nominal thickness are termed unequal welds. The analysis details and results for these welds are given in **Section 5**.

**Table 5** Types of welds analyzed

S.no	Type of weld	No. of FE models
1	Equal weld between 6-inch pipe and winghub	2
2	Unequal weld between 6-inch pipe and winghub	2
3	Fillet weld between doubler plate and pipe	1
4	Equal welds between HIP headers and hubs	8
5	Unequal welds between HIP headers and hubs	8
6	Welds between HIP headers and Valves	8

## 5. Finite Element Analysis and Results

### 5.1 Equal weld between 6-inch pipe and winghub

#### 5.1.1 Analysis model dimensions

The analysis model dimensions for the equal weld between the 6-inch pipe and the winghub are shown in **Figure 19**. The model includes the hub transition (1:4) from a larger OD to the same OD (nominal) as the pipe. The nominal dimensions of both the hub and pipe sides are equal. However, for the analysis, the difference between nominal and max/min tolerance can be used (DNVGL, 2019). Nominal dimensions on the hub and max/min dimensions on the pipe are used here to be on the conservative side.

#### Analysis Model Dimensions

Tolerance combination considered:

##### Hub Side

OD = 168.3 (Nominal OD)

ID = 124.5 (Nominal ID)

Reference: Drawings from TechnipFMC

##### Pipe Side

OD = 168.3 + 1.6 = 169.9 mm (maximum OD)

thickness (t) = 21.95 – 12.5%(t) = 19.2 mm  
(minimum thickness)

ID = 131.5 mm

Reference: ASTM A999/A999M

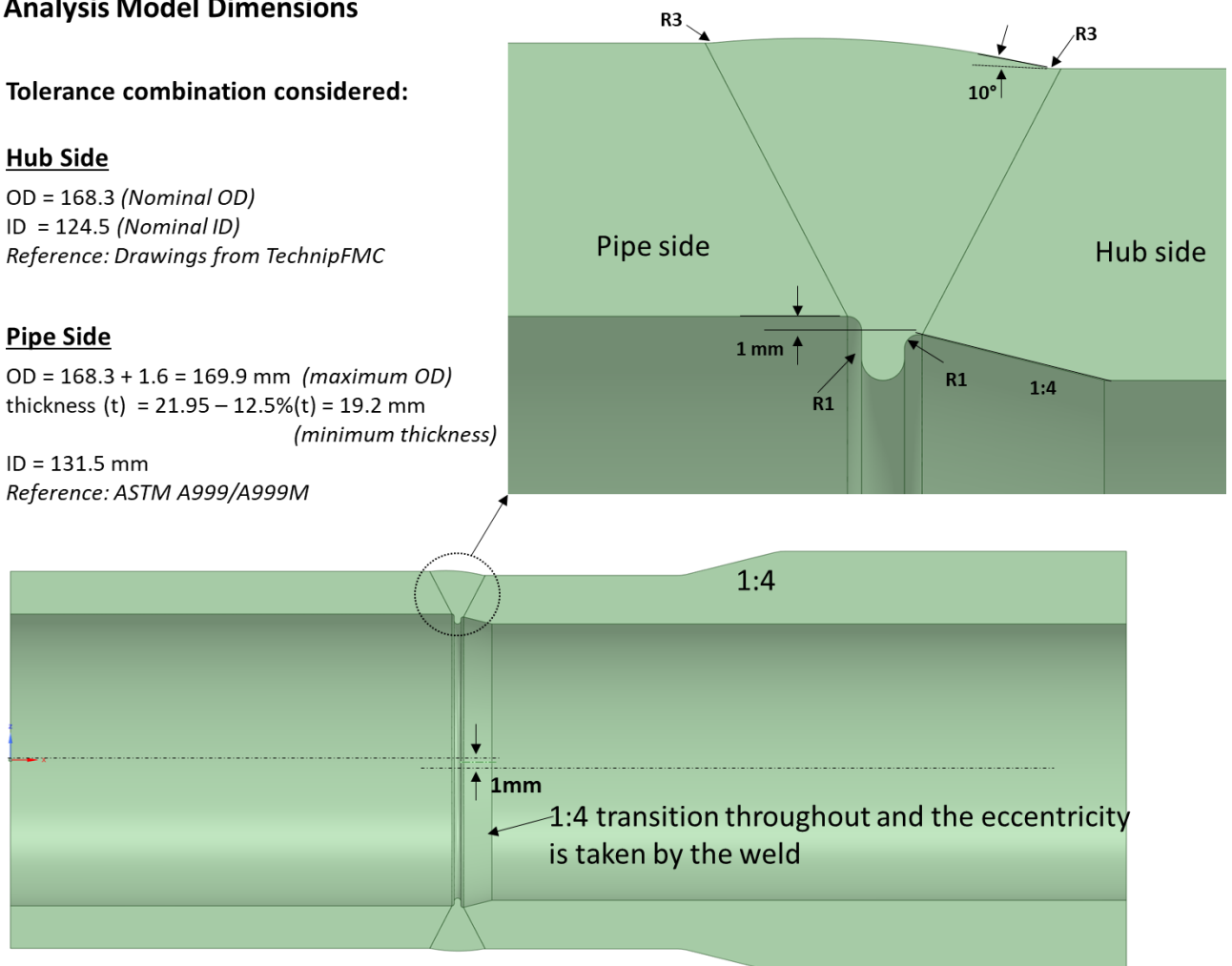


**Figure 19** Analysis model dimensions - equal weld between 6" pipe and winghub

The hub and pipe ID are matched with a 1:4 transition. A centerline misalignment of 1 mm is modeled in 3D between the hub and the pipe. This centerline misalignment is expected to induce secondary bending moments in the model and increase the stress concentration significantly. A flank angle of 10° is considered for the weld cap and the toe radius is 3mm. However, the analysis is also done for a model with a flat transition without a convex-shaped weld cap. The radial root protrusion of 4.5 mm (maximum), with the axial length of the protrusion as 3mm and the root fillet radius of 1mm are assumed for the analysis based on the weld specification requirements from TechnipFMC.

### 5.1.2 Analysis model mesh details

The analysis model is meshed using higher-order 3D 20-node solid elements (SOLID186 in Ansys) in the weld area and linear 3D 8-node solid elements (SOLID185 in Ansys) in the remaining locations, which are not of primary interest for the SCF study. In the critical areas like the weld toe and root, the mesh is finely refined in both directions, as shown in the *Figure 20*. The model is checked for the mesh convergence criteria and the meshing presented here is the most refined mesh after convergence.

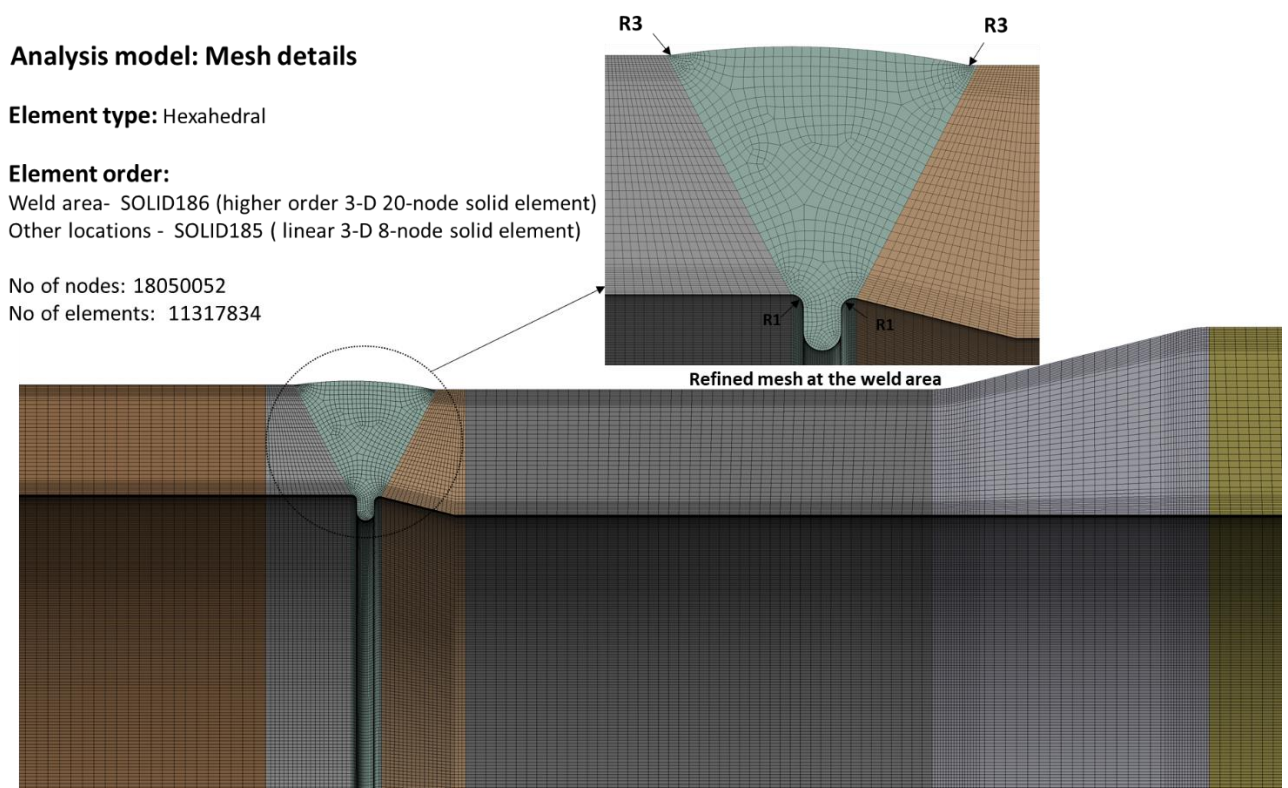


**Figure 20** Analysis model mesh details - equal weld between 6” pipe and winghub

### 5.1.3 Boundary conditions

As the analysis aims to just calculate the stress concentration factors, for simplicity, the analysis model is loaded with a simple tensile force at one end (pipe side) and is rigidly fixed at the other end (hub side). No other external loads (like pressure, temperature, or bending moments) are applied. **Figure 21** shows the boundary conditions applied to the analysis model.

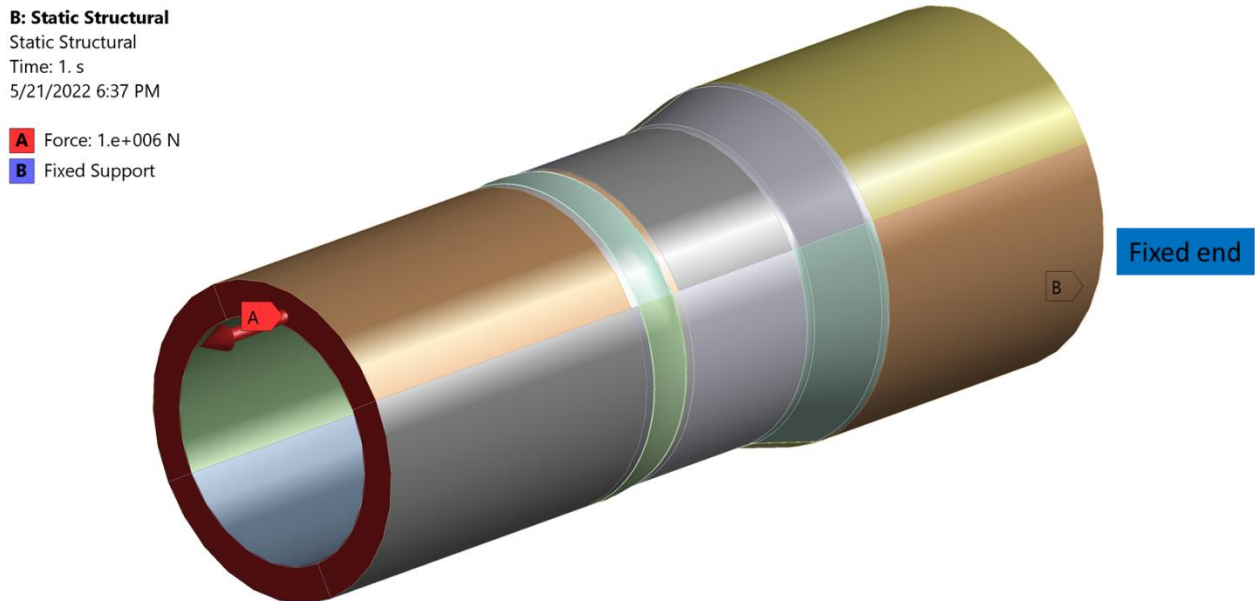


**Figure 21** Analysis model boundary conditions - equal weld between 6” pipe and winghub

### 5.1.4 Analysis results

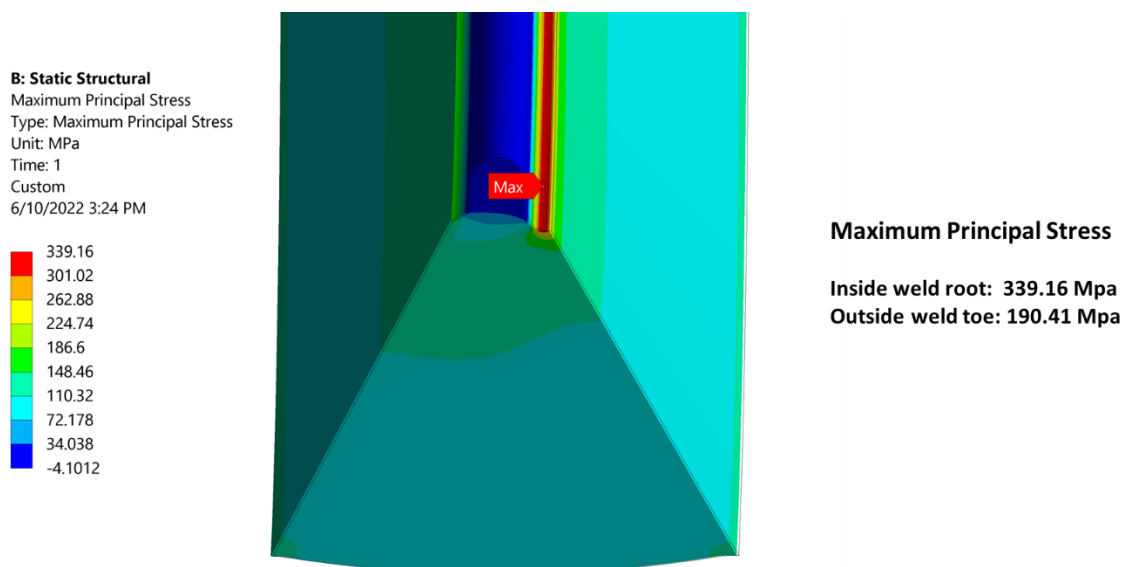


**Figure 22** Maximum principal stress plot - equal weld between 6” pipe and winghub

The analysis results show that the stress at the root of the weld is much higher compared to the outside weld toe. This is because of the large tolerances on the ID of the pipe side and the center-line misalignment between the pipe and hub. The maximum principal stress plot for the weld is shown in **Figure 22**. The stress is linearized along the stress classification path from the peak stress point on the weld root to the external surface of the weld, and the factors LSPF and  $S_{mag}$  are calculated for the hotspot at the weld root, as shown in **Figure 23**.

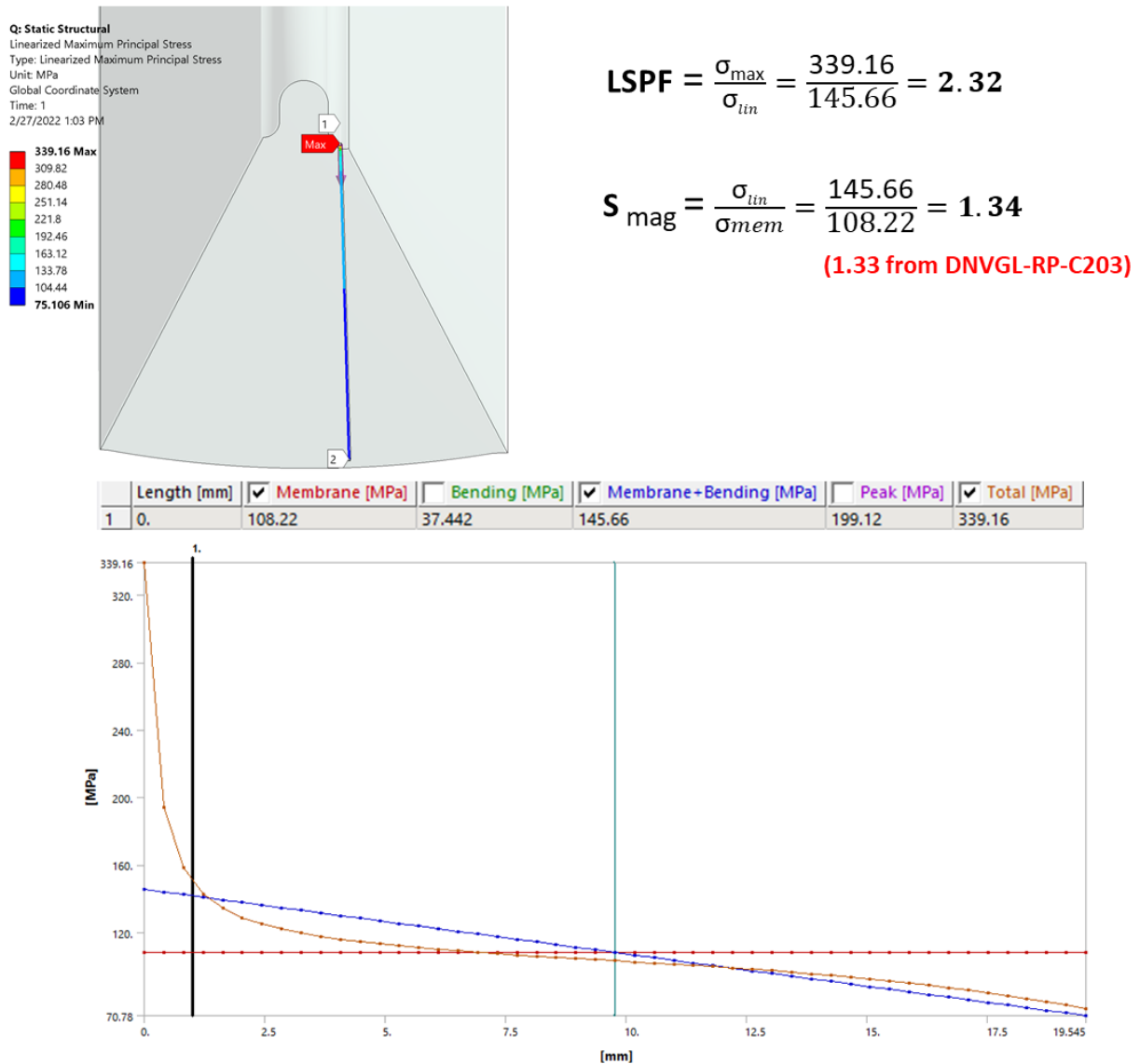
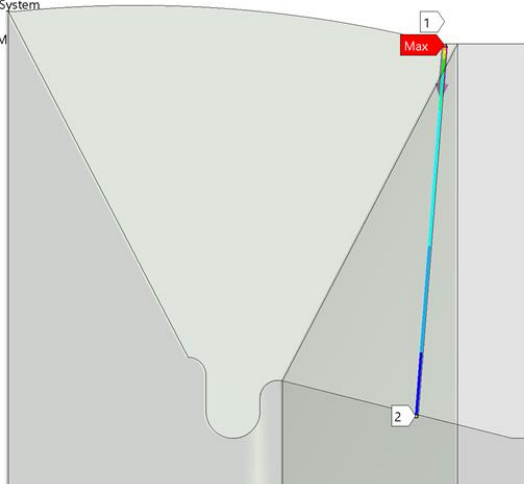
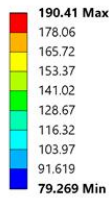


**Figure 23** Calculation of LSPF and  $S_{mag}$  using linearization of stress – weld root of the equal weld between 6” pipe and winghub

Similarly, LSPF and  $S_{mag}$  for the weld toe are calculated by linearizing the stress along the path from the peak stress point on the weld toe to the internal surface of the pipe, as shown in **Figure 24**. The  $S_{mag}$  values from FEM are compared with the values calculated using the formulae from DNVGL-RP-C203, and they are in line with the analytical calculations.



Q: Static Structural  
 Linearized Maximum Principal Stress 2  
 Type: Linearized Maximum Principal Stress  
 Unit: MPa  
 Global Coordinate System  
 Time: 1  
 2/27/2022 12:57 PM



$$LSPF = \frac{\sigma_{max}}{\sigma_{lin}} = \frac{190.41}{131.84} = 1.44$$

$$S_{mag} = \frac{\sigma_{lin}}{\sigma_{mem}} = \frac{131.84}{105.81} = 1.24$$

(1.23 from DNVGL-RP-C203)

Length [mm]	<input checked="" type="checkbox"/> Membrane [MPa]	<input type="checkbox"/> Bending [MPa]	<input checked="" type="checkbox"/> Membrane+Bending [MPa]	<input type="checkbox"/> Peak [MPa]	<input checked="" type="checkbox"/> Total [MPa]
1 0.	105.81	26.924	131.84	58.865	190.41

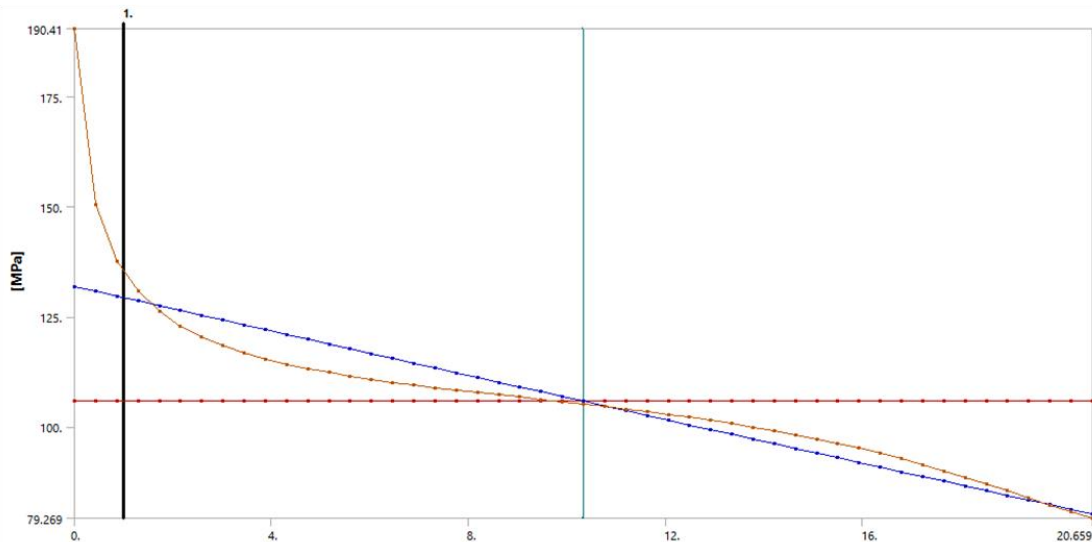


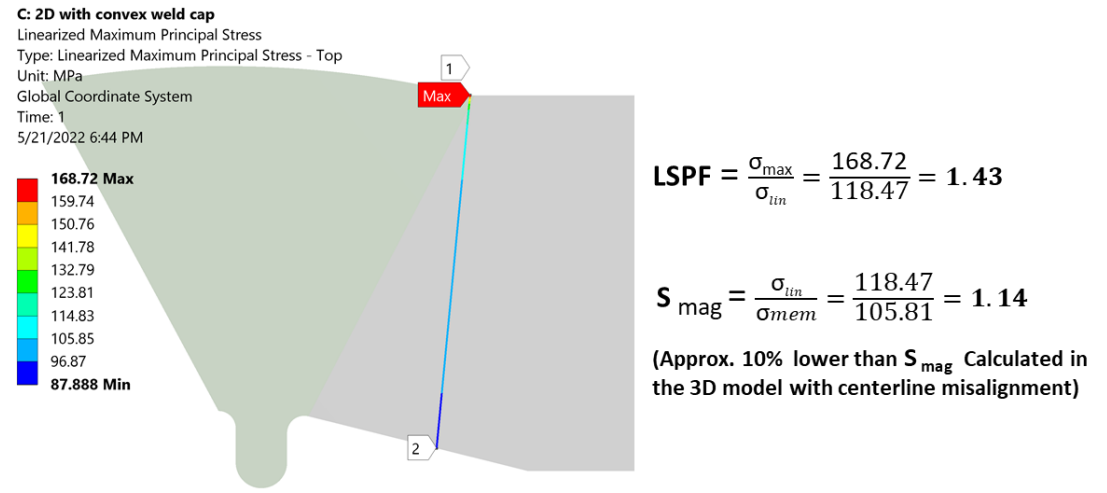
**Figure 24** Calculation of LSPF and  $S_{mag}$  using linearization of stress – weld toe of the equal weld between 6” pipe and winghub

### 5.1.5 Analysis results with flat transition on the weld

To calculate the stress concentration factors at the weld toe when there is no convex weld cap (zero flank angle/ flat transition), a 2D axisymmetric analysis is done to save the analysis time. The effect of centerline misalignment cannot be captured using an axisymmetric model, which is significant for calculating the  $S_{mag}$ . To include this effect, a comparison is made by recreating 3D the model of the previous section in 2D and the difference in the  $S_{mag}$  captured.

The results from this assessment, as given in **Figure 25**, show that there is about a 10% difference in  $S_{mag}$  between both the models, and this shall be used as a reference to calculate the  $S_{mag}$  for the model with a flat transition in the next step.

### Analysis results comparison: 2D Axisymmetric model (no centerline misalignment)



	Length [mm]	Membrane [MPa]	Bending [MPa]	Membrane+Bending [MPa]	Peak [MPa]	Total [MPa]
1	0.	103.92	16.283	118.47	53.97	168.72

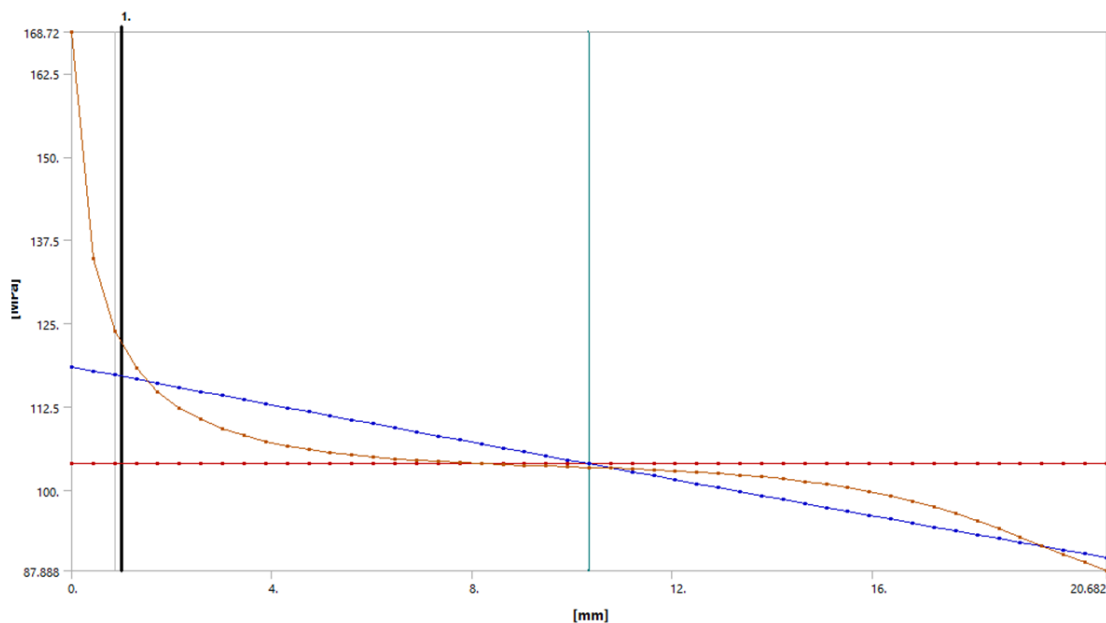


**Figure 25** Analysis results comparison between 2D axisymmetric model and 3D model with centerline misalignment - weld toe of the equal weld between 6” pipe and winghub

Now, the weld is modeled in an axisymmetric analysis with a flat transition on the outside. The LSPF value is calculated similarly, but the  $S_{mag}$  value is increased by 10% to include the effect of secondary bending stresses caused by the centerline misalignment. The calculated stress concentration factors for this model are shown in **Figure 26** below.

## 2D Axisymmetric model with flat transition (no centerline misalignment)

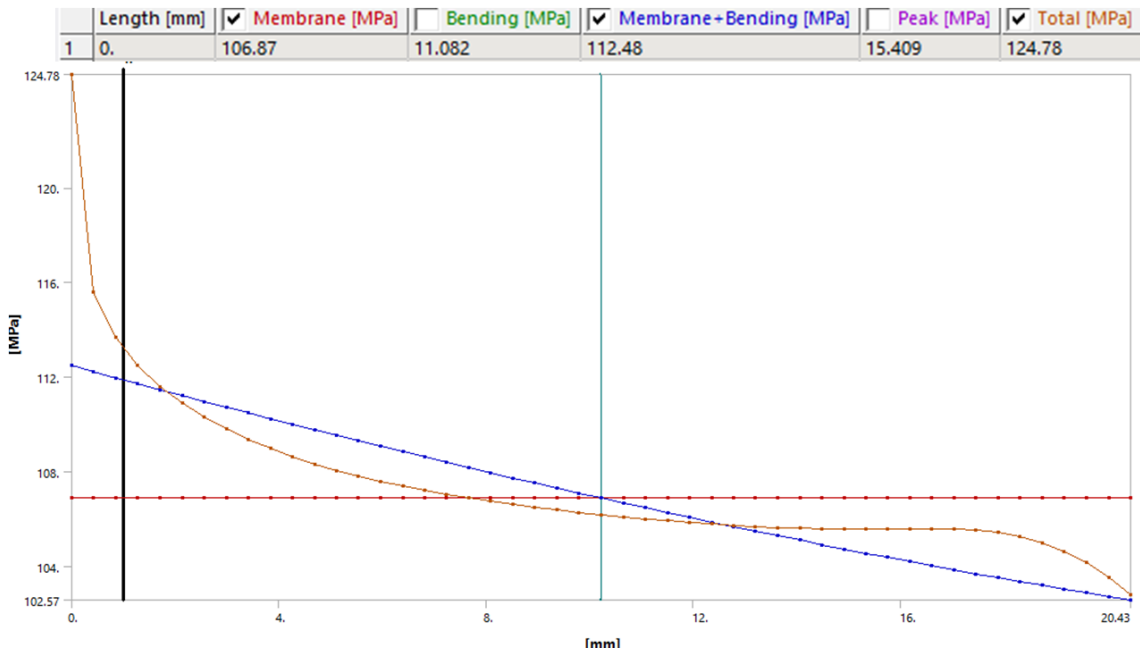
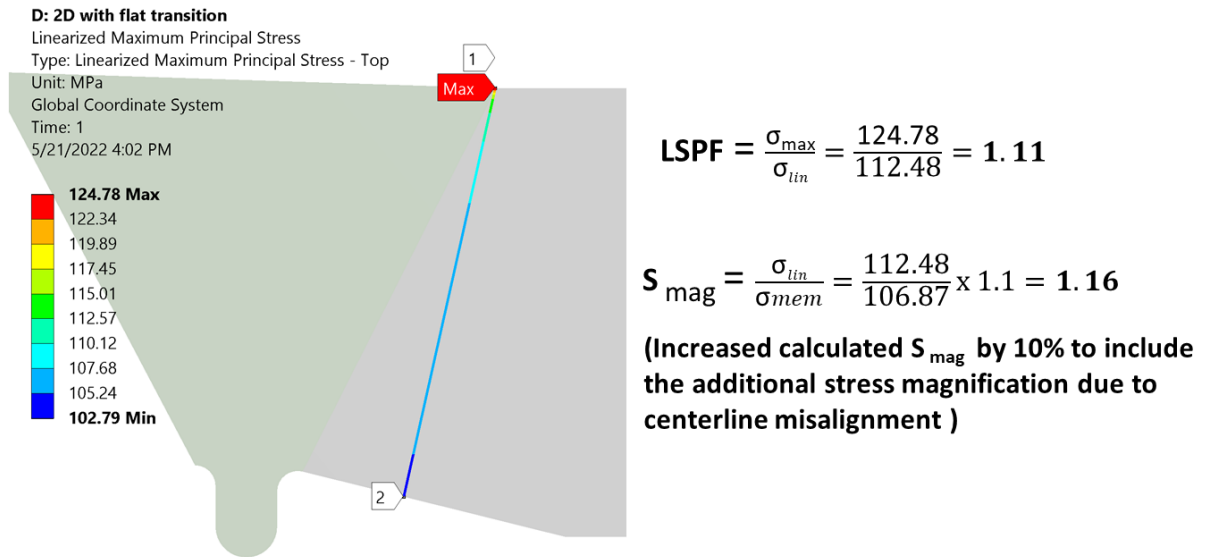


**Figure 26** Calculation of LSPF and  $S_{mag}$  using linearization of stress – weld toe of the equal weld with the flat transition between 6” pipe and winghub

### 5.1.6 Analysis Result Summary

**Table 6** Analysis result summary - equal weld between 6” pipe and winghub

Location	Geometry	LSPF	Smag
Weld toe	Convex weld cap (10° flank angle & 3mm toe fillet radius)	1.44	1.24
	Flat transition (3mm toe fillet radius)	1.11	1.16
Weld root	1mm root fillet radius	2.32	1.34

## 5.2 Unequal weld between 6-inch pipe and winghub

### 5.2.1 Analysis model dimensions

The analysis model dimensions for the unequal weld between the 6-inch pipe and the winghub are shown in **Figure 27**. The hub side, which is made of carbon steel (F65), has larger OD and thickness compared to the pipe side, which is made of super duplex stainless steel. The weld is made of Alloy 59 material. For the analysis, the difference between nominal and max/min tolerance is used, taking dimensions on the hub and max/min dimensions on the pipe to be on the conservative side. The hub and pipe ID are matched with a 1:4 transition. A centerline misalignment of 1 mm is modeled in 3D between the hub and the pipe. A flank angle of  $10^\circ$  is considered for the weld cap and the toe radius is 3mm. The root fillet radius of 1mm is assumed.

#### Analysis Model Dimensions

##### Tolerance combination considered

###### Hub Side

OD = 179.6 (Nominal OD)

ID = 132.4 (Nominal ID. Cladding not considered for analysis)

Reference: Drawings from TechnipFMC

###### Pipe Side

OD =  $168.3 - 0.8 = 167.5$  mm (minimum OD)

thickness (t) =  $21.95 - 12.5\%(t) = 19.2$  mm (minimum thickness)

ID = 129.1 mm

Reference: ASTM A999/A999M

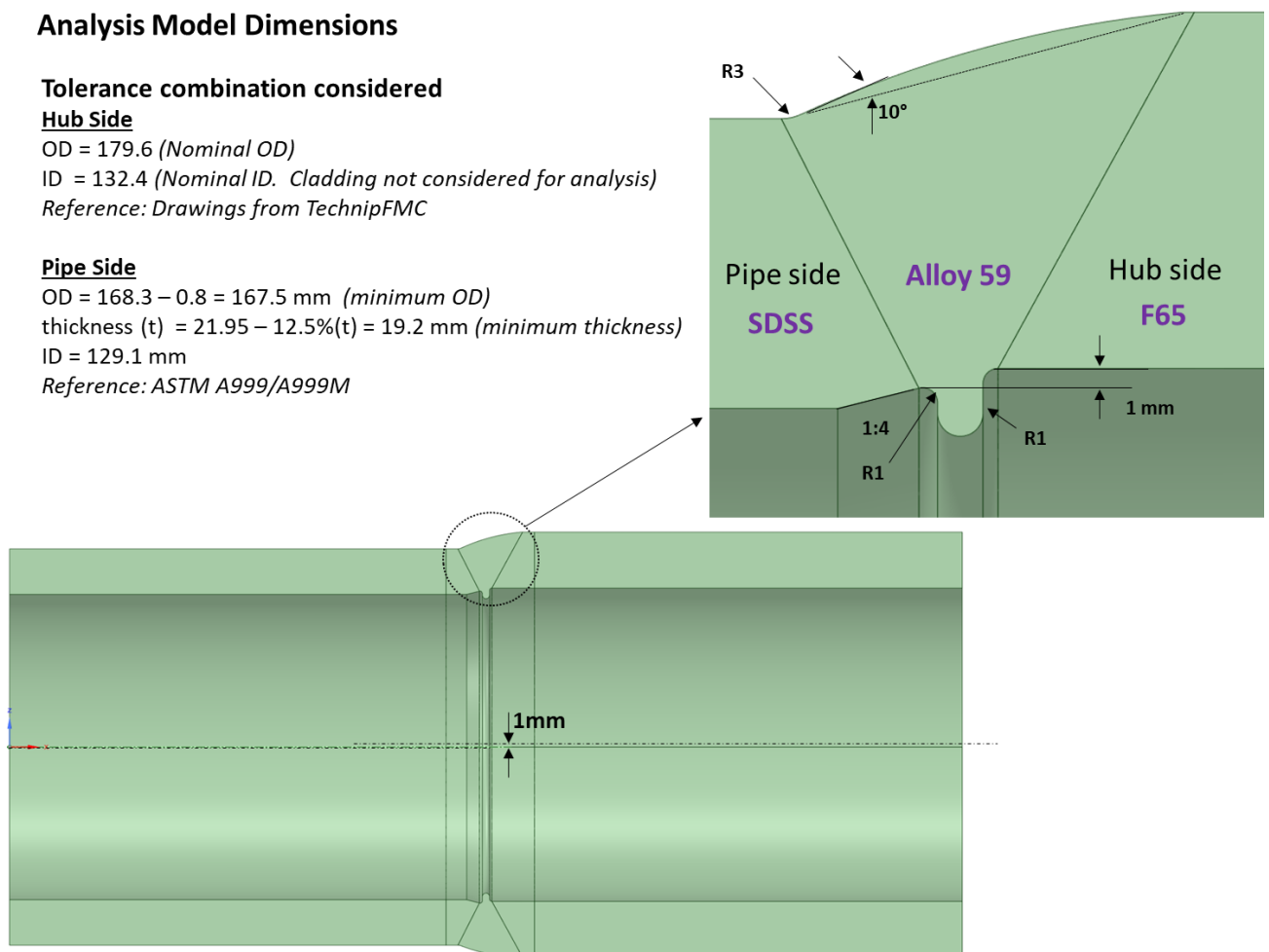


**Figure 27** Analysis model dimensions - unequal weld between 6-inch pipe and winghub

### 5.2.2 Analysis model mesh details

The analysis model is meshed using higher-order 3D 20-node solid elements (SOLID186 in Ansys) in the weld area and linear 3D 8-node solid elements (SOLID185 in Ansys) in the remaining locations, which are not of primary interest for the SCF study to reduce the computational time. In the critical areas like the weld toe and root, the mesh is finely refined in both directions, as shown in *Figure 28* below.

#### Analysis model: Mesh details

**Element type:** Hexahedral

**Element order:**

Weld area- SOLID186 (higher order 3-D 20-node solid element)

Other locations - SOLID185 ( linear 3-D 8-node solid element)

No of nodes: 17667000

No of elements: 8901000

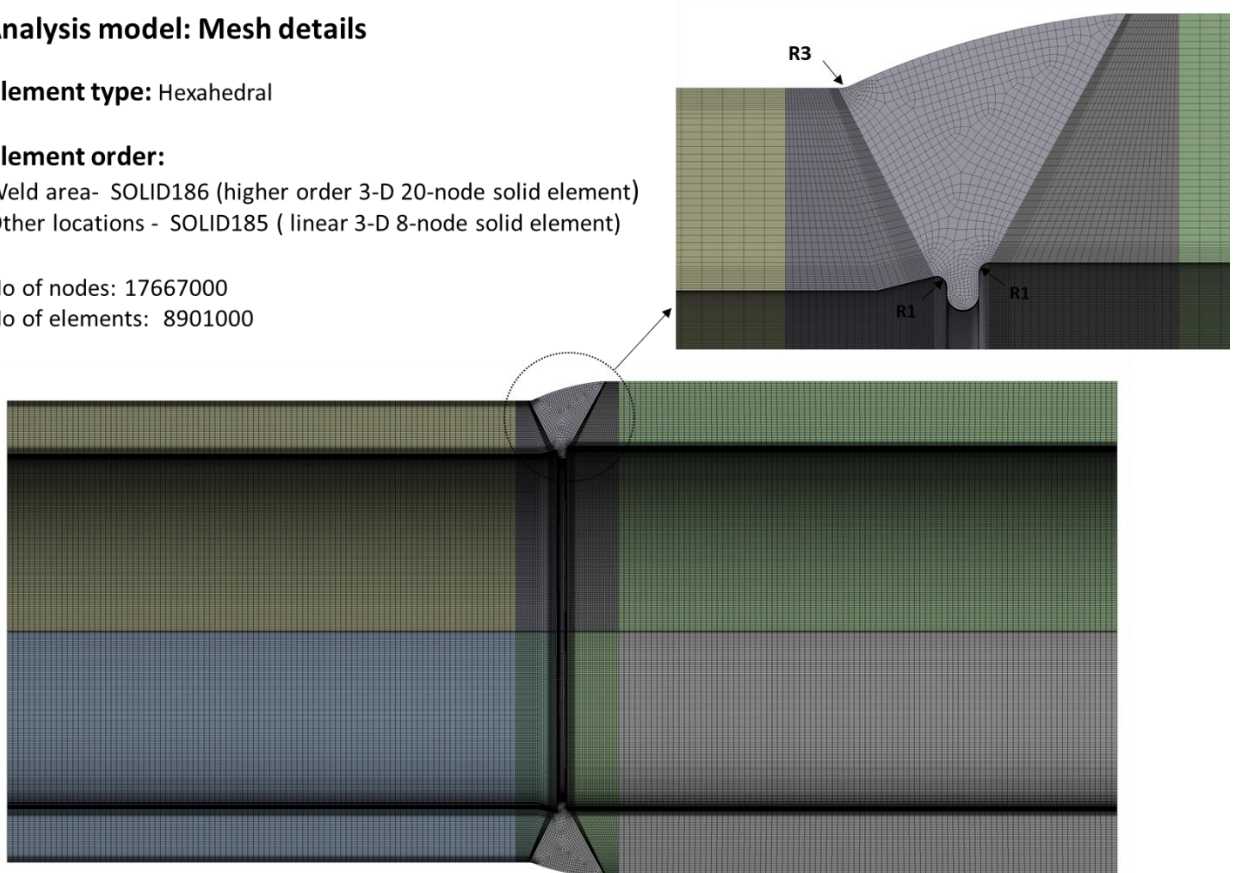


**Figure 28** Analysis model mesh details - unequal weld between 6” pipe and winghub

### 5.2.3 Boundary conditions

The analysis model is loaded with a simple tensile force at one end (pipe side) and is rigidly fixed at the other end (hub side). No other external loads (like pressure, temperature, or bending moments) are applied. *Figure 29* shows the boundary conditions applied to the analysis model.

### Analysis model: Boundary conditions

**B: Static Structural**  
Static Structural  
Time: 1. s  
5/21/2022 6:50 PM

- A** Remote Displacement
- B** Remote Force: 5.e+005 N

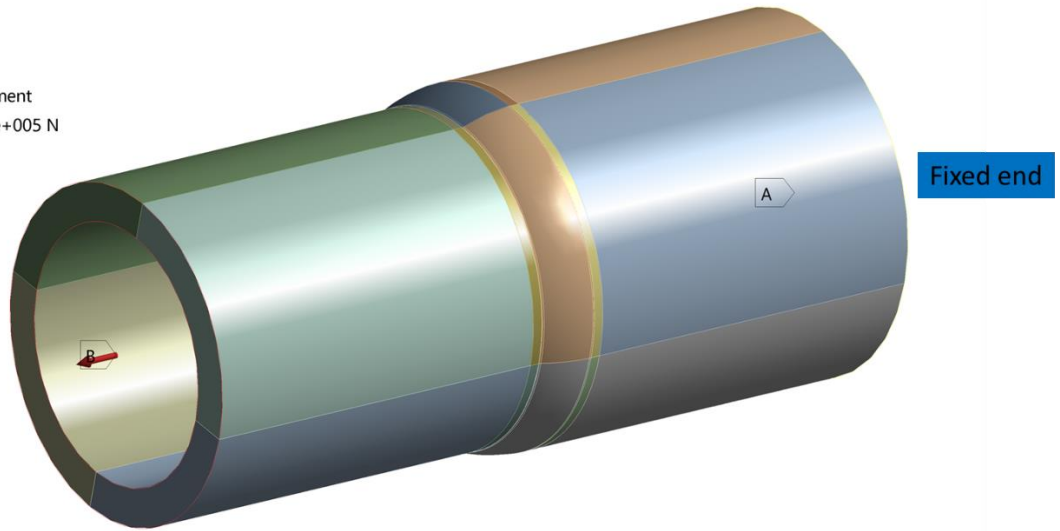


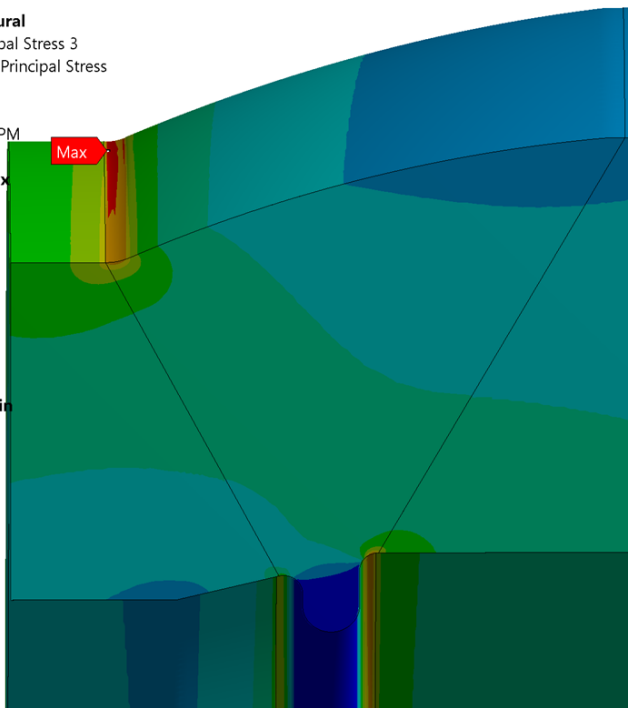
**Figure 29** Analysis model boundary conditions - unequal weld between 6” pipe and winghub

### 5.2.4 Analysis results

The analysis results show the highest stress at the outside toe of the weld. This is because of the larger OD and thickness on the hub side compared to the pipe side. The maximum principal stress plot for the weld is shown in *Figure 30* below.

**B: Static Structural**  
Maximum Principal Stress 3  
Type: Maximum Principal Stress  
Unit: MPa  
Time: 1  
3/5/2022 10:08 PM

- 151.09 Max
- 134.1
- 117.11
- 100.11
- 83.12
- 66.127
- 49.133
- 32.139
- 15.146
- 1.8477 Min



**Maximum Principal Stress**

**Outside weld toe: 151.09 Mpa**

**Inside weld root: 141.62 Mpa**

**Figure 30** Maximum principal stress plot - unequal weld between 6” pipe and winghub

The stress is linearized along the stress linearization path from the peak stress point on the weld toe to the inside of the pipe, and the factors LSPF and  $S_{mag}$  are calculated for the hotspot at the weld toe as shown in **Figure 31**.

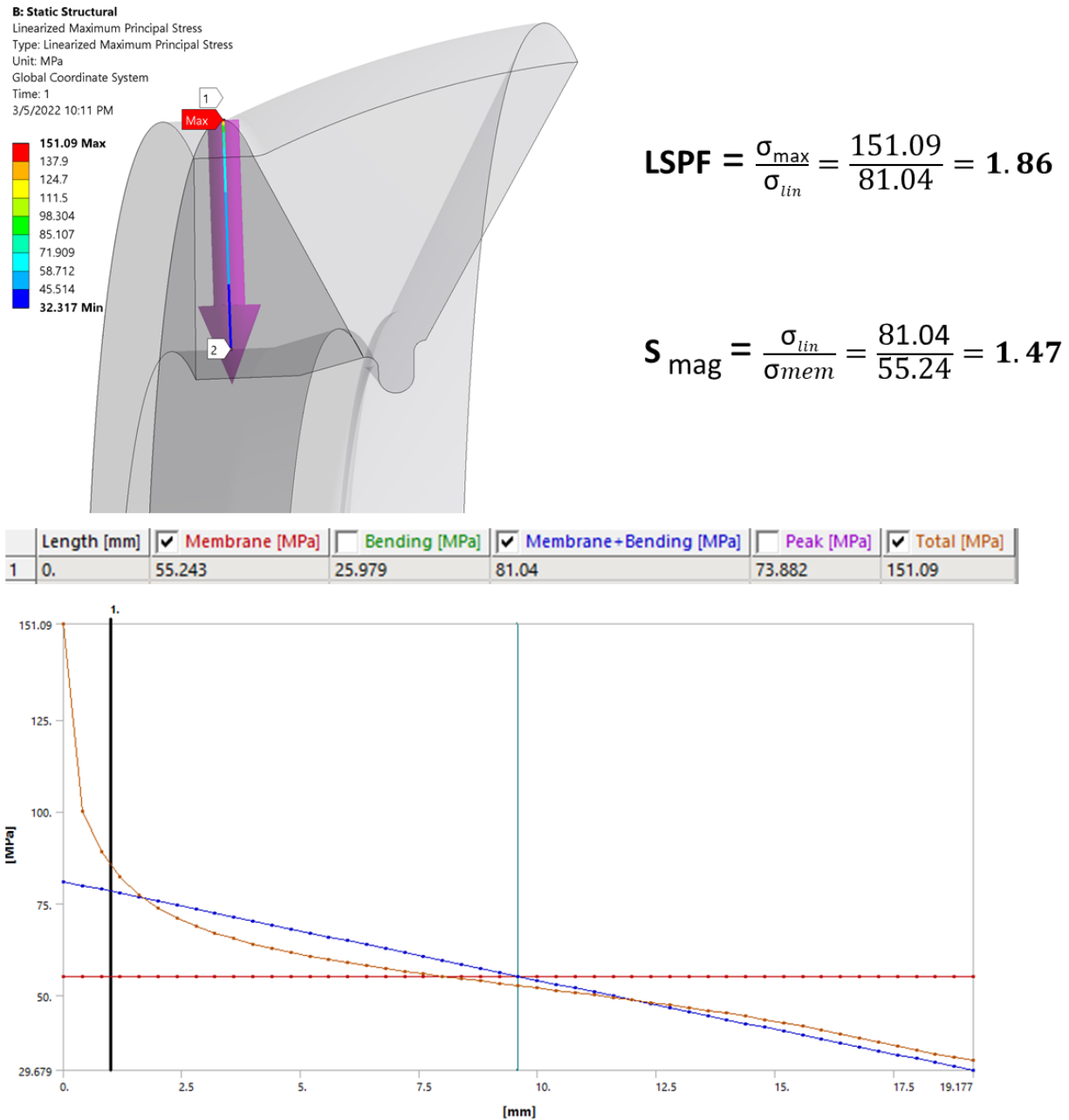
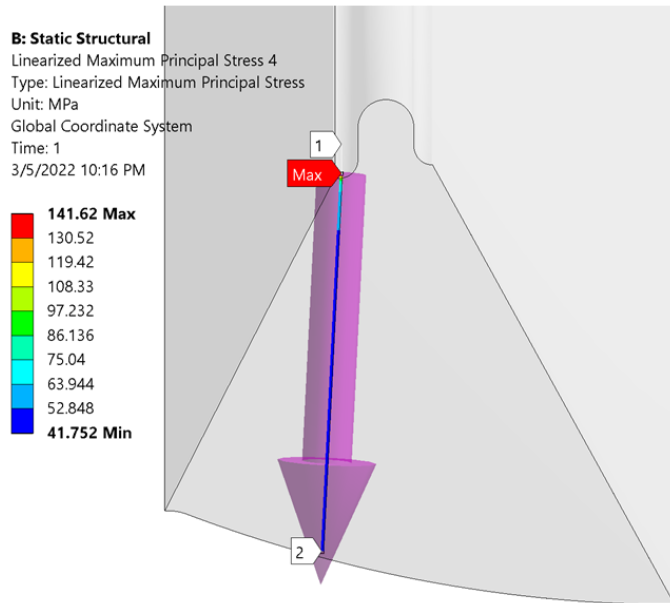


**Figure 31** Calculation of LSPF and  $S_{mag}$  using linearization of stress – weld toe of the unequal weld between 6” pipe and winghub

Similarly, LSPF and  $S_{mag}$  for the inside weld root are calculated by linearizing the stress along the path from the peak stress point on the weld root to the external surface of the weld, as shown in **Figure 32**.



$$LSPF = \frac{\sigma_{max}}{\sigma_{lin}} = \frac{141.62}{62.58} = 2.26$$

$$S_{mag} = \frac{\sigma_{lin}}{\sigma_{mem}} = \frac{62.58}{52.3} = 1.2$$

	Length [mm]	<input checked="" type="checkbox"/> Membrane [MPa]	<input type="checkbox"/> Bending [MPa]	<input checked="" type="checkbox"/> Membrane+Bending [MPa]	<input type="checkbox"/> Peak [MPa]	<input checked="" type="checkbox"/> Total [MPa]
1	0.	52.3	13.924	62.583	79.871	141.62

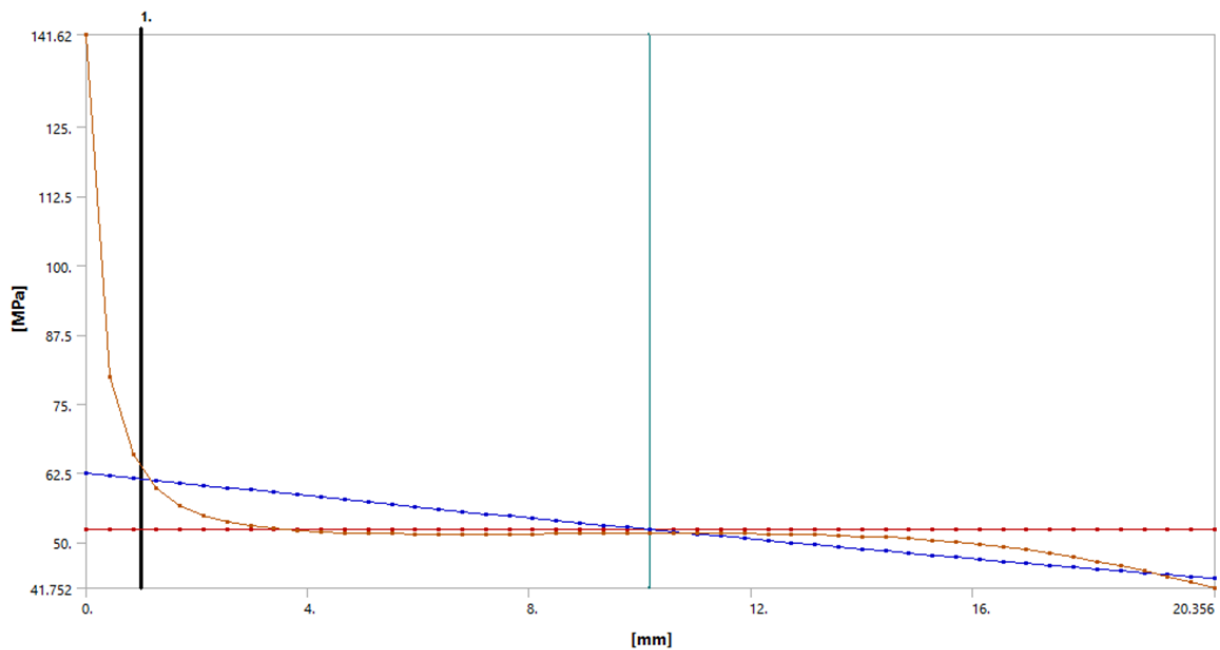


**Figure 32** Calculation of LSPF and  $S_{mag}$  using linearization of stress – weld root of the equal weld between 6” pipe and winghub

### 5.2.5 Analysis results with flat transition on the weld

The analysis model is prepared using the same dimensions, tolerances, and misalignments as the model in the previous section, except that the convex weld cap is not modeled. The transition of the weld is modeled flat, and the results with this flat transition are shown in

*Figure 33.*



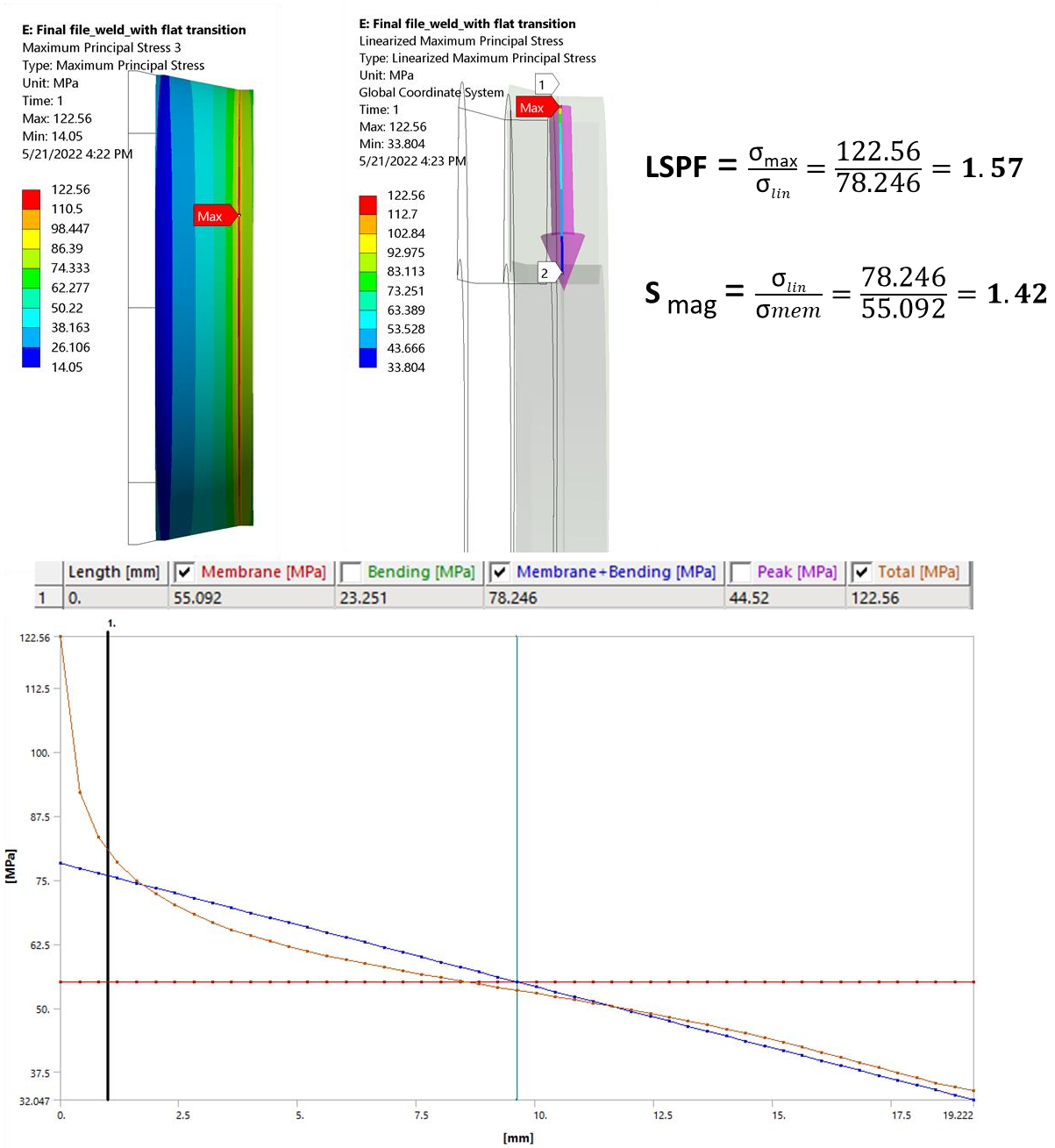


**Figure 33** Calculation of LSPF and  $S_{mag}$  using linearization of stress – weld toe of the unequal weld with the flat transition between 6” pipe and winghub

### 5.2.6 Analysis result summary

**Table 7** Analysis result summary - unequal weld between 6” pipe and winghub

Location	Geometry	LSPF	S <sub>mag</sub>
Weld toe	Convex weld cap (10° flank angle & 3mm toe fillet radius)	1.86	1.47
	Flat transition (3mm toe fillet radius)	1.57	1.42
Weld root	1mm root fillet radius	2.26	1.2

## 5.3 Fillet weld between 6-inch pipe and doubler Plate

### 5.3.1 Analysis model dimensions

The doubler plate, made of 22 Cr duplex steel, looks like a sleeve on top of the hub is joined by fillet welds on either side. The analysis model is simplified to capture only one of the two welds. The geometry is modeled as a 2D axisymmetric model with a clearance of 1mm between the pipe and the plate. The weld made of 25 Cr duplex steel is modeled with a throat thickness of 8mm and a toe radius of 3mm. The analysis model dimensions are shown in *Figure 34*. For this analysis, nominal dimensions are used for both pipe and the doubler plate.

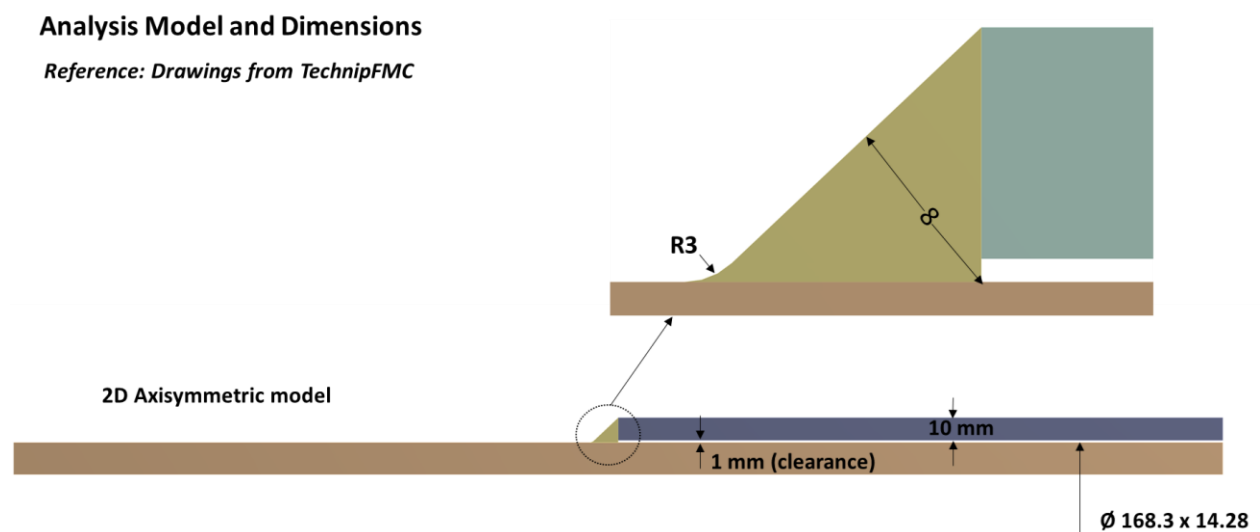


**Figure 34** Analysis model dimensions – fillet weld between the 6-inch pipe and doubler plate. Since the weld transition is very steep, high stress concentration is expected at the weld toe and the weld might not meet the category 1 (linear elastic) assessment. So, the weld is directly checked for category 2 (non-linear) assessment with the available direct loads from the project (piping stress analysis) provided by TechnipFMC.

### 5.3.2 Analysis model mesh details

The analysis model is meshed using higher-order 2D 8-node plane elements (PLANE183 in Ansys). The mesh is very finely refined at the weld toe, which is the area of interest in this case. The model is checked for mesh convergence, and the details of the most refined mesh are presented in *Figure 35*.

### Analysis model: Mesh details

**Element type and order:** PLANE183 (higher order 2-D, 8-node)  
axisymmetric  
No of nodes: 139860  
No of elements: 45529

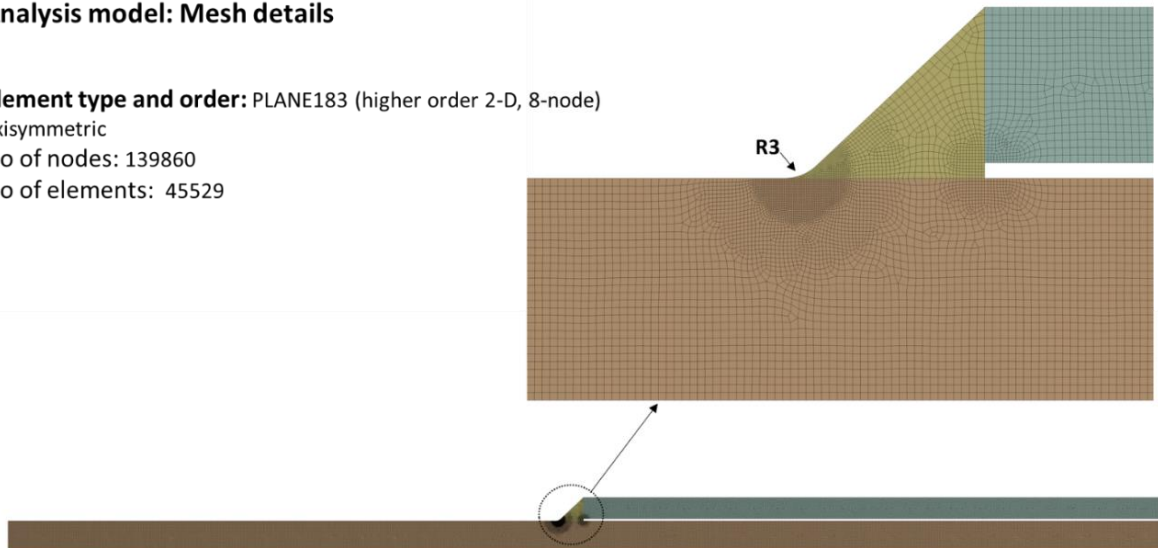


**Figure 35** Analysis model mesh details – fillet weld between 6” pipe and doubler plate

### 5.3.3 Steady-state thermal analysis

Initially, a steady-state thermal analysis is done with the fluid temperature inside the pipe at 85°C (Reference: production fluid temperature from the operating case) and external temperature of 4°C (Seawater). Both the pipe and the doubler plate made of duplex stainless steel are considered uninsulated and coated with an epoxy paint of thickness 0.35mm with paint thermal conductivity of 0.35 W/mK. Forced convection coefficients are calculated for the external surfaces assuming a water current of 0.7 m/s. **Figure 36** below shows the output temperature plot from the steady-state thermal analysis showing the temperature gradient across the thickness of the component.

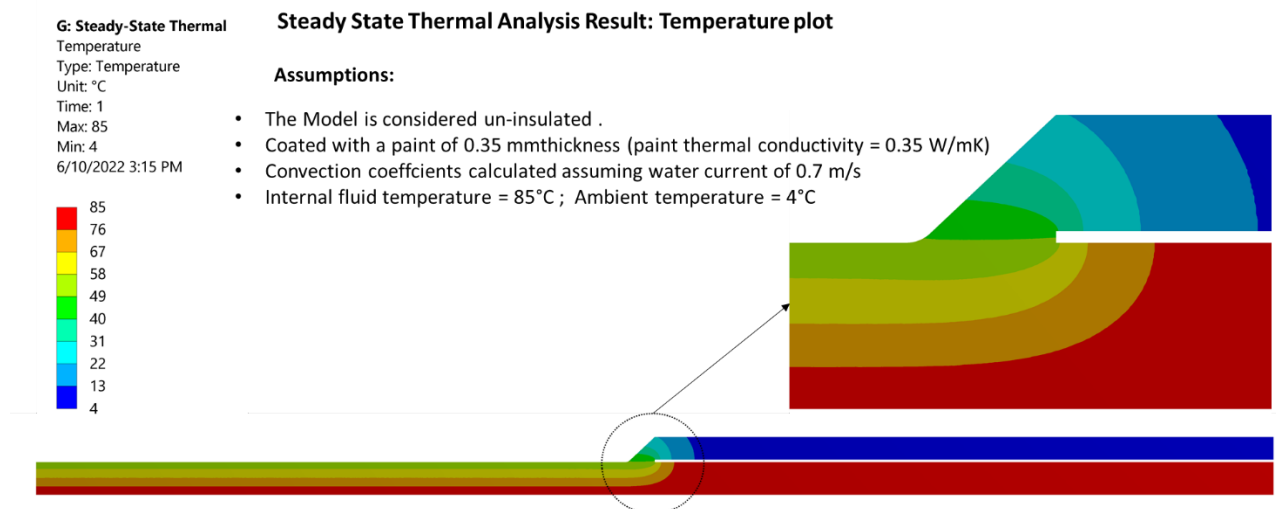


**Figure 36** Temperature plot from the steady-state thermal analysis - 6” pipe and doubler plate

### 5.3.4 Loads and boundary conditions

Thermal load for the static structural analysis is imported as temperature gradient from the steady-state thermal analysis. The effective internal pressure of the pipe is taken as 452 bar (Reference: production fluid pressure from the operating case). The external loads (forces & moments) from the project pipe stress analysis are not directly applied to the model. Instead, an effective tensile load of 288 MPa (Reference: maximum longitudinal stress from piping stress analysis of the operating case) is applied at one end of the pipe, fixing the other end of the pipe and doubler plate as shown in **Figure 37** below. Note that the effective tension of 288 MPa includes the end cap effect due to internal pressure.

#### Loads and boundary conditions applied:

- Pipe Internal pressure = 452 bar
- Temperature imported from steady state thermal analysis
- Fixed support at one end as shown in the figure below
- Tension of 288 Mpa applied as shown in the figure below (Ref: maximum longitudinal stress from piping analysis operating case)

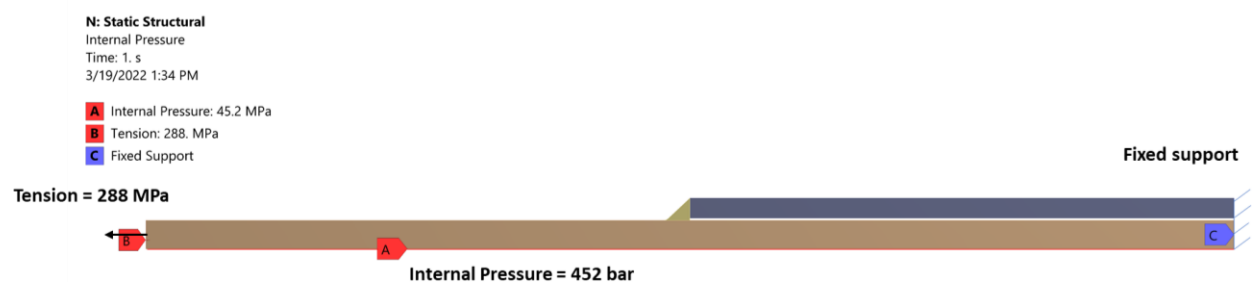


**Figure 37** Analysis boundary conditions - weld between the 6-inch pipe and doubler plate

### 5.3.5 Non-linear analysis results

The non-linear analysis as shown in **Figure 38** indicates a peak strain of 0.77% at the weld toe which is lower than the maximum allowable peak strain calculated as per category 2 assessment criteria defined in DNVGL-RP-F112. The calculation of LSMF is shown in **Section 5.3.6**.

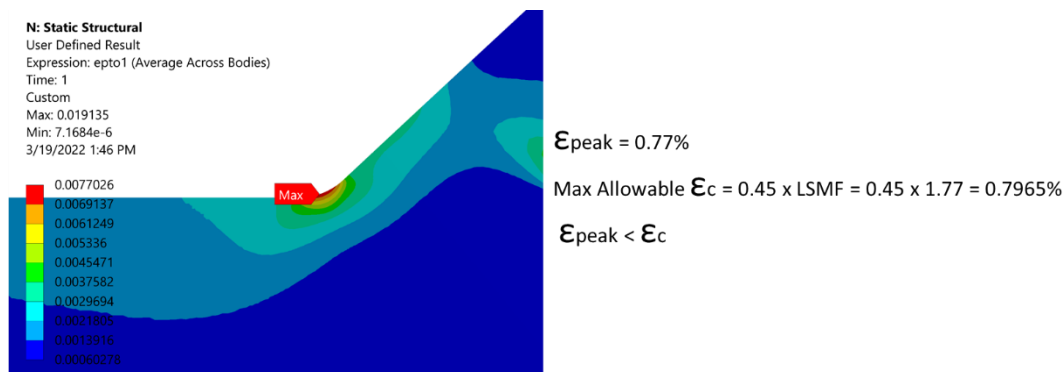
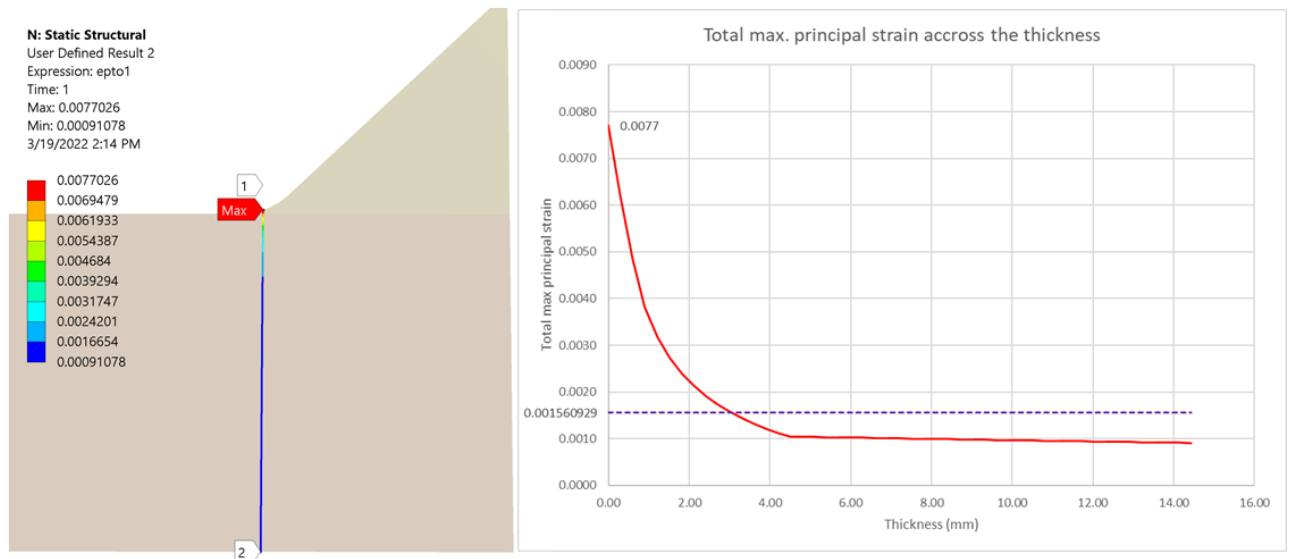


**Figure 38** Total maximum principal strain plot - weld between the 6” pipe and doubler plate

To calculate the membrane strain, as a conservative approach, the total maximum principal strain is averaged across the thickness from weld toe until inside of the pipe along the shortest path, as shown in **Figure 39** below. For a more accurate result, the strains only in the direction of the maximum principal strain of the hotspot should be averaged across the thickness, which would give a lower membrane strain than the one calculated below. However, the calculated membrane strain is much lower than the maximum allowable membrane strain defined in the category 2 assessment criteria defined in DNVGL-RP-F112.



$$\epsilon_{\text{mem}} = 0.156\%$$

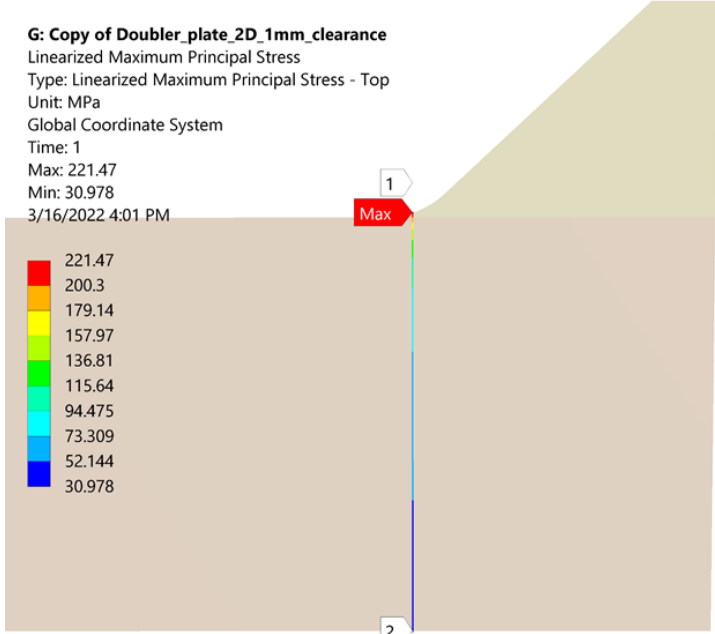
$$\text{Max. allowable } \epsilon_{\text{mem}} = 0.3\%$$

$$\epsilon_{\text{mem}} < \text{Allowable } \epsilon_{\text{mem}}$$

**Figure 39** Calculation of membrane strain - weld between the 6-inch pipe and doubler plate

### 5.3.6 Calculation of LSMF using linear elastic analysis

It was needed to calculate the local surface magnification factor (LSMF) at the weld toe to estimate the maximum allowable peak strain for the non-linear assessment of the weld in **Section 5.3.5**. A linear elastic analysis is done with a simple tensile force at one end (pipe side) and is rigidly fixed at the other end (hub side). No other external loads are applied. The stress is linearized along the stress linearization path from the peak stress point on the weld toe to the inside of the pipe, and the factors LSMF is calculated for the hotspot at the weld toe as shown in **Figure 40**.



$$LSMF = \frac{\sigma_{max}}{\sigma_{lin}} = \frac{221.47}{124.81} = 1.77$$

	Length [mm]	<input checked="" type="checkbox"/> Membrane [MPa]	<input type="checkbox"/> Bending [MPa]	<input checked="" type="checkbox"/> Membrane+Bending [MPa]	<input type="checkbox"/> Peak [MPa]	<input checked="" type="checkbox"/> Total [MPa]
1	0.	70.904	56.323	124.81	97.614	221.47

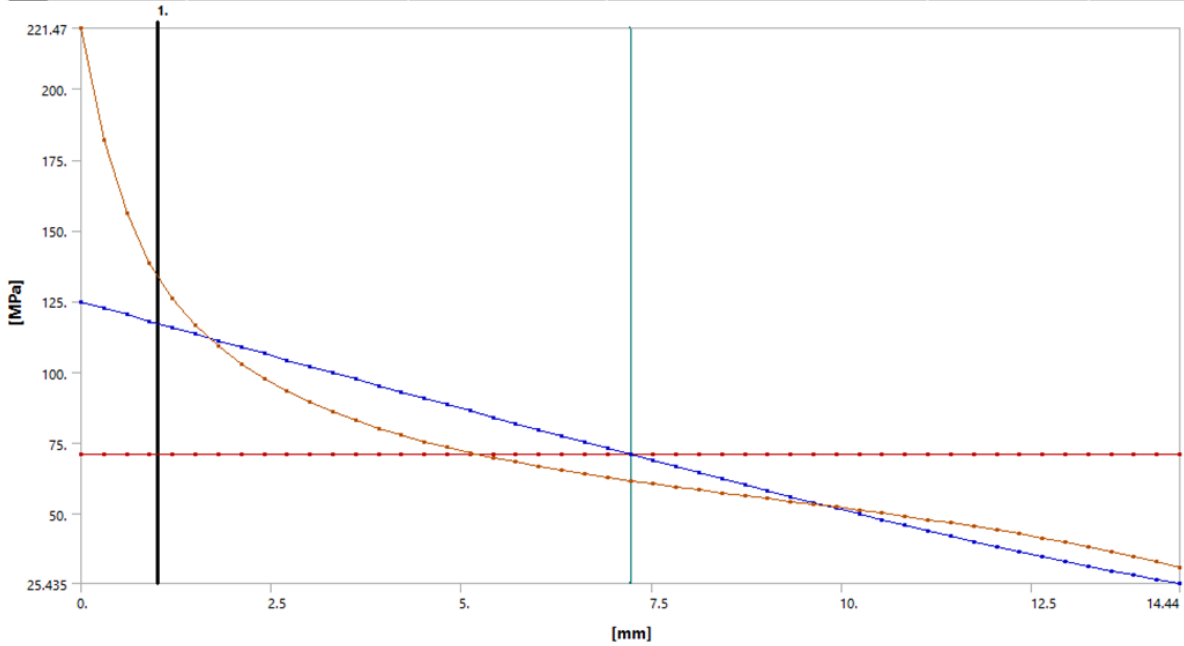


**Figure 40** Calculation of LSMF from linear elastic analysis - weld between the 6-inch pipe and doubler plate

## 5.4 Equal welds between HIP headers and hubs

The analysis has been done for the four different header sizes (8, 9, 10, and 12-inch ID) with two different thicknesses for 22 Cr and 25 Cr duplex steel, making it a total of 8 analysis models of the equal welds between HIP headers and hubs. The analysis details of one of the models are shown in this section. The result plots for the rest of the models are attached to **Appendix A** of this report.

### 5.4.1 Analysis model dimensions

The analysis model dimensions for the equal welds between HIP headers and hubs are shown in **Figure 41**. The nominal dimensions of both the hub and pipe sides are equal. However, for the analysis, the difference between Nominal and max/min tolerance can be used (DNVGL, 2019). Nominal dimensions on the hub and maximum dimensions on the header are used here to be on the conservative side.

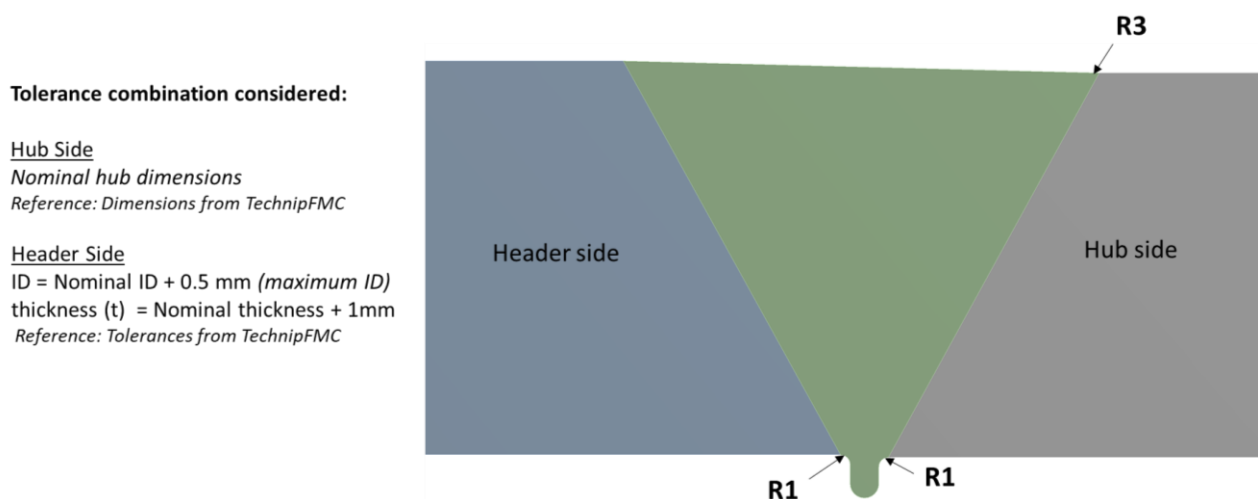


**Figure 41** Analysis model dimensions – equal welds between HIP headers and hubs

### 5.4.2 Analysis model mesh details

The analysis model is meshed using higher-order 2D 8-node plane elements (PLANE183 in Ansys). The mesh is very finely refined at the weld toe and root, which are the areas of interest in this case. The model is checked for mesh convergence, and the details of the most refined mesh are presented in **Figure 42**.

### Analysis model: Mesh details

Element type and order: PLANE183 (higher order 2-D, 8-node) axisymmetric

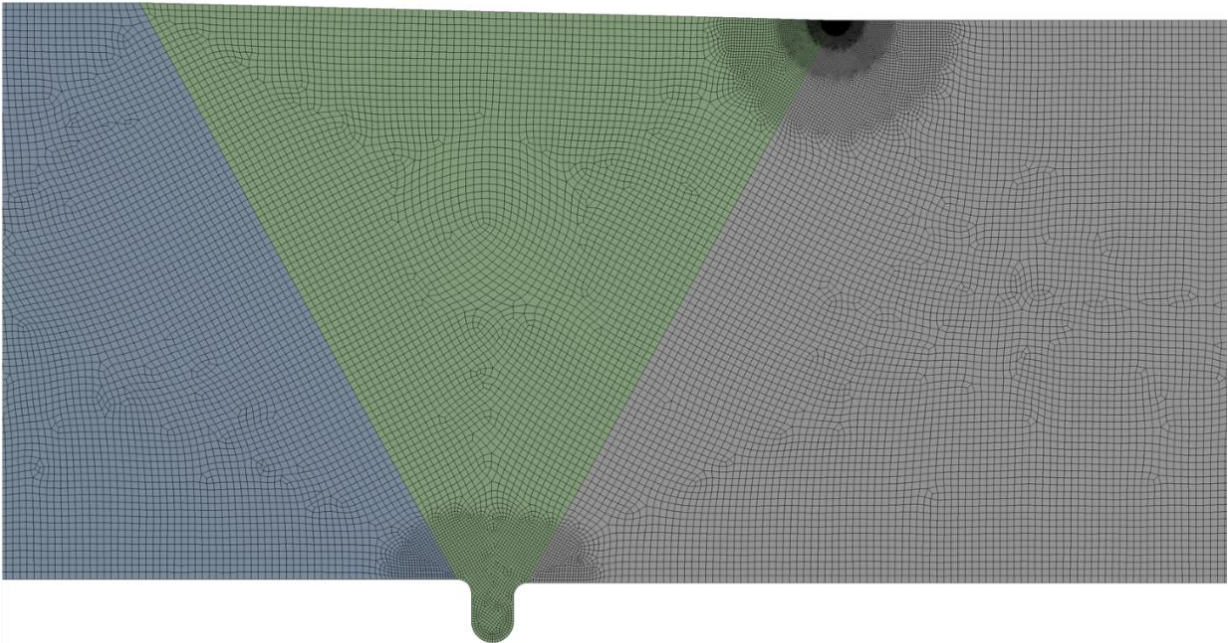


**Figure 42** Analysis model mesh details – equal welds between HIP headers and hubs

### 5.4.3 Boundary conditions

The analysis model is loaded with a simple tensile force at one end (hub side) and is rigidly fixed at the other end (header side). No other external loads (like pressure, temperature, or bending moments) are applied. **Figure 43** shows the boundary conditions applied to the analysis model.



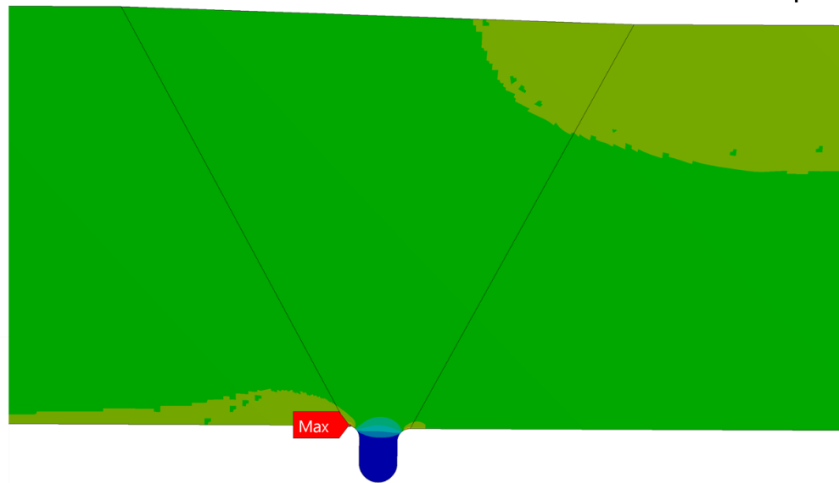
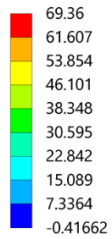
**Figure 43** Analysis model boundary conditions - equal welds between HIP headers and hubs

### 5.4.4 Analysis results

The analysis results show that the stress at the root of the weld is higher compared to the outside weld toe. The maximum principal stress plot for one of the welds (9-inch 25 Cr duplex) is shown in **Figure 44**. The stress is linearized along the stress classification path from the peak stress point on the weld root to the external surface of the weld, and the factors LSPF and  $S_{mag}$  are calculated for the hotspot at the weld root, as shown in **Figure 45**.



C: 9 inch 2D  
 Maximum Principal Stress  
 Type: Maximum Principal Stress - Top/Bottom  
 Unit: MPa  
 Time: 1  
 Custom  
 6/10/2022 3:06 PM



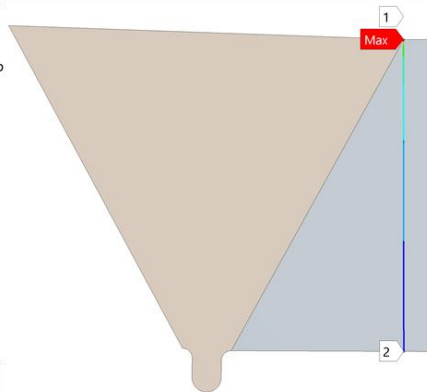
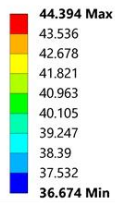
**Maximum Principal Stress:**  
 Inside weld root: 69.36 Mpa  
 Outside weld toe: 44.4 Mpa

**Figure 44** Maximum principal stress plot - equal welds between HIP headers and hubs

Linearized Maximum Principal Stress - Weld toe

	Length [mm]	Membrane [MPa]	Bending [MPa]	Membrane+Bending [MPa]	Peak [MPa]	Total [MPa]
1	0.	38.129	1.8426	39.921	4.4731	44.394

C: 9 inch 2D  
 Linearized Maximum Principal Stress  
 Type: Linearized Maximum Principal Stress - Top  
 Unit: MPa  
 Global Coordinate System  
 Time: 1  
 6/10/2022 3:06 PM



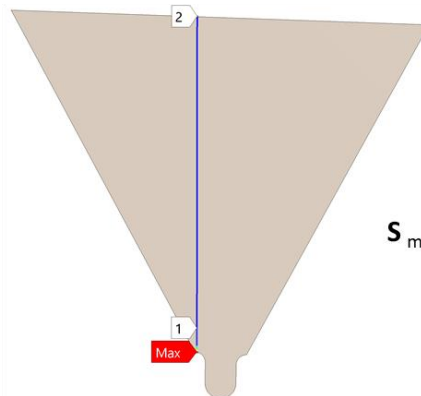
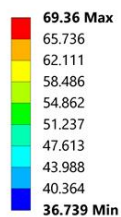
$$LSPF = \frac{\sigma_{max}}{\sigma_{lin}} = \frac{44.394}{39.921} = 1.11$$

$$S_{mag} = \frac{\sigma_{lin}}{\sigma_{mem}} = \frac{39.921}{38.129} \times 1.1 = 1.15$$

Linearized Maximum Principal Stress - Inside Weld root

	Length [mm]	Membrane [MPa]	Bending [MPa]	Membrane+Bending [MPa]	Peak [MPa]	Total [MPa]
1	0.	37.671	1.0197	38.66	33.367	69.36

C: 9 inch 2D  
 Linearized Maximum Principal Stress 2  
 Type: Linearized Maximum Principal Stress - Top  
 Unit: MPa  
 Global Coordinate System  
 Time: 1  
 6/10/2022 3:07 PM



$$LSPF = \frac{\sigma_{max}}{\sigma_{lin}} = \frac{69.36}{38.66} = 1.79$$

$$S_{mag} = \frac{\sigma_{lin}}{\sigma_{mem}} = \frac{38.66}{37.671} \times 1.1 = 1.13$$

**Figure 45** Calculation of LSPF and  $S_{mag}$  using linearization of stress – equal welds between HIP headers and hubs

Similarly, the analysis is done for the other header sizes. **Table 8** shows the LSPF and  $S_{mag}$  values calculated for different header sizes. It can be observed that these values are approximately the same, with only a small difference showing that the stress concentration factors at the weld are least dependent on the header size in this case. In this case, the high LSPF values on the inside root may not be of real concern in relation to HISC. This is because the minimum wall thickness of headers analyzed is 32 mm, which is high enough that sufficient hydrogen might not diffuse to the inside surface of the header in its project lifetime. For reference, it takes about 25 years for the hydrogen to diffuse through a thickness of 28 mm of the component whose surface temperature is 121°C according to the diffusion depth table in DNVGL-RP-F112.

**Table 8** Analysis result summary - equal welds between HIP headers and hubs

Header size	Dimensions	Header [max] (mm)	Hub [nom] (mm)	LSPF (toe)	LSPF (root)	Smag (toe)	Smag (root)
8" ID (25 Cr)	ID	203.7	203.2	1.11	1.78	1.14	1.1
	WT	33	32				
	OD	269.7	267.2				
9" ID (25 Cr)	ID	229.1	228.6	1.11	1.79	1.15	1.13
	WT	33	32				
	OD	295.1	292.6				
10" ID (25 Cr)	ID	254.5	254	1.11	1.79	1.15	1.13
	WT	33	32				
	OD	320.5	318				
12" ID (25 Cr)	ID	305.3	304.8	1.12	1.79	1.16	1.11
	WT	36	35				
	OD	377.3	374.8				
8" ID (22 Cr)	ID	203.7	203.2	1.1	1.8	1.14	1.12
	WT	38	37				
	OD	279.7	277.2				
9" ID (22 Cr)	ID	229.1	228.6	1.1	1.81	1.15	1.12
	WT	38	37				
	OD	305.1	302.6				
10" ID (22 Cr)	ID	254.5	254	1.11	1.8	1.15	1.12
	WT	38	37				
	OD	330.5	328				
12" ID (22 Cr)	ID	305.3	304.8	1.11	1.8	1.14	1.13
	WT	41	40				
	OD	387.3	384.8				

## 5.5 Unequal welds between HIP headers and hubs

The analysis has been done for the four different header sizes (8, 9, 10 and 12-inch ID) with two different thicknesses for 22 Cr and 25 Cr duplex steel, making it a total of 8 analysis models of the unequal welds between HIP headers and hubs. The analysis details of one of the models are shown in this section. The result plots for the rest of the models are attached to **Appendix B** of this report.

### 5.5.1 Analysis model dimensions

The analysis model dimensions for the unequal welds between HIP headers and hubs are shown in **Figure 46**. The nominal thickness on the hub side is assumed as 1.3 times the nominal thickness on the header side. The weld toe fillet radius is taken as 3mm. For the analysis model, nominal dimensions on the header and max/min dimensions on the hub are used here to be conservative. The hub is made of F65 material, and the header is of duplex/super duplex steel. The fusion line between the header and the weld is the area of interest for HISC assessment.

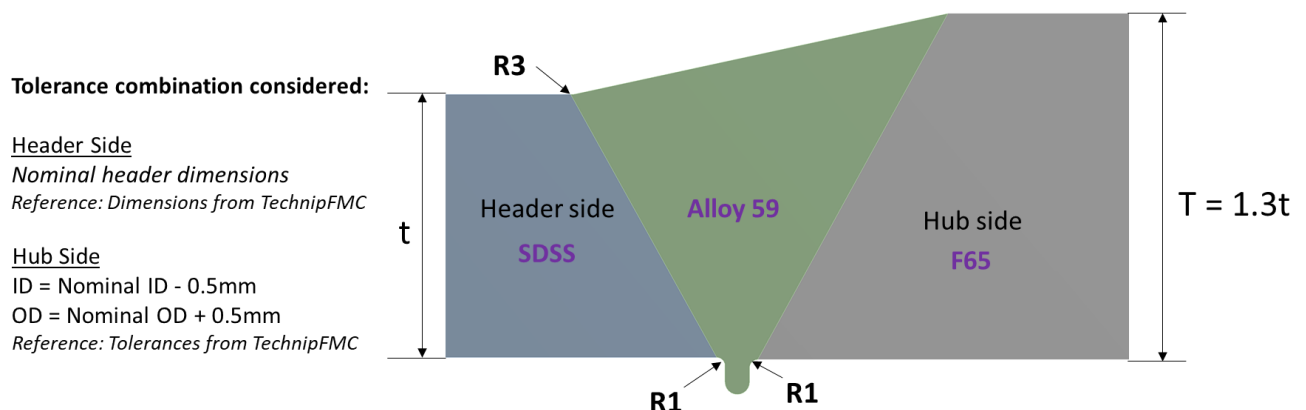


**Figure 46** Analysis model dimensions – unequal welds between HIP headers and hubs

### 5.5.2 Analysis model mesh details

The analysis model is meshed using higher-order 2D 8-node plane elements (PLANE183 in Ansys). The mesh is very finely refined at the weld toe and root, which are the areas of interest in this case. The model is checked for mesh convergence, and the details of the most refined mesh are presented in **Figure 47**.

## Analysis model: Mesh details

**Element type and order:** PLANE183 (higher order 2-D, 8-node)  
axisymmetric

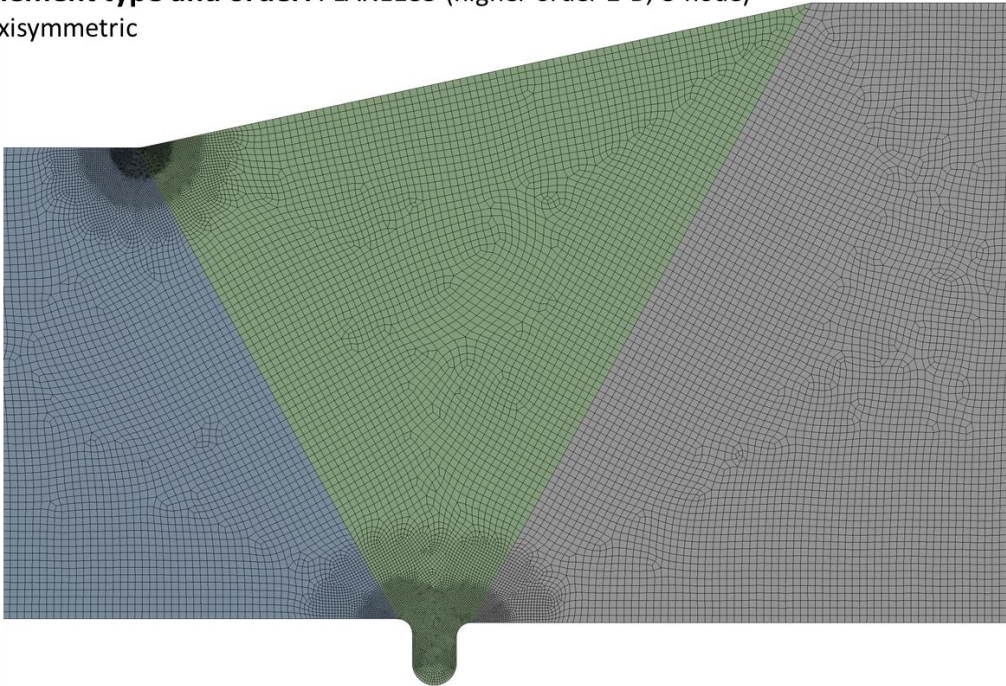


**Figure 47** Analysis model mesh details – unequal welds between HIP headers and hubs

### 5.5.3 Boundary conditions

The analysis model is loaded with a simple tensile force at one end (header side) and is rigidly fixed at the other end (hub side). No other external loads (like pressure, temperature, or bending moments) are applied. **Figure 48** shows the boundary conditions applied.



**Figure 48** Analysis model boundary conditions - unequal welds between HIP headers and hubs

### 5.5.4 Analysis results

The analysis results show that the maximum stress is at the outside weld toe. The maximum principal stress plot for one of the welds (8-inch 25 Cr duplex) is shown in **Figure 49**. The stress is linearized along the stress classification path, and the factors LSPF and  $S_{mag}$  are calculated for the hotspots at the weld toe and root, as shown in **Figure 50**.

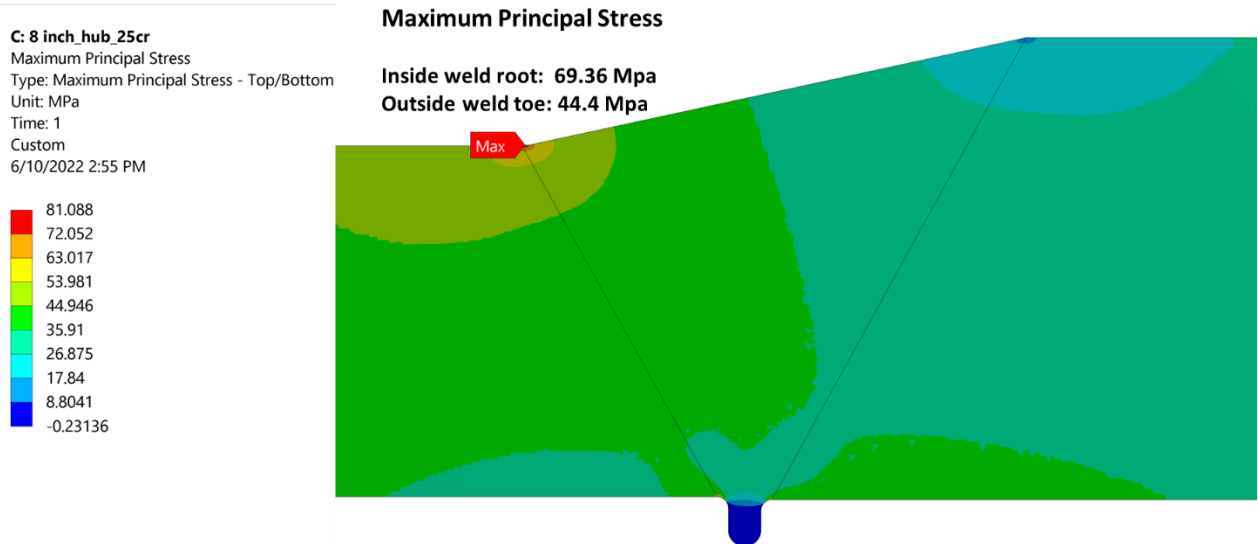


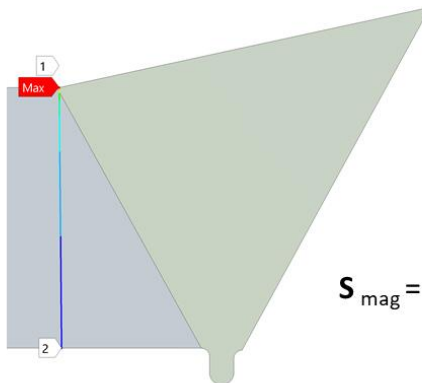
**Figure 49** Maximum principal stress plot - unequal welds between HIP headers and hubs

**Linearized Maximum Principal Stress - Weld toe**

	Length [mm]	Membrane [MPa]	Bending [MPa]	Membrane+Bending [MPa]	Peak [MPa]	Total [MPa]
1	0.	41.973	10.798	52.293	28.798	81.083

**C: 8 inch\_hub\_25cr**  
 Linearized Maximum Principal Stress  
 Type: Linearized Maximum Principal Stress - Top  
 Unit: MPa  
 Global Coordinate System  
 Time: 1  
 6/10/2022 2:55 PM

81.088 Max  
75.867  
70.646  
65.425  
60.204  
54.983  
49.762  
44.542  
39.321  
34.1 Min



$$LSPF = \frac{\sigma_{max}}{\sigma_{lin}} = \frac{81.083}{52.293} = 1.55$$

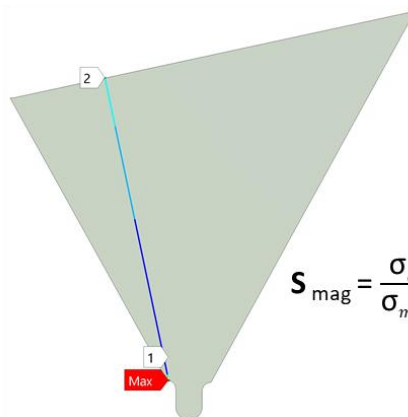
$$S_{mag} = \frac{\sigma_{lin}}{\sigma_{mem}} = \frac{52.293}{41.973} \times 1.06 = 1.32$$

**Linearized Maximum Principal Stress – Inside Weld root**

	Length [mm]	Membrane [MPa]	Bending [MPa]	Membrane+Bending [MPa]	Peak [MPa]	Total [MPa]
1	0.	38.779	3.5657	36.304	29.924	65.35

**C: 8 inch\_hub\_25cr**  
 Linearized Maximum Principal Stress 2  
 Type: Linearized Maximum Principal Stress - Top  
 Unit: MPa  
 Global Coordinate System  
 Time: 1  
 6/10/2022 2:55 PM

65.031 Max  
61.715  
58.399  
55.083  
51.766  
48.45  
45.134  
41.818  
38.502  
35.185 Min



$$LSPF = \frac{\sigma_{max}}{\sigma_{lin}} = \frac{65.35}{36.304} = 1.8$$

$$S_{mag} = \frac{\sigma_{lin}}{\sigma_{mem}} = \frac{38.779 + 3.5657}{38.779} \times 1.06 = 1.16$$

**Figure 50** Calculation of LSPF and  $S_{mag}$  using linearization of stress – unequal welds between HIP headers and hubs

Similarly, the analysis is done for the other header sizes. **Table 9** shows the LSPF and  $S_{mag}$  values calculated for different header sizes. The variation of LSPF at the toe of valve- header welds for different thicknesses and toe radii is given in **Section 6** of this report which is closely related to the unequal welds between headers and hubs.

**Table 9** Analysis result summary - unequal welds between HIP headers and hubs

Header size	Dimensions	Header [nom] (mm)	Hub [max/min] (mm)	LSPF (toe)	LSPF (root)	Smag (toe)	Smag (root)
8" ID (25 Cr)	ID	203.2	202.7	1.55	1.8	1.32	1.2
	WT	32	42.1				
	OD	267.2	286.9				
9" ID (25 Cr)	ID	228.6	228.1	1.55	1.79	1.33	1.2
	WT	32	42.1				
	OD	292.6	312.3				
10" ID (25 Cr)	ID	254	253.5	1.55	1.79	1.33	1.2
	WT	32	42.1				
	OD	318	337.7				
12" ID (25 Cr)	ID	304.8	304.3	1.57	1.8	1.34	1.2
	WT	35	46				
	OD	374.8	396.3				
8" ID (22 Cr)	ID	203.2	202.7	1.58	1.8	1.32	1.2
	WT	37	48.6				
	OD	277.2	299.9				
9" ID (22 Cr)	ID	228.6	228.1	1.58	1.8	1.32	1.2
	WT	37	48.6				
	OD	302.6	325.3				
10" ID (22 Cr)	ID	254	253.5	1.58	1.8	1.33	1.2
	WT	37	48.6				
	OD	328	350.7				
12" ID (22 Cr)	ID	304.8	304.3	1.59	1.81	1.33	1.19
	WT	40	52.5				
	OD	384.8	409.3				

## 5.6 Welds between HIP headers and valves

For the welds between headers and valves, the analysis has been done for the four different header sizes (8, 9, 10, and 12-inch ID) with two different thicknesses each for 22 Cr and 25 Cr duplex steel, making it a total of 8 analysis models. The analysis details of one of the models are shown in this section. The result plots for the rest of the models are attached to **Appendix C** of this report.

### 5.6.1 Analysis model dimensions

The analysis model dimensions for the welds between HIP headers and valves are shown in **Figure 51**. Thickness at the valve side of the weld is assumed 1.3 times the header pipe wall thickness. The transition angles on the valve are taken as 30° and 45° as shown in the figure below. The weld toe and root fillet radii are taken as 3mm and 1mm respectively. For the analysis model, nominal dimensions on the header and max/ min dimensions on the valve side are used here to be conservative. The valve is made of F60 material, and the header is of duplex/ super duplex steel. The fusion line between the header and the weld is the area of interest for HISC assessment.

#### Tolerance combination considered:

##### Header Side

Nominal hub dimensions

Reference: Dimensions from TechnipFMC

##### Valve Side

ID = Nominal ID – 1 mm

OD = Nominal OD + 0.5% (nom. OD)

Reference: Tolerances from TechnipFMC

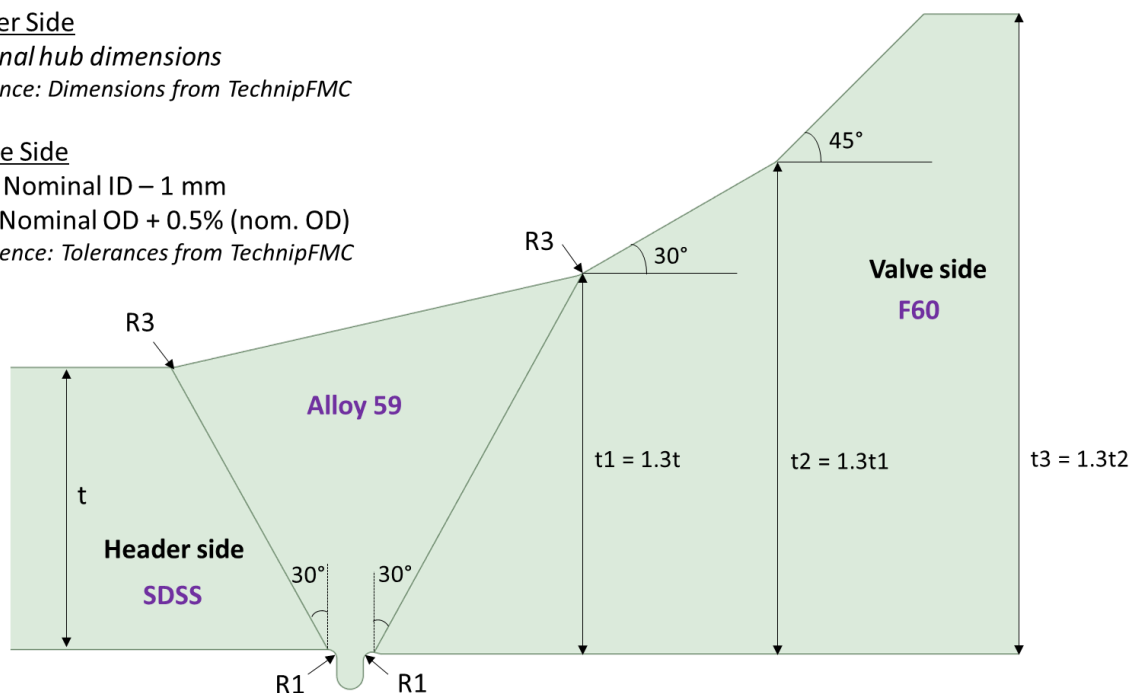


**Figure 51** Analysis model dimensions –welds between HIP headers and valves

### 5.6.2 Analysis model mesh details

The analysis model is meshed using higher-order 2D 8-node plane elements (PLANE183 in Ansys). The mesh is very finely refined at both the weld toes and root. However, the weld toe towards the hub which is at the fusion line with duplex material is of more interest for this HISC assessment study than the weld toe towards the valve which is made of F60 material. The model is checked for mesh convergence, and the details of the most refined mesh are presented in *Figure 52*.

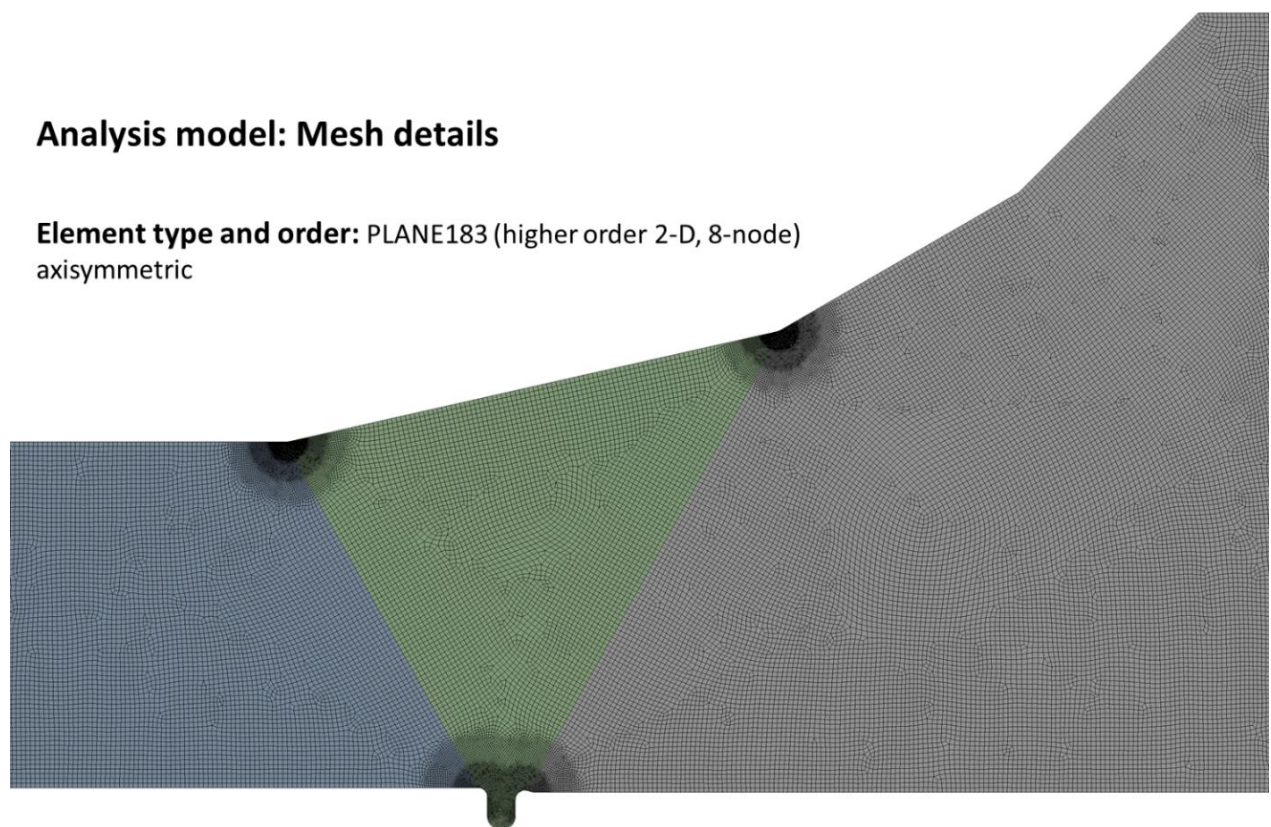


**Figure 52** Analysis model mesh details – welds between HIP headers and valves

### 5.6.3 Boundary conditions

The analysis model is loaded with a simple tensile force at one end (header side) and is rigidly fixed at the other end (valve side). No other external loads (like pressure, temperature, or bending moments) are applied. *Figure 53* shows the boundary conditions applied.



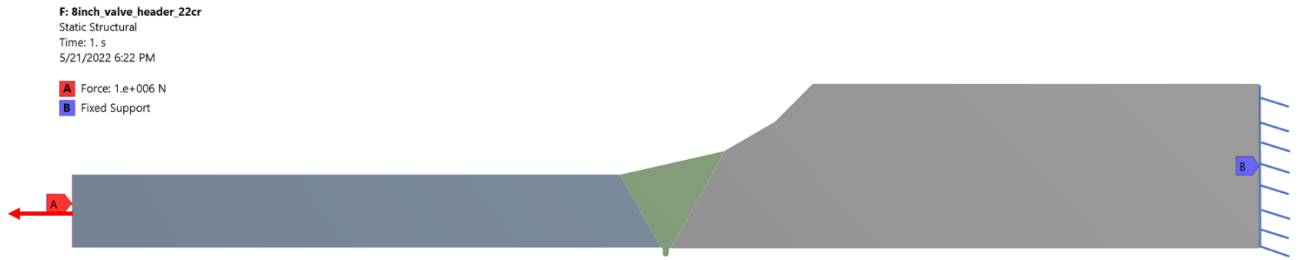


**Figure 53** Analysis model boundary conditions - welds between HIP headers and valves

### 5.6.4 Analysis results

The analysis results show that the maximum stress is at the outside weld toe towards the header, which is also the area of interest for HISC assessment. The maximum principal stress plot for one of the welds (8-inch 25 Cr duplex) is shown in **Figure 54**. The stress is linearized along the stress classification path, and the factors LSPF and  $S_{mag}$  are calculated for the hotspots at the weld toe and root, as shown in **Figure 55**.

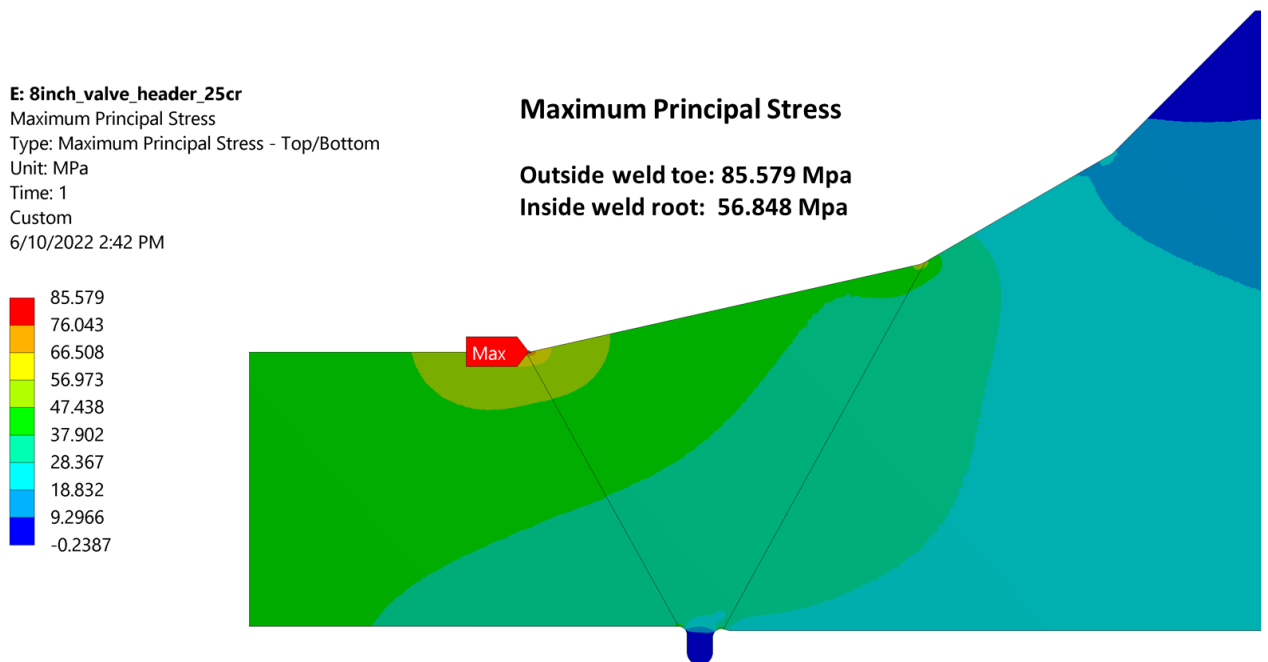
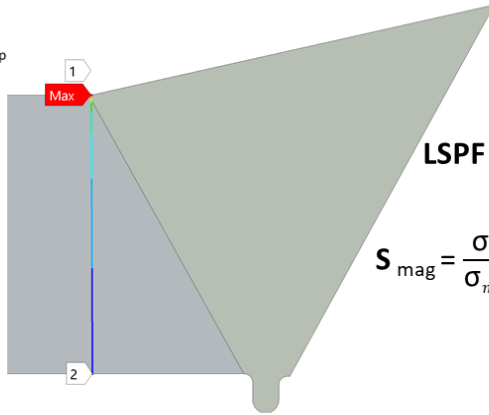
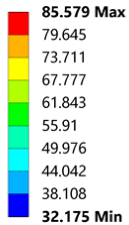


**Figure 54** Maximum principal stress plot - welds between HIP headers and valves

**Linearized Maximum Principal Stress - Weld toe**

	Length [mm]	<input checked="" type="checkbox"/> Membrane [MPa]	<input type="checkbox"/> Bending [MPa]	<input checked="" type="checkbox"/> Membrane+Bending [MPa]	<input type="checkbox"/> Peak [MPa]	<input checked="" type="checkbox"/> Total [MPa]
1	0.	42.004	13.023	54.681	30.915	85.579

E: 8inch\_valve\_header\_25cr  
 Linearized Maximum Principal Stress  
 Type: Linearized Maximum Principal Stress - Top  
 Unit: MPa  
 Global Coordinate System  
 Time: 1  
 6/10/2022 2:49 PM



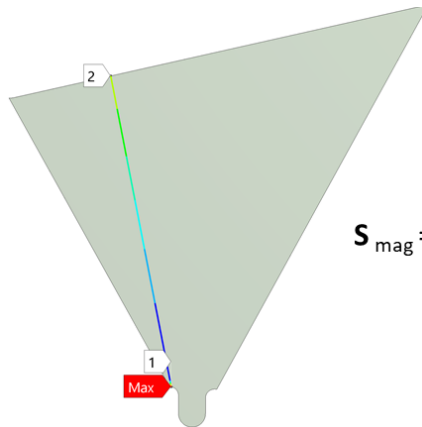
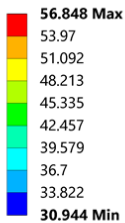
$$LSPF = \frac{\sigma_{max}}{\sigma_{lin}} = \frac{85.579}{54.681} = 1.57$$

$$S_{mag} = \frac{\sigma_{lin}}{\sigma_{mem}} = \frac{54.681}{42.004} \times 1.06 = 1.38$$

**Linearized Maximum Principal Stress – Inside Weld root**

	Length [mm]	<input checked="" type="checkbox"/> Membrane [MPa]	<input type="checkbox"/> Bending [MPa]	<input checked="" type="checkbox"/> Membrane+Bending [MPa]	<input type="checkbox"/> Peak [MPa]	<input checked="" type="checkbox"/> Total [MPa]
1	0.	38.216	2.7713	31.13	26.685	56.848

E: 8inch\_valve\_header\_25cr  
 Linearized Maximum Principal Stress 2  
 Type: Linearized Maximum Principal Stress - Top  
 Unit: MPa  
 Global Coordinate System  
 Time: 1  
 6/10/2022 2:49 PM



$$LSPF = \frac{\sigma_{max}}{\sigma_{lin}} = \frac{56.848}{31.13} = 1.83$$

$$S_{mag} = \frac{\sigma_{lin}}{\sigma_{mem}} = \frac{38.216+2.7713}{38.216} \times 1.06 = 1.14$$

**Figure 55** Calculation of LSPF and  $S_{mag}$  using linearization of stress – welds between HIP headers and valves

Similarly, the analysis is done for the other header sizes. **Table 10** shows the LSPF and  $S_{mag}$  values calculated for different header sizes. It can be observed that the LSPF values at the weld toe are comparable with the values from the unequal weld between headers and hubs calculated in **section 5.5**. The variation of LSPF at the toe of valve- header welds for different thicknesses and toe radii estimated using response surface modeling is given in **Section 6** of this report.

**Table 10** Analysis result summary - welds between HIP headers and valves

Header size	Dimensions	Header [nom] (mm)	Valve [max/ min] (mm)	LSPF (toe)	LSPF (root)	Smag (toe)	Smag (root)
8" ID (25 Cr)	ID	203.2	202.2	1.57	1.83	1.38	1.14
	WT	32	42.8				
	OD	267.2	287.8				
9" ID (25 Cr)	ID	228.6	227.6	1.57	1.83	1.4	1.13
	WT	32	42.9				
	OD	292.6	313.4				
10" ID (25 Cr)	ID	254	253	1.57	1.83	1.41	1.13
	WT	32	42.95				
	OD	318	338.9				
12" ID (25 Cr)	ID	304.8	303.8	1.6	1.83	1.43	1.13
	WT	35	47				
	OD	374.8	397.8				
8" ID (22 Cr)	ID	203.2	202.2	1.59	1.84	1.36	1.13
	WT	37	49.35				
	OD	277.2	300.9				
9" ID (22 Cr)	ID	228.6	227.6	1.6	1.84	1.38	1.13
	WT	37	49.4				
	OD	302.6	326.4				
10" ID (22 Cr)	ID	254	253	1.6	1.85	1.39	1.13
	WT	37	49.5				
	OD	328	352				
12" ID (22 Cr)	ID	304.8	303.8	1.62	1.86	1.41	1.13
	WT	40	53.5				
	OD	384.8	410.8				

These welds are also checked at lower wall thickness to see how it affects the stress concentrations. The result summary of one of such models checked for lower header thickness (20 mm) compared with the results of higher thickness models is presented in **Appendix D** attached with this report. It is observed that LSPF is increasing with thickness, Smag is decreasing with increase in thickness.

## **6. Response Surface Modeling and Results**

The response surface modeling (RSM), also known as surrogate modeling or meta-modeling, is a mathematical and statistical method commonly used for an approximate estimation or optimization of one or more output variables called response variables based on the governing input variables (Gramacy, 2020). RSMs can be used to predict the behavior of input/output (I/O) variables by using the available limited set of computationally expensive simulations (CES) (Donthi and Keprate, 2021a).

This method is based on surface placement, aiming to understand the topography of the response surface, including the local maximum, local minimum, and ridge lines, and finding the region where the most appropriate response occurs (Bradley, 2007). The design of experiments (DoE) is a crucial aspect of RSM that deals with the selection of the most appropriate training points where the response should be well examined, and this has a significant effect on determining the accuracy of the response surface construction (Aydar, 2018).

The two basic steps in constructing an RSM are training and testing. The first corresponds to fitting a model to the intelligently chosen training points, while the second step involves comparing the predictions of the model to the actual response. RSMs act as a 'curve fit' to the training data and thereafter may be used to estimate the quantity of interest without running the expensive simulation code. The RSMs must not be mistaken as a simplified version of the CES; conversely, they emulate the behavior of the CES as accurately as possible, coupled with low computational cost (Donthi and Keprate, 2021).

### **6.1 RSM coupled with FEM**

HISC assessment generally involves individual analysis and assessment of the welds through the finite element method (FEM). This practice can be time-consuming and computationally expensive, especially when there are a group of welds that are geometrically similar but dimensionally different. This practice can be improved by collecting data from a limited number of FEM assessments and using response surface models (RSM) to estimate the stress concentration factors (SCF) of similar welds. The intention here is not about using RSM as a replacement to the FEM but to use it along with FEM wherever applicable to estimate usefully accurate results to save computational time and expense.

The advantages offered by the RSM can be summarized as determining the interaction between the independent variables, modeling the system mathematically, and saving time and cost by reducing the number of trials. However, the most important disadvantage of the response surface method is that the experimental data are fitted to a polynomial model at the second order. It is not correct to say that all systems with curvature are compatible with a second-order polynomial model. In addition, experimental verification of the estimated values in the model should be done absolutely.

## 6.2 Gaussian process regression

Gaussian process regression (GPR), built on the fundamentals of spatial statistics, is a non-parametric kernel-based stochastic technique used to design an approximate model to estimate the relationship between input and output variables based on the data that is available from the observations (McFarland, 2008; Keprate et al., 2017). Unlike most machine learning models where a given input produces a single number as an output prediction, Gaussian Process offers a distribution to reflect the uncertainty in the prediction. The main aim of a GPR model (GPRM) is to use the training data obtained from expensive computer simulation to emulate the underlying relationship and thereafter to use GPRM in the future to estimate the quantity of interest without running expensive simulation code (McFarland, 2008). Furthermore, the main idea of GPRM is that the output variables (SCF for our case) assessed at different values of the input variables (pipe dimensions, weld toe radius, flank angle, centerline misalignment etc.), are modeled as a Gaussian random field, with relevant mean and covariance functions (Sankararaman, 2012).

### 6.2.1 Theory

Gaussian Process Regression is based on the idea of evaluating the response values  $Y$  at known values of the governing input variables  $X$ , modeled as a Gaussian random field, with relevant mean and covariance functions (Sankararaman, 2012). Let's say in a  $d$ -dimensional input vector there are  $m$  training points,  $x_1, x_2, x_3 \dots x_m$  corresponding to each, governing the output values  $Y(x_1), Y(x_2), Y(x_3) \dots Y(x_m)$ . These training points can be written as  $x_t$  vs.  $y_t$  where,  $x_t$  is a  $m \times n$  and  $y_t$  is a  $m \times 1$  vector. To estimate the response ( $y_p$ ) corresponding to an input vector  $x_p$  ( $p \times d$  matrix), the joint density of the output values  $y_p$  can be calculated as:

$$P(y_p | x_p, x_t, y_t, \theta) \sim N(m, s)$$

Here,  $\theta$  denotes the hyper-parameters of the GP, the value of which is evaluated by the training data. The prediction mean ( $m$ ) and covariance matrix ( $S$ ) are given by:

$$m = K_{PT}(K_{TT} + \sigma_n^2 I)^{-1} y_T$$

$$S = K_{PP} - K_{PT}(K_{TT} + \sigma_n^2 I)^{-1} K_{TP}$$

Here,  $K_{TT}$  is the covariance function matrix (also known as Kernel) for the input training points ( $x_t$ ), and  $K_{PT}$  is the covariance function matrix for the input prediction point ( $x_p$ ) and the input training points ( $x_t$ ) (Sankararaman, 2012).

### Matern kernel

The Matern kernel in GPR is a stationary kernel parameterized by a length-scale parameter ( $l$ ) and  $\nu$ , which controls the smoothness of the resulting function (Rasmussen and Williams, 2006) and this can be written as,

$$K_{ij} = K(x_i, x_j, \theta) = \sigma^2 \frac{2^{1-\nu}}{\Gamma(\nu)} \left( \frac{\sqrt{2\nu}r}{l} \right)^\nu K_\nu \left( \frac{\sqrt{2\nu}r}{l} \right)$$

Here,  $r$  is the Euclidean distance,  $K_\nu(\cdot)$  is a modified Bessel function and  $\Gamma(\cdot)$  is the gamma function. The flexibility of controlling the smoothness of the learned function via ' $\nu$ ' allows adapting to the properties of the true underlying functional relation (scikit-learn, 2022). The computation of the Kernel matrix requires the computation of hyper parameters  $\Theta$ , which include the length scale ( $l$ ), the noise standard deviation ( $\sigma$ ), and the parameter ' $\nu$ '. These hyper parameters are calculated using the input training data and maximizing the following log-likelihood function (Sankararaman, 2012):

$$\log(y_t|x_t; \theta) = \frac{y_T^T}{2} (K_{TT} + \sigma_n^2 I)^{-1} y_T - \frac{1}{2} \log|K_{TT} + \sigma_n^2 I| + \frac{d}{2} \log(2\pi)$$

## 6.3 LSPF estimation using Gaussian process regression

### 6.3.1 Training the GPR model

Welds between headers and valves of an on-template manifold are used for this study by varying the weld geometric parameters. Initially, the LSPF at the weld toe is calculated using

FEA for a limited number of models by varying the parameters like the header size, wall thickness, and toe radius as given in **Figure 56** below. The data is used to train the GPR model to estimate the LSPF for different combinations of these parameters. The FEA data used to train the model is given in **Appendix E** of this report.

### Weld parameters for GPRM

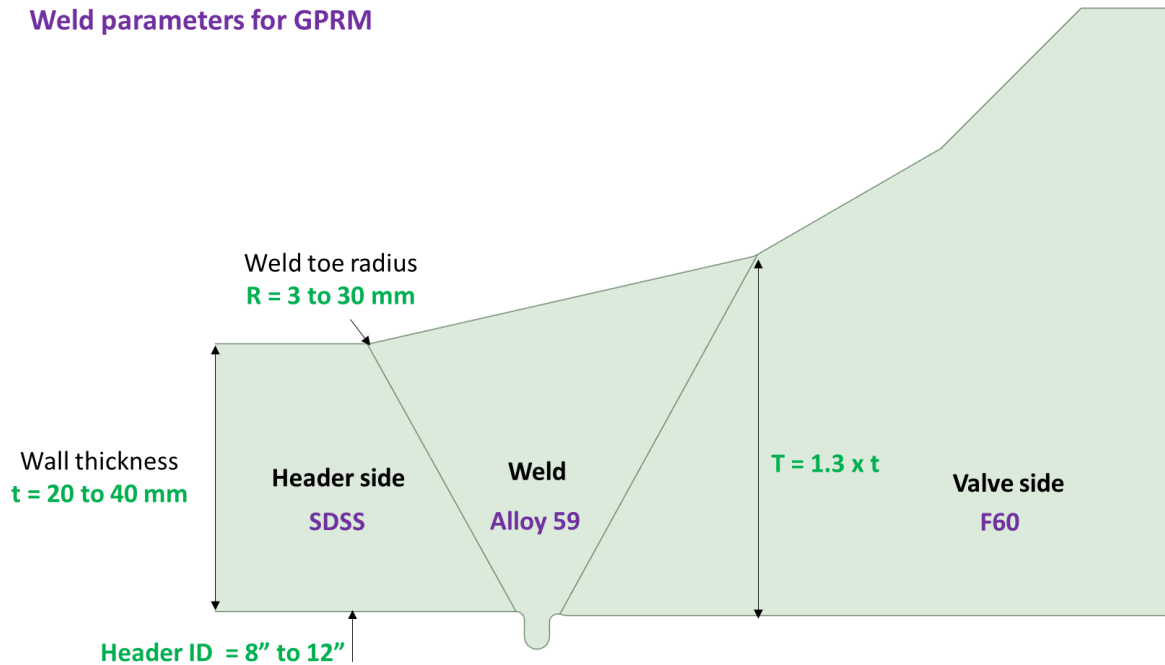


**Figure 56** Variation of weld parameters used for GPRM training

To check the dependency of LSPF on various geometric parameters, by calculating the correlation coefficients, it is found that the header size (ID of the header) has minimal impact on the LSPF at the weld toe, suggesting that the LSPF for different headers with IDs between 8-inch and 12-inch are approximately the same provided they are of the same thickness and have same weld toe radius. Weld toe radius is found to be the most influential geometric parameter affecting the LSPF. As shown in **Figure 57**, weld toe radius (R) has the highest correlation to LSPF, and the negative sign indicates that an increase in weld toe radius will decrease the LSPF and vice versa.

It can also be observed that the thickness of the header/ valve has a significant influence on the LSPF. Higher wall thickness would increase the LSPF at the weld toe and lower wall thickness would help the stress distribute more evenly resulting in a decrease in the stress concentration at the hotspot.

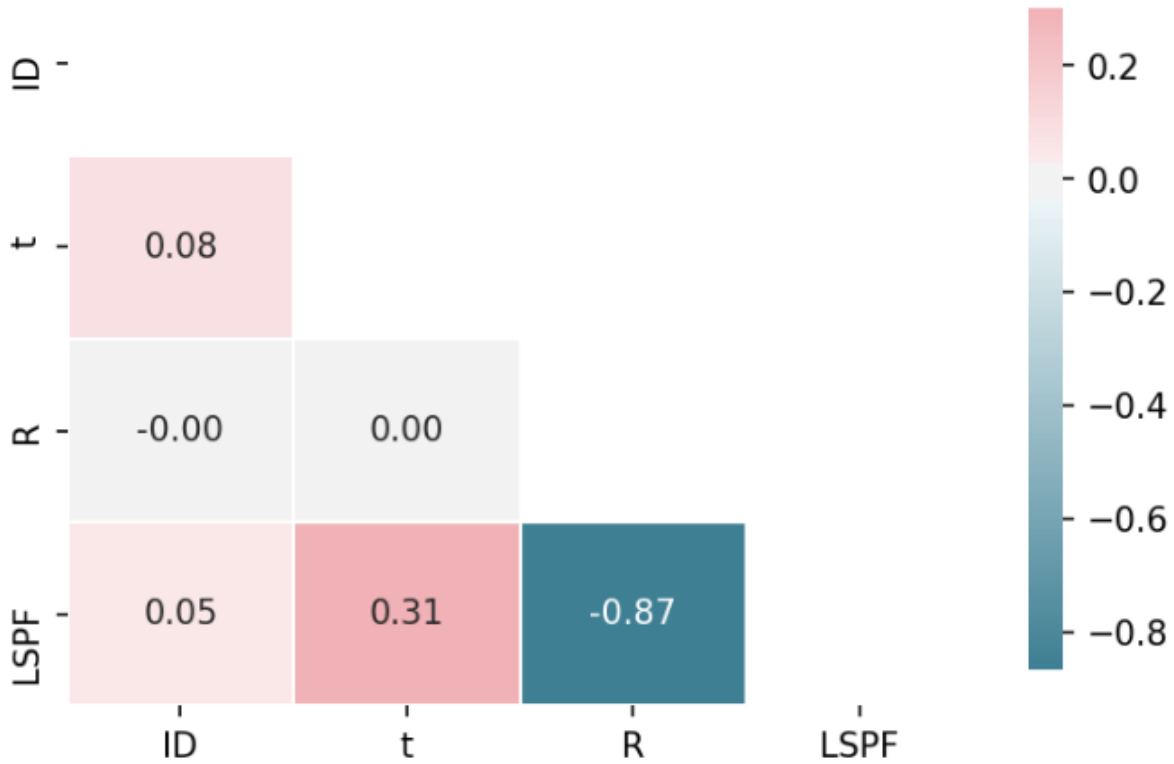


**Figure 57** Correlation coefficients between the input and output variables

### 6.3.2 Testing the GPR model

To test the GPR model, random values from the same training input data as well as some new values specifically used for testing the model generated from FEA are used. K-fold cross validation technique can be used to evaluate the accuracy of the GPR Algorithm by calculating the performance metrics called Root Mean Square Error (RMSE), Mean Absolute Error (MAE), and Explained Variance Score (EVS) (Donthi and Keprate, 2021). These metrics can be mathematically written as:

$$RMSE = \sqrt{\frac{[\sum_{i=1}^n (y_i - \bar{y}_i)^2]}{n}}$$

$$MAE = \sum_{i=1}^n \frac{|y_i - \bar{y}_i|}{n}$$

$$EVS = 1 - \frac{var(y_i - \bar{y}_i)}{var(y_i)}$$



Where,  $y_i$  and  $\bar{y}_i$  are actual and predicted output variables and  $n$  is the number of data points used for the GPRM.

The RMSE and MAE values of the GPR model should be as low as possible (closer to 0) and the EVS closer to 1 for the model to be called accurate. The calculated performance metrics for the current GPR model are given below:

**Table 11** performance metrics for the GPR model

Root Mean Square Error (RMSE)	0.0096
Mean Absolute Error (MAE)	0.0081
Explained Variance Score (EVS)	0.9869

The plot between actual (FEA) and predicted LSPF (from GPRM) values are in **Figure 58** given below, and it shows that the general trend is almost linear with only a few outliers indicating a good accuracy of the GPR model.

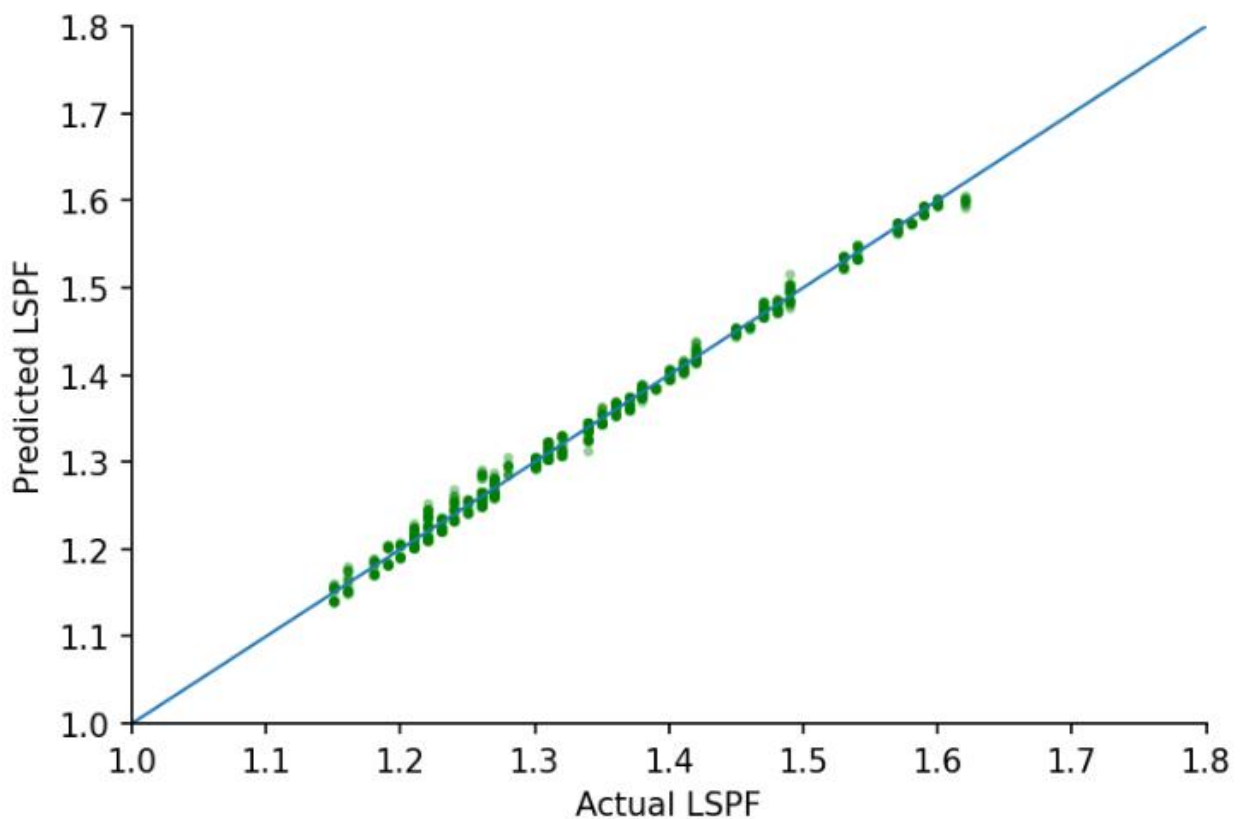


**Figure 58** Actual (FEA) vs. Predicted (GPRM) LSPF values for the weld toe (70 test points)

## 6.4 Estimated LSPF values

**Figure 59** shows the LSPF plots for headers with various thicknesses ranging from 20mm to 40mm against varying the weld toe radius from 3mm to 30mm. From observations that ID of the header had the least influence on the LSPF, these values can be used as same for all the header sizes from 8-inch ID and 12-inch ID. The values used for plotting these graphs are given in a tabular form in **Appendix E** of this report. LSPF values can be estimated for more combinations of thickness and toe radii id required using the same GPR model.

These LSPF plots shown in **Figure 59** can also be used for the unequal welds between headers and hubs conservatively, as they have similar stress distribution and slightly lower LSPF values at the weld toe (near the header- weld fusion line).

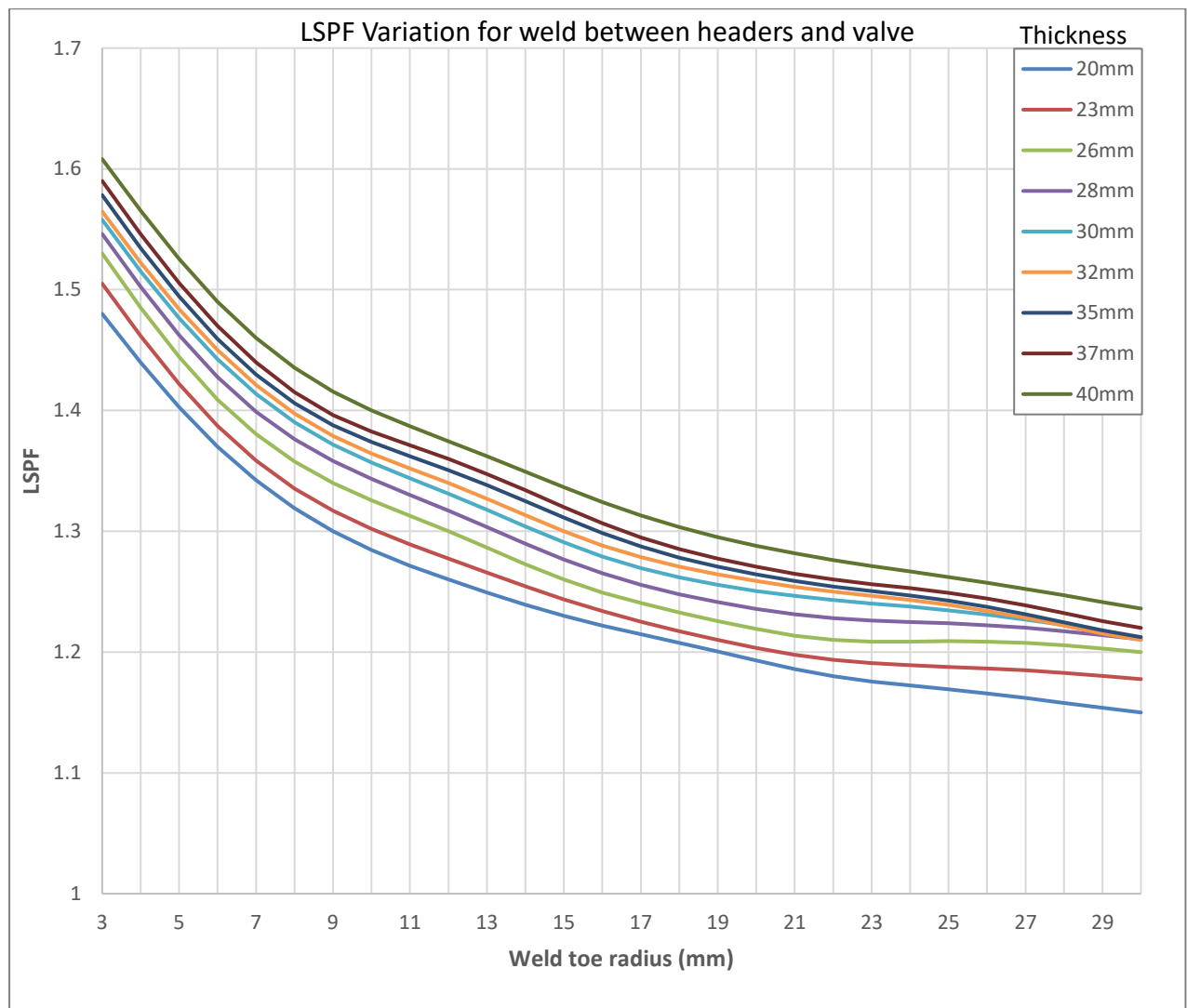


**Figure 59** Estimated LSPF variation for welds between headers and valves

## 7. Result Discussion and Conclusions

The FEA results of the equal weld between 6-inch pipe and winghub show high stress concentration on the internal surface at the root of the weld. This is because of the large tolerances on the ID of the pipe combined with the centerline misalignment between the welded components. The stress concentration on the external surface at the weld toe is relatively lower and using a flat transition instead of convex-shaped weld cap is helping to reduce the local surface penalty factor significantly.

For the unequal weld between the 6-inch pipe and winghub, the highest stress is at the outside toe of the weld. This is because of the larger OD and thickness on the hub side compared to the pipe side. The stress concentration can be reduced significantly by increasing the toe fillet radius if required. The stress magnification factors estimated at some weld geometries are compared with the values calculated using the formulae from DNVGL-RP-C203, wherever applicable, and found that they are in line with the analytical calculations.

The fillet weld between doubler plate and pipe with high stress concentrations that couldn't meet the linear elastic assessment criteria is checked and qualified with the actual loads from project pipe stress analysis. The results indicate that the peak and membrane strains at the weld toe are lower than, but still very close to, the maximum allowable peak and membrane strains calculated as per category 2 assessment criteria.

For the equal welds between headers and hubs, the highest stress is on the internal surface at the root of the weld. In this case, the high LSPF values on the inside root may not be of real concern in relation to HISC. This is because the minimum wall thickness of headers analyzed is high enough that sufficient hydrogen might not diffuse to the inside surface of the header in its project lifetime. However, if it is required to use headers of lower wall thickness the stress at the root could be concerning.

The FEA results of the unequal welds of header – hub and header – valve show the highest stress concentration at the outside toe near the fusion line between the duplex/ super duplex header and the Alloy 59 weld, which is the primary area of interest for HISC assessment. When checked for headers with different thicknesses it is observed that LSPF is increasing with thickness,  $S_{mag}$  is decreasing with an increase in thickness.

The additional stress concentration induced by the secondary bending moments in the welds due to centerline misalignment between the components is estimated using a 3D finite element model of the weld. It is found that this additional stress is about 10% for the pipe – winghub welds and equal welds of header – hub. For unequal welds of header – hub and header – valve, the additional stress due to centerline misalignment is about 5-6%. Based on these results, the analysis models are simplified to axisymmetric models and  $S_{mag}$  values are increased by the same amount to approximately estimate the values without doing a 3D assessment saving the computational time and expense.

The Gaussian process regression model is used to predict the stress concentration factors at different combinations of geometric parameters based on the available FEA data and is found to be reasonably accurate when tested with random values from the estimated FEA data. It was found that the local surface penalty/ magnification factors are almost the same for different header sizes checked, provided they are of the same thickness and weld parameters. Variation of the local surface penalty/ magnification factors for different combinations of wall thickness and toe fillet radius is calculated and plotted which can be used as a reasonable estimation. These LSPF plots can also be used for the unequal welds between headers and hubs conservatively, as they have similar stress distribution and slightly lower LSPF values.

### **Scope for future work**

As the weld parameters like flank angle and centerline misalignment were checked for some fixed values, it would be interesting to study the variation of the stress concentration factors for different values of these parameters. Another area of interest is developing some simple formulae instead of using GPRM to approximately calculate the LSPF and  $S_{mag}$  values at the welds wherever possible.

The GPRM can be extended to more input variables if it is required to include any other geometric parameters of the welds that are not considered now. The  $S_{mag}$  variation for different header sizes and thicknesses can be estimated similarly if the data is available from a reasonable number of FE models.

## References

- ANSYS Mechanical, Finite Element Analysis Software for Structural Engineering, 2021: Canonsburg, Pennsylvania, United States, ANSYS, Inc.
- ANSYS SpaceClaim - 3D CAD Modeling Software, 2021: Canonsburg, Pennsylvania, United States, ANSYS, Inc.
- ASME, 2019, Industry Standard BPVC-VIII-2 Rules for Construction of Pressure Vessels Division: American Petroleum Institute, Washington, D.C.
- Aydar, A. Y., 2018, Utilization of Response Surface Methodology in Optimization of Extraction of Plant Materials, *in* V. Silva, ed., Statistical Approaches with Emphasis on Design of Experiments Applied to Chemical Processes: Rijeka, Intech Open, doi:10.5772/intechopen.73690.
- Bradley, N., 2007, The Response Surface Methodology: Indiana University South Bend.
- Cassagne, T., and F. Busschaert, 2005, A Review on Hydrogen Embrittlement of Duplex Stainless Steels.
- DNV, 2008, Recommended Practice DNV-RP-F112 Design of Duplex Stainless Steel Subsea Equipment Exposed to Cathodic Protection: Det Norske Veritas, Høvik, Norway.
- DNVGL, 2016, Recommended Practice DNVGL-RP-C203 Fatigue design of offshore steel structures: Det Norske Veritas, Høvik, Norway.
- DNVGL, 2019, Recommended Practice DNVGL-RP-F112 Duplex stainless steel – design against hydrogen induced stress cracking: Det Norske Veritas, Høvik, Norway.
- Donthi, N., and A. Keprate, 2021, Prediction of Stress Correction Factor for Welded Joints Using Response Surface Models, *in* Proceedings of the ASME 2021 40th International Conference on Ocean, Offshore and Arctic Engineering, OMAE2021, Virtual, online: ASME.
- Gramacy, R. B., 2020, Surrogates: Gaussian process modeling, design and optimization for the applied sciences: Boca Raton, Florida, Chapman Hall/CRC.
- HAIHAO Piping, 2021, What is Hydrogen-Induced Cracking (HIC)? accessed November 2, 2021, [www.haihaopiping.com](http://www.haihaopiping.com).
- Keprate, A., R. M. Ratnayake, and S. Shankar, 2017, Adaptive Gaussian process regression as an alternative to FEM for prediction of stress intensity factor to assess fatigue degradation in offshore pipeline: International Journal of Pressure Vessels and Piping, v. 153.
- Krosness, O. M., 2014, Connection Between Critical Stress and Hydrogen Content for SDSS under Cathodic Protection: NTNU, Trondheim, Norway (Master Thesis), <https://ntnuopen.ntnu.no/ntnu-xmlui/handle/11250/249554>.

- McFarland, J. M., 2008, Uncertainty analysis for computer simulations through validation and calibration, (Doctoral dissertation), <https://core.ac.uk/download/pdf/46926696.pdf>
- Paul, S., 2022, FORMS OF CORROSION: accessed May 30, 2022, <http://education.sptech.xyz>.
- Press, W. H., W. H. Press, B. P. Flannery, S. A. Teukolsky, W. T. Vetterling, B. P. Flannery, and W. T. Vetterling, 1989, Numerical Recipes in Pascal (First Edition): The Art of Scientific Computing: Cambridge University Press.
- Rasmussen, C. E., and C. K. I. Williams, 2006, Gaussian processes for machine learning: Cambridge, Mass, MIT Press, Adaptive computation and machine learning, 248 p.
- Sankararaman, S., 2012, Uncertainty quantification and integration in engineering systems, PhD Dissertation: Vanderbilt University.
- scikit-learn, 2022, Gaussian Processes Kernels: accessed May 25, 2022, [https://scikit-learn/stable/modules/gaussian\\_process.html](https://scikit-learn/stable/modules/gaussian_process.html).
- Skotny, Ł., 2019, Why is a Triangular Element Stiffer? ,[www.enterfea.com](http://www.enterfea.com).
- Solnørdal, M., S. Wästberg, G. Heiberg, and O. Hauås-Eide, 2009, Hydrogen induced stress cracking (HISC) and DNV-RP-F112: Measurement and Control, v. 42, p. 145–148, doi:10.1177/002029400904200504.
- TechnipFMC.com, 2021, TechnipFMC plc: accessed March 24, 2022, [www.technipfmc.com](http://www.technipfmc.com).

# Appendix - A

**SCF calculation at the equal weld between HIP header and hub**

LSFP<sub>Cat 1</sub> & S<sub>mag</sub> calculations using FEA

## Analysis results Summary

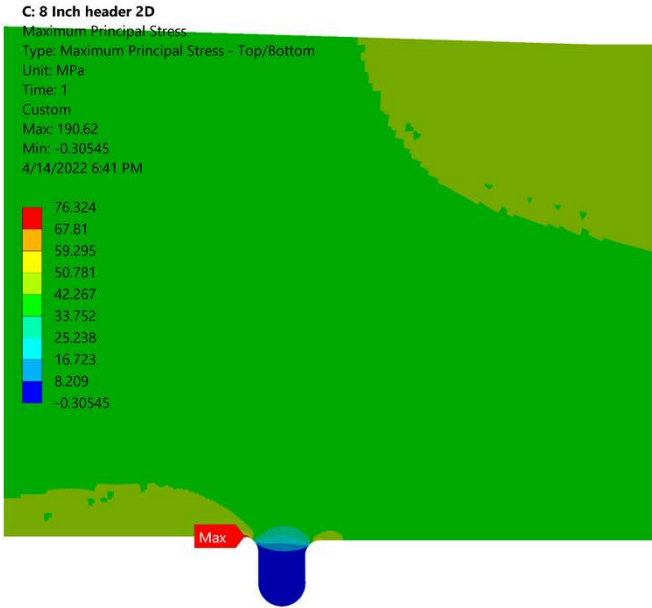
25%Cr duplex				
8" ID	Header (max)	Hub/ valve (nom)	LSPF	Smag
ID	203.7 (203.2+0.5)	203.2	1.11 (outside toe)	1.14 (outside toe)
WT	33 (32+1)	32	1.78 (inside root)	1.1 (inside root)
OD	269.7 (ID + 2WT)	267.2		
9" ID	Header (max)	Hub/ valve (nom)	LSPF	Smag
ID	229.1 (228.6+0.5)	228.6	1.11 (outside toe)	1.15 (outside toe)
WT	33 (32+1)	32	1.79 (inside root)	1.13 (inside root)
OD	295.1 (ID + 2WT)	292.6		
10" ID	Header (max)	Hub/ valve (nom)	LSPF	Smag
ID	254.5 (254+0.5)	254	1.11 (outside toe)	1.15 (outside toe)
WT	33 (32+1)	32	1.79 (inside root)	1.13 (inside root)
OD	320.5 (ID + 2WT)	318		
12" ID	Header (max)	Hub/ valve (nom)	LSPF	Smag
ID	305.3 (304.8+0.5)	304.8	1.12 (outside toe)	1.16 (outside toe)
WT	36 (35+1)	35	1.79 (inside root)	1.11 (inside root)
OD	377.3 (ID + 2WT)	374.8		

22%Cr duplex				
8" ID	Header (max)	Hub/ valve (nom)	LSPF	Smag
ID	203.7 (203.7+0.5)	203.2	1.1 (outside toe)	1.14 (outside toe)
WT	38 (37+1)	37	1.8 (inside root)	1.12 (inside root)
OD	279.7 (ID + 2WT)	277.2		
9" ID	Header (max)	Hub/ valve (nom)	LSPF	Smag
ID	229.1 (228.6+0.5)	228.6	1.1 (outside toe)	1.15 (outside toe)
WT	38 (37+1)	37	1.81 (inside root)	1.12 (inside root)
OD	305.1 (ID + 2WT)	302.6		
10" ID	Header (max)	Hub/ valve (nom)	LSPF	Smag
ID	254.5 (254+0.5)	254	1.1 (outside toe)	1.15 (outside toe)
WT	38 (37+1)	37	1.8 (inside root)	1.12 (inside root)
OD	330.5 (ID + 2WT)	328		
12" ID	Header (max)	Hub/ valve (nom)	LSPF	Smag
ID	305.3 (304.8+0.5)	304.8	1.11 (outside toe)	1.14 (outside toe)
WT	41 (40+1)	40	1.8 (inside root)	1.13 (inside root)
OD	387.3 (ID + 2WT)	384.8		

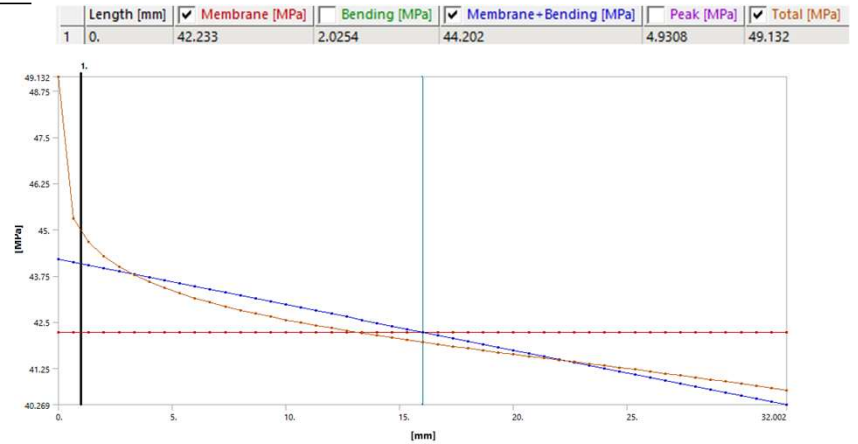
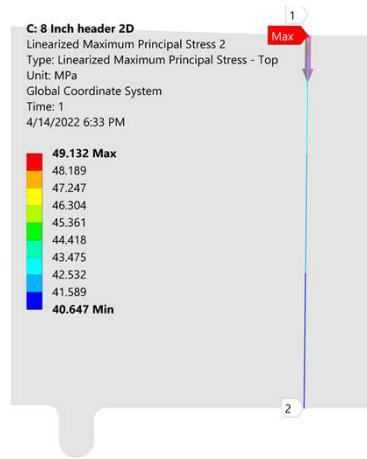


# 2D Axisymmetric analysis Results 8 inch Header 25Cr

## Maximum Principal Stress



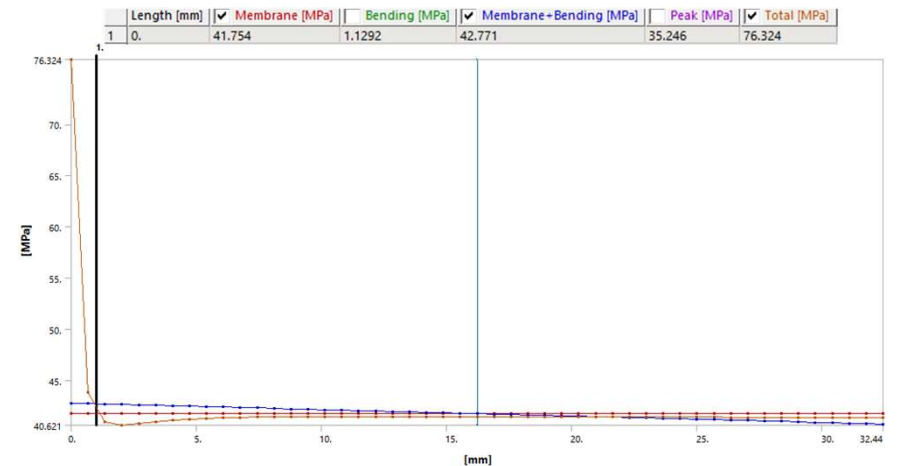
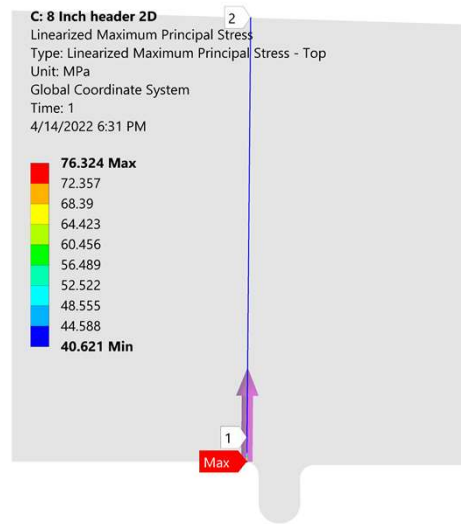
### Linearized Maximum Principal Stress - Weld toe



$$LSPF = \frac{\sigma_{max}}{\sigma_{lin}} = \frac{49.132}{44.202} = 1.11$$

$$S_{mag} = \frac{\sigma_{lin}}{\sigma_{mem}} = \frac{44.202}{42.233} = 1.04$$

### Linearized Maximum Principal Stress - Inside Weld root

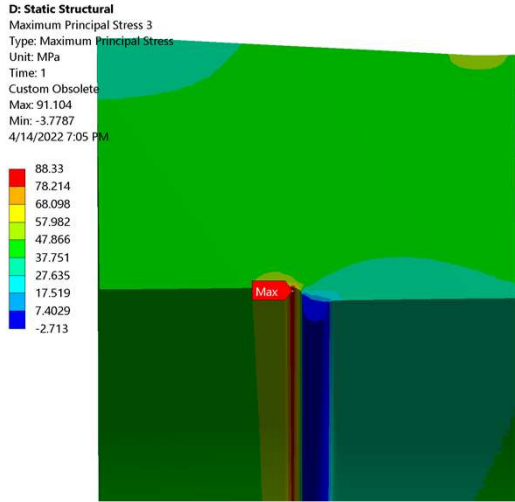


$$LSPF = \frac{\sigma_{max}}{\sigma_{lin}} = \frac{76.324}{42.771} = 1.78$$

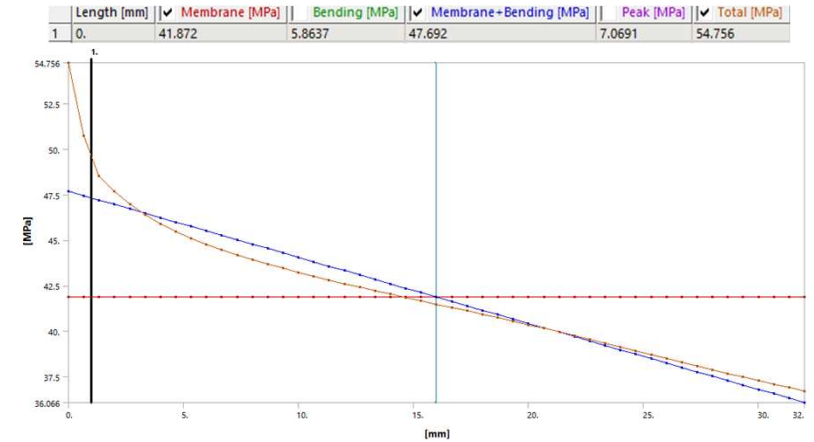
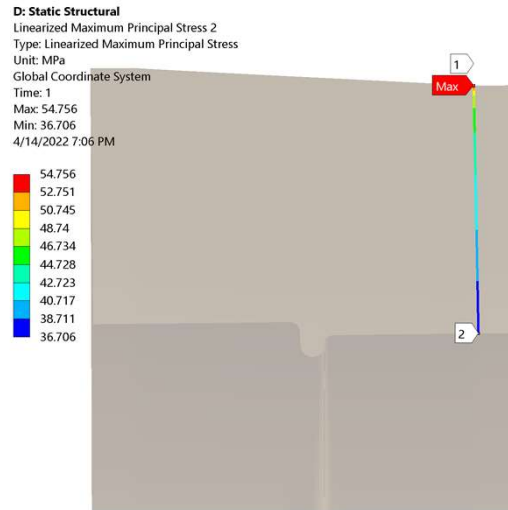
$$S_{mag} = \frac{\sigma_{lin}}{\sigma_{mem}} = \frac{42.771}{41.754} = 1.02$$

### 3D analysis Results 8 inch Header 25Cr (with 1.6mm Center line misalignment )

#### Maximum Principal Stress

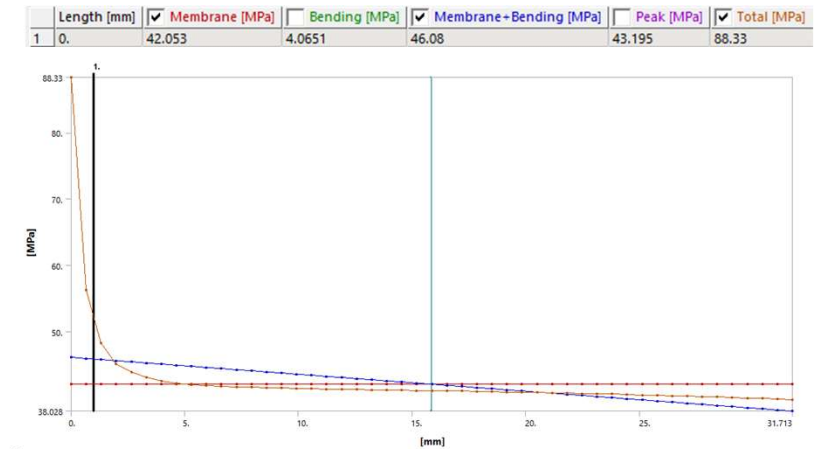
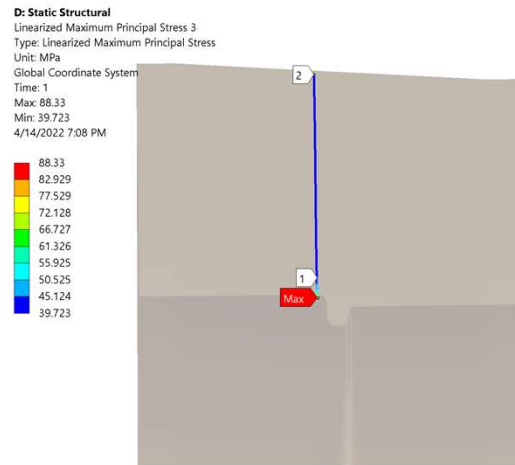


### Linearized Maximum Principal Stress - Weld toe



$$S_{mag} = \frac{\sigma_{lin}}{\sigma_{mem}} = \frac{47.69}{41.87} = 1.14$$

### Linearized Maximum Principal Stress – Inside Weld root



$$S_{mag} = \frac{\sigma_{lin}}{\sigma_{mem}} = \frac{46.08}{42.05} = 1.1$$

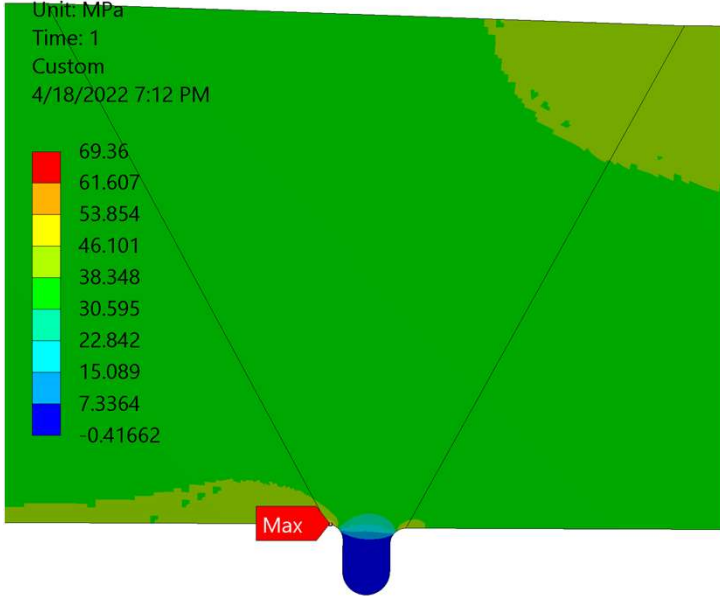
**Note:** It is observed that the  $S_{mag}$  was approx. 10% higher in case of model with center-line misalignment compared to no center-line misalignment.

Going by this, only axisymmetric 2D analysis is done for the remaining header sizes and the  $S_{mag}$  value is increased by 10%.

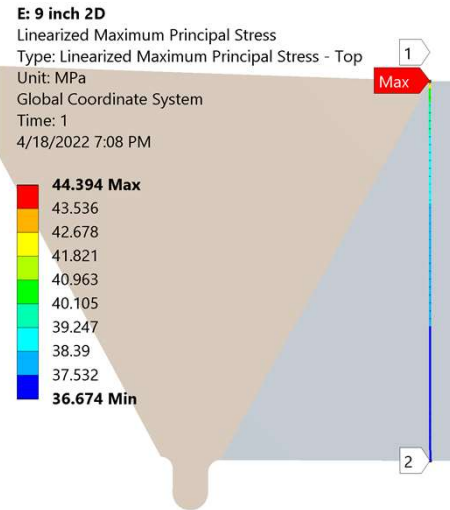
# 9 inch Header 25Cr

## Maximum Principal Stress

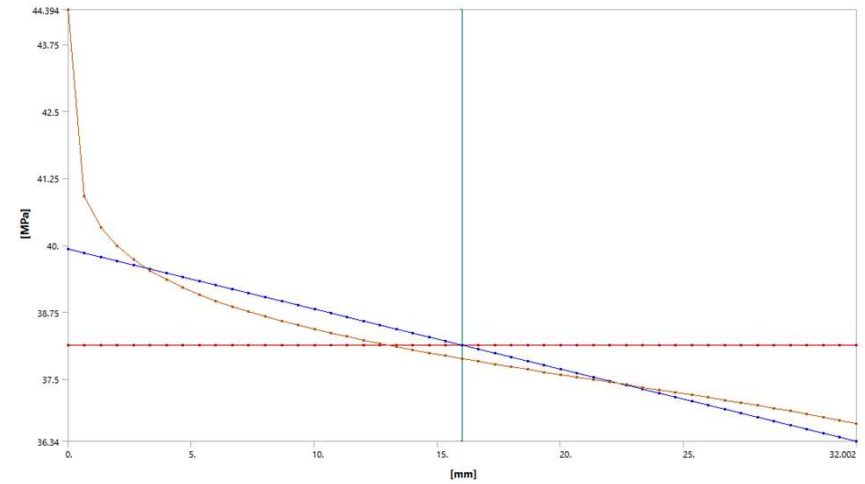
**E: 9 inch 2D**  
 Maximum Principal Stress  
 Type: Maximum Principal Stress - Top/Bottom  
 Unit: MPa  
 Time: 1  
 Custom  
 4/18/2022 7:12 PM



## Linearized Maximum Principal Stress - Weld toe

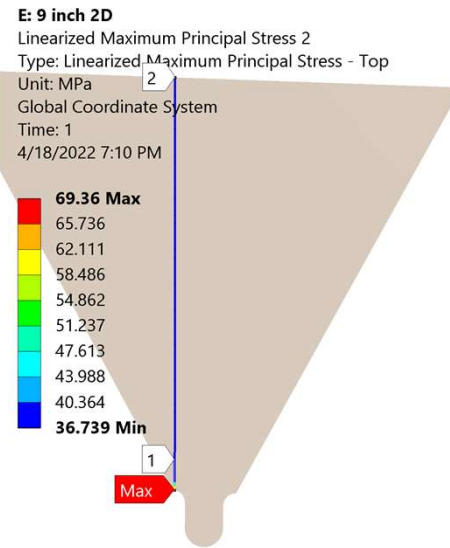


Length [mm]	Membrane [MPa]	Bending [MPa]	Membrane+Bending [MPa]	Peak [MPa]	Total [MPa]
1	0.	38.129	1.8426	39.921	4.4731

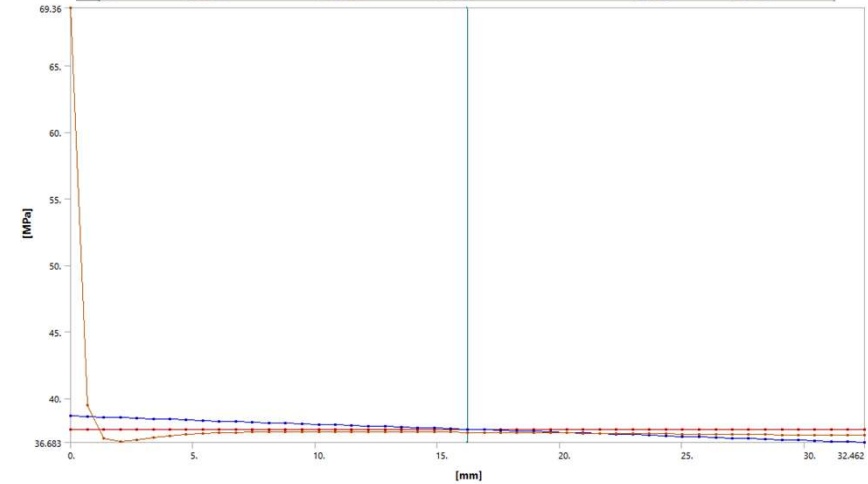


$$LSPF = \frac{\sigma_{max}}{\sigma_{lin}} = \frac{44.394}{39.921} = 1.11 \quad S_{mag} = \frac{\sigma_{lin}}{\sigma_{mem}} = \frac{39.921}{38.129} \times 1.1 = 1.15$$

## Linearized Maximum Principal Stress - Inside Weld root



Length [mm]	Membrane [MPa]	Bending [MPa]	Membrane+Bending [MPa]	Peak [MPa]	Total [MPa]
1	0.	37.671	1.0197	38.66	33.367

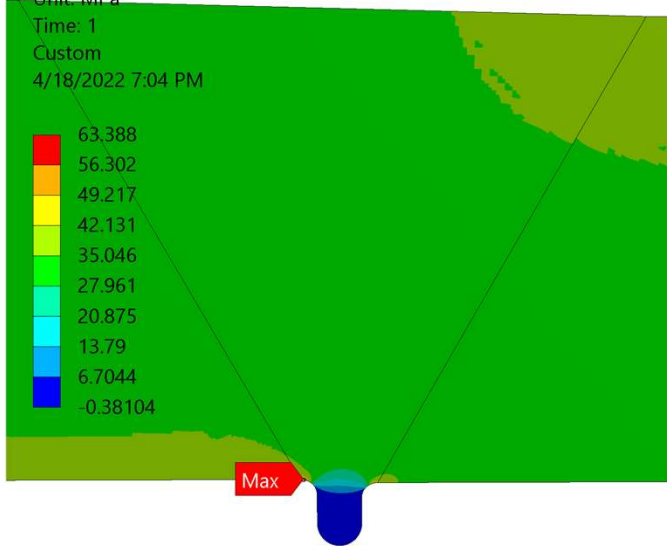


$$LSPF = \frac{\sigma_{max}}{\sigma_{lin}} = \frac{69.36}{38.66} = 1.79 \quad S_{mag} = \frac{\sigma_{lin}}{\sigma_{mem}} = \frac{38.66}{37.671} \times 1.1 = 1.13$$

# 10 inch Header 25Cr

## Maximum Principal Stress

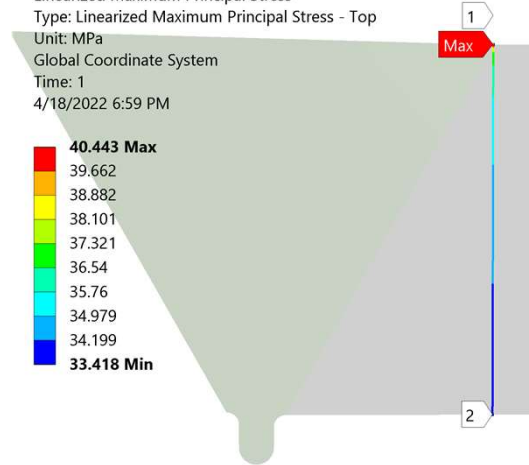
F: 10 inch 2D  
 Maximum Principal Stress  
 Type: Maximum Principal Stress - Top/Bottom  
 Unit: MPa  
 Time: 1  
 Custom  
 4/18/2022 7:04 PM



## Linearized Maximum Principal Stress - Weld toe

F: 10 inch 2D  
 Linearized Maximum Principal Stress  
 Type: Linearized Maximum Principal Stress - Top  
 Unit: MPa  
 Global Coordinate System  
 Time: 1  
 4/18/2022 6:59 PM

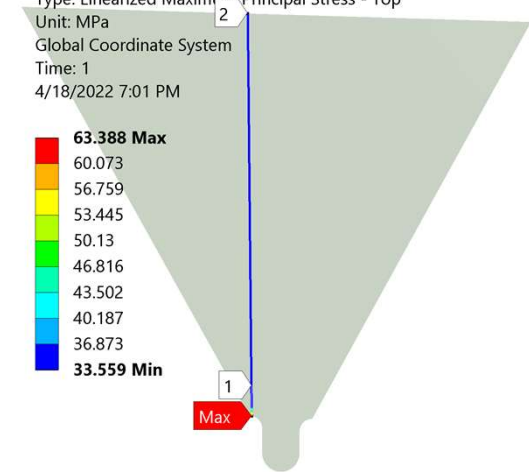
40.443 Max  
 39.662  
 38.882  
 38.101  
 37.321  
 36.54  
 35.76  
 34.979  
 34.199  
 33.418 Min



## Linearized Maximum Principal Stress - Inside Weld root

F: 10 inch 2D  
 Linearized Maximum Principal Stress 2  
 Type: Linearized Maximum Principal Stress - Top  
 Unit: MPa  
 Global Coordinate System  
 Time: 1  
 4/18/2022 7:01 PM

63.388 Max  
 60.073  
 56.759  
 53.445  
 50.13  
 46.816  
 43.502  
 40.187  
 36.873  
 33.559 Min

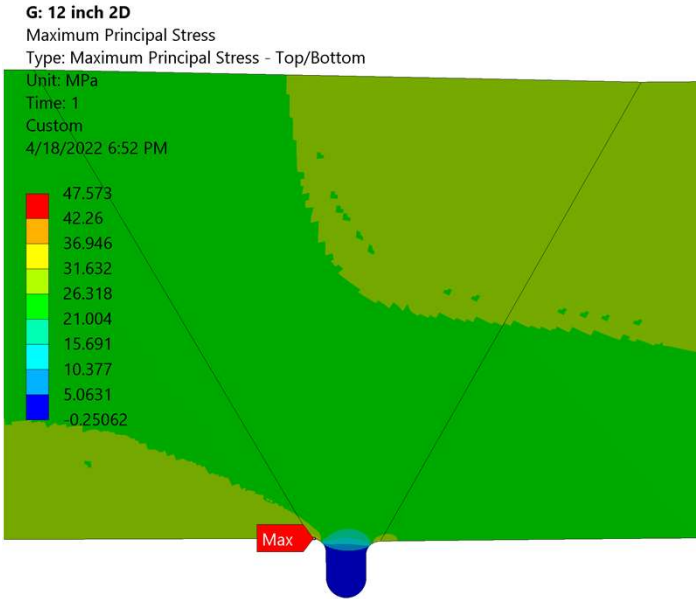


$$LSPF = \frac{\sigma_{max}}{\sigma_{lin}} = \frac{40.443}{36.377} = 1.11 \quad S_{mag} = \frac{\sigma_{lin}}{\sigma_{mem}} = \frac{36.377}{34.744} \times 1.1 = 1.15$$

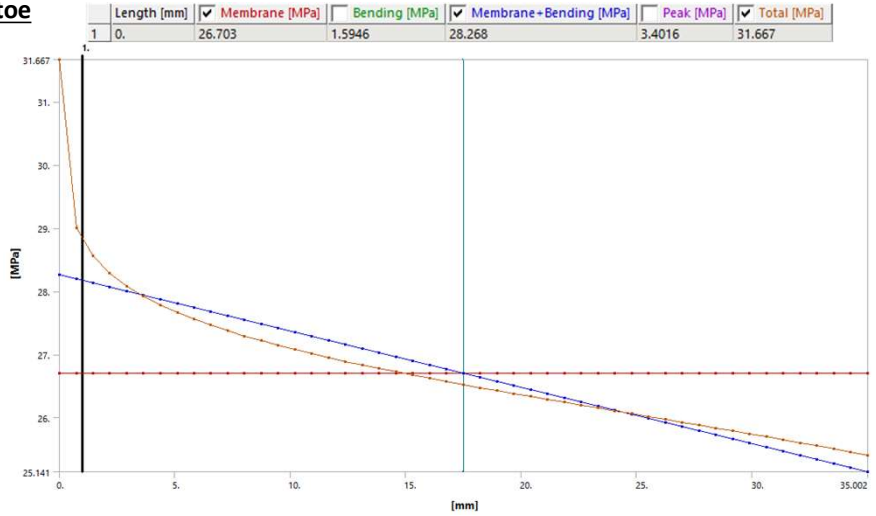
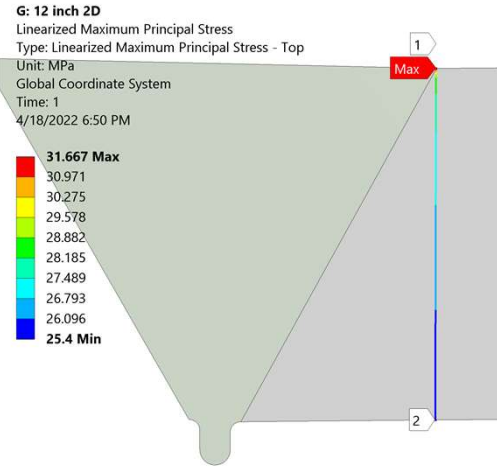
$$LSPF = \frac{\sigma_{max}}{\sigma_{lin}} = \frac{63.388}{35.324} = 1.79 \quad S_{mag} = \frac{\sigma_{lin}}{\sigma_{mem}} = \frac{35.324}{34.336} \times 1.1 = 1.13$$

# 12 inch Header 25Cr

## Maximum Principal Stress

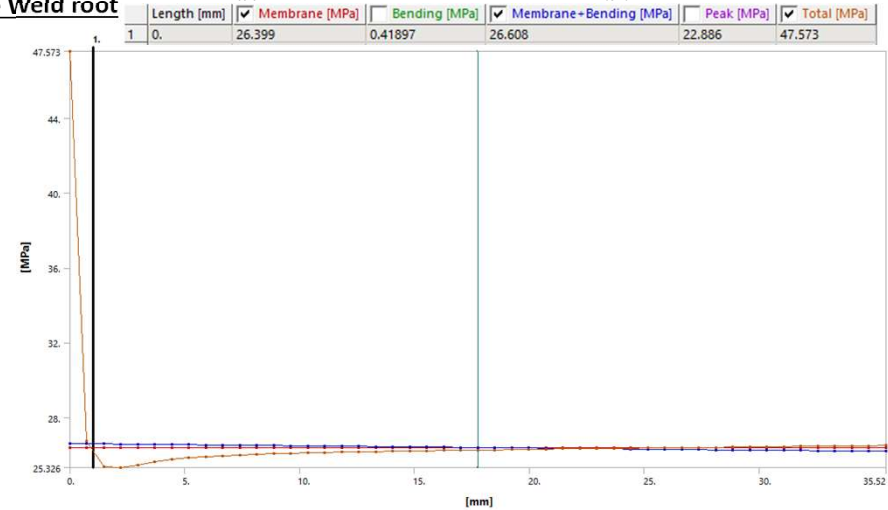
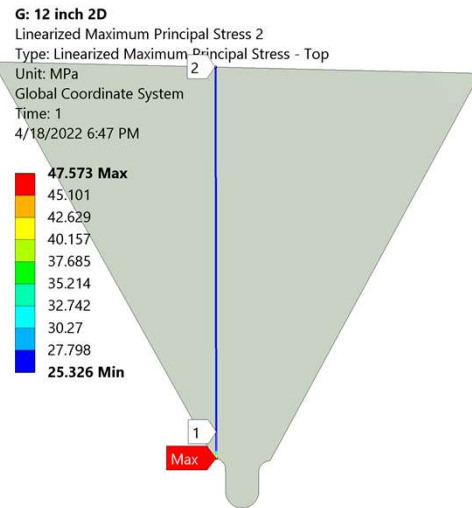


## Linearized Maximum Principal Stress - Weld toe



$$LSPF = \frac{\sigma_{max}}{\sigma_{lin}} = \frac{31.667}{28.268} = 1.12 \quad S_{mag} = \frac{\sigma_{lin}}{\sigma_{mem}} = \frac{28.268}{26.703} \times 1.1 = 1.16$$

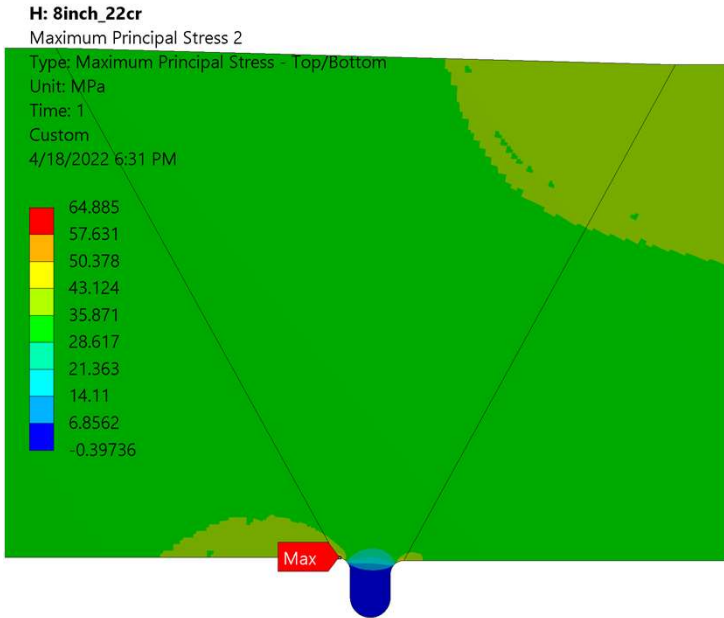
## Linearized Maximum Principal Stress - Inside Weld root



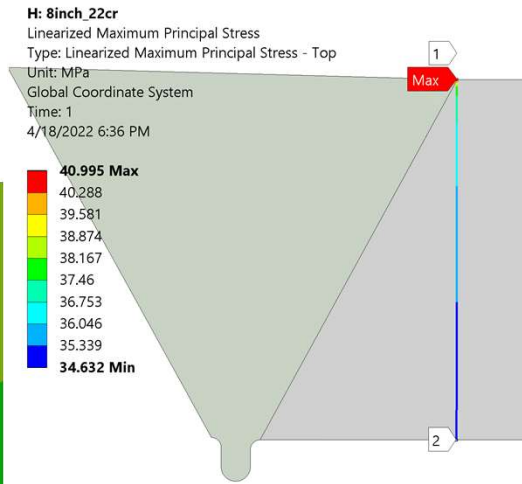
$$LSPF = \frac{\sigma_{max}}{\sigma_{lin}} = \frac{47.573}{26.608} = 1.79 \quad S_{mag} = \frac{\sigma_{lin}}{\sigma_{mem}} = \frac{26.608}{26.399} \times 1.1 = 1.11$$

# 8 inch Header 22Cr

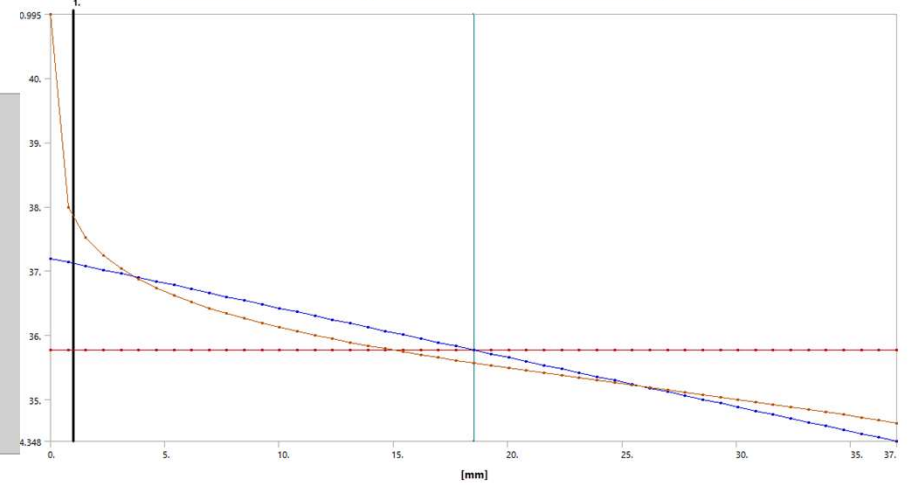
## Maximum Principal Stress



## Linearized Maximum Principal Stress - Weld toe

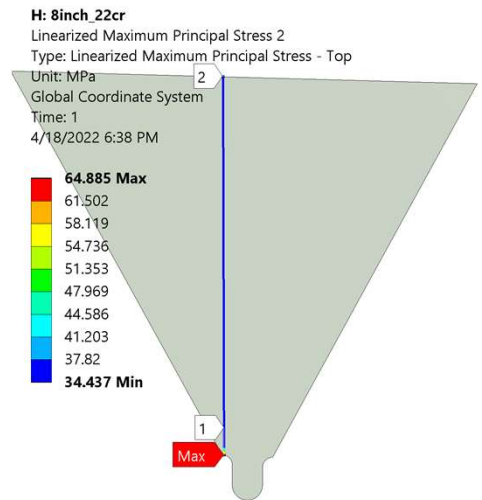


Length [mm]	Membrane [MPa]	Bending [MPa]	Membrane+Bending [MPa]	Peak [MPa]	Total [MPa]	
1	0.	35.769	1.4667	37.194	3.8016	40.995

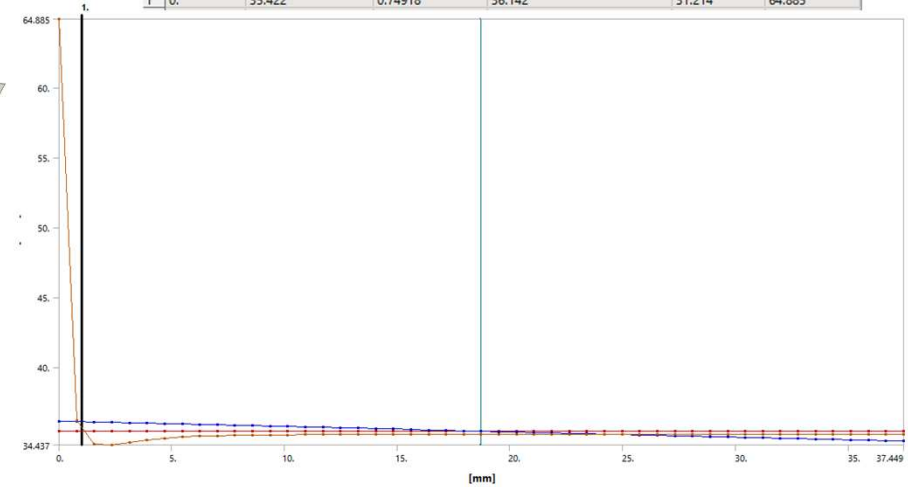


$$LSPF = \frac{\sigma_{max}}{\sigma_{lin}} = \frac{40.995}{37.194} = 1.1 \quad S_{mag} = \frac{\sigma_{lin}}{\sigma_{mem}} = \frac{37.194}{35.769} \times 1.1 = 1.14$$

## Linearized Maximum Principal Stress - Inside Weld root



Length [mm]	Membrane [MPa]	Bending [MPa]	Membrane+Bending [MPa]	Peak [MPa]	Total [MPa]	
1	0.	35.422	0.74918	36.142	31.214	64.885



$$LSPF = \frac{\sigma_{max}}{\sigma_{lin}} = \frac{64.885}{36.142} = 1.8 \quad S_{mag} = \frac{\sigma_{lin}}{\sigma_{mem}} = \frac{36.142}{35.422} \times 1.1 = 1.12$$

# 9 inch Header 22Cr

## Maximum Principal Stress

I: 9inch\_22cr

Maximum Principal Stress

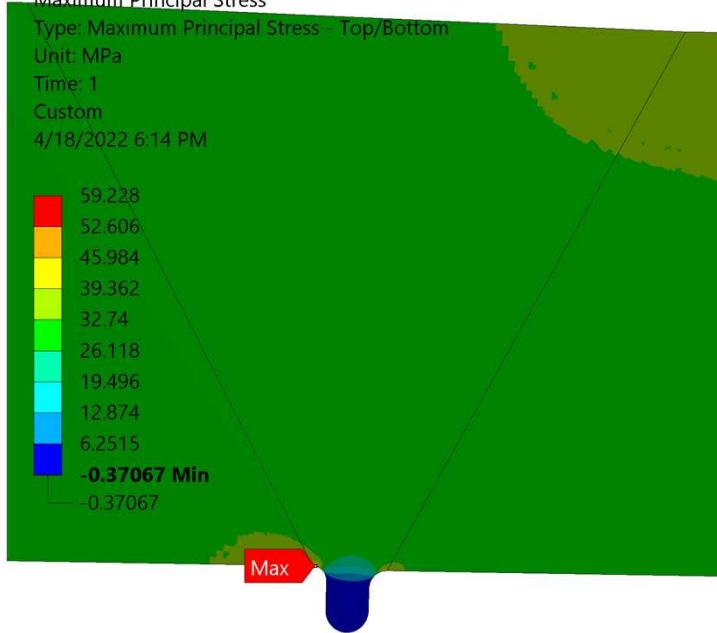
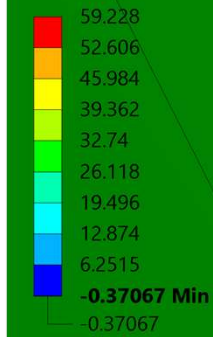
Type: Maximum Principal Stress - Top/Bottom

Unit: MPa

Time: 1

Custom

4/18/2022 6:14 PM



## Linearized Maximum Principal Stress - Weld toe

I: 9inch\_22cr

Linearized Maximum Principal Stress

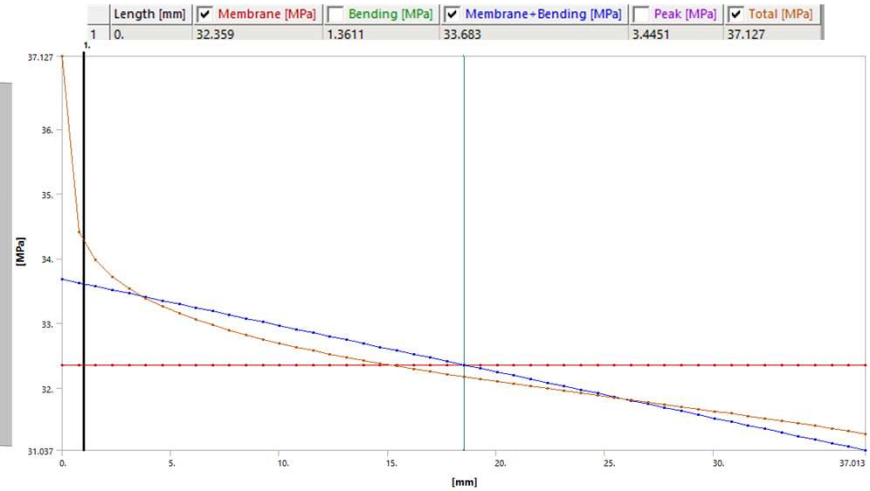
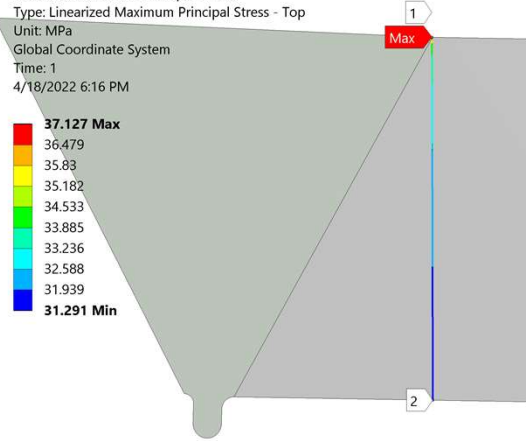
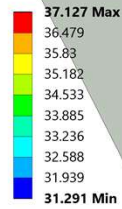
Type: Linearized Maximum Principal Stress - Top

Unit: MPa

Global Coordinate System

Time: 1

4/18/2022 6:16 PM



$$LSPF = \frac{\sigma_{max}}{\sigma_{lin}} = \frac{37.127}{33.686} = 1.1 \quad S_{mag} = \frac{\sigma_{lin}}{\sigma_{mem}} = \frac{33.686}{32.359} \times 1.1 = 1.15$$

## Linearized Maximum Principal Stress - Inside Weld root

I: 9inch\_22cr

Linearized Maximum Principal Stress 2

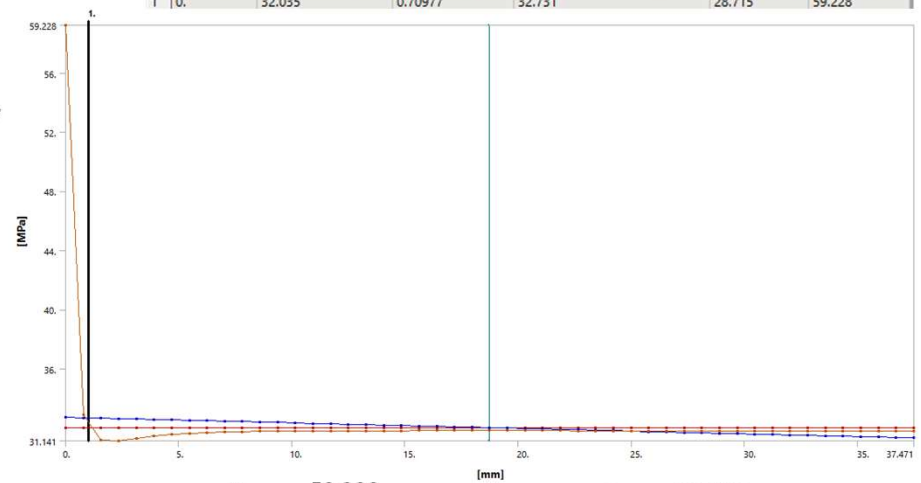
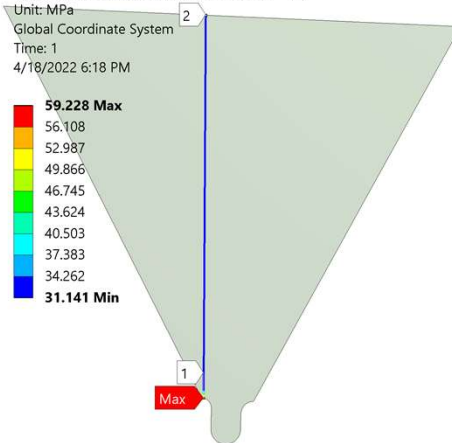
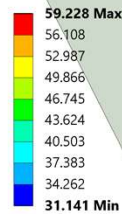
Type: Linearized Maximum Principal Stress - Top

Unit: MPa

Global Coordinate System

Time: 1

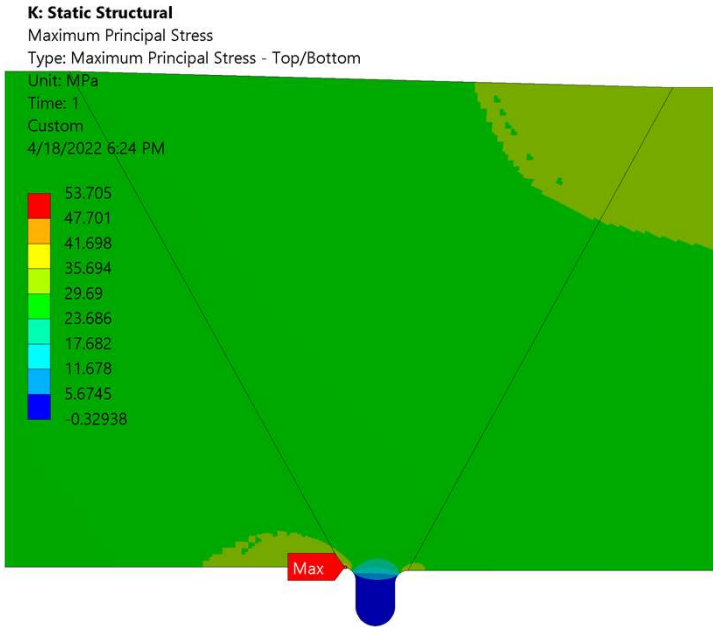
4/18/2022 6:18 PM



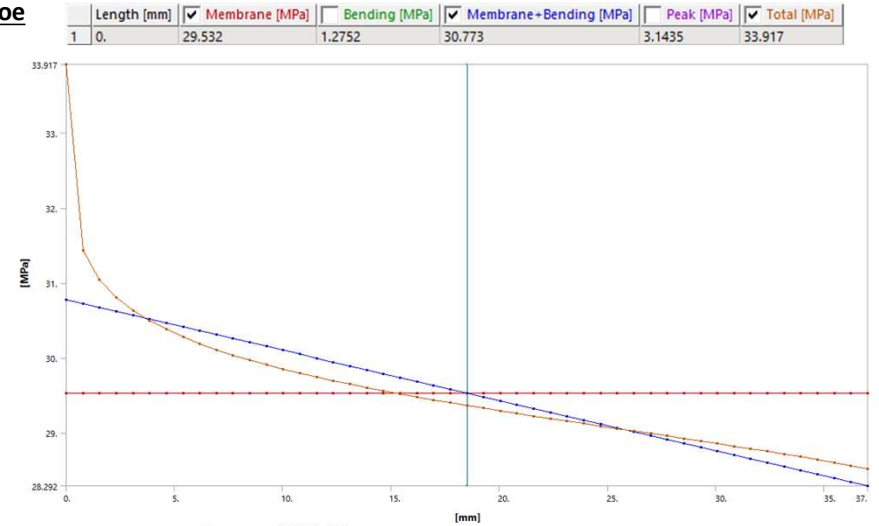
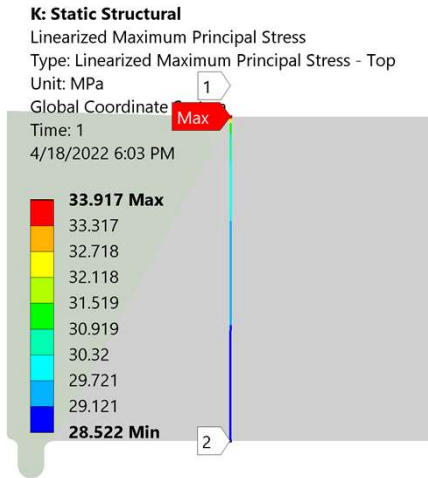
$$LSPF = \frac{\sigma_{max}}{\sigma_{lin}} = \frac{59.228}{32.731} = 1.81 \quad S_{mag} = \frac{\sigma_{lin}}{\sigma_{mem}} = \frac{32.731}{32.035} \times 1.1 = 1.12$$

# 10 inch Header 22Cr

## Maximum Principal Stress

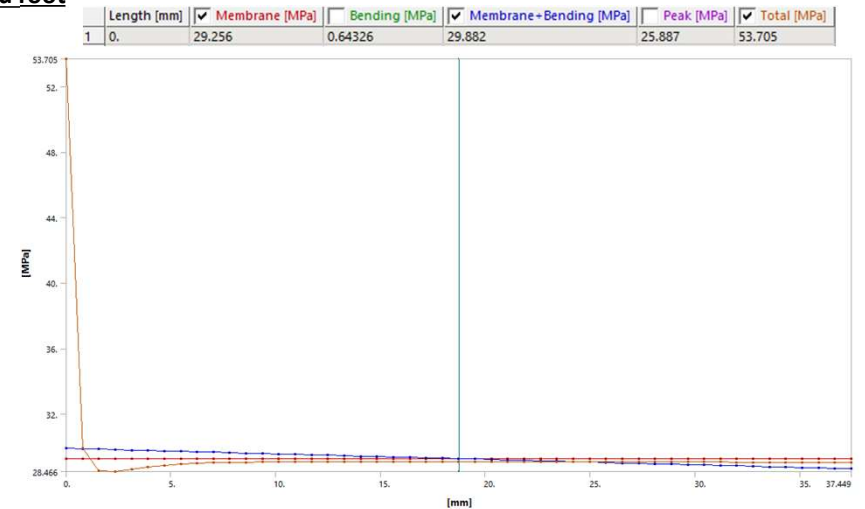
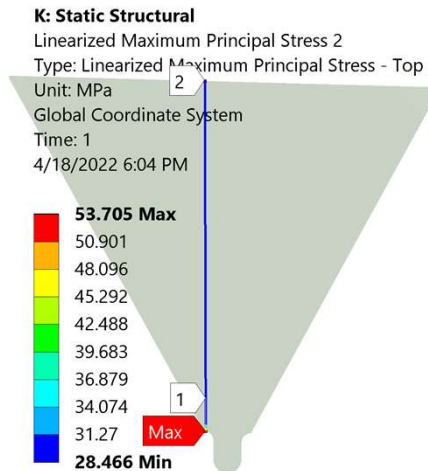


## Linearized Maximum Principal Stress - Weld toe



$$LSPF = \frac{\sigma_{max}}{\sigma_{lin}} = \frac{33.917}{30.773} = 1.1 \quad S_{mag} = \frac{\sigma_{lin}}{\sigma_{mem}} = \frac{30.773}{29.532} \times 1.1 = 1.15$$

## Linearized Maximum Principal Stress - Inside Weld root



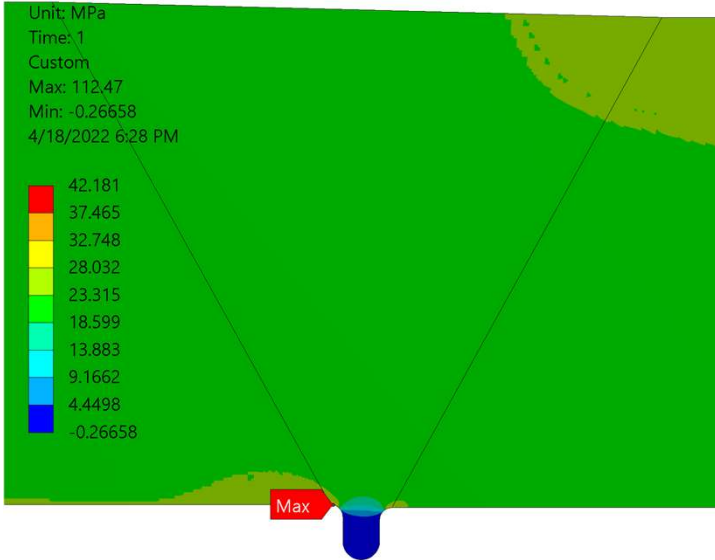
$$LSPF = \frac{\sigma_{max}}{\sigma_{lin}} = \frac{53.705}{29.882} = 1.8 \quad S_{mag} = \frac{\sigma_{lin}}{\sigma_{mem}} = \frac{29.882}{29.256} \times 1.1 = 1.12$$



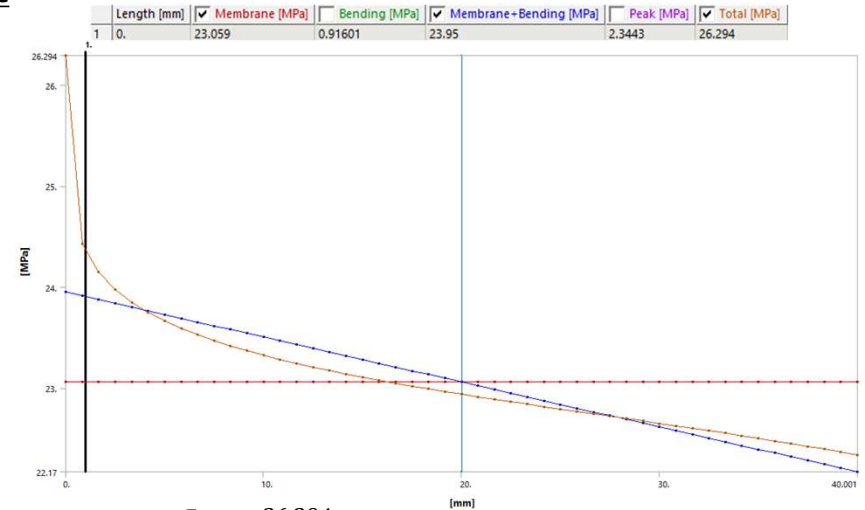
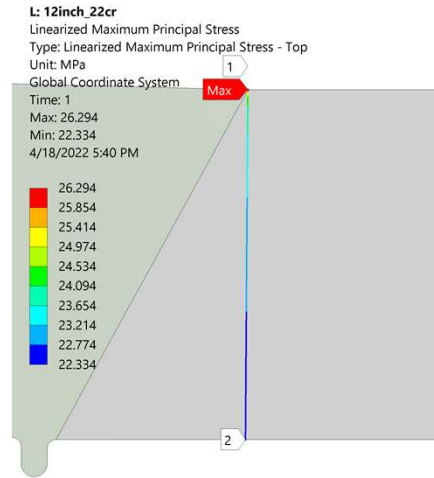
# 12 inch Header 22Cr

## Maximum Principal Stress

L: 12inch\_22cr  
 Maximum Principal Stress 2  
 Type: Maximum Principal Stress - Top/Bottom  
 Unit: MPa  
 Time: 1  
 Custom  
 Max: 112.47  
 Min: -0.26658  
 4/18/2022 6:28 PM



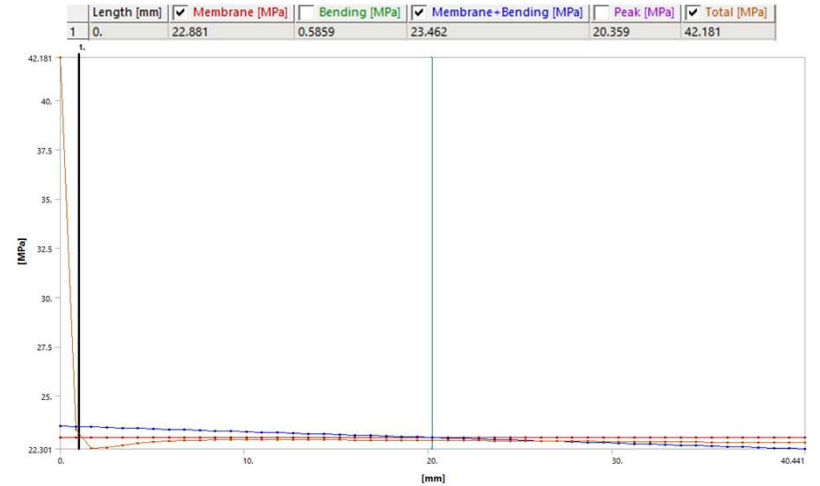
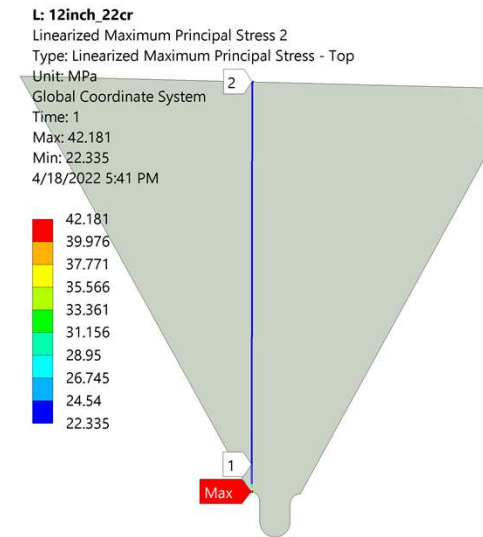
## Linearized Maximum Principal Stress - Weld toe



$$LSPF = \frac{\sigma_{max}}{\sigma_{lin}} = \frac{26.294}{23.95} = 1.1$$

$$S_{mag} = \frac{\sigma_{lin}}{\sigma_{mem}} = \frac{23.95}{23.059} \times 1.1 = 1.14$$

## Linearized Maximum Principal Stress - Inside Weld root



$$LSPF = \frac{\sigma_{max}}{\sigma_{lin}} = \frac{42.181}{23.462} = 1.8$$

$$S_{mag} = \frac{\sigma_{lin}}{\sigma_{mem}} = \frac{23.462}{22.881} \times 1.1 = 1.13$$

## **Appendix - B**

**SCF calculation at the unequal weld between Header and hub**  
LSFP<sub>Cat 1</sub> & S<sub>mag</sub> calculations using FEA

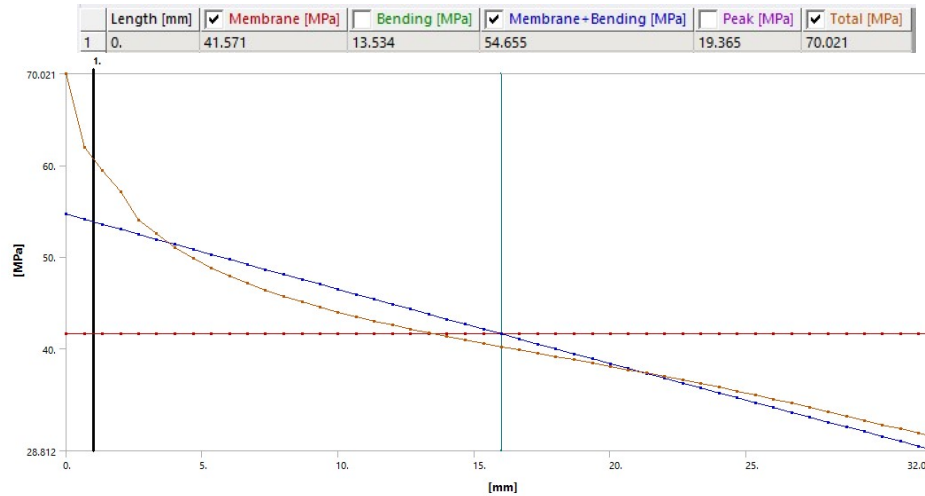
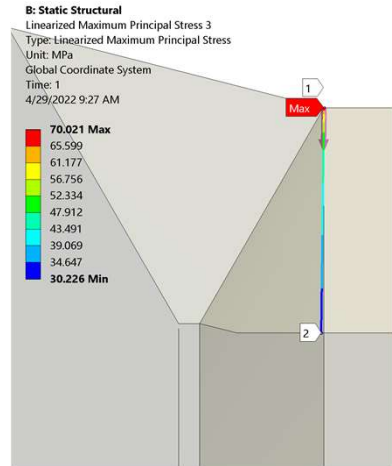
## Analysis results Summary

25%Cr duplex					22%Cr duplex				
8" ID	Header (nom)	Hub (max)	LSPF	Smag	8" ID	Header (nom)	Hub (max)	LSPF	Smag
ID	203.2	202.7 (203.2 -0.5)	1.55 (outside toe)	1.32 (outside toe)	ID	203.2	202.7 (203.2 -0.5)	1.58 (outside toe)	1.32 (outside toe)
WT	32	42.1 (OD-ID)/2	1.8 (inside root)	1.16 (inside root)	WT	37	48.6 (OD-ID)/2	1.8 (inside root)	1.16 (inside root)
OD	267.2	286.9 (286.4+0.5)			OD	277.2	299.9 (299.4+0.5)		
9" ID	Header (nom)	Hub (max)	LSPF	Smag	9" ID	Header (nom)	Hub (max)	LSPF	Smag
ID	228.6	228.1 (228.6 -0.5)	1.55 (outside toe)	1.33 (outside toe)	ID	228.6	228.1 (228.6 -0.5)	1.58 (outside toe)	1.32 (outside toe)
WT	32	42.1 (OD-ID)/2	1.79 (inside root)	1.16 (inside root)	WT	37	48.6 (OD-ID)/2	1.8 (inside root)	1.16 (inside root)
OD	292.6	312.3 (311.8+0.5)			OD	302.6	325.3 (324.8+0.5)		
10" ID	Header (nom)	Hub (max)	LSPF	Smag	10" ID	Header (nom)	Hub (max)	LSPF	Smag
ID	254	253.5 (254 -0.5)	1.55 (outside toe)	1.33 (outside toe)	ID	254	253.5 (254 -0.5)	1.58 (outside toe)	1.33 (outside toe)
WT	32	42.1 (OD-ID)/2	1.79 (inside root)	1.16 (inside root)	WT	37	48.6 (OD-ID)/2	1.8 (inside root)	1.16 (inside root)
OD	318	337.7 (337.2+0.5)			OD	328	350.7 (350.2+0.5)		
12" ID	Header (nom)	Hub (max)	LSPF	Smag	12" ID	Header (nom)	Hub (max)	LSPF	Smag
ID	304.8	304.3 (304.8 -0.5)	1.57 (outside toe)	1.34 (outside toe)	ID	304.8	304.3 (304.8 -0.5)	1.59 (outside toe)	1.33 (outside toe)
WT	35	46 (OD-ID)/2	1.8 (inside root)	1.16 (inside root)	WT	40	52.5 (OD-ID)/2	1.81 (inside root)	1.15 (inside root)
OD	374.8	396.3 (395.8+0.5)			OD	384.8	409.3 (408.8+0.5)		

### 3D analysis Results (Modeled only for Smag comparison)

(with 1.6mm Center line misalignment )

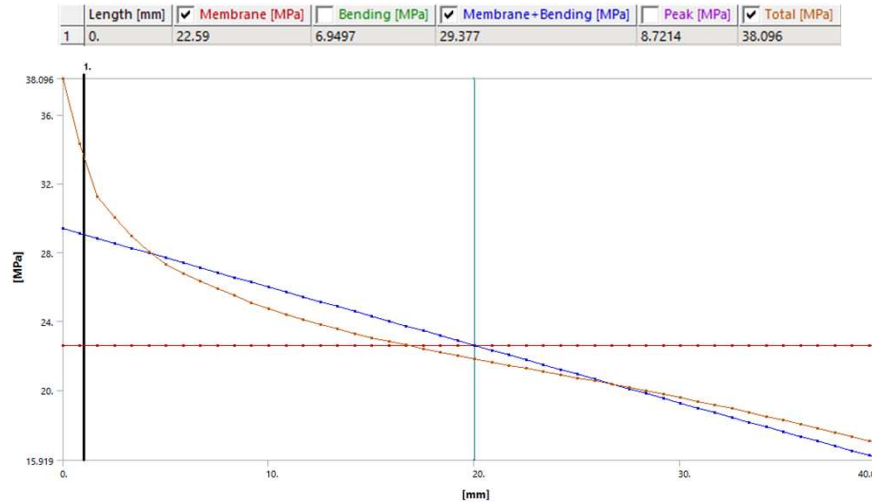
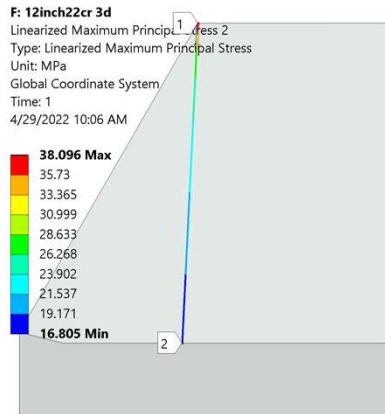
#### 8 inch Header 25Cr



$$S_{mag} = \frac{\sigma_{lin}}{\sigma_{mem}} = \frac{54.655}{41.571} = 1.32$$

$$S_{mag} (w/0 clm) = 1.24$$

#### 12 inch Header 22Cr



$$S_{mag} = \frac{\sigma_{lin}}{\sigma_{mem}} = \frac{29.377}{22.59} = 1.3$$

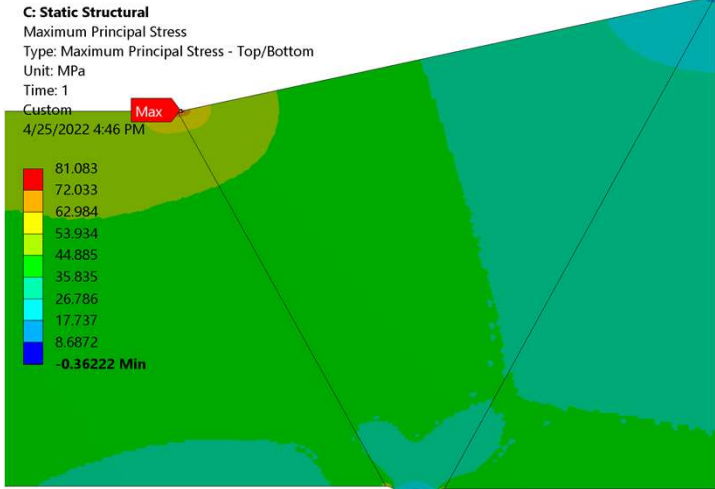
$$S_{mag} (w/0 clm) = 1.25$$

**Note:** It is observed that the Smag was approx. 5-6% higher in case of model with center-line misalignment compared to no center-line misalignment.

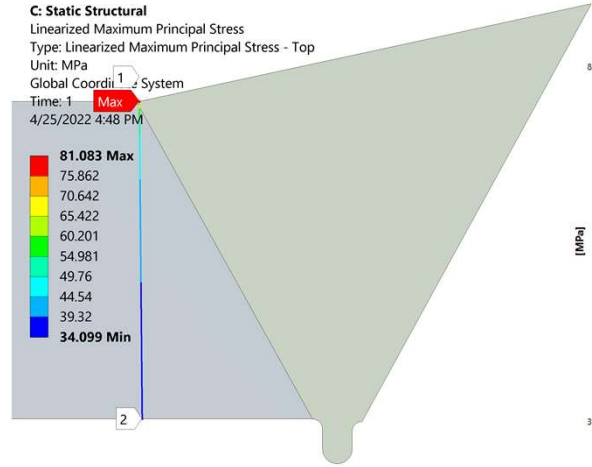
Going by this, only axisymmetric 2D analysis is done for the remaining sizes and the Smag value is increased by 6% .

# 8 inch Header 25Cr

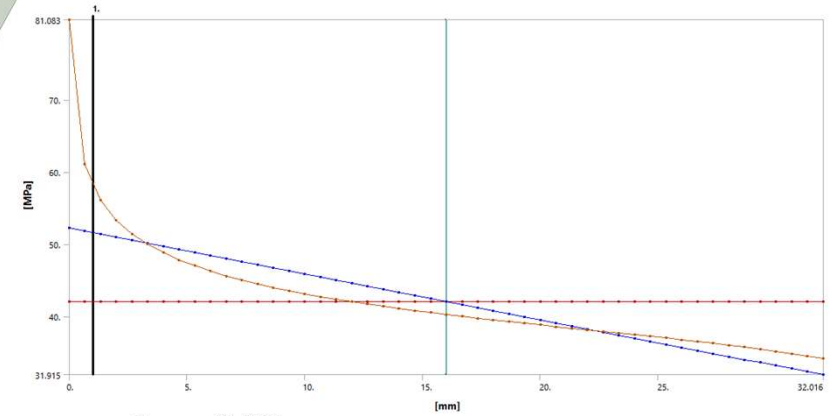
## Maximum Principal Stress



## Linearized Maximum Principal Stress - Weld toe

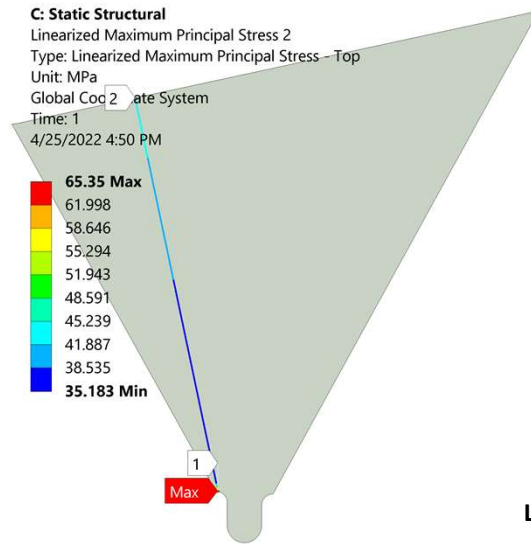


Length [mm]	Membrane [MPa]	Bending [MPa]	Membrane+Bending [MPa]	Peak [MPa]	Total [MPa]
1 0.	41.973	10.798	52.293	28.798	81.083

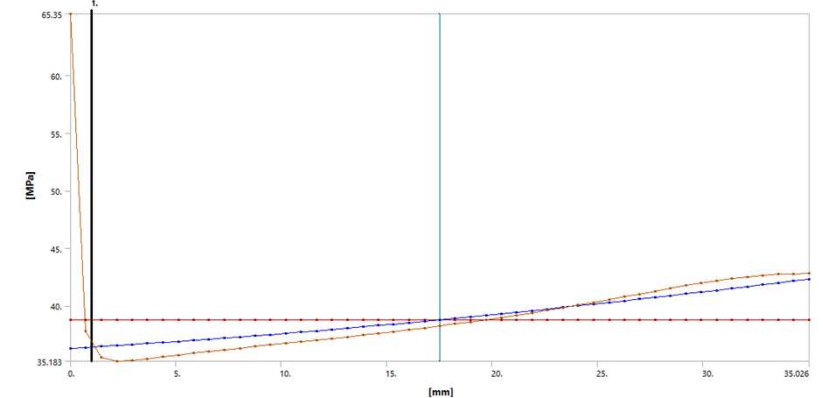


$$LSPF = \frac{\sigma_{max}}{\sigma_{lin}} = \frac{81.083}{52.293} = 1.55 \quad S_{mag} = \frac{\sigma_{lin}}{\sigma_{mem}} = \frac{52.293}{41.973} \times 1.06 = 1.32$$

## Linearized Maximum Principal Stress - Inside Weld root



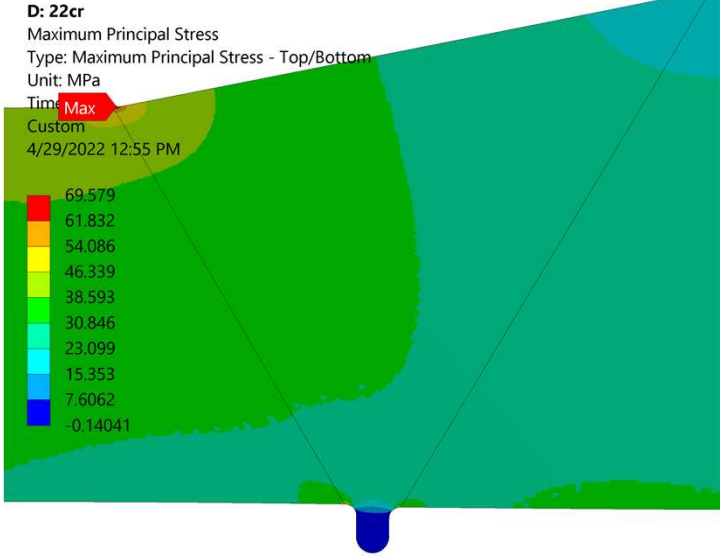
Length [mm]	Membrane [MPa]	Bending [MPa]	Membrane+Bending [MPa]	Peak [MPa]	Total [MPa]
1 0.	38.779	3.5657	36.304	29.924	65.35



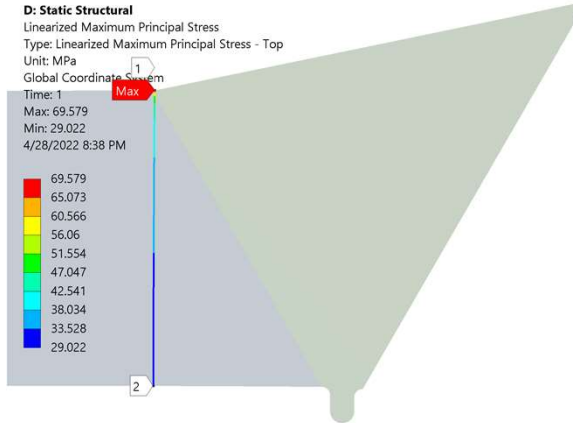
$$LSPF = \frac{\sigma_{max}}{\sigma_{lin}} = \frac{65.35}{36.304} = 1.8 \quad S_{mag} = \frac{\sigma_{lin}}{\sigma_{mem}} = \frac{38.779+3.5657}{38.779} \times 1.06 = 1.16$$

# 8 inch Header 22Cr

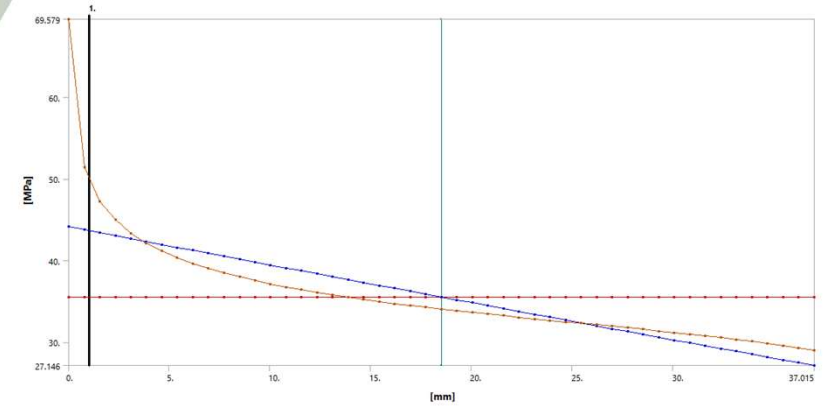
## Maximum Principal Stress



## Linearized Maximum Principal Stress - Weld toe

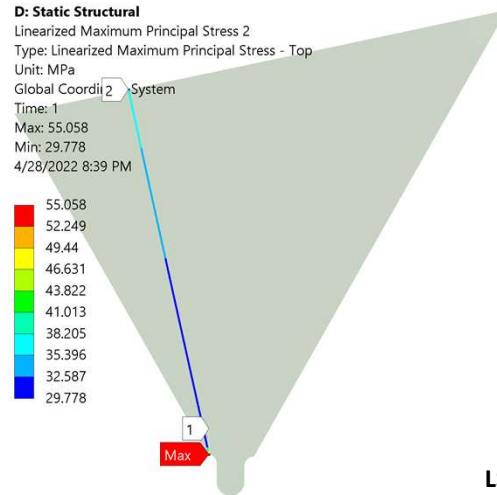


Length [mm]	Membrane [MPa]	Bending [MPa]	Membrane+Bending [MPa]	Peak [MPa]	Total [MPa]
1 0.	35.534	9.0141	44.141	25.442	69.579

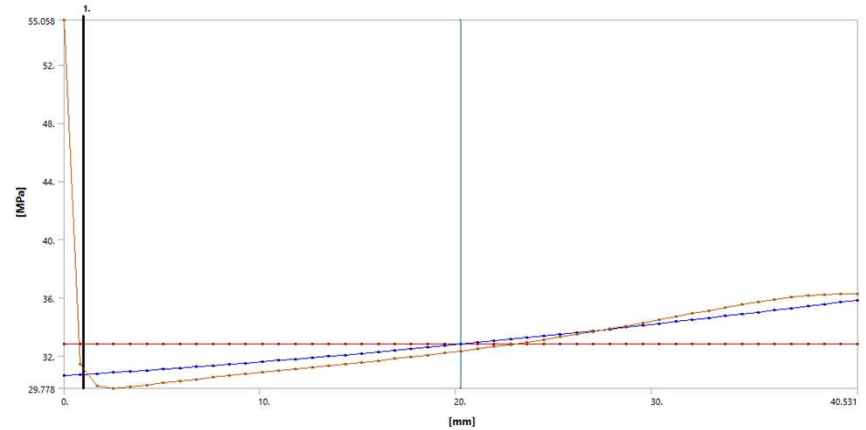


$$LSPF = \frac{\sigma_{max}}{\sigma_{lin}} = \frac{69.579}{44.141} = 1.58 \quad S_{mag} = \frac{\sigma_{lin}}{\sigma_{mem}} = \frac{44.141}{35.534} \times 1.06 = 1.32$$

## Linearized Maximum Principal Stress - Inside Weld root

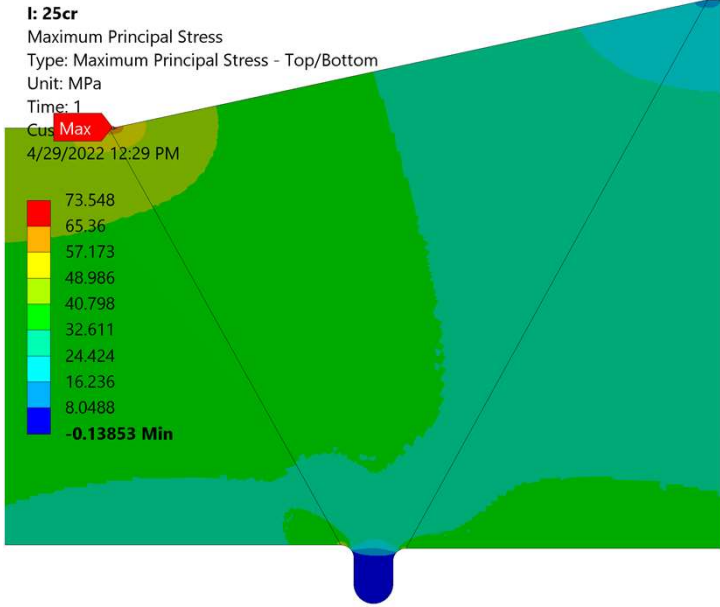


Length [mm]	Membrane [MPa]	Bending [MPa]	Membrane+Bending [MPa]	Peak [MPa]	Total [MPa]
1 0.	32.805	2.9054	30.657	25.24	55.058

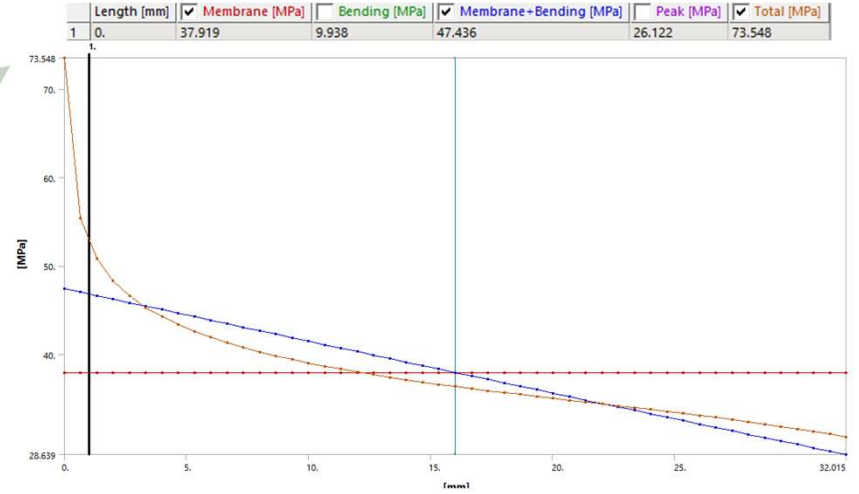
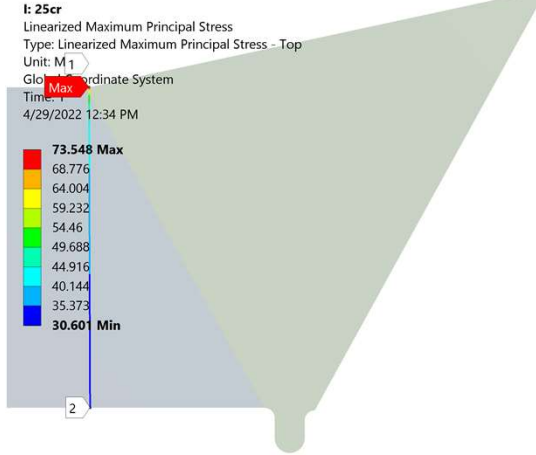


$$LSPF = \frac{\sigma_{max}}{\sigma_{lin}} = \frac{55.058}{30.657} = 1.8 \quad S_{mag} = \frac{\sigma_{lin}}{\sigma_{mem}} = \frac{32.805 + 2.905}{32.805} \times 1.06 = 1.16$$

# 9 inch Header 25Cr

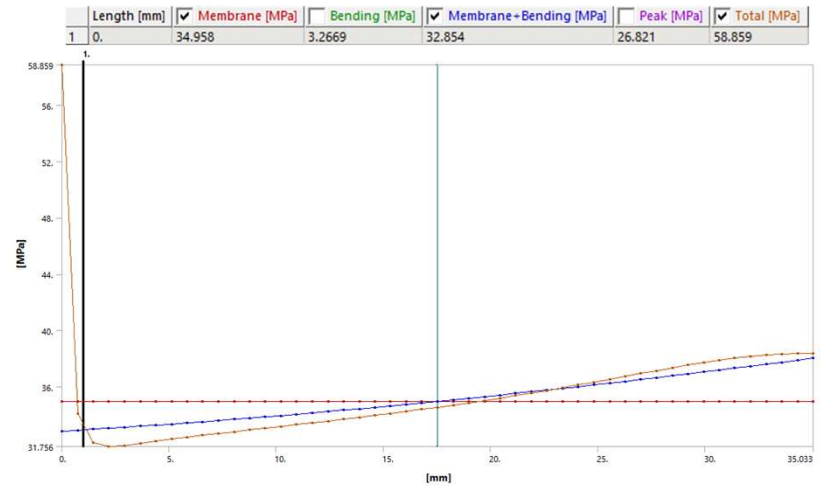
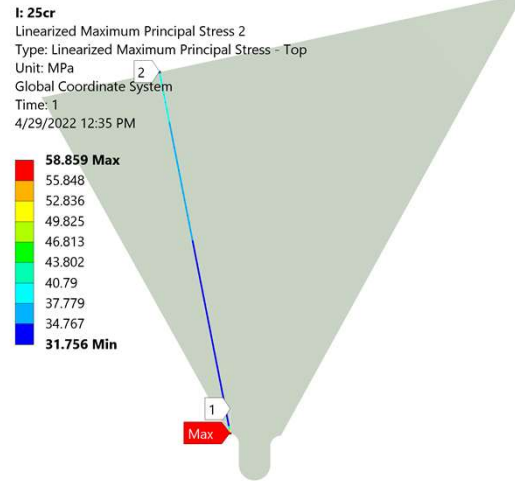


## Linearized Maximum Principal Stress - Weld toe



$$LSPF = \frac{\sigma_{max}}{\sigma_{lin}} = \frac{73.548}{47.436} = 1.55 \quad S_{mag} = \frac{\sigma_{lin}}{\sigma_{mem}} = \frac{47.436}{37.919} \times 1.06 = 1.33$$

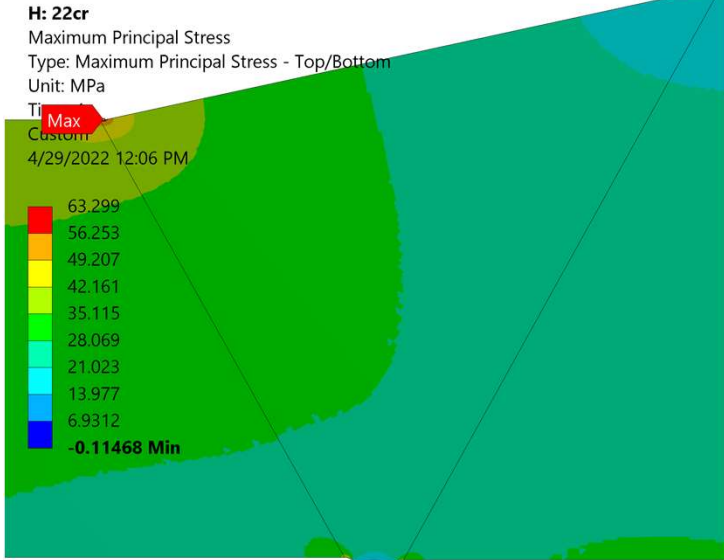
## Linearized Maximum Principal Stress - Inside Weld root



$$LSPF = \frac{\sigma_{max}}{\sigma_{lin}} = \frac{58.859}{32.854} = 1.79 \quad S_{mag} = \frac{\sigma_{lin}}{\sigma_{mem}} = \frac{34.958 + 3.2669}{34.958} \times 1.06 = 1.16$$

# 9 inch Header 22Cr

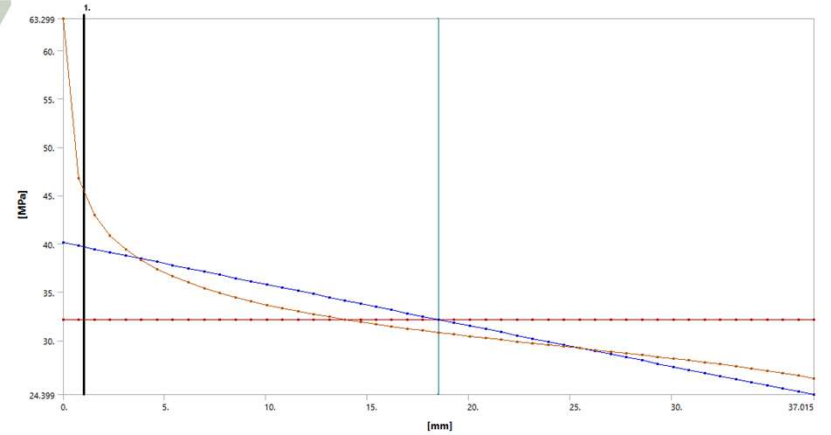
## Maximum Principal Stress



## Linearized Maximum Principal Stress - Weld toe

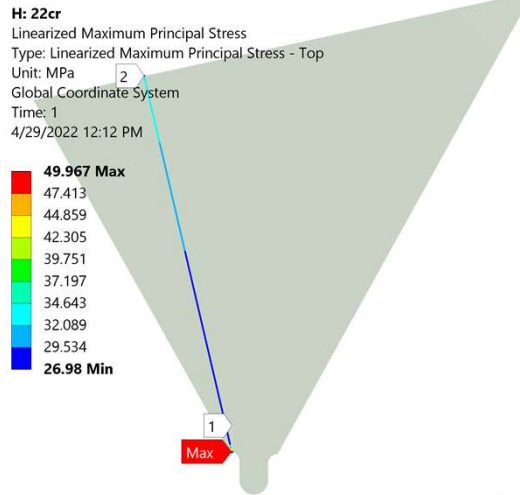


Length [mm]	Membrane [MPa]	Bending [MPa]	Membrane-Bending [MPa]	Peak [MPa]	Total [MPa]
1 0.	32.16	8.3247	40.122	23.183	63.299

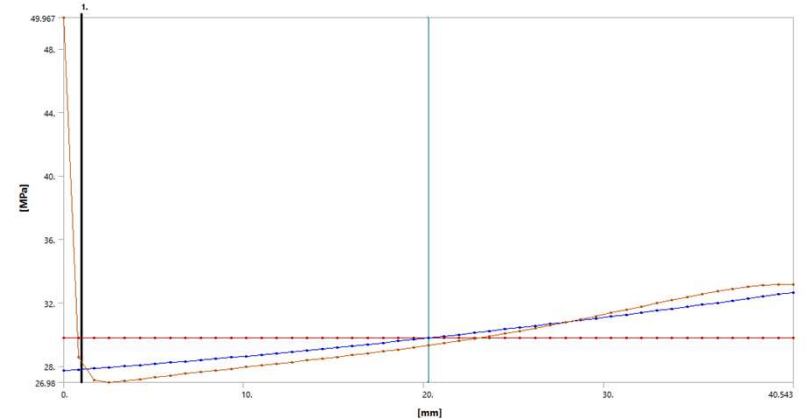


$$LSPF = \frac{\sigma_{max}}{\sigma_{lin}} = \frac{63.299}{40.122} = 1.58 \quad S_{mag} = \frac{\sigma_{lin}}{\sigma_{mem}} = \frac{40.122}{32.16} \times 1.06 = 1.32$$

## Linearized Maximum Principal Stress - Inside Weld root



Length [mm]	Membrane [MPa]	Bending [MPa]	Membrane-Bending [MPa]	Peak [MPa]	Total [MPa]
1 0.	29.782	2.5967	27.713	22.964	49.967

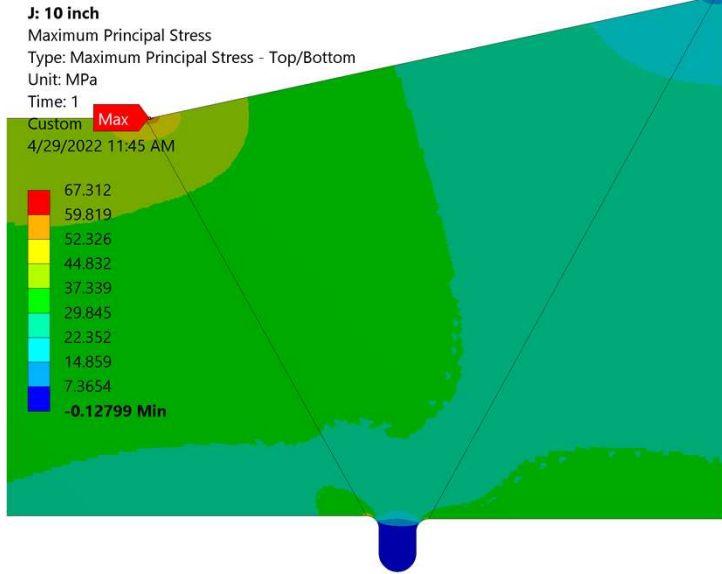


$$LSPF = \frac{\sigma_{max}}{\sigma_{lin}} = \frac{49.967}{27.713} = 1.8 \quad S_{mag} = \frac{\sigma_{lin}}{\sigma_{mem}} = \frac{29.782 + 2.5967}{29.782} \times 1.06 = 1.16$$

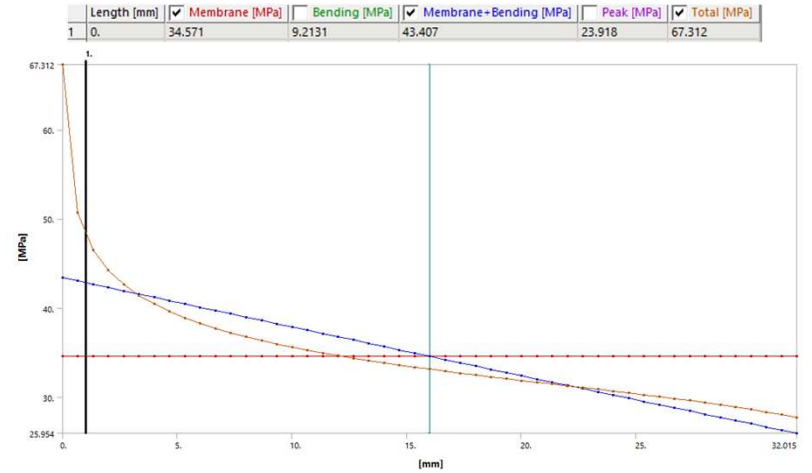
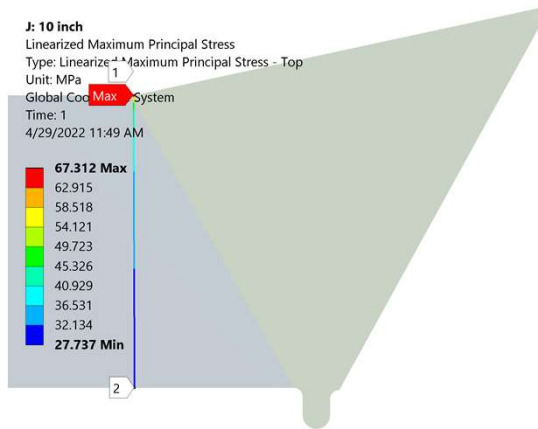


# 10 inch Header 25Cr

## Maximum Principal Stress

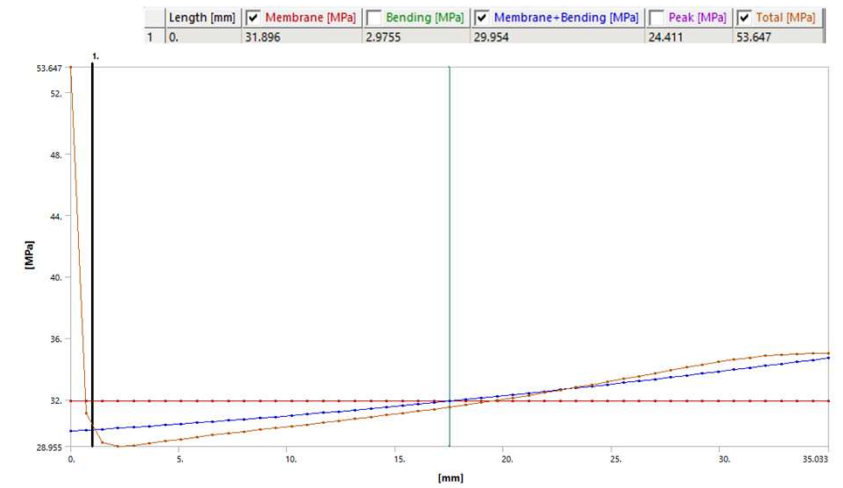
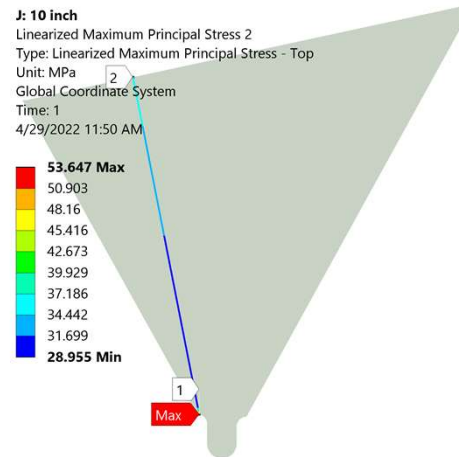


## Linearized Maximum Principal Stress - Weld toe



$$LSPF = \frac{\sigma_{max}}{\sigma_{lin}} = \frac{67.312}{43.407} = 1.55 \quad S_{mag} = \frac{\sigma_{lin}}{\sigma_{mem}} = \frac{43.407}{34.571} \times 1.06 = 1.33$$

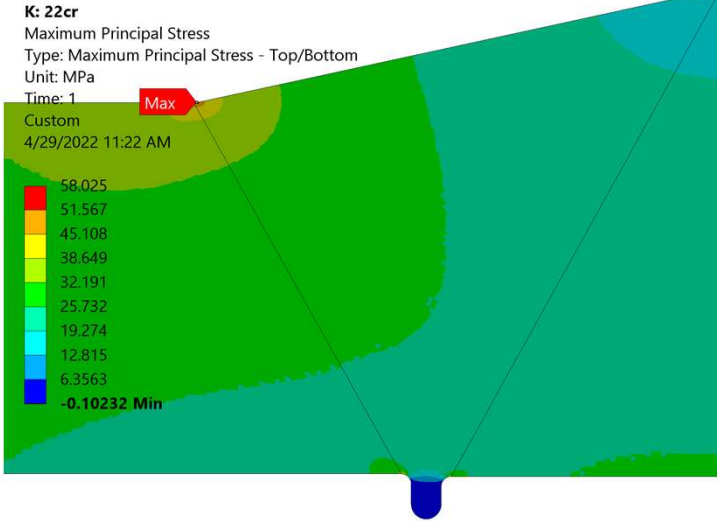
## Linearized Maximum Principal Stress - Inside Weld root



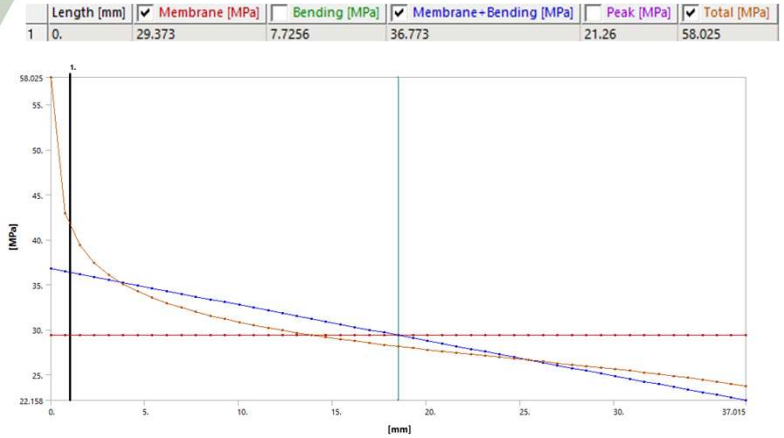
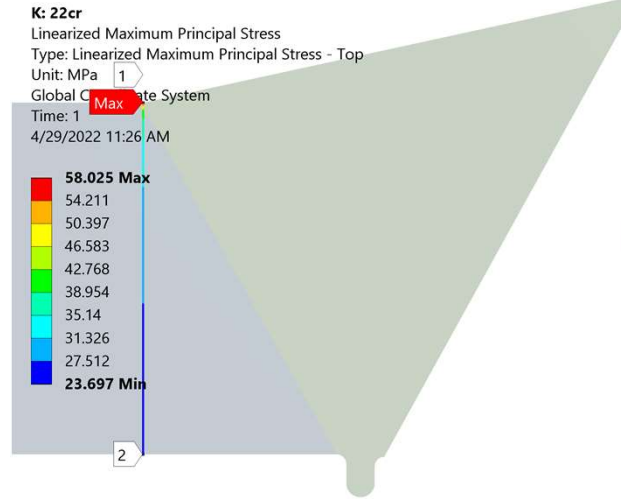
$$LSPF = \frac{\sigma_{max}}{\sigma_{lin}} = \frac{53.647}{29.954} = 1.79 \quad S_{mag} = \frac{\sigma_{lin}}{\sigma_{mem}} = \frac{31.896 + 2.9755}{31.896} \times 1.06 = 1.16$$

# 10 inch Header 22Cr

## Maximum Principal Stress

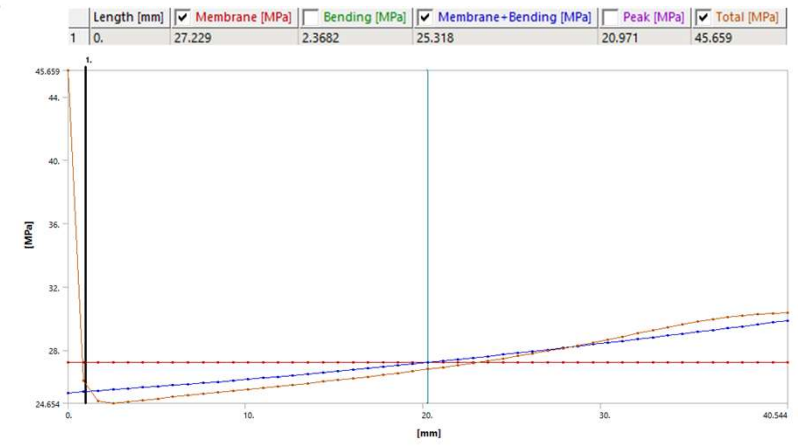
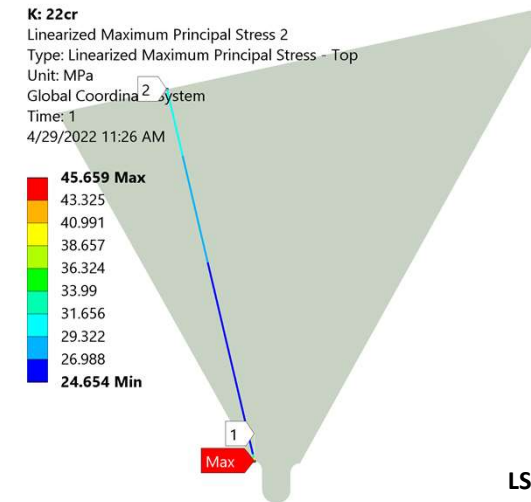


## Linearized Maximum Principal Stress - Weld toe



$$LSPF = \frac{\sigma_{max}}{\sigma_{lin}} = \frac{58.025}{36.773} = 1.58 \quad S_{mag} = \frac{\sigma_{lin}}{\sigma_{mem}} = \frac{36.773}{29.373} \times 1.06 = 1.33$$

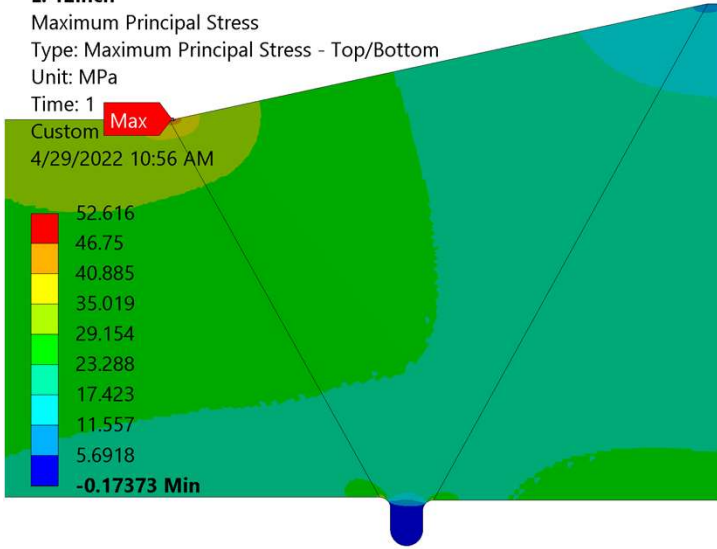
## Linearized Maximum Principal Stress - Inside Weld root



$$LSPF = \frac{\sigma_{max}}{\sigma_{lin}} = \frac{45.659}{25.318} = 1.8 \quad S_{mag} = \frac{\sigma_{lin}}{\sigma_{mem}} = \frac{27.229 + 2.3682}{27.229} \times 1.06 = 1.16$$

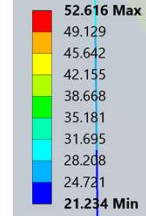
# 12 inch Header 25Cr

L: 12inch  
 Maximum Principal Stress  
 Type: Maximum Principal Stress - Top/Bottom  
 Unit: MPa  
 Time: 1  
 Custom Max  
 4/29/2022 10:56 AM

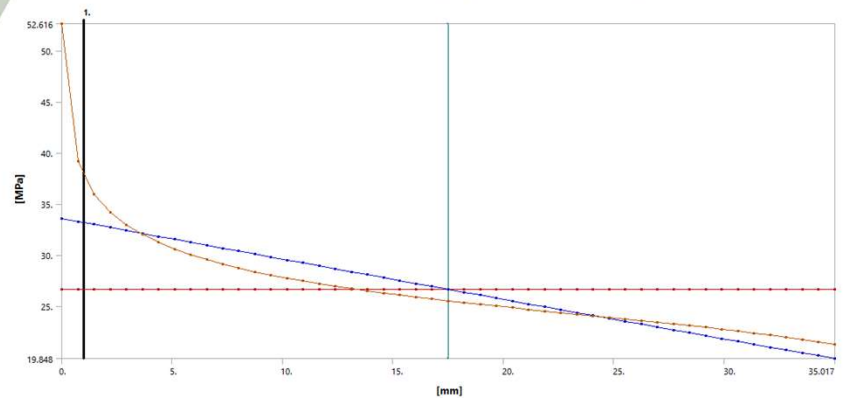


## Linearized Maximum Principal Stress - Weld toe

L: 12inch  
 Linearized Maximum Principal Stress  
 Type: Linearized Maximum Principal Stress - Top  
 Unit: 1  
 Global Coordinate System  
 Time: 1  
 4/29/2022 11:04 AM



Length [mm]	Membrane [MPa]	Bending [MPa]	Membrane+Bending [MPa]	Peak [MPa]	Total [MPa]
1	0.	26.613	7.2243	33.548	52.616

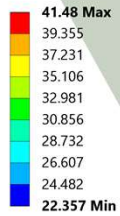


$$LSPF = \frac{\sigma_{max}}{\sigma_{lin}} = \frac{52.616}{33.548} = 1.57$$

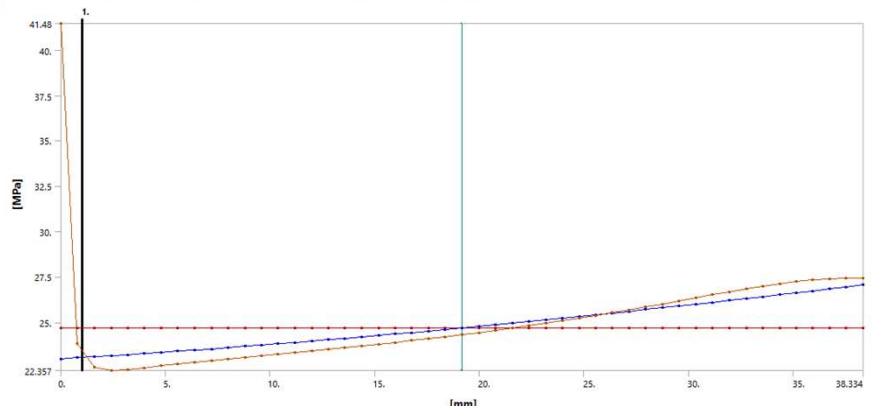
$$S_{mag} = \frac{\sigma_{lin}}{\sigma_{mem}} = \frac{33.548}{26.613} \times 1.06 = 1.34$$

## Linearized Maximum Principal Stress - Inside Weld root

L: 12inch  
 Linearized Maximum Principal Stress 2  
 Type: Linearized Maximum Principal Stress - Top  
 Unit: MPa  
 Global Coordinate System  
 Time: 1  
 4/29/2022 11:05 AM



Length [mm]	Membrane [MPa]	Bending [MPa]	Membrane+Bending [MPa]	Peak [MPa]	Total [MPa]
1	0.	24.691	2.1957	23.005	41.48

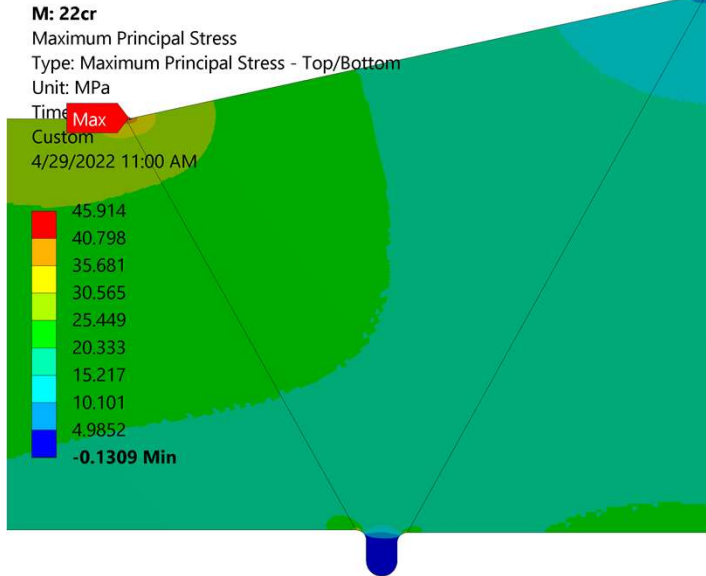


$$LSPF = \frac{\sigma_{max}}{\sigma_{lin}} = \frac{41.48}{23.005} = 1.8$$

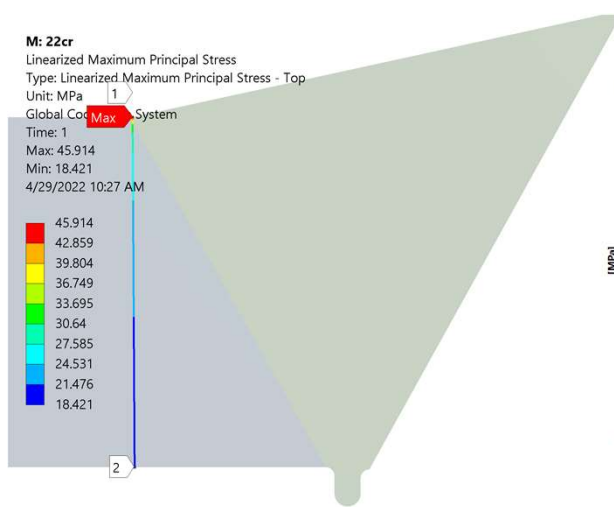
$$S_{mag} = \frac{\sigma_{lin}}{\sigma_{mem}} = \frac{24.691 + 2.1957}{24.691} \times 1.06 = 1.16$$

# 12 inch Header 22Cr

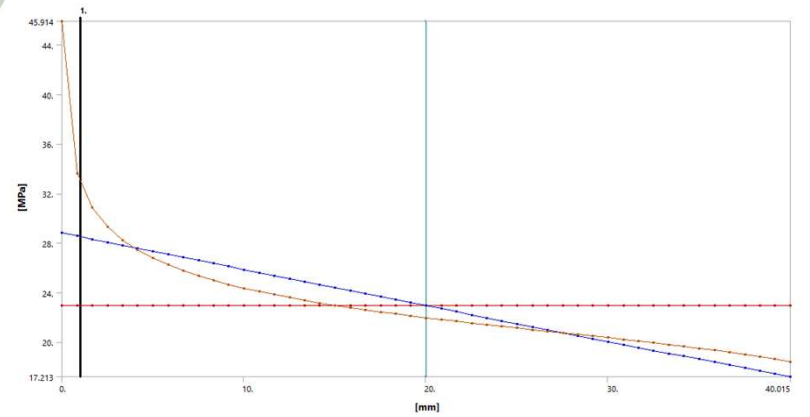
## Maximum Principal Stress



## Linearized Maximum Principal Stress - Weld toe

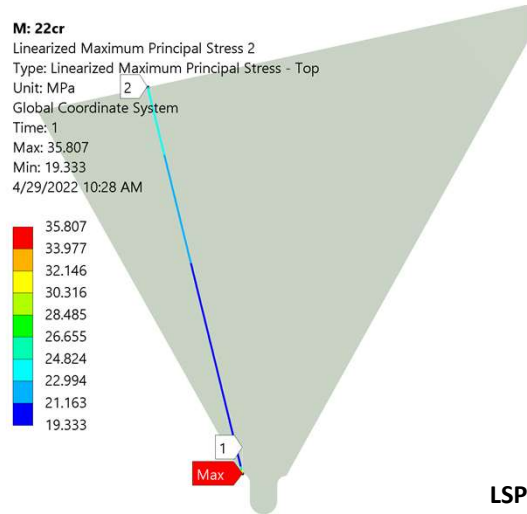


Length [mm]	Membrane [MPa]	Bending [MPa]	Membrane+Bending [MPa]	Peak [MPa]	Total [MPa]
1 0.	22.942	6.129	28.817	17.105	45.914

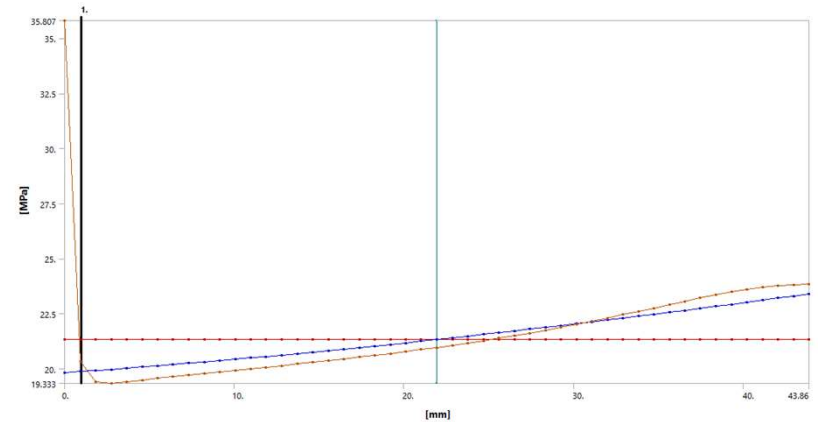


$$LSPF = \frac{\sigma_{max}}{\sigma_{lin}} = \frac{45.914}{28.817} = 1.59 \quad S_{mag} = \frac{\sigma_{lin}}{\sigma_{mem}} = \frac{28.817}{22.942} \times 1.06 = 1.33$$

## Linearized Maximum Principal Stress - Inside Weld root



Length [mm]	Membrane [MPa]	Bending [MPa]	Membrane+Bending [MPa]	Peak [MPa]	Total [MPa]
1 0.	21.321	1.8186	19.817	16.465	35.807



$$LSPF = \frac{\sigma_{max}}{\sigma_{lin}} = \frac{35.807}{19.817} = 1.81 \quad S_{mag} = \frac{\sigma_{lin}}{\sigma_{mem}} = \frac{21.321 + 1.8186}{21.321} \times 1.06 = 1.15$$

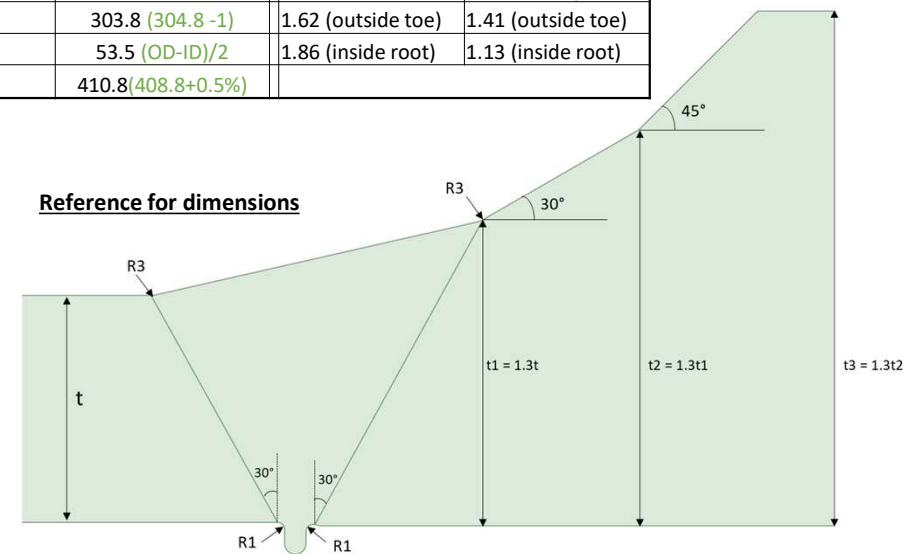
## Appendix - C

**SCF calculation at the unequal weld between Header and valve**

LSFP<sub>Cat 1</sub> & S<sub>mag</sub> calculations using FEA

## Analysis results Summary

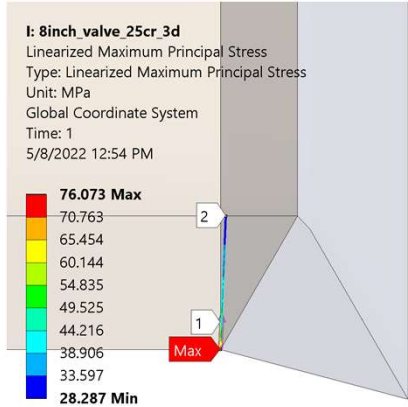
25%Cr duplex					22%Cr duplex				
8" ID	Header (nom)	valve (max)	LSPF	Smag	8" ID	Header (nom)	valve (max)	LSPF	Smag
ID	203.2	202.2 (203.2 -1)	1.57 (outside toe)	1.38 (outside toe)	ID	203.2	202.2 (203.2 -1)	1.59 (outside toe)	1.36 (outside toe)
WT	32	42.8 (OD-ID)/2	1.83 (inside root)	1.14 (inside root)	WT	37	49.35 (OD-ID)/2	1.84 (inside root)	1.13 (inside root)
OD	267.2	287.8 (286.4+0.5%)			OD	277.2	300.9 (299.4+0.5%)		
9" ID	Header (nom)	valve (max)	LSPF	Smag	9" ID	Header (nom)	valve (max)	LSPF	Smag
ID	228.6	227.6 (228.6 -1)	1.57 (outside toe)	1.4 (outside toe)	ID	228.6	227.6 (228.6 -1)	1.6 (outside toe)	1.38 (outside toe)
WT	32	42.9 (OD-ID)/2	1.83 (inside root)	1.13 (inside root)	WT	37	49.4 (OD-ID)/2	1.84 (inside root)	1.13 (inside root)
OD	292.6	313.4 (311.8+0.5%)			OD	302.6	326.4 (324.8+0.5%)		
10" ID	Header (nom)	valve (max)	LSPF	Smag	10" ID	Header (nom)	valve (max)	LSPF	Smag
ID	254	253 (254 -1)	1.57 (outside toe)	1.41 (outside toe)	ID	254	253 (254 -1)	1.6 (outside toe)	1.39 (outside toe)
WT	32	42.95 (OD-ID)/2	1.83 (inside root)	1.13 (inside root)	WT	37	49.5 (OD-ID)/2	1.85 (inside root)	1.13 (inside root)
OD	318	338.9 (337.2+0.5%)			OD	328	352 (350.2+0.5%)		
12" ID	Header (nom)	valve (max)	LSPF	Smag	12" ID	Header (nom)	valve (max)	LSPF	Smag
ID	304.8	303.8 (304.8 -1)	1.6 (outside toe)	1.43 (outside toe)	ID	304.8	303.8 (304.8 -1)	1.62 (outside toe)	1.41 (outside toe)
WT	35	47 (OD-ID)/2	1.83 (inside root)	1.13 (inside root)	WT	40	53.5 (OD-ID)/2	1.86 (inside root)	1.13 (inside root)
OD	374.8	397.8(395.8+0.5%)			OD	384.8	410.8(408.8+0.5%)		



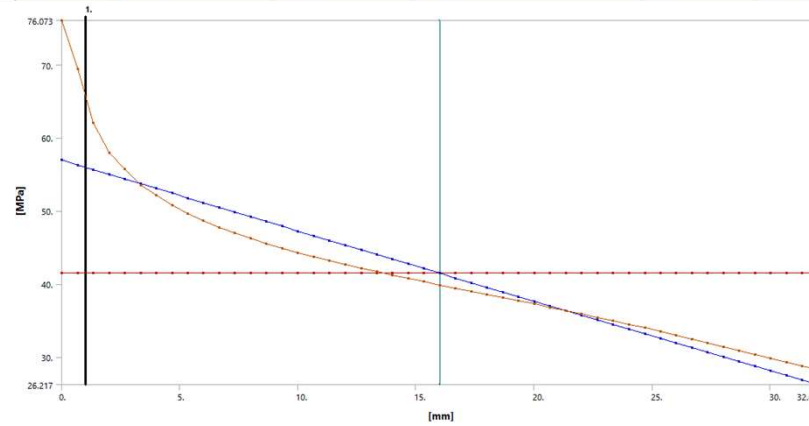
### 3D analysis Results (Modeled only for Smag comparison)

(with 1.6mm Center line misalignment )

#### 8 inch Header 25Cr



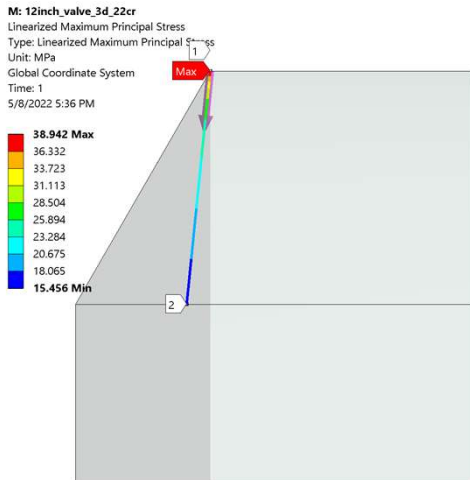
Length [mm]	Membrane [MPa]	Bending [MPa]	Membrane+Bending [MPa]	Peak [MPa]	Total [MPa]
1 0.	41.454	15.747	56.944	21.417	76.073



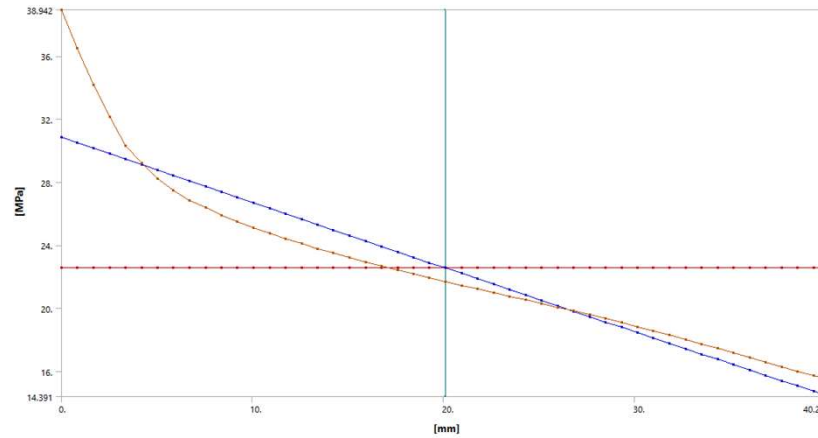
$$S_{mag} = \frac{\sigma_{lin}}{\sigma_{mem}} = \frac{56.944}{41.454} = 1.37$$

$$S_{mag} (w/0 clm) = 1.3$$

#### 12 inch Header 22Cr



Length [mm]	Membrane [MPa]	Bending [MPa]	Membrane+Bending [MPa]	Peak [MPa]	Total [MPa]
1 0.	22.55	8.4111	30.834	8.1165	38.942



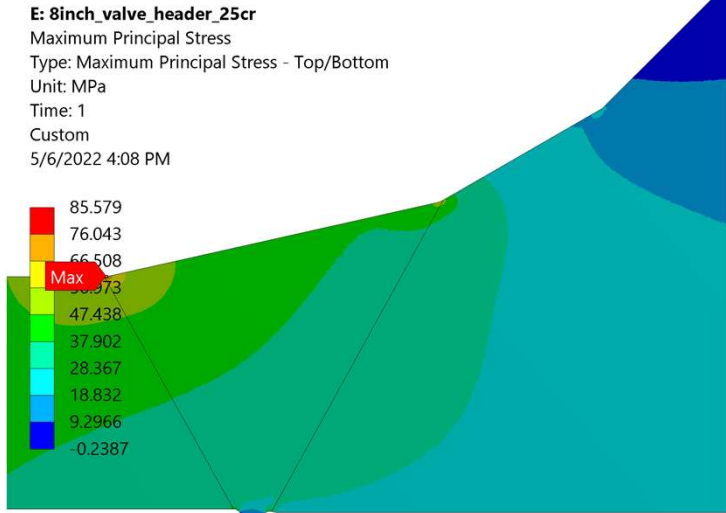
$$S_{mag} = \frac{\sigma_{lin}}{\sigma_{mem}} = \frac{30.834}{22.55} = 1.37$$

$$S_{mag} (w/0 clm) = 1.32$$

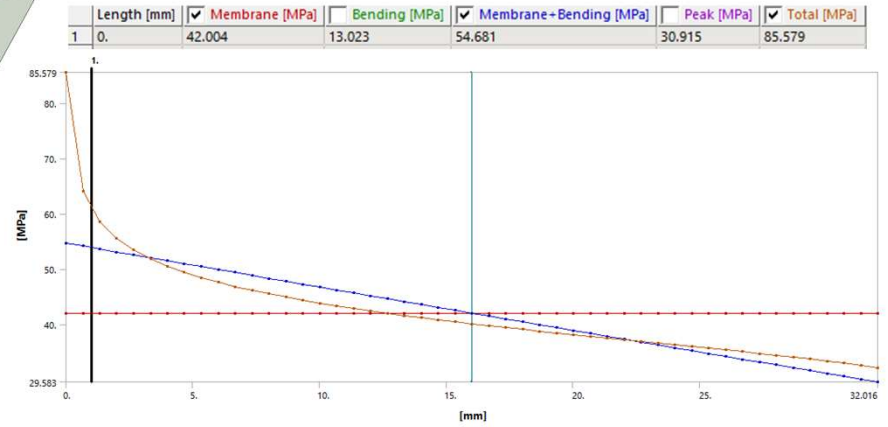
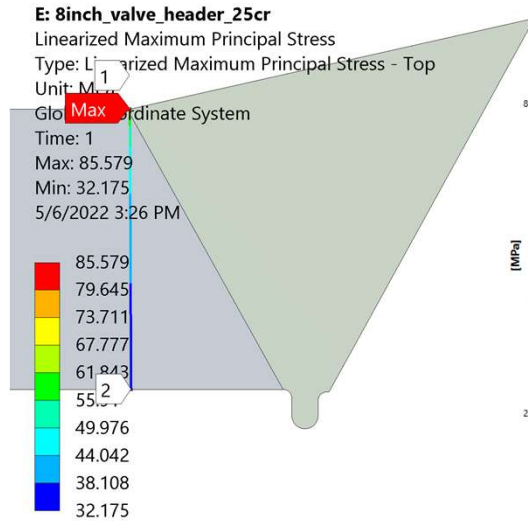
**Note:** It is observed that the Smag was approx. 4-6% higher in case of model with center-line misalignment compared to no center-line misalignment.

# 8 inch Header 25Cr

## Maximum Principal Stress

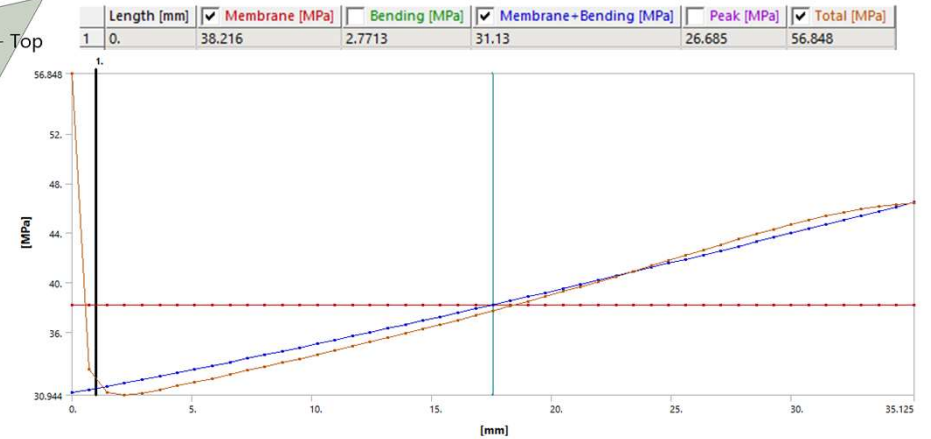
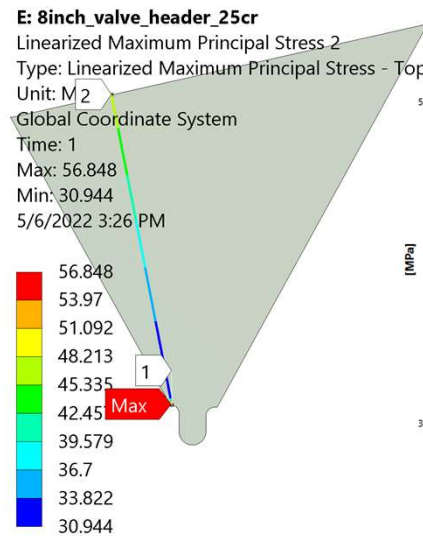


## Linearized Maximum Principal Stress - Weld toe



$$LSPF = \frac{\sigma_{max}}{\sigma_{lin}} = \frac{85.579}{54.681} = 1.57 \quad S_{mag} = \frac{\sigma_{lin}}{\sigma_{mem}} = \frac{54.681}{42.004} \times 1.06 = 1.38$$

## Linearized Maximum Principal Stress - Inside Weld root

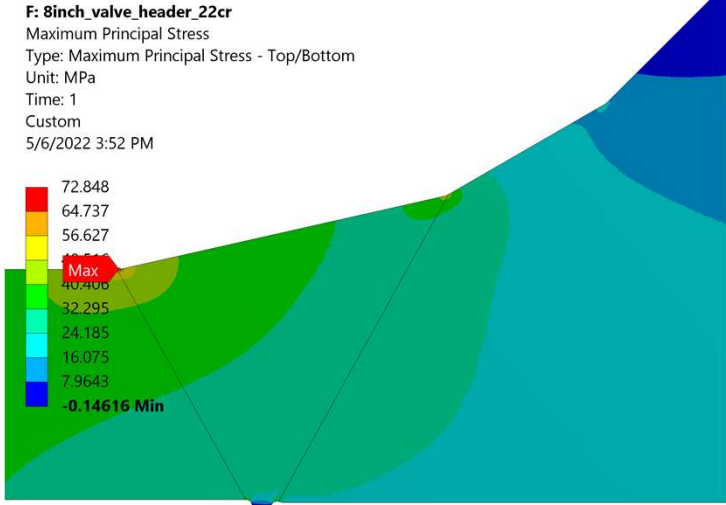


$$LSPF = \frac{\sigma_{max}}{\sigma_{lin}} = \frac{56.848}{31.13} = 1.83 \quad S_{mag} = \frac{\sigma_{lin}}{\sigma_{mem}} = \frac{38.216+2.7713}{38.216} \times 1.06 = 1.14$$

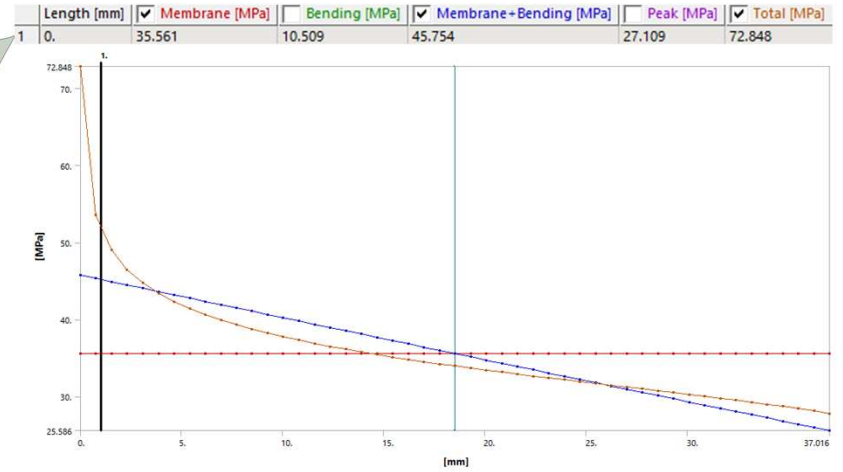
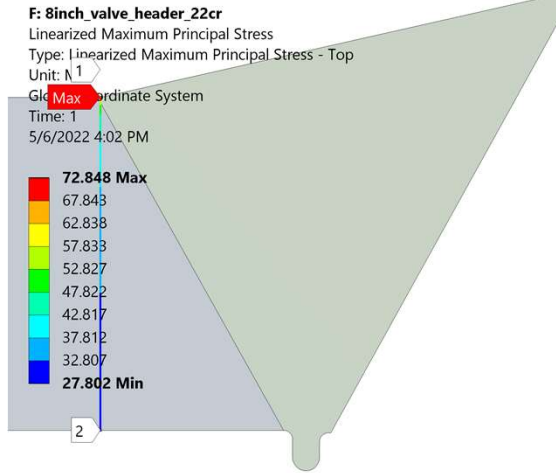


# 8 inch Header 22Cr

## Maximum Principal Stress

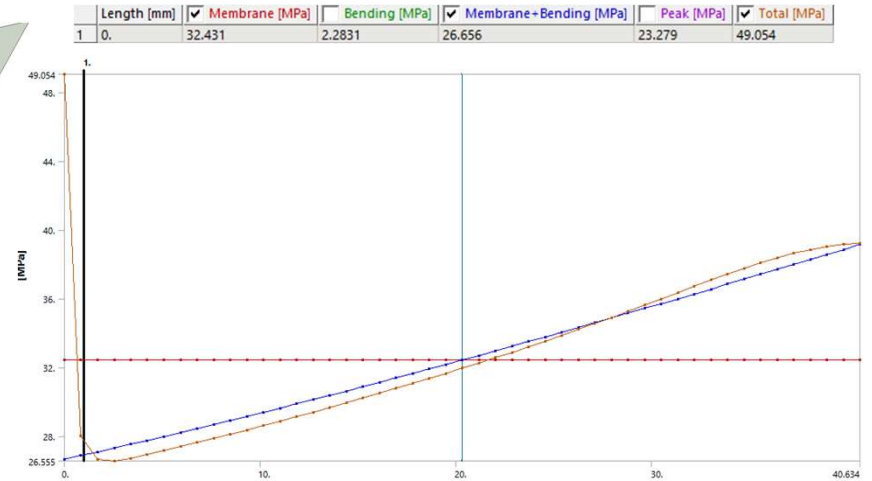
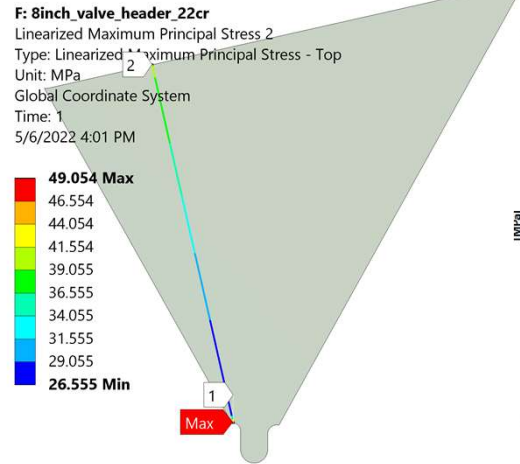


## Linearized Maximum Principal Stress - Weld toe



$$LSPF = \frac{\sigma_{max}}{\sigma_{lin}} = \frac{72.848}{45.754} = 1.59 \quad S_{mag} = \frac{\sigma_{lin}}{\sigma_{mem}} = \frac{45.754}{35.561} \times 1.06 = 1.36$$

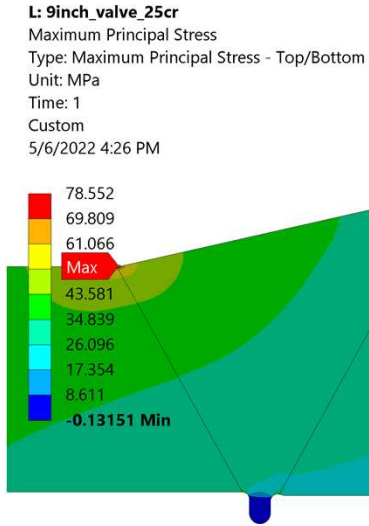
## Linearized Maximum Principal Stress - Inside Weld root



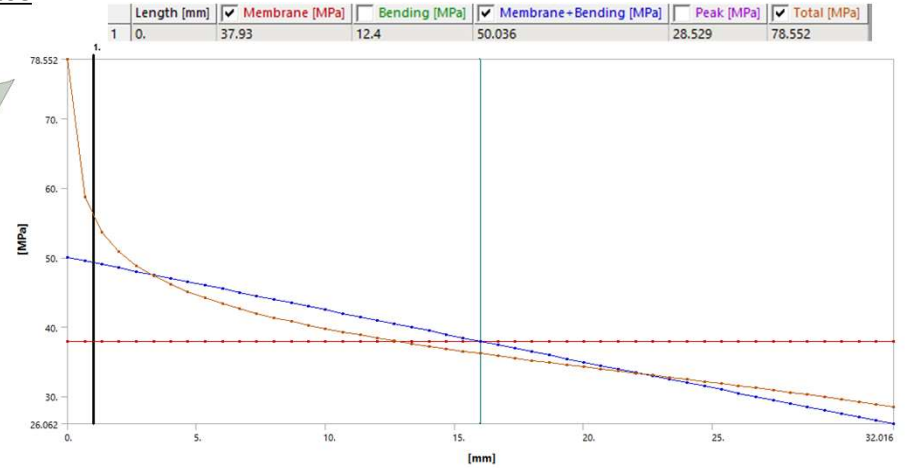
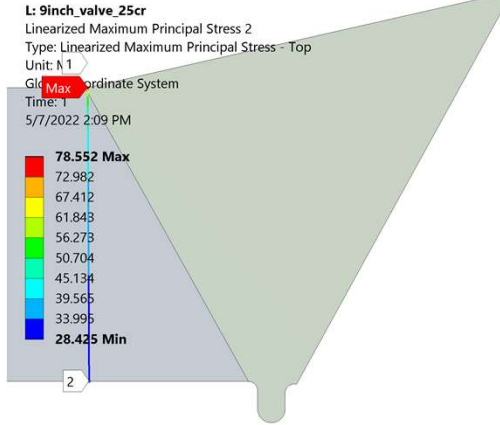
$$LSPF = \frac{\sigma_{max}}{\sigma_{lin}} = \frac{49.054}{26.656} = 1.84 \quad S_{mag} = \frac{\sigma_{lin}}{\sigma_{mem}} = \frac{32.431 + 2.2831}{32.431} \times 1.06 = 1.13$$

# 9 inch Header 25Cr

## Maximum Principal Stress

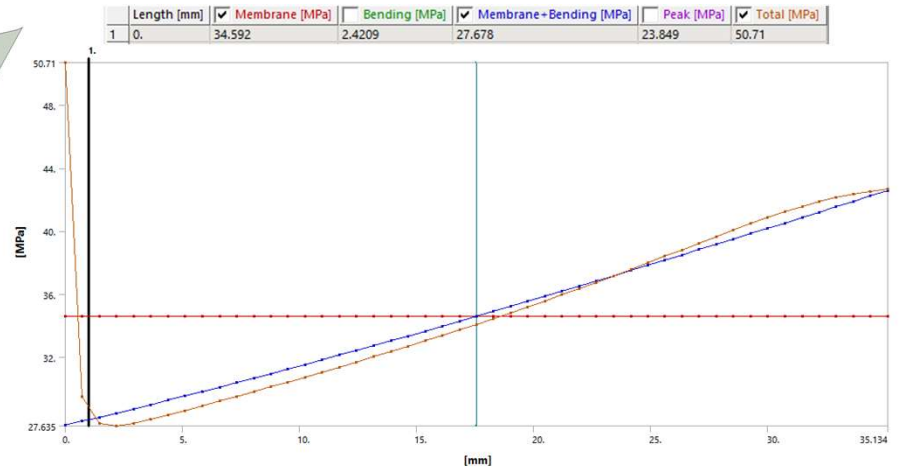
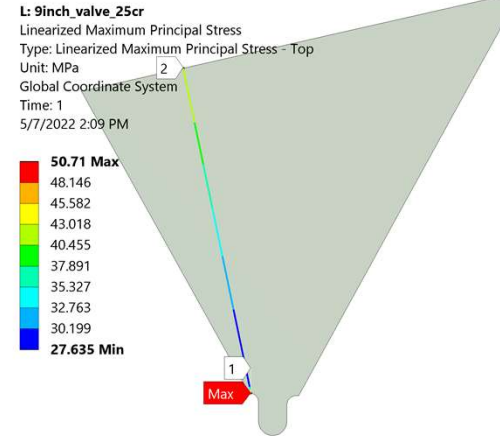


## Linearized Maximum Principal Stress - Weld toe



$$LSPF = \frac{\sigma_{max}}{\sigma_{lin}} = \frac{78.552}{50.036} = 1.57 \quad S_{mag} = \frac{\sigma_{lin}}{\sigma_{mem}} = \frac{50.036}{37.93} \times 1.06 = 1.4$$

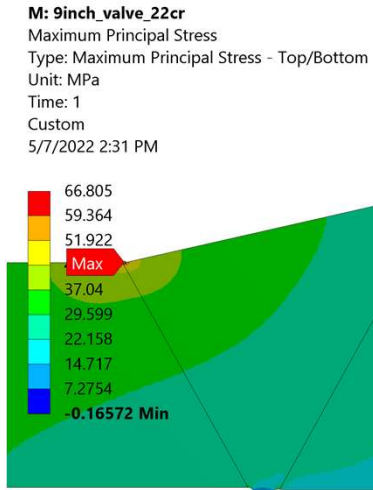
## Linearized Maximum Principal Stress - Inside Weld root



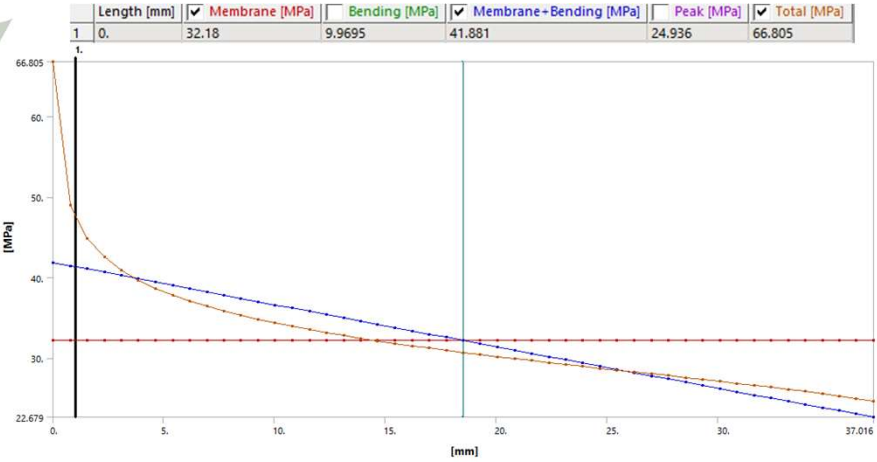
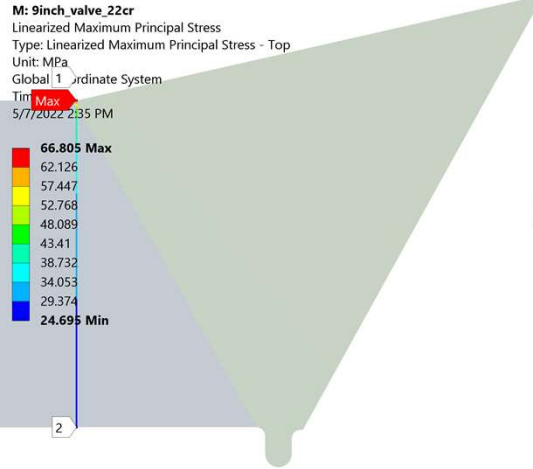
$$LSPF = \frac{\sigma_{max}}{\sigma_{lin}} = \frac{50.71}{27.678} = 1.83 \quad S_{mag} = \frac{\sigma_{lin}}{\sigma_{mem}} = \frac{34.592 + 2.4209}{34.592} \times 1.06 = 1.13$$

# 9 inch Header 22Cr

## Maximum Principal Stress

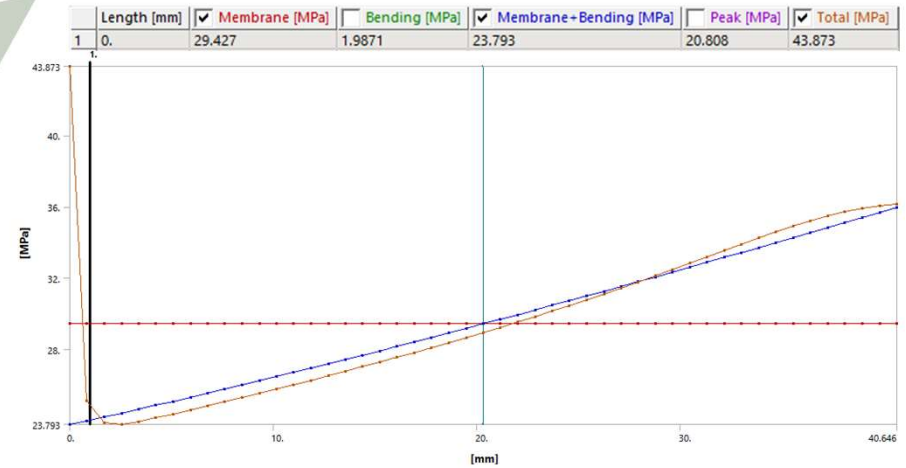
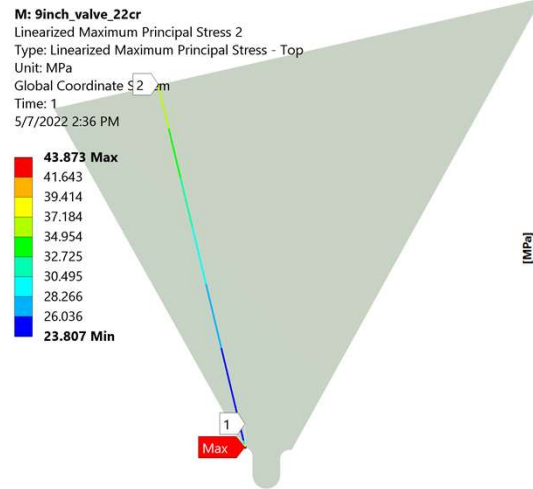


## Linearized Maximum Principal Stress - Weld toe



$$LSPF = \frac{\sigma_{max}}{\sigma_{lin}} = \frac{66.805}{41.881} = 1.6 \quad S_{mag} = \frac{\sigma_{lin}}{\sigma_{mem}} = \frac{41.881}{32.18} \times 1.06 = 1.38$$

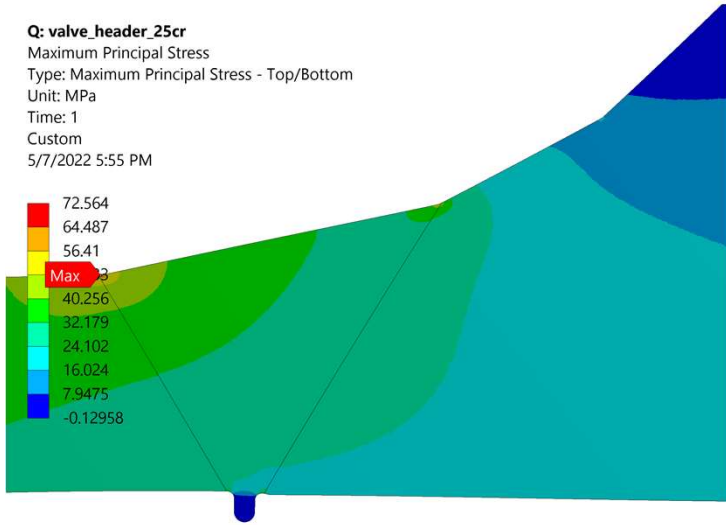
## Linearized Maximum Principal Stress - Inside Weld root



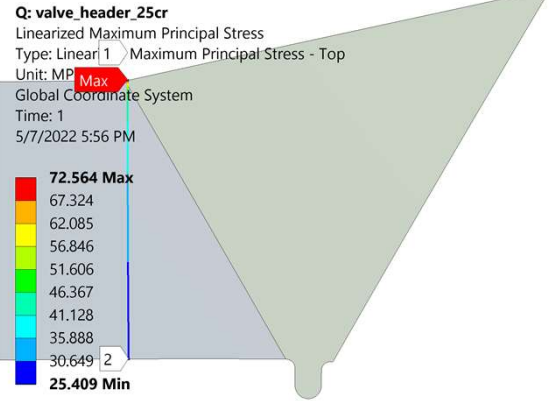
$$LSPF = \frac{\sigma_{max}}{\sigma_{lin}} = \frac{43.873}{23.793} = 1.84 \quad S_{mag} = \frac{\sigma_{lin}}{\sigma_{mem}} = \frac{29.427 + 1.9871}{29.427} \times 1.06 = 1.13$$

# 10 inch Header 25Cr

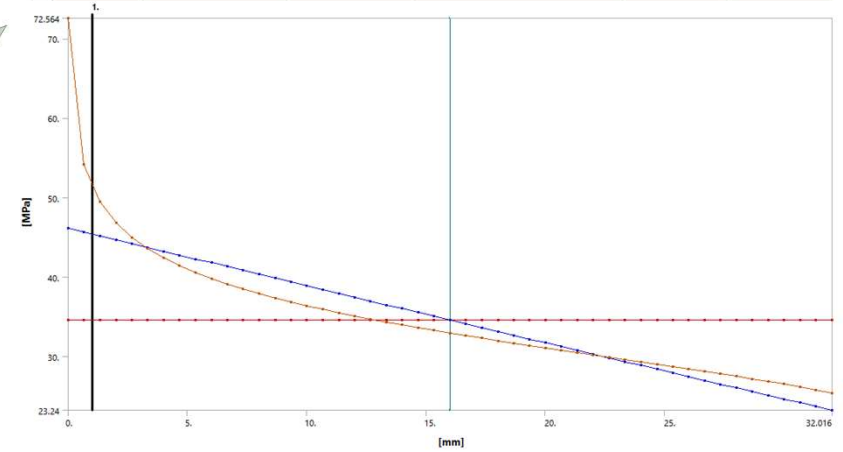
## Maximum Principal Stress



## Linearized Maximum Principal Stress - Weld toe

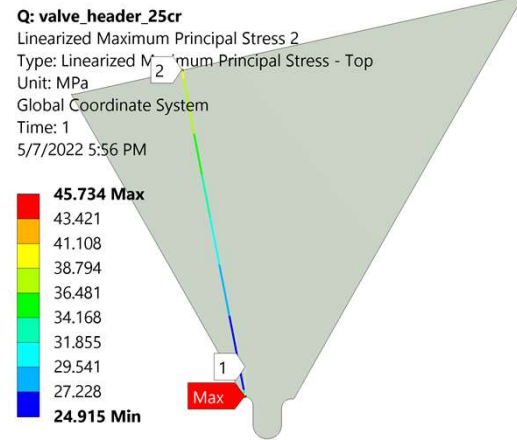


Length [mm]	Membrane [MPa]	Bending [MPa]	Membrane+Bending [MPa]	Peak [MPa]	Total [MPa]
1 0.	34.58	11.813	46.14	26.434	72.564

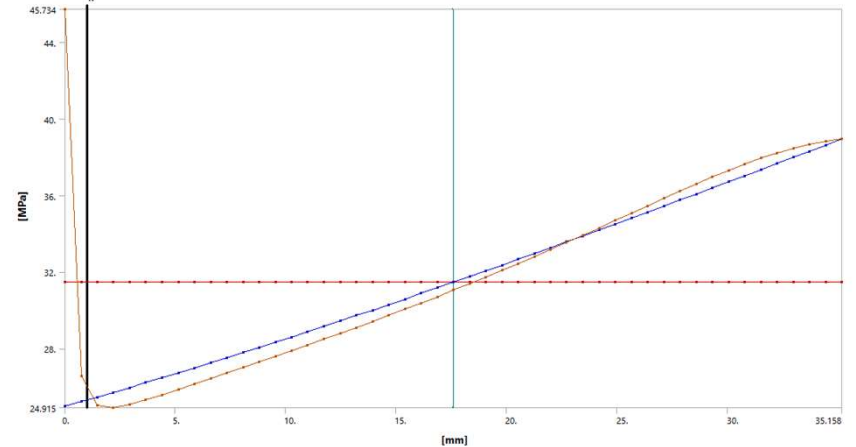


$$LSPF = \frac{\sigma_{max}}{\sigma_{lin}} = \frac{72.564}{46.14} = 1.57 \quad S_{mag} = \frac{\sigma_{lin}}{\sigma_{mem}} = \frac{46.14}{34.58} \times 1.06 = 1.41$$

## Linearized Maximum Principal Stress - Inside Weld root



Length [mm]	Membrane [MPa]	Bending [MPa]	Membrane+Bending [MPa]	Peak [MPa]	Total [MPa]
1 0.	31.474	2.1851	24.989	21.406	45.734

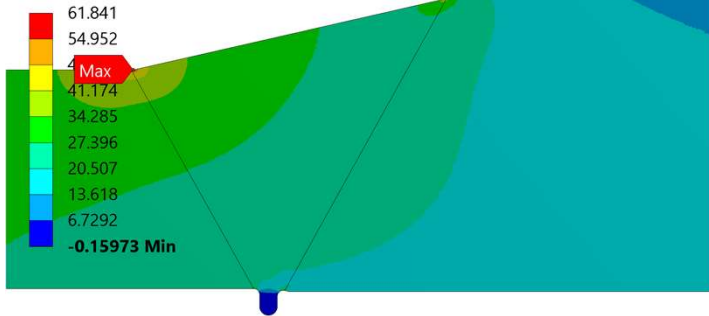


$$LSPF = \frac{\sigma_{max}}{\sigma_{lin}} = \frac{45.734}{24.989} = 1.83 \quad S_{mag} = \frac{\sigma_{lin}}{\sigma_{mem}} = \frac{31.474 + 2.1851}{31.474} \times 1.06 = 1.13$$

# 10 inch Header 22Cr

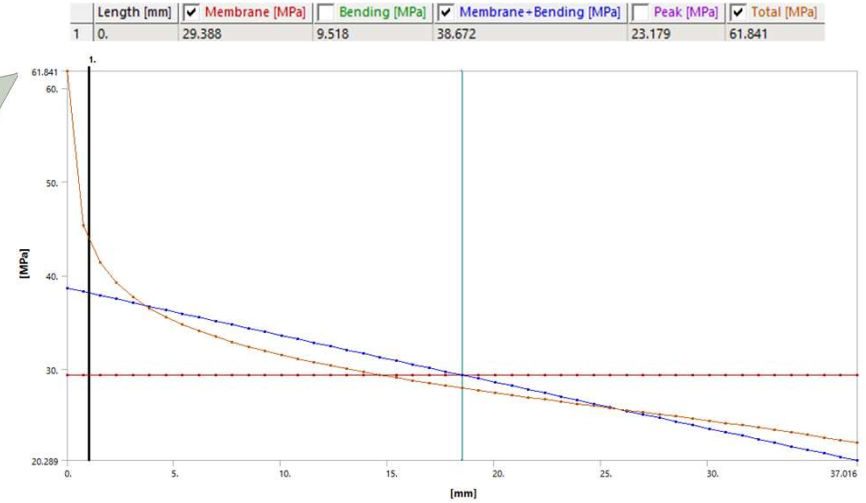
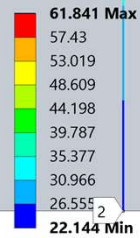
## Maximum Principal Stress

**R: 10inch\_header\_valve\_22cr**  
 Maximum Principal Stress  
 Type: Maximum Principal Stress - Top/Bottom  
 Unit: MPa  
 Time: 1  
 Custom  
 5/7/2022 5:44 PM



## Linearized Maximum Principal Stress - Weld toe

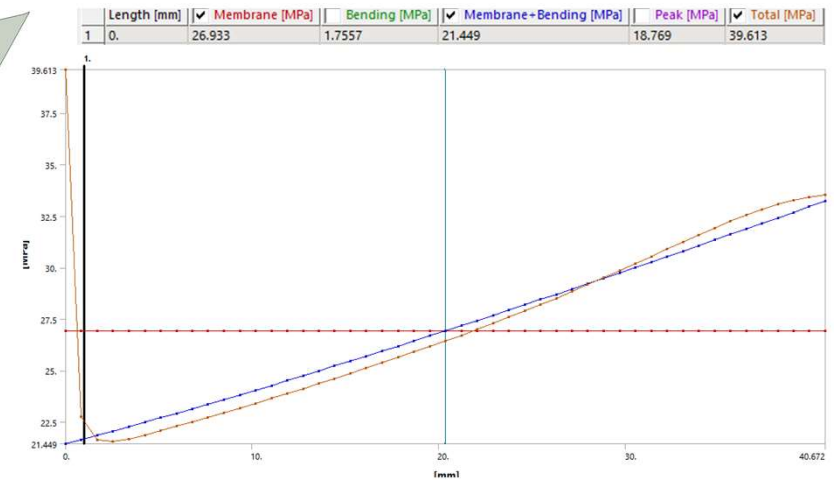
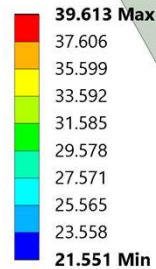
**R: 10inch\_header\_valve\_22cr**  
 Linearized Maximum Principal Stress  
 Type: Linearized Maximum Principal Stress - Top  
 Unit: MPa  
 Global Coordinate System  
 Time: 1  
 5/7/2022 5:48 PM



$$LSPF = \frac{\sigma_{max}}{\sigma_{lin}} = \frac{61.841}{38.672} = 1.6 \quad S_{mag} = \frac{\sigma_{lin}}{\sigma_{mem}} = \frac{38.672}{29.388} \times 1.06 = 1.39$$

## Linearized Maximum Principal Stress - Inside Weld root

**R: 10inch\_header\_valve\_22cr**  
 Linearized Maximum Principal Stress 2  
 Type: Linearized Maximum Principal Stress - Top  
 Unit: MPa  
 Global Coordinate System  
 Time: 1  
 5/7/2022 5:49 PM

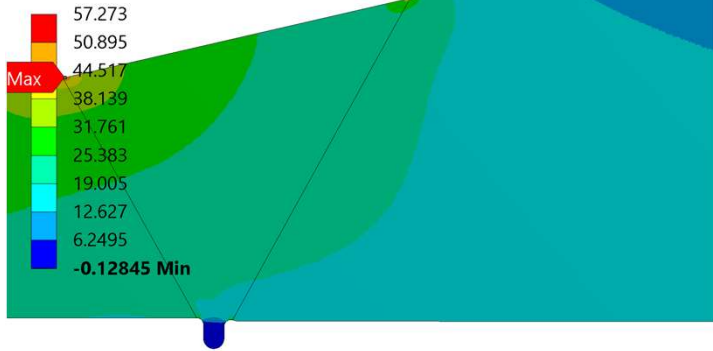


$$LSPF = \frac{\sigma_{max}}{\sigma_{lin}} = \frac{39.613}{21.449} = 1.85 \quad S_{mag} = \frac{\sigma_{lin}}{\sigma_{mem}} = \frac{26.933+1.7557}{26.933} \times 1.06 = 1.13$$

# 12 inch Header 25Cr

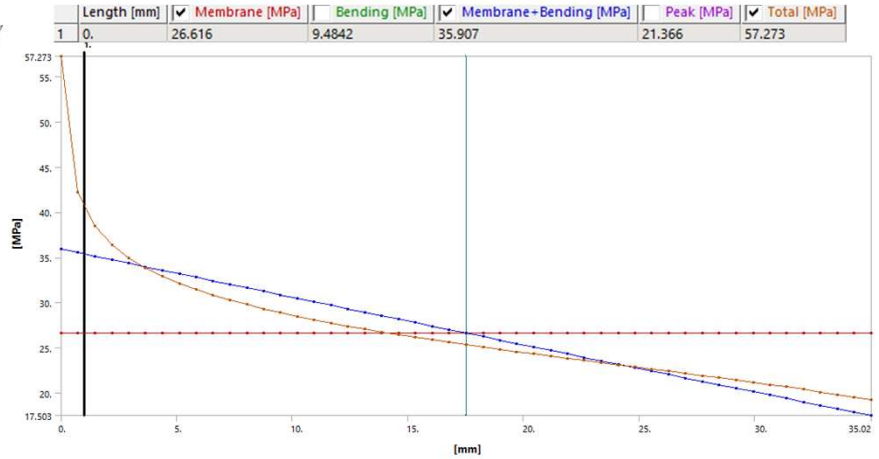
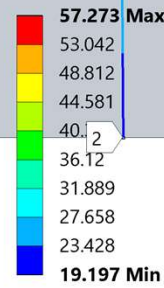
## Maximum Principal Stress

V: 12inch\_valve25cr  
 Maximum Principal Stress  
 Type: Maximum Principal Stress - Top/Bottom  
 Unit: MPa  
 Time: 1  
 Custom  
 5/7/2022 4:38 PM



## Linearized Maximum Principal Stress - Weld toe

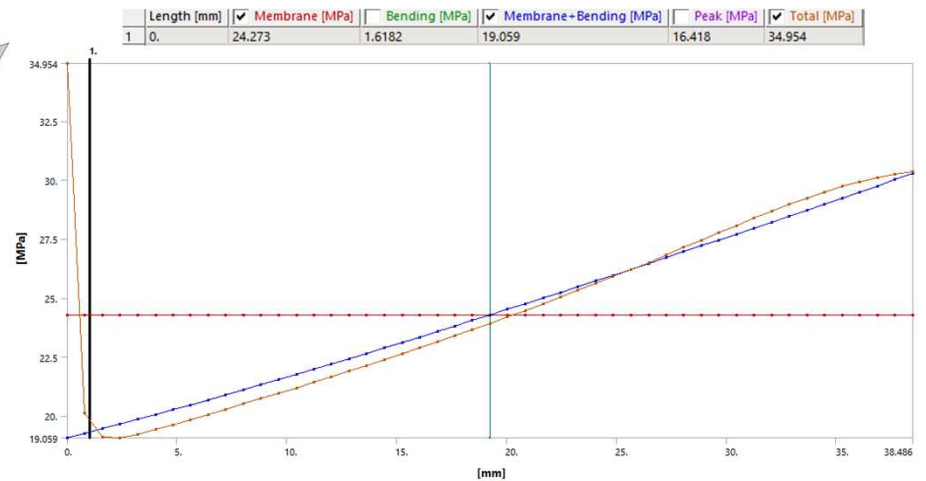
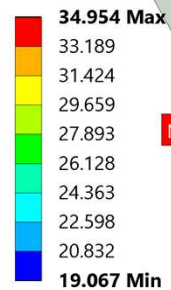
V: 12inch\_valve25cr  
 Linearized Maximum Principal Stress  
 Type: Linearized Maximum Principal Stress - Top  
 Unit: MPa  
 Global Coordinate System  
 Time: 1  
 5/7/2022 4:40 PM



$$LSPF = \frac{\sigma_{max}}{\sigma_{lin}} = \frac{57.273}{35.907} = 1.6 \quad S_{mag} = \frac{\sigma_{lin}}{\sigma_{mem}} = \frac{35.907}{26.616} \times 1.06 = 1.43$$

## Linearized Maximum Principal Stress - Inside Weld root

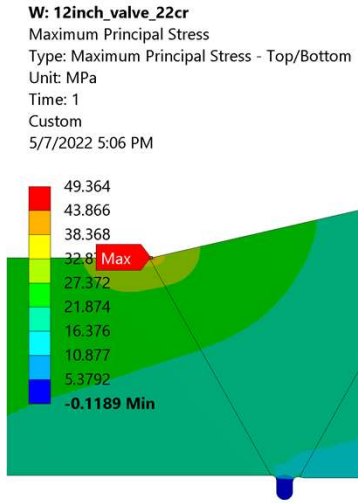
V: 12inch\_valve25cr  
 Linearized Maximum Principal Stress 2  
 Type: Linearized Maximum Principal Stress - Top  
 Unit: MPa  
 Global Coordinate System  
 Time: 1  
 5/7/2022 4:39 PM



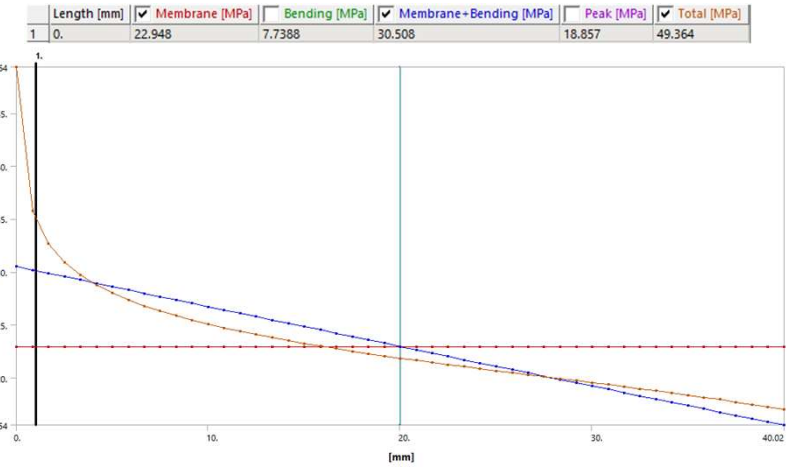
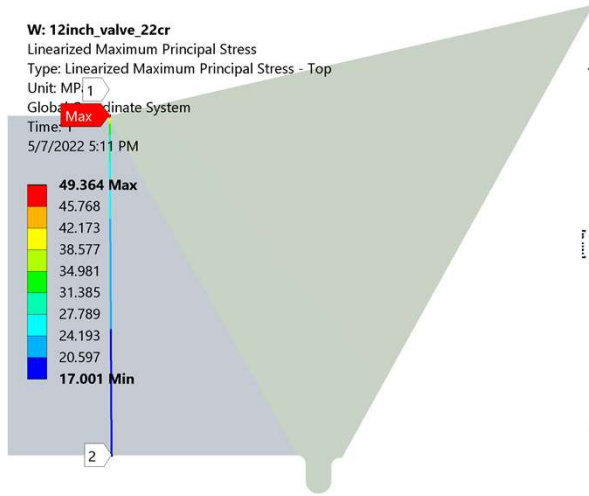
$$LSPF = \frac{\sigma_{max}}{\sigma_{lin}} = \frac{34.954}{19.059} = 1.83 \quad S_{mag} = \frac{\sigma_{lin}}{\sigma_{mem}} = \frac{24.273+1.6182}{24.273} \times 1.06 = 1.13$$

# 12 inch Header 22Cr

## Maximum Principal Stress

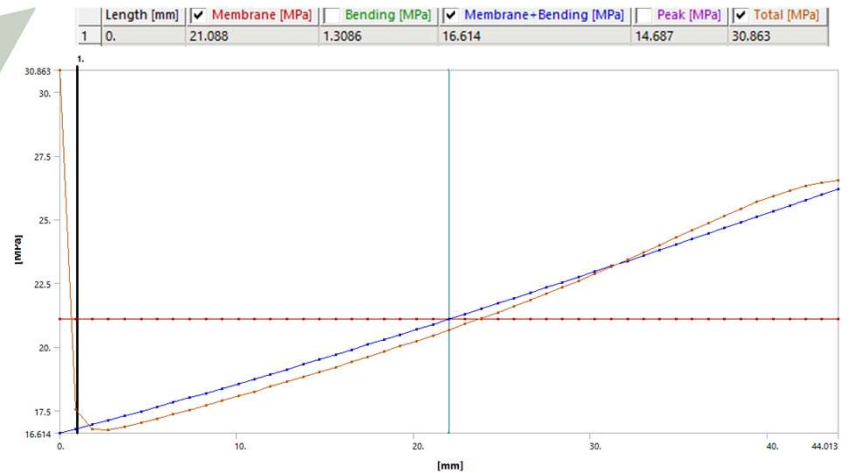
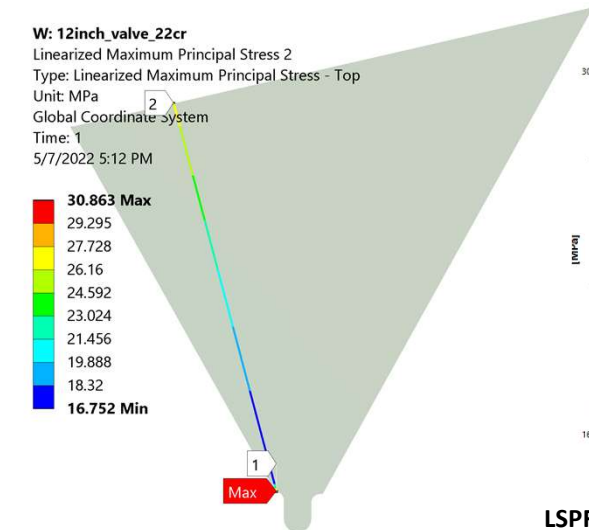


## Linearized Maximum Principal Stress - Weld toe



$$LSPF = \frac{\sigma_{max}}{\sigma_{lin}} = \frac{49.364}{30.508} = 1.62 \quad S_{mag} = \frac{\sigma_{lin}}{\sigma_{mem}} = \frac{30.508}{22.948} \times 1.06 = 1.41$$

## Linearized Maximum Principal Stress - Inside Weld root



$$LSPF = \frac{\sigma_{max}}{\sigma_{lin}} = \frac{30.863}{16.614} = 1.86 \quad S_{mag} = \frac{\sigma_{lin}}{\sigma_{mem}} = \frac{21.088 + 1.3086}{21.088} \times 1.06 = 1.13$$

## Appendix - D

**SCF calculation for valve/hub welds - headers with lower wall thickness**

LSFP<sub>cat 1</sub> & S<sub>mag</sub> calculations using FEA

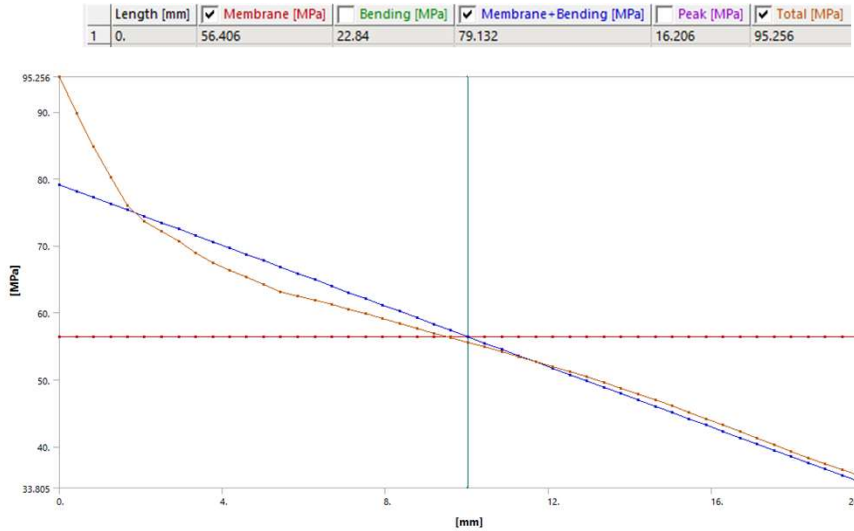
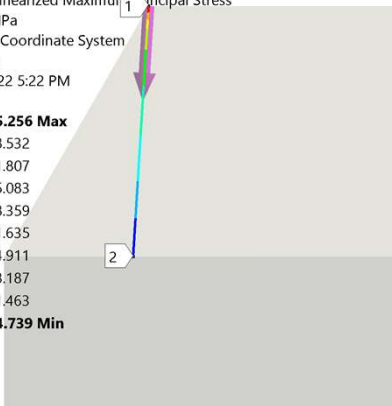
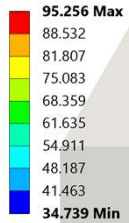


# SCF calculation for Headers with lower thickness (t = 20 mm)

## 10 inch Header (t=20mm) to hub

N: 10inch\_20mm\_hub\_3d

Linearized Maximum Principal Stress  
 Type: Linearized Maximum Principal Stress  
 Unit: MPa  
 Global Coordinate System  
 Time: 1  
 5/8/2022 5:22 PM



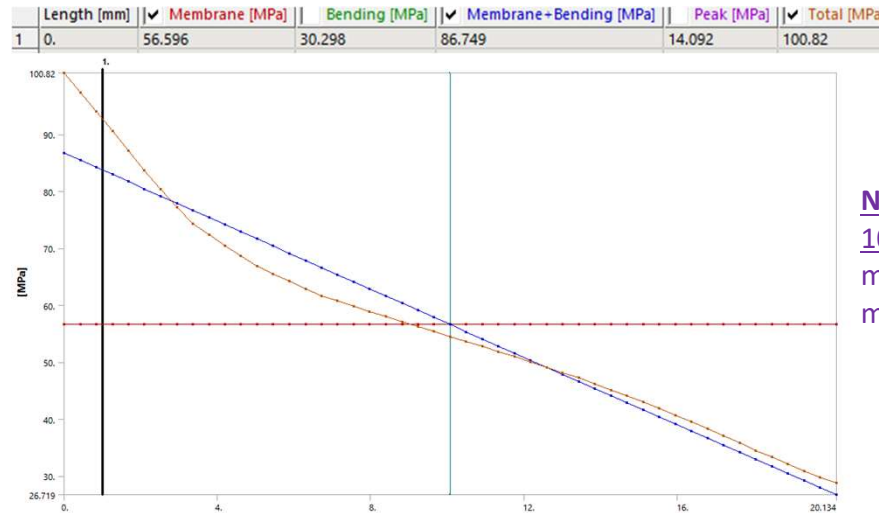
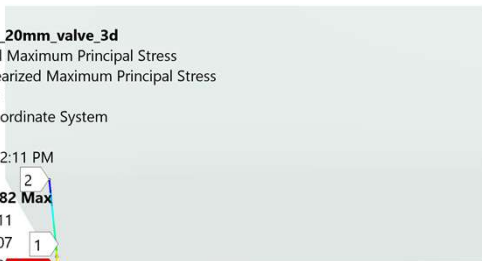
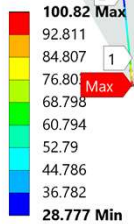
$$S_{mag} = \frac{\sigma_{lin}}{\sigma_{mem}} = \frac{79.132}{56.406} = 1.4$$

$$S_{mag} (w/o clm) = 1.26$$

## 10 inch Header (t=20mm) to valve

L: 10inch\_20mm\_valve\_3d

Linearized Maximum Principal Stress  
 Type: Linearized Maximum Principal Stress  
 Unit: MPa  
 Global Coordinate System  
 Time: 1  
 5/8/2022 2:11 PM



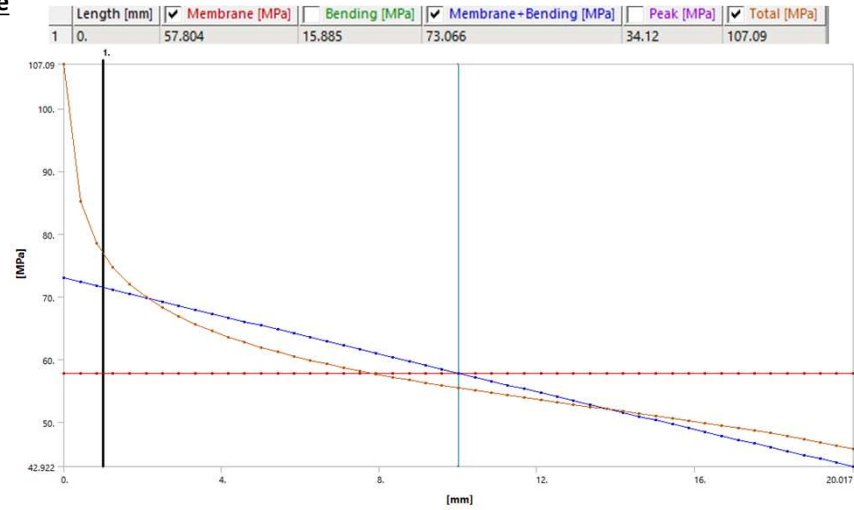
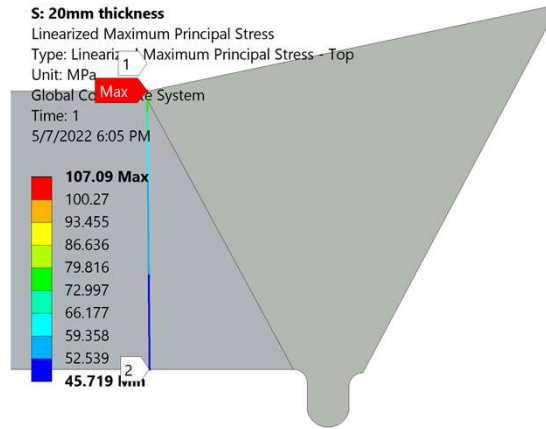
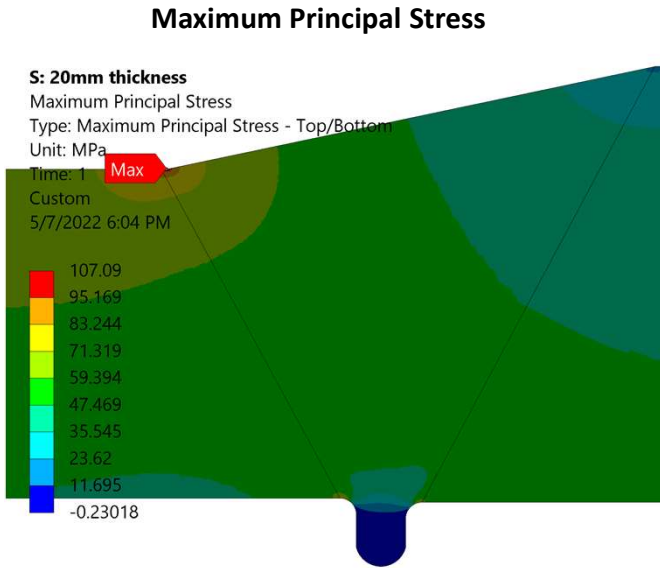
$$S_{mag} = \frac{\sigma_{lin}}{\sigma_{mem}} = \frac{86.749}{56.596} = 1.53$$

$$S_{mag} (w/o clm) = 1.39$$

**Note:** It is observed that the  $S_{mag}$  was approx. 10% higher in case of model with center-line misalignment compared to no center-line misalignment.

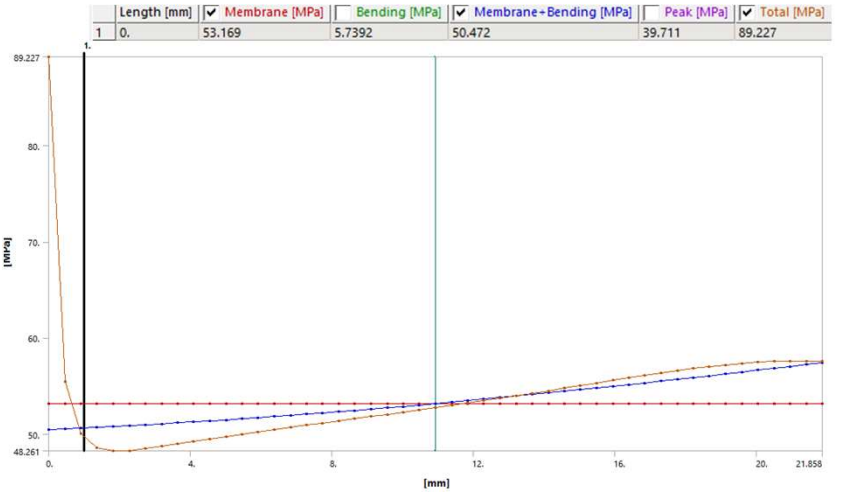
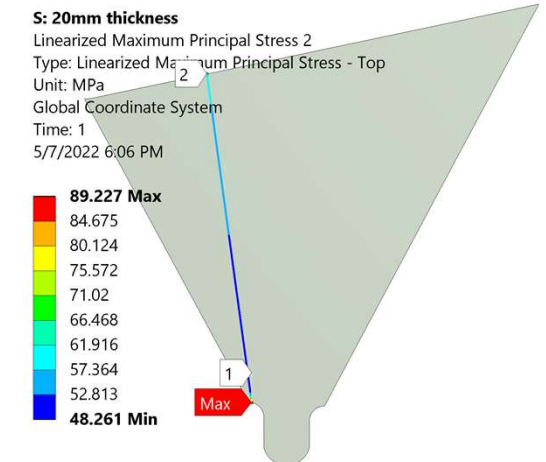
# 10 inch Header (20 mm thickness) to hub

## Linearized Maximum Principal Stress - Weld toe



$$LSPF = \frac{\sigma_{max}}{\sigma_{lin}} = \frac{107.09}{73.066} = 1.47 \quad S_{mag} = \frac{\sigma_{lin}}{\sigma_{mem}} = \frac{73.066}{57.804} \times 1.1 = 1.4$$

## Linearized Maximum Principal Stress - Inside Weld root

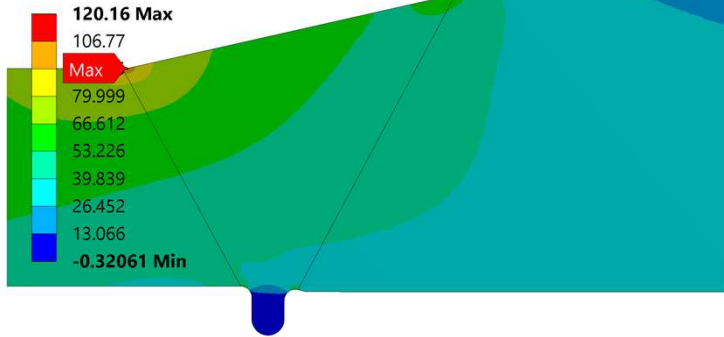


$$LSPF = \frac{\sigma_{max}}{\sigma_{lin}} = \frac{89.227}{50.472} = 1.77 \quad S_{mag} = \frac{\sigma_{lin}}{\sigma_{mem}} = \frac{53.169 + 5.7392}{53.169} \times 1.1 = 1.22$$

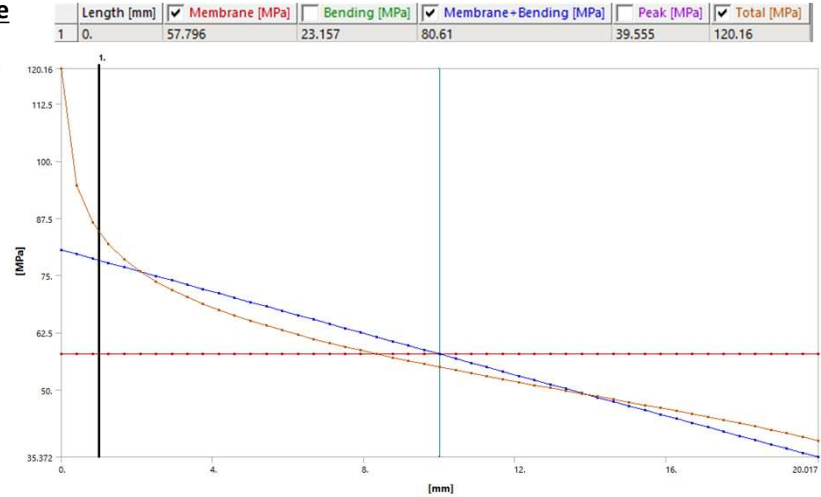
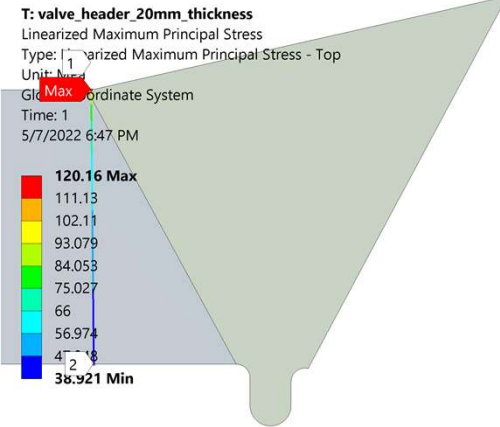
# 10 inch Header (20 mm thickness) to valve

## Maximum Principal Stress

T: valve\_header\_20mm\_thickness  
 Maximum Principal Stress  
 Type: Maximum Principal Stress - Top/Bottom  
 Unit: MPa  
 Time: 1  
 Custom  
 5/7/2022 6:49 PM

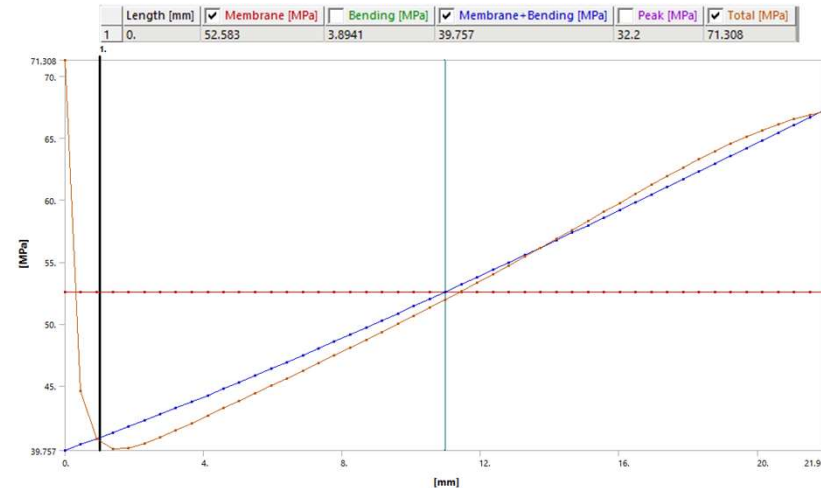
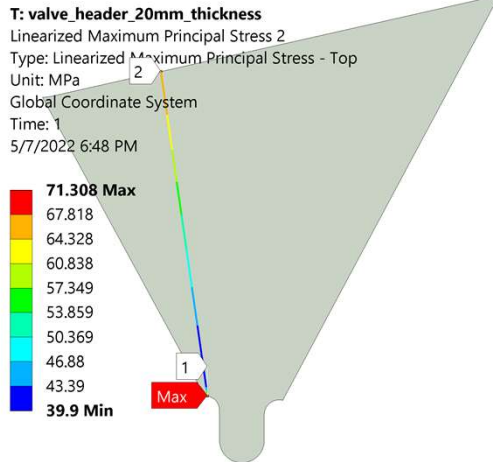


## Linearized Maximum Principal Stress - Weld toe



$$LSPF = \frac{\sigma_{max}}{\sigma_{lin}} = \frac{120.16}{80.61} = 1.49 \quad S_{mag} = \frac{\sigma_{lin}}{\sigma_{mem}} = \frac{80.61}{57.796} \times 1.1 = 1.53$$

## Linearized Maximum Principal Stress - Inside Weld root



$$LSPF = \frac{\sigma_{max}}{\sigma_{lin}} = \frac{71.308}{39.757} = 1.79 \quad S_{mag} = \frac{\sigma_{lin}}{\sigma_{mem}} = \frac{52.583+3.8941}{52.583} \times 1.1 = 1.18$$

## Comparison of 10 inch headers with different thickness:

### 10 Inch header with thickness = 20 mm

10" ID	Header (nom)	valve (max)	LSPF	Smag
ID	254	253 (254 -1)	1.49 (outside toe)	1.53 (outside toe)
WT	20	27.265 (OD-ID)/2	1.79 (inside root)	1.18 (inside root)
OD	294	307.53(306+0.5%)		

10" ID	Header (nom)	Hub (max)	LSPF	Smag
ID	254	253.5 (254 -0.5)	1.47 (outside toe)	1.4 (outside toe)
WT	20	26.5 (OD-ID)/2	1.77 (inside root)	1.22 (inside root)
OD	294	306.5 (306+0.5)		

### 10 Inch header with thickness = 32 mm

10" ID	Header (nom)	valve (max)	LSPF	Smag
ID	254	253 (254 -1)	1.57 (outside toe)	1.41 (outside toe)
WT	32	42.95 (OD-ID)/2	1.83 (inside root)	1.13 (inside root)
OD	318	338.9 (337.2+0.5%)		

10" ID	Header (nom)	Hub (max)	LSPF	Smag
ID	254	253.5 (254 -0.5)	1.55 (outside toe)	1.38 (outside toe)
WT	32	42.1 (OD-ID)/2	1.79 (inside root)	1.2 (inside root)
OD	318	337.7 (337.2+0.5)		

### 10 Inch header with thickness = 37 mm (22cr)

10" ID	Header (nom)	valve (max)	LSPF	Smag
ID	254	253 (254 -1)	1.6 (outside toe)	1.39 (outside toe)
WT	37	49.5 (OD-ID)/2	1.85 (inside root)	1.13 (inside root)
OD	328	352 (350.2+0.5%)		

10" ID	Header (nom)	Hub (max)	LSPF	Smag
ID	254	253.5 (254 -0.5)	1.58 (outside toe)	1.38 (outside toe)
WT	37	48.6 (OD-ID)/2	1.8 (inside root)	1.2 (inside root)
OD	328	350.7 (350.2+0.5)		

While LSPF is increasing with thickness, Smag is decreasing with increase in thickness.

## Appendix - E

### Input for GPRM training from FEA calculated LSPF data

<b>8" &amp; 9" ID</b>	<b>LSPF</b>						
<b>t</b>	R3	R6	R9	R12	R15	R22	R30
20	1.48	1.37	1.3	1.26	1.23	1.18	1.15
26	1.53	1.41	1.34	1.30	1.26	1.21	1.20
32	1.57	1.45	1.38	1.34	1.3	1.25	1.21
37	1.59	1.47	1.4	1.36	1.32	1.26	1.22

<b>10" ID</b>	<b>LSPF</b>						
<b>t</b>	R3	R6	R9	R12	R15	R22	R30
20	1.49	1.38	1.31	1.27	1.24	1.19	1.16
26	1.54	1.42	1.35	1.31	1.27	1.22	1.21
32	1.58	1.46	1.39	1.35	1.31	1.27	1.23
37	1.6	1.48	1.41	1.37	1.31	1.27	1.23

<b>12" ID</b>	<b>LSPF</b>						
<b>t</b>	R3	R6	R9	R12	R15	R22	R30
35	1.6	1.47	1.4	1.36	1.32	1.26	1.22
40	1.62	1.49	1.42	1.38	1.34	1.28	1.24

## Estimated LSPF Values for Unequal Welds between Header and Valve/ Hubs

(Applicable for headers sizes of 8" ID to 12"ID)

<b>Estimated LSPF</b>									
<b>Toe radius (mm)</b>	<b>Thickness (mm)</b>								
	<b>20</b>	<b>23</b>	<b>26</b>	<b>28</b>	<b>30</b>	<b>32</b>	<b>35</b>	<b>37</b>	<b>40</b>
3	1.48	1.51	1.53	1.55	1.56	1.56	1.58	1.59	1.61
4	1.44	1.46	1.49	1.50	1.52	1.52	1.53	1.55	1.57
5	1.40	1.42	1.44	1.46	1.48	1.48	1.49	1.51	1.53
6	1.37	1.39	1.41	1.43	1.44	1.45	1.46	1.47	1.49
7	1.34	1.36	1.38	1.40	1.41	1.42	1.43	1.44	1.46
8	1.32	1.34	1.36	1.38	1.39	1.40	1.41	1.42	1.44
9	1.30	1.32	1.34	1.36	1.37	1.38	1.39	1.40	1.42
10	1.28	1.30	1.33	1.34	1.36	1.36	1.37	1.38	1.40
11	1.27	1.29	1.31	1.33	1.34	1.35	1.36	1.37	1.39
12	1.26	1.28	1.30	1.32	1.33	1.34	1.35	1.36	1.37
13	1.25	1.27	1.29	1.30	1.32	1.33	1.34	1.35	1.36
14	1.24	1.25	1.27	1.29	1.30	1.31	1.32	1.33	1.35
15	1.23	1.24	1.26	1.28	1.29	1.30	1.31	1.32	1.34
16	1.22	1.23	1.25	1.27	1.28	1.29	1.30	1.31	1.32
17	1.21	1.23	1.24	1.26	1.27	1.28	1.29	1.29	1.31
18	1.21	1.22	1.23	1.25	1.26	1.27	1.28	1.29	1.30
19	1.20	1.21	1.23	1.24	1.26	1.26	1.27	1.28	1.30
20	1.19	1.20	1.22	1.24	1.25	1.26	1.26	1.27	1.29
21	1.19	1.20	1.21	1.23	1.25	1.25	1.26	1.26	1.28
22	1.18	1.19	1.21	1.23	1.24	1.25	1.25	1.26	1.28
23	1.18	1.19	1.21	1.23	1.24	1.25	1.25	1.26	1.27
24	1.17	1.19	1.21	1.22	1.24	1.24	1.25	1.25	1.27
25	1.17	1.19	1.21	1.22	1.23	1.24	1.24	1.25	1.26
26	1.17	1.19	1.21	1.22	1.23	1.23	1.24	1.24	1.26
27	1.16	1.18	1.21	1.22	1.23	1.23	1.23	1.24	1.25
28	1.16	1.18	1.21	1.22	1.22	1.22	1.22	1.23	1.25
29	1.15	1.18	1.20	1.21	1.22	1.22	1.22	1.23	1.24
30	1.15	1.18	1.20	1.21	1.21	1.21	1.21	1.22	1.24

# Appendix - F

## Stress linearization data and calculations

Data from FEA analysis - ANSYS						
Length	Membrane (M)	Bending (B)	M + B	Peak (P)	Total (M+B+P)	$\sigma (t/2 - x)$
0	100.79	23.756	124.12	19.022	139.84	1534.744
0.45729	100.79	22.766	123.14	14.211	135.4	1424.098
0.91458	100.79	21.776	122.17	9.621	131.07	1318.619
1.3719	100.79	20.787	121.19	6.9092	127.81	1227.372
1.8292	100.79	19.797	120.22	4.4728	124.67	1140.207
2.2865	100.79	18.807	119.24	2.8467	122.07	1060.605
2.7438	100.79	17.817	118.27	1.6656	119.58	984.2869
3.201	100.79	16.827	117.3	1.2579	117.42	912.8231
3.6583	100.79	15.837	116.32	1.28	115.39	844.274
4.1156	100.79	14.848	115.35	1.3795	113.59	779.1592
4.5729	100.79	13.858	114.38	1.4753	111.91	716.459
5.0302	100.79	12.868	113.4	1.5409	110.39	656.2465
5.4875	100.79	11.878	112.43	1.5742	108.98	598.0278
5.9448	100.79	10.888	111.46	1.5866	107.67	541.6016
6.4021	100.79	9.8984	110.49	1.5711	106.46	486.8309
6.8594	100.79	8.9085	109.52	1.5443	105.32	433.455
7.3167	100.79	7.9187	108.54	1.4962	104.26	381.4144
7.774	100.79	6.9289	107.57	1.4426	103.25	330.5033
8.2313	100.79	5.939	106.6	1.3729	102.32	280.7354
8.6885	100.79	4.9492	105.63	1.301	101.41	231.874
9.1458	100.79	3.9594	104.66	1.2171	100.57	183.9626
9.6031	100.79	2.9695	103.69	1.1325	99.747	136.8429
10.06	100.79	1.9797	102.72	1.0394	98.984	90.57036
10.518	100.79	0.98984	101.75	0.94637	98.223	44.88791
10.975	100.79	1.55E-14	100.79	0.84731	97.516	0
11.432	100.79	-7.23E-02	99.818	0.74852	96.809	-44.2417
11.89	100.79	-0.14466	98.851	0.64654	96.142	-87.9699
12.347	100.79	-0.21698	97.883	0.54462	95.478	-130.996
12.804	100.79	-0.28931	96.917	0.44171	94.84	-173.462
13.261	100.79	-0.36164	95.95	0.33888	94.206	-215.355
13.719	100.79	-0.43397	94.985	0.23697	93.588	-256.805
14.176	100.79	-0.5063	94.019	0.13585	92.974	-297.61
14.633	100.79	-0.57863	93.054	3.85E-02	92.367	-337.878
15.091	100.79	-0.65095	92.09	-4.87E-02	91.763	-377.697
15.548	100.79	-0.72328	91.126	7.21E-02	91.16	-416.875
16.005	100.79	-0.79561	90.163	0.42259	90.557	-455.502
16.463	100.79	-0.86794	89.2	0.77893	89.949	-493.64
16.92	100.79	-0.94027	88.237	1.132	89.338	-531.114
17.377	100.79	-1.0126	87.276	1.4771	88.718	-567.973
17.834	100.79	-1.0849	86.315	1.8114	88.088	-604.196
18.292	100.79	-1.1573	85.354	2.1355	87.447	-639.85
18.749	100.79	-1.2296	84.394	2.4404	86.788	-674.69
19.206	100.79	-1.3019	83.435	2.7349	86.119	-708.845
19.664	100.79	-1.3742	82.476	2.9998	85.419	-742.206
20.121	100.79	-1.4466	81.519	3.2556	84.71	-774.758
20.578	100.79	-1.5189	80.561	3.4683	83.956	-806.229
21.035	100.79	-1.5912	79.605	3.6763	83.197	-836.962
21.493	100.79	-1.6635	78.649	3.8313	82.377	-866.441
21.95	100.79	-1.7359	77.695	3.9883	81.559	-895.11
Membrane ( manual calc)					100.8479063	

$$\sigma_{mem} = \frac{1}{t} \int_0^t \sigma_{ij} dx$$

Bending stress (outer) manual calc.	23.21467
-------------------------------------	----------

$$\sigma_{bending} = \frac{6}{t^2} \int_0^t \sigma_{ij} \left( \frac{t}{2} - x \right) dx$$

$$\int_a^b f(x) dx \approx \frac{h}{48} \left[ 17f(x_0) + 59f(x_1) + 43f(x_2) + 49f(x_3) + 48 \sum_{i=4}^{n-4} f(x_i) + 49f(x_{n-3}) + 43f(x_{n-2}) + 59f(x_{n-1}) + 17f(x_n) \right]$$